UDK 66:54(05) CODEN HMIDA 8 ISSN 0367–598 X

4 Hemijska industrija

Vol. 70

Časopis Saveza hemijskih inženjera Srbije

Chemical Industry

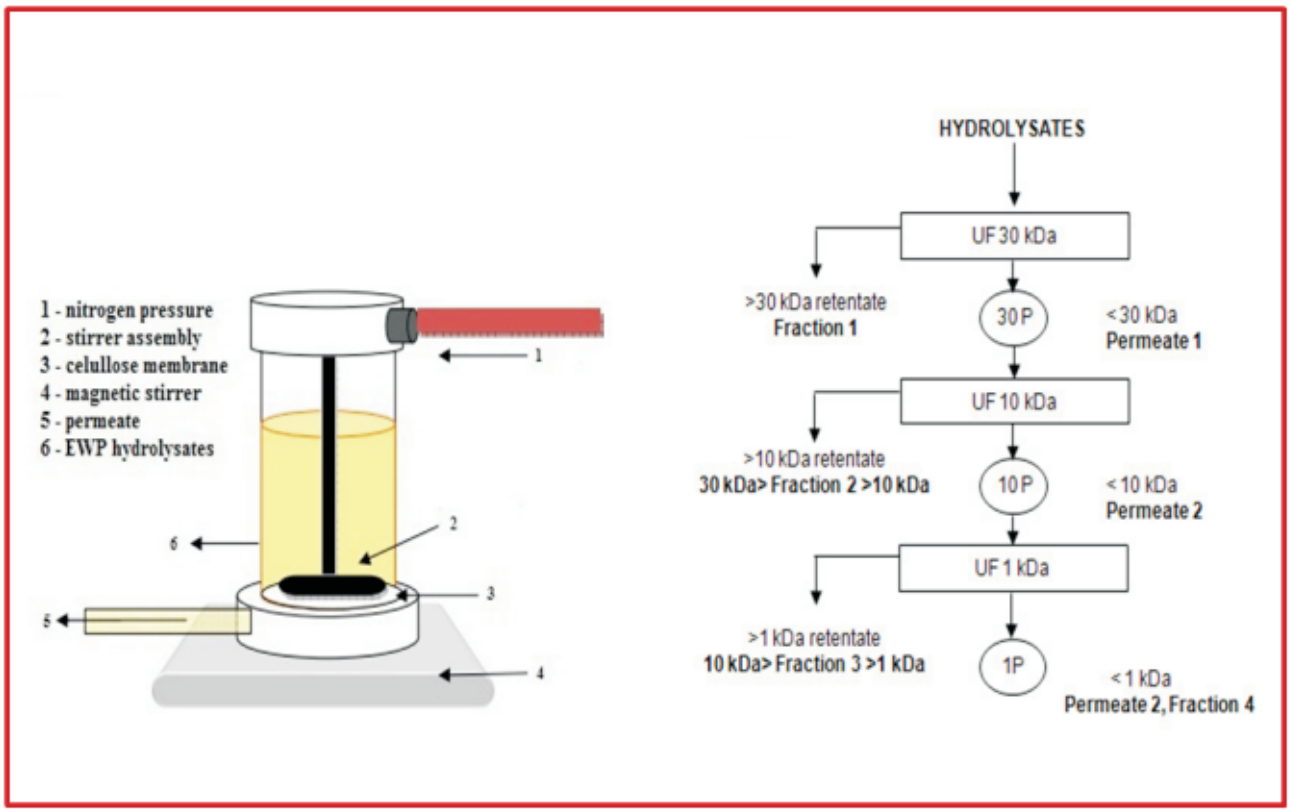

Aktivnosti Saveza hemijskih inženjera Srbije pomažu:

MINISTARSTVO PROSVETE, NAUKE I TEHNOLOŠKOG RAZVOJA REPUBLIKE SRBIJE

Tehnološko-metalurški fakultet
Univerziteta u Beogradu, Beograd

Prirodno-matematički fakultet Univerziteta
u Novom Sadu, Novi Sad

Hemijski fakutet
Univerziteta u Beogradu
Beograd

ITNMS
Institut za tehnologiju nuklearnih i drugih
mineralnih sirovina, Beograd

Institut za opštu i fizičku hemiju,
Beograd

Tehnološki fakultet Univerziteta
u Novom Sadu, Novi Sad

Hipol
Hipol a.d., Odžaci

Tehnološki fakultet Univerziteta
u Nišu, Leskovac

NU Institut za hemiju,
tehnologiju i metalurgiju
Univerziteta u Beogradu,
Beograd

Fakultet tehničkih nauka,
Kosovska Mitrovica

Beograd Srbija SHI

Chemical Industry
Химическая промышленность

Hemijska industrija

Časopis Saveza hemijskih inženjera Srbije
Journal of the Association of Chemical Engineers of Serbia
Журнал Союза химических инженеров Сербии

VOL. 70 **Beograd, jul–avgust 2016** **Broj 4**

Izdavač
Savez hemijskih inženjera Srbije
Beograd, Kneza Miloša 9/I

Glavni urednik
Bojana Obradović

Urednici
Katarina Jeremić, Ivana Banković-Ilić, Maja Obradović, Dušan Mijin, Mirjana Ristić, Z orica Knežević Jugović

Članovi uredništva
Nikolaj Ostrovski, Milorad Cakić, Željko Čupić, Katarina Jeremić, Miodrag Lazić, Slobodan Petrović, Milovan Purenović, Aleksandar Spasić, Dragoslav Stoiljković, Radmila Šećerov-Sokolović, Slobodan Šerbanović, Nikola Nikačević, Svetomir Milojević

Članovi uredništva iz inostranstva
Dragomir Bukur (SAD), Jiri Hanika (Češka Republika), Valerij Meshalkin (Rusija), Ljubiša Radović (SAD), Constantinos Vayenas (Grčka)

Likovno-grafičko rešenje naslovne strane
Ivana Drvenica

Redakcija
11000 Beograd, Kneza Miloša 9/I
Tel/fax: 011/3240-018
E-pošta: shi@ache.org.rs
www.ache.org.rs

Izlazi dvomesečno, rukopisi se ne vraćaju

Za izdavača
Tatijana Duduković

Sekretar redakcije
Slavica Desnica

Izdavanje časopisa pomaže
Republika Srbija, Ministarstvo prosvete, nauke i tehnološkog razvoja

Uplata pretplate i oglasnog prostora vrši se na tekući račun Saveza hemijskih inženjera Srbije, Beograd, broj 205-2172-71, Komercijalna banka a.d., Beograd

Kompjuterska priprema
Vladimir Panić

Štampa
Razvojno-istraživački centar grafičkog inženjerstva, Tehnološko-metalurški fakultet, Univerzitet u Beogradu, Karnegijeva 4, 11000 Beograd

Indeksiranje
Radovi koji se publikuju u časopisu *Hemijska Industrija* ideksiraju se preko *Thompson Reuters Scietific®* servisa *Science Citation Index - Expanded™* i *Journal Citation Report (JCR)*

SADRŽAJ/CONTENTS

SADRŽAJ nastavak
CONTENTS continued

Hazelnut oil production using pressing and supercritical CO_2 extraction

Stela Jokić[1], Tihomir Moslavac[1], Krunoslav Aladić[2], Mate Bilić[1], Đurđica Ačkar[1], Drago Šubarić[1]

[1]*Josip Juraj Strossmayer University of Osijek, Faculty of Food Technology Osijek, Osijek, Croatia*
[2]*Croatian Veterinary Institute, Branch – Veterinary Institute Vinkovci, Vinkovci, Croatia*

Abstract

In the hazelnut oil production it is very important to find an appropriate method to recover the oil from kernels. The objective of this study was to evaluate the oil extraction process from hazelnuts by screw pressing followed by extraction with supercritical CO_2. The effects of temperature head presses, frequency and nozzle size in pressing experiments on oil temperature and recovery were monitored. The optimal pressing condition using response surface methodology was determined. In obtained hazelnut oil the following quality parameters were determined: peroxide value 0 mmol O_2/kg, free fatty acids 0.23%, insoluble impurities 0.42%, moisture content 0.045%, iodine value 91.55 g I_2/100 g, saponification value 191.46 mg KOH/g and *p*-anisidine value 0.19. Rosemary extract was the most effective in protecting the oil from oxidative deterioration. The residual oil that remained in the cake after pressing was extracted totally with supercritical CO_2 and such defatted cake, free of toxic solvents, can be used further in other processes.

Keywords: hazelnut oil, quality, screw pressing, supercritical CO_2 extraction, response surface methodology.

Available online at the Journal website: http://www.ache.org.rs/HI/

SCIENTIFIC PAPER

UDC 634.54:665:66.06

Hem. Ind. **70** (4) 359–366 (2016)

doi: 10.2298/HEMIND150428043J

Hazelnuts (*Corylus sp.* L.) are an important commercial crop in many countries including Croatia. Hazelnut has a high nutritional value, containing, generally, 65% oil, 14% protein, and 16% carbohydrates. More than 90% of its oil consists of unsaturated fatty acids, especially oleic (80%) and linoleic (6–12%) acids. Several authors have studied the physicochemical characteristics and nutritional values of different hazelnut oils [1–5] and they concluded that hazelnut oil is appreciated as valuable edible oil for health food. It is a good source of vitamin E (*α*-tocopherol) and may be used as food value improving the shelf-life of the product by its antioxidant function. At the same time it belongs to the non-drying oils with an excellent stability and is used in the cosmetic industry as well as in the production of oleic acid. These unsaturated fatty acids, as well as sterols and tocopherols also present in the oil, play a preventive role in many diseases, especially cardiovascular ones, as they contribute to lower the low density of lipoprotein cholesterol. Currently, hazelnut oil is used mainly in salad dressings and cosmetic and pharmaceutical products.

Two main types of processes for obtaining oil are physical and chemical [6]. The physical process involves the use of mechanical power to remove oil from material, such as hydraulic pressing and screw pressing. Extraction is a process based on chemical characteristics of solute and solvent. Conventional solvent extraction produces low-quality oil that requires extensive purification operations while screw pressing does not require the use of organic solvent and is able to retain bioactive compounds such as essential fatty acids, phenolics, flavonoids and tocopherols in the oils [7], as well as the possibility of using cake free of toxic solvents in other processes. Unfortunately, the main disadvantage of this process is low oil extraction yield. But nowadays, technologies such as supercritical fluid extraction (SFE) are more often applied in the extraction of fatty oils [8]. All these mentioned extraction processes can be combined in commercial operations i.e. continuous mechanical pressing followed by supercritical CO_2 extraction by which is an environmentally-friendly solvent [9]. Eggers *et al*. [10] studied process of fatty oil SFE from rapeseed and soybean and explained that the oil containing cell wall had to be disrupted in order to enable successful extraction. They showed that the mechanical pre-deoiling remained the superior pretreatment in the supercritical extraction of oilseeds. Extracts obtained using CO_2 as the extraction solvent are solvent-free / without any trace of toxic extraction solvents, and are thereby highly valued [6,8]. Use of SFE as a replacement of organic solvents in fatty oil extraction was considered in early 1980's [10–13]. At present moment, SFE on a commercial scale are limited to decaffeination, production of soluble hops extracts, sesame seed oil production, extraction of certain petroleum products, high-value compounds from spices, herbs, and other vegetable material, animal tissue, and microalgae [14,15]. Despite industrial application for almost four decades, there is reluctance in some world

Correspondence: S. Jokić, Josip Juraj Strossmayer University of Osijek, Faculty of Food Technology Osijek, Franje Kuhača 20, 31000 Osijek, Croatia.
E-mail: stela.jokic@ptfos.hr
Paper received: 28 April, 2015
Paper accepted: 15 July, 2015

regions to adopt SFE because of the wrong perception that it is not fully competitive [14].

In the production of hazelnut oil, the amount and quality of extracted oil are crucial for determining feasibility of commercial production. So, the objective of this work was to investigate the effects of process parameters during the screw pressing of hazelnuts using response surface methodology (RSM) and to check the possibility to complete recovery of the residual oil from pressed cake using green solvent-supercritical CO_2.

MATERIAL AND METHODS

Materials

Hazelnuts without shell were kindly provided from company PP Orahovica d.d. (Orahovica, Croatia) in 2014. Rosemary extract Oxy.Less CS, green tea extract, and pomegranate extract were supplied from Naturex (France). Olive leaf extract was supplied from Exxentia (Spain). Essential oils of oregano (*Origanum vulgare*), sage (*Salvia officinalis*) and winter savory (*Satureja Montana*) were produced by steam distillation according to the standard Ph. Jug. IV procedure [16].

The purity of CO_2 used for extraction was 99.97 mass% (Messer, Osijek, Croatia). *n*-hexane was provided from Merck KGaA (Darmstadt, Germany). All other chemicals and reagents were of analytical reagent grade.

Determination of initial oil and water content

The initial oil content in hazelnuts as well as the cake residual oil was measured by traditional laboratory Soxhlet-extraction with *n*-hexane as solvent [17]. The measurement was done in triplicate. Moisture content of hazelnuts was determined according to AOAC Official Method 925.40 [18].

Screw press extraction

The pressing of the hazelnuts was performed in a screw expeller (Model SPU 20, Senta, Serbia). The hazelnut oil was obtained by pressing 500 g of cleaned hazelnuts per each experiment using different process conditions. The minimum and maximum nozzle size used was 8 and 12 mm, respectively. The frequency had a minimum of 20 Hz and a maximum of 40 Hz. The temperature of head presses was between 70 and 100 °C. After pressing, the volume of screw pressed oils and their temperature were measured and after that the oil was centrifuged. The sedimented solids were recovered and solid percentage of the oils was calculated by weight difference.

Oil quality parameters

Free fatty acids, iodine value and saponification value were determined according to AOAC official methods 940.28, 920.185 and 920.160 [19]. Peroxide value (*PV*) of oil samples was determined according to ISO 3960 [20] and is expressed as mmol O_2/kg of oil. Insoluble impurities were determined according to ISO 663 [21]. *p*-Anisidine value (AV) was determined according to ISO 6885 [22]. Totox value was calculated as 2PV+AV [23]. All these determinations were carried out in triplicate.

Determination of oxidative stability

The oxidative stability was determined by rapid oil oxidation test – Schaal or Oven Test (63 °C) [24]. The influence of the addition of natural antioxidants, namely rosemary extract, green tea extract, olive leaf extract, and pomegranate extract in concentrations of 0.1 and 0.3%, and essential oils of oregano, sage and winter savory in the concentration of 0.05%, on the oxidative stability of hazelnut oil were monitored. The result of oil oxidation was expressed as peroxide value during 4 days of the test. All determinations were carried out in duplicate.

Experimental design

Box-Behnken design which includes three variables and three factorial levels was chosen in this study [25]. The ranges for the variables, namely temperature head presses (70, 85 and 100 °C), frequency (20, 30 and 40 Hz) and nozzle size (8, 10 and 12 mm) were selected to approximate the optimal conditions for screw pressing of hazelnut oil. Coded and uncoded levels of the independent variables and the experimental design are given in Table 1. Coded value 0 stands for center point of the variables and repeated for experimental error. Factorial points are coded as ±1.

Table 1. The uncoded and coded levels of independent variables used in the RSM design in pressing experiments

Independent variable	Symbol	Level		
		Low (–1)	Middle (0)	High (+1)
Nozzle, mm	X_1	8	10	12
Temperature, °C	X_2	70	85	100
Frequency, Hz	X_3	20	30	40

Second-order polynomial equation was used to express the investigated responses (*Y*) after pressing, namely the volume of screw press oil (mL), oil temperature (°C) and residual oil in pressed cake (%) as a function of the coded independent variables, where X_1, X_2,..., X_k are the independent variables affecting the responses *Y*'s; β_0, β_j (i = 1, 2,..., k), β_{ii} (i = 1, 2,..., k) and β_{ij} (i = 1, 2,..., k; j = 1, 2,.. , k) are regression coefficients for intercept, linear, quadratic, and interaction terms, respectively; k is the number of variables.

$$Y = \beta_0 + \sum_{i=1}^{k} \beta_i X_i + \sum_{i=1}^{k} \beta_{ii} X_i^2 + \sum_{\substack{i=1 \\ i<j}}^{k-1} \sum_{j=2}^{k} \beta_{ij} X_i X_j \quad (1)$$

Statistical analysis was performed using RSM software Design-Expert®, v. 7 (Stat Ease, Minneapolis, MN, USA). The results were statistically tested by the analysis of variance (ANOVA) at the significance level of p = = 0.05. The adequacy of the model was evaluated by the coefficient of determination (R^2) and model p-value. Mathematical models were established to describe the influence of single process parameter and/or interaction of multiple parameters on each investigated response. Response surface plots were generated with the same software and drawn by using the function of two factors, and keeping the other constant.

Supercritical CO_2 extraction

The experiment was performed in supercritical fluid extraction system described in detail elsewhere [9,26]. The pressed cake of 100 g was placed into an extractor vessel to recover the residual cake oil using supercritical CO_2. The extracts were collected in previously weighed glass tubes. The amount of extract obtained at regular intervals of time was established by weight using a balance with a precision of ±0.0001 g. Extraction was performed at the following conditions: pressure of 30 MPa, temperature of 40 °C and a CO_2 mass flow rate of 1.73 kg/h. Separator conditions were 1.5 MPa and 25 °C.

RESULTS AND DISCUSSION

Screw pressing experiments

The cold pressing method was used to extract oil from hazelnuts. Before pressing experiments, the initial oil and moisture content of hazelnuts were determined. The average of the initial oil content was 65.17±0.38% and moisture content was 4.08±0.09%. The oil content was consistent with reported values [27–29]. The experimental design of 17 pressing experiments was carried out using the described factors and levels (Table 2). Effects of temperature head presses, nozzle size and frequency on recovery and quality parameters of hazelnut oil were studied by RSM. In all 17 experimental runs only a small percentage of moisture was found in the obtained oils (average value 0.045%) and the peroxide value of all experimental runs was 0 mmol O_2/kg. The oil temperature in all experimental runs was in the range from 30 to 54 °C.

Model for prediction the investigated responses and his coefficients are obtained by using linear regression statistical method of the experimental data, and the obtained model provides a functional dependence between the independent and dependent variables. Table 3 shows the regression coefficients obtained by fitting experimental data to the second order response models for investigated responses. The coefficients are related to coded variables. The first-order term of temperature (X_2) had significant effect ($p < 0.05$) on the oil temperature on the amount of cake residual oil. The first-order term of frequency (X_3) had significant effects on oil temperature. The second-order term of nozzle size (X_1^2) had significant effect ($p < 0.05$) on cake residual oil, while second-order term of frequency (X_3^2) had significant effect on oil content and temperature. The interactions between the pressing temperature and frequency (X_2X_3) had significant effect on the oil content. Other interactions had no significant ($p > 0.05$) effect on investigated responses.

Table 2. Experimental matrix and values of the observed response

Run	Nozzle mm	Temperature °C	Frequency Hz	Oil volume mL	Oil yield g/500 g	Oil temperature °C	Cake oil %	Recovery % of total oil
1	12	85	40	240	230.40	53	15.92	72.82
2	8	100	30	270	259.20	52	15.43	81.92
3	10	70	20	195	187.20	41	9.79	59.17
4	12	70	30	255	244.80	42	13.53	77.37
5	10	85	30	295	283.20	41	12.83	89.51
6	8	70	30	245	235.20	38	12.32	74.34
7	10	85	30	285	273.60	45	12.08	86.47
8	12	100	30	270	259.20	52	15.94	81.92
9	10	85	30	260	249.60	43	15.05	78.89
10	10	85	30	275	264.00	46	13.23	83.44
11	10	85	30	280	268.80	45	14.33	84.96
12	12	85	20	225	216.00	45	15.08	68.27
13	10	70	40	270	259.20	46	13.18	81.92
14	8	85	40	265	254.40	54	14.06	80.40
15	10	100	40	220	211.20	50	13.2	66.75
16	8	85	20	265	254.40	47	14.32	80.40
17	10	100	20	245	235.20	50	15.53	74.34

*Table 3. Estimated coefficient of the second order polynomial equation; X_1: nozzle size; X_2: temperature; X_3: frequency; *: significant at $p \leq 0.05$*

Term	Coefficient[a]	Oil volume	Oil temperature	Cake oil
Intercept	β_0	279.00*	44.00*	13.50*
X_1	β_1	-6.88	0.13	0.54
X_2	β_2	5.00	4.63*	1.41*
X_3	β_3	8.13	2.50*	0.21
X_1^2	β_{11}	-1.38	2.50	1.36*
X_2^2	β_{22}	-17.62	-0.50	-0.56
X_3^2	β_{33}	-28.88*	3.25*	-0.020
X_1X_2	β_{12}	-2.50	-1.00	-0.18
X_1X_3	β_{13}	3.75	0.25	0.28
X_2X_3	β_{23}	-25.00*	-1.25	-1.43*

[a] $y=\beta_0+\beta_1x_1+\beta_2x_2+\beta_3x_3+\beta_{11}x_1^2++\beta_{22}x_2^2+\beta_{33}x_3^2+\beta_{12}x_1x_2+$ $+\beta_{13}x_1x_3+\beta_{23}x_2x_3$

The ANOVA results for modeled responses are reported in Table 4. Joglekar and May [30] suggested that for a good fit of a model, R^2 should be at least 0.80. In our study, the R^2 values for these response variables were higher than 0.80, indicating the adequacy of the applied regression models. Table 4 shows the test statistics for the model (*F*-test and probability) of oil recovery and oil quality. The probability (*p*-value) of all regression models was below 0.05, which means that there was a statistically significant multiple regression relationship between the independent variables and the response variable.

The best way of expressing the effect of screw pressing parameters on oil recovery and oil temperature within the investigated experimental range was to generate response surfaces of the model (Fig. 1). From Fig. 1 can be seen that the amount of obtained oil significantly increased with the increase of pressing temperature, and maximum oil yield is obtained using electromotor frequency of 30 Hz. In our earlier paper [9] where the walnut oil extraction using screw pressing were investigated, oil temperature was also significantly influenced by used temperature for heating the output press head.

Furthermore, increasing the nozzle size ID the volume of oil decreases. The amount of residual oil in cake increased also with the nozzle size from 10 to 12 mm and decreased with increase of temperature. It can be seen that the oil temperature is significantly influenced by used temperature for heating the output press head and by used frequency, while nozzle size did not have significant influence on oil temperature. The ANOVA showed that the models were acceptable and could be used for optimization the pressing parameters with respect to oil recovery and temperature.

Optimization of screw pressing of hazelnut oil

The final goal of RSM is the process optimization. Thus, the developed models can be used for simulation and optimization. Optimization is an essential tool in food engineering for the efficient operation of different processes to yield a highly acceptable product [31]. During optimization of screw pressing process, several response variables describe the oil quality characteris-

Table 4. Analysis of variance (ANOVA) of the modelled responses; the recovery

Source	Sum of squares	Degree of freedom	Mean square	*F*-value	*p*-value
		Oil volume			
Model	8811.99	9	979.11	3.97	0.0413
Residual	1726.25	7	246.61		
Lack of fit	1056.25	3	352.08	2.10	0.2427
Pure error	670.00	4	167.50		
Total	10538.24	16			
		Oil temperature			
Model	306.49	9	34.05	4.79	0.0254
Residual	49.75	7	7.11		
Lack of fit	33.75	3	11.25	2.81	0.1717
Pure error	16.00	4	4.00		
Total	356.24	16			
		Cake oil			
Model	36.00	9	4.00	4.86	0.0246
Residual	5.77	7	0.82		
Lack of fit	0.14	3	0.046	0.033	0.9910
Pure error	5.63	4	1.41		
Total	41.77	16			

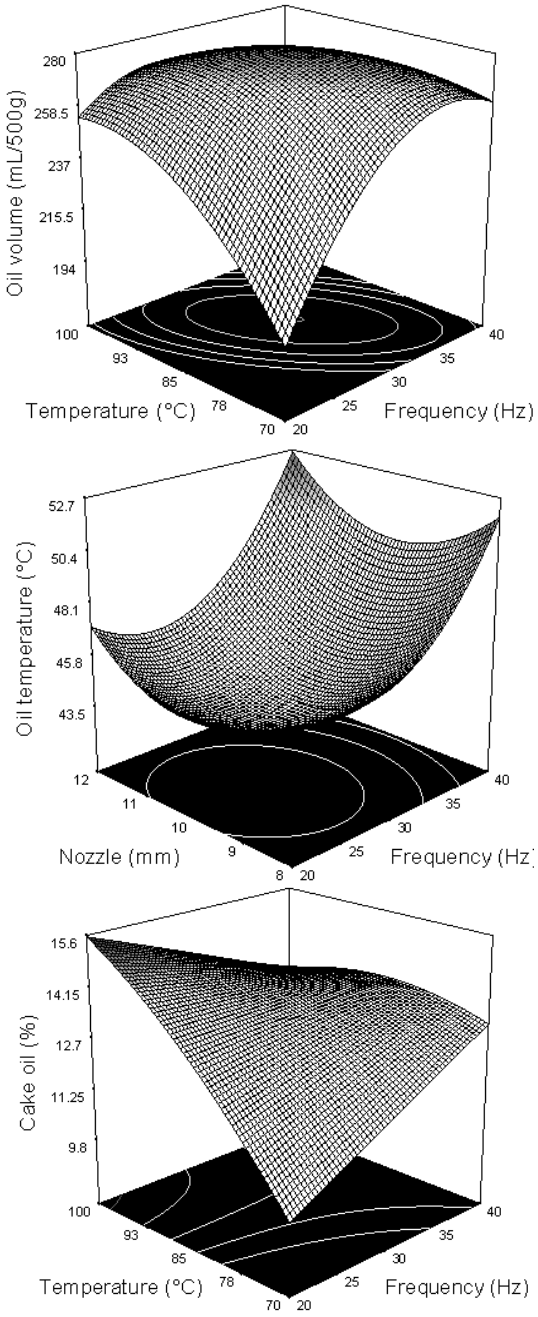

Figure 1. Response surface plots showing the effects of investigated variables on oil temperature and recovery.

tics and had influence on oil recovery [9]. Some of these variables need to be maximized, while others need to be minimized. In this study the following optimization conditions were proposed for calculations: the maximum oil yield and the minimum oil temperature. The goal of this research was to find the best settings for the screw pressing, *i.e.*, the best temperature, frequency and nozzle size. By applying desirability function method [32], the optimum screw pressing conditions were obtained: temperature of 70 °C, frequency of 30 Hz and using nozzle of ID 9 mm. Screw press oil volume was calculated to be 256.8 ml, oil temperature 41.7 °C and cake residual oil 11.4%, which is in very close agreement with experimental obtained data.

Oil quality

In obtained hazelnut oil at calculated optimal screw pressing conditions given in the text above, the oil quality parameters were determined. From Table 5 it can be seen that the produced hazelnut oil had excellent quality. Peroxide is one of the oil quality indicators and its value in obtained hazelnut oil was 0 mmol O_2/kg. Primary oxidation processes in oil mainly form hydroperoxides, which are measured by the peroxide value. In general, the lower the peroxide value the better is the oil quality [33]. This obtained peroxide value indicates that the investigated oil had good quality according to excellent quality of used raw material-hazelnuts, which is very important because such obtained oil is not necessary to pass further refining.

Table 5. Physicochemical properties of hazelnut oil

Property	Value
Iodine value, g I_2/100 g of oil	91.55
Saponification value, mg KOH/g of oil	191.46
Peroxide value, mmol O_2/kg of oil	0
Free fatty acids, %	0.23
Insoluble impurities, %	0.42
Moisture content, %	0.045
p-Anisidine value	0.19
Totox value	0.19

Moisture content (mentioned earlier) in the oil was 0.045%, free fatty acids 0.23% and insoluble impurities 0.42% which are also the another parameters of oil quality. Water contributes to the hydrolysis of oil during processing, which generates free fatty acids and glycerol products. It is very important that cold pressed oils are low in moisture content and free fatty acids to maintain the quality and shelf life of the oils [7].

Furthermore, other physicochemical properties of hazelnut oil were also determined. Iodine value was expressed as the grams of iodine absorbed per 100 g of lipid and was determined to be 91.55 g I_2/100 g. Saponification value, which is the number of milligrams of KOH required to neutralize the fatty acids resulting from complete hydrolysis of one gram of oil was determined to be 191.46 mg KOH/g. Good quality oil should have *p*-anisidine value of less than two, and Totox oxidation value, so called Totox value less than four [33]. The hazelnut oil in this study had *p*-anisidine value 0.19. The calculated Totox value was 0.19.

Oxidative stability of hazelnut oil

Oxidative stability of cold pressed hazelnut oil with and without the addition of natural antioxidants is

shown in Table 6. The stability of oil is determined by the accelerated oxidation test, the Schaal oven test (63 °C). Hazelnut oil without added antioxidants (control sample) after four days of the test had a peroxide value 10.35 mmol O_2/kg. The addition of the OxyLess CS rosemary extract in concentrations of 0.1 % and 0.3% achieved the best stability of oil to oxidative deterioration (peroxide value was 0.98 and 0.74 mmol O_2/kg after four days) in relation to the use of other investigated natural antioxidants. Green tea extract leads to an increase in the stability of the hazelnut oil, in relation to hazelnut oil with addition of the pomegranate extract and olive leaf extract. Winter savory essential oil (0.05%) effectively protected this oil against oxidative deterioration compared to essential oil of oregano. However, the addition of sage essential oil did not affect the stability of hazelnut oil to oxidative deterioration; on the contrary, peroxide value was higher than the control sample after 4 days of the test.

Extraction of residual oil from pressed cake with CO_2

The cake resulting from pressing at optimal conditions (temperature of 70 °C, frequency of 30 Hz and nozzle ID 9 mm) was extracted with supercritical CO_2 and the obtained kinetic curve for this experiment is shown in Fig. 2. The amount of residual oil in pressed cake at optimal conditions was 11.81% (obtained by Soxhlet extraction). From Fig. 2 it can be seen that after 4 h of extraction the residual oil in the press cake was totally extracted by supercritical CO_2. From the shape of the extraction curve can be seen that the extraction process is divided in three periods: rapid extraction period, transition period and slow extraction period [34]. The first period is the constant extraction rate period, where the external surface of the particles is covered with solute and the convection is the dominant mass transfer mechanism. The amount of oil is ultimately limited by the solubility of the oil in the supercritical CO_2. The second is the falling extraction rate period where failures in the external surface oil layer appear and the diffusion mechanism starts combined with convection. In the third period the mass transfer occurs mainly by the diffusion. The similar shape of extraction curves was also obtained by other authors [28,29] who investigated supercritical CO_2 extraction of hazelnut oil.

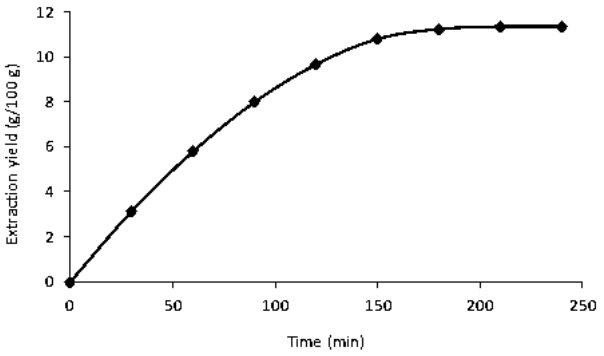

Figure 2. Extraction of cake residual oil with supercritical CO_2.

Table 6. Influence of natural antioxidants on oxidative stability of hazelnut oil

Sample	Concentration of antioxidants, %	Peroxide value, mmol O_2/kg				
		0 day	1 day	2 day	3 day	4 day
Hazelnut oil	–	0	1.97	4.44	8.46	10.35
Rosemary extract (Oxy Less CS)	0.1		0.24	0.50	0.75	0.98
	0.3		0.25	0.37	0.50	0.74
Green tea extract	0.1		1.00	1.47	1.96	2.45
	0.3		0.48	0.99	1.48	2.00
Pomegranate extract	0.1		1.46	2.91	5.88	8.50
	0.3		1.21	2.88	5.39	6.86
Olive leaf extract	0.1		1.46	4.25	7.28	9.90
	0.3		1.48	3.43	6.80	9.41
Oregano essential oil	0.05		1.98	4.41	7.84	10.00
Sage essential oil	0.05		2.02	4.41	8.01	11.38
Winter savory essential oil	0.05		0.75	2.48	6.93	8.42

CONCLUSION

The results of this study showed that the screw pressing conditions influenced the hazelnut oil extraction. Obtained hazelnut oil showed excellent quality as it had very small percentages of moisture, insoluble impurities and free fatty acids, as well as its peroxide value is 0 mmol O_2/kg. The optimal condition to obtain the best oil recovery and quality using response surface methodology was at temperature of head presses 70 °C, frequency of 30 Hz and using nozzle of ID 9 mm. The influence of different natural antioxidants on the oxid-

ative stability of hazelnut oil was investigated, and the rosemary extract was the most efficient in protecting the hazelnut oil against oxidative deterioration. Residual oil content in pressed cake was totally extracted with supercritical CO_2. Such defatted cake, free of toxic solvents, can be used further in other processes, for example, in development of new functional and enriched products based on extrusion process which is our area of interest in future research.

Acknowledgements

This work has been fully supported by Croatian Science Foundation under the project 1321.

REFERENCES

[1] J.C. Bada, M. León-Camacho, M. Prieto, L. Alonso, Characterization of oils of hazelnuts from Asturias, Spain, Eur. J. Lipid Sci. Technol. **106** (2004) 294–300.

[2] C. Bertoli, L.B. Fay, M. Stancanelli, D. Gumy, P. Lambelet, Characterization of chilean hazelnut (*Gevuina avellana* mol) seed oil, J. Am. Oil Chem. Soc. **75** (1998) 1037––1040.

[3] G.P. Savage, D.L. McNeil, P.C. Dutta, Lipid composition and oxidative stability of oils in hazelnuts (*Corylus avellana* L.) grown in New Zealand, J. Am. Oil Chem. Soc. **74** (1997) 755–759.

[4] J. Parcerisa, R. Codony, J. Boatella, M. Rafecas, Triacylglycerol and phospholipid composition of hazelnut (*Corylus avellana* L.) lipid fraction during fruit development, J. Agric. Food Chem. **47** (1999) 1410–1415.

[5] J. Parcerisa, M. Rafecas, A. Castellote, R. Codony, A. Farrán, J. García, A. López, A. Romero, J. Boatella, Influence of variety and geographical origin on the lipid fraction of hazelnuts (*Corylus avellana* L.) Food Chem. **50** (1994) 245–249.

[6] S. Jokić, S. Vidović, K. Aladić, in: J. Osborne (Ed.), Supercritical Fluids: Fundamentals, Properties and Applications: Supercritical Fluid Extraction of Edible Oils, Nova Science Publishers, Inc., New York, 2014, pp. 205–228.

[7] S.S. Teh, J. Birch, Physicochemical and quality characteristics of cold-pressed hemp, flax and canola seed oils, J. Food Compos. Anal. **30** (2013) 26–31.

[8] M. Cvjetko Bubalo, S. Vidović, I. Radojčić Redovniković, S. Jokić, Green solvents for green technologies, J. Chem. Technol. Biot. (2015), DOI: 10.1002/jctb.4668

[9] S. Jokić, T. Moslavac, A. Bošnjak, K. Aladić, M. Rajić, M. Bilić, Optimization of walnut oil production, Croat. J. Food Sci. Technol. **6** (2014) 27–35.

[10] R. Eggers, U. Sievers, W. Stein, High Pressure Extraction of Oil Seed, J. Am. Oil Chem. Soc. **62** (1985) 1222–1230.

[11] J.P. Friedrich, G.R. List, Characterization of soybean oil extracted by supercritical carbon dioxide and hexane, J. Agr. Food Chem. **30** (1982) 192–193.

[12] J.P. Friedrich, E.H. Pryde, Supercritical CO_2 extraction of lipid-bearing materials and characterization of the products, J. Am. Oil Chem. Soc. **61** (1984) 223–228.

[13] J. Chrastil, Solubility of solids and liquids in supercritical gases, J. Phys. Chem. **86** (1982) 3016–3021.

[14] J.M. del Valle, Extraction of natural compounds using supercritical CO_2: Going from the laboratory to the industrial application, J. Supercrit. Fluid. (2015), doi: 10.1016/j.supflu.2014.10.001

[15] T. Gamse, Industrial applications and current trends in supercritical fluid technologies, Hem. Ind. **59** (2005) 207–212.

[16] Pharmacopoea Jugoslavica, Editio Quarta (Ph. Jug. IV), Vol. 1, Federal Institute of Public-Health, Belgrade, 1984.

[17] T. Moslavac, S. Jokić, D. Šubarić, K. Aladić, J. Vukoja, N. Prce, Pressing and supercritical CO_2 extraction of *Camelina sativa* oil, Ind. Crop. Prod. **54** (2014) 122–129.

[18] AOAC, Official Methods of Analysis, seventeenth ed. Association of Official Analytical Chemists, Washington DC, 2000.

[19] AOAC, Official Methods of Analysis, sixteenth ed. AOAC International, Gaithersburg, 1999.

[20] ISO 3960, Animal and vegetable fats and oils – Determination of peroxide value, 1998.

[21] ISO 663, Animal and vegetable fats and oils – Determination of insoluble impurities content, 1992.

[22] ISO 6885, Animal and vegetable fats and oils – Determination of anisidine value, 2006.

[23] R.S. Hamilton, J.B. Rossell, Analysis of oils and fats, Elsevier Applied Science, London, 1986.

[24] N.T. Joyner, J.E. McIntyre, The oven test as an index of keeping quality, Oil Soap. **15** (1938) 184–186.

[25] D. Baş, I.H. Boyacı, Modeling and optimization I: Usability of response surface methodology, J. Food Eng. **78** (2007) 836–845.

[26] S. Jokić, G. Horvat, K. Aladić, in: J. Lindy (Ed.), Supercritical Fluid Extraction: Technology, Applications and Limitations: Design of SFE system using a holistic approach - problems and challenges, Nova Science Publishers, Inc., New York, 2014, pp. 95–123.

[27] M.G. Bernardo-Gil, J. Grenha, J. Santos, P. Cardoso, Supercritical fluid extraction and characterisation of oil from hazelnut, Eur. J. Lipid Sci. Technol. **104** (2002) 402–409.

[28] M.G. Bernardo-Gil, M. Casquilho, Modeling the supercritical fluid extraction of hazelnut and walnut oils. AIChE J. **53** (2007) 2980–2985.

[29] S.G. Özkal, U. Salgın, M.E. Yener, Supercritical carbon dioxide extraction of hazelnut oil, J. Food Eng. **69** (2005) 217–223.

[30] A.M. Joglekar, A.T. May, Product excellence through design of experiments, Cereal Food. World **32** (1987) 857–868.

[31] Z. Šumić, A. Tepić, S. Jokić, R. Malbaša, Optimization of frozen wild blueberry vacuum drying process, Hem. Ind. **69** (2015) 77–84.

[32] C. Cojocaru, M. Khayet, G. Zakrzewska-Trznadel, A. Jaworska, Modeling and multi-response optimization of pervaporation of organic aqueous solutions using desirability function approach, J. Hazard. Mater. **167** (2009) 52–63.

[33] E.N. Frankel, Lipid Oxidation, 2nd ed., The Oily Press, Bridgwater, 2005.

[34] H. Sovová, Rate of the vegetable oil extraction with supercritical CO_2 – I modelling of extraction curves, Chem. Eng. Sci. **49** (1994) 409–414.

IZVOD

PROIZVODNJA LEŠNJAKOVOG ULJA PRIMJENOM METODE PREŠANJA I EKSTRAKCIJE POMOĆU SUPERKRITIČNOG CO_2

Stela Jokić[1], Tihomir Moslavac[1], Krunoslav Aladić[2], Mate Bilić[1], Đurđica Ačkar[1], Drago Šubarić[1]

[1]*Josip Juraj Strossmayer University of Osijek, Faculty of Food Technology Osijek, Osijek, Croatia*
[2]*Croatian Veterinary Institute, Branch – Veterinary Institute Vinkovci, Vinkovci, Croatia*

(Naučni rad)

U proizvodnji lješnjakovog ulja vrlo je važno pronaći odgovarajući postupak za što veće iskorištenje ulja iz jezgre lješnjaka. Cilj ovog istraživanja bio je ispitati utjecaj različitih procesa ekstrakcije ulja iz lješnjaka procesom hladnog prešanja, nakon čega je provedena ekstrakcija zaostalog ulja unutar pogače pomoću superkritičnog CO_2. U eksperimentima prešanja korištena je metoda odzivnih površina (RSM) pomoću koje je ispitan utjecaj temperature zagrijavanja glave preše, frekvencije elektromotora i veličine otvora pužne preše na temperaturu i iskorištenje ulja. U dobivenom lješnjakovom ulju određeni su parametri kvalitete ulja: peroksidni broj 0 mmol O_2/kg, slobodne masne kiseline 0.23%, netopljive nečistoće, 0.42%, vlaga u ulju 0.045%, jodni broj 91.55 g I_2/100 g, saponifikacijski broj 191.46 mg KOH/g i anisidinski broj 0.19. Najbolje antioksidacijsko djelovanje kod ispitivanog ulja pokazala je primjena ekstrakta ružmarina. Količina zaostalog ulja u pogači nakon hladnog prešanja potpuno je ekstrahirana pomoću superkritičnog CO_2, te tako odmašćena pogača može se dalje koristiti u drugim procesima.

Ključne reči: Lješnjakovo ulje • Kvaliteta • Hladno prešanje • Superkritična ekstrakcija • Metoda odzivnih površina

Liquid–liquid separation using steady-state bed coalescer

Radmila M. Šećerov Sokolović[1], Dunja S. Sokolović[2], Dragan D. Govedarica[1]

[1]*Faculty of Technology, University of Novi Sad, Novi Sad, Serbia*
[2]*Faculty of Technical Sciences, University of Novi Sad, Novi Sad, Serbia*

Abstract

This paper presents a literature review on the current understanding of liquid-liquid separation that is immensely widespread in practice, highlighting the steady-state bed coalescer being a good solution in various engineering application. Generally, the fibre bed coalescence has proven to be very effective separation method in the industry. Due to the complexity of bed coalescence phenomenon coalescer design and sizing procedure relies on experimental test. This review provides a research overview of the key phenomena essential for the efficient bed coalescence, such as mechanisms of droplet coalescence and emulsion flow through the fibre bed. In addition to this provides an overview of the current knowledge about coalescer´s design properties and variables such as: fluid velocity, fluid flow orientation/flow mode, fibre bed geometry, and bed length.

Keywords: liquid–liquid separation, droplet coalescence, fibre bed, bed coalescers.

Available online at the Journal website: http://www.ache.org.rs/HI/

REVIEW PAPER

UDC 66:66.066.3

Hem. Ind. **70** (4) 367–381 (2016)

doi: 10.2298/HEMIND150309041S

During the crude oil production on oil fields, two types of separation must be carried out. Since the crude oil always contains a certain amount of water, the first step is to remove this water. Two fractions are formed after this separation: crude oil with a residual dispersed water and water with a residual amount of dispersed crude oil (formation water). Further preparation of crude oil for transport consists of additional dehydration, whereas the optimal care of formation water implies its injection into abandoned wells [1–5]. In order to prevent clogging of the pore space, prior to the injection the suspended particles and the remaining content of crude oil must be removed from the water. For all of these separations regarding the liquid––liquid systems, bed coalescers have been commonly used.

Oily water is extremely widespread in the industry. Water is often the main cooling fluid. Maintenance of vehicles and heavy machinery also cause the formation of significant quantities of oily wastewater. Oily wastewater can also be formed in specific operations that use oil or other organic solvents such as quenching, extraction and other similar operations [1–5].

In addition, the application of bed coalescence significantly improves the productivity of the process furnaces during the steam reforming process. In this way, the control and reduction of the emission of waste gases is achieved. In order to eliminate the water droplets from the output material flow of gas oil, modern facilities for hydrodesulphurization of gas oil incurporate coalescers. Since the petroleum products are often highly acidic in the oil and gas industry, their neutralization with base solvents is needed. The base treatment is applied in the following processes: during the mercaptans oxidation process, removal of hydrogen sulfide, the production of LPG (liquefied petroleum gas), kerosene, FCC (fluid catalytic cracking) gasoline, olefins, alkylates and etc. The residual base solvent affects the petroleum product turbidity and increases the sodium concentration. The bed coalescers are used to remove the excess base solvent from the petroleum products [3,5].

MECHANISMS OF COALESCENCE

Introduction

Coalescence is defined as droplets drowning either in its formed continuous phase or as merging two droplets into a larger one. Three main types of coalescence can be distinguished: droplet coalescence at the liquid-liquid interface, coalescence of the adjacent droplets and droplet coalescence in the porous bed.

The beginning of the investigation of coalescence phenomenon is based on the analogy with the DLVO theory. In 1941 Derjaguin and Landau presented a theory of stability of colloidal particles as a function of the attractive and repulsive forces [6]. Seven years later, independently of the previous theory, Varwey and Overbeek proposed the same theory of stability [7]. The DLVO theory takes into account only the attractive van der Waals forces and the repulsive force of the electrical double layer. The authors concluded that the colloidal particles stability depends on the total potential energy, which has three components. One component represents the energy contribution of

Correspondence: R. Šećerov Sokolović, Faculty of Technology, University of Novi Sad, Bulevar cara Lazara 1, 21000 Novi Sad, Serbia.
E-mail: radost@uns.ac.rs
Paper received: 9 March, 2015
Paper accepted: 14 July, 2015

attractive forces; the second component is the energy contribution of repulsion forces, whereas the third is potential energy of a solvent. The potential energy of the solvent can be neglected due to the low intensity and a short action radius of a few nanometers. The most important attractive forces between particles are the London-van der Waals forces. The energy contribution of the repulsive forces comes from the presence of the electrical double layer. With the increase of ion concentration the thickness of the electrical double layer decreases and thus the system becomes unstable. Another group of repulsive forces that occur between particles are the Borne forces. These forces are the result of interactions between electrons in the electron shells that occur at shorter distances being the main difference from the electrical double layer force [6,7].

Elimelech *et al.* pointed out that all the forces acting between the particles are of electromagnetic nature [8,9]. However, there are also other forces that influence the particles/droplets interactions and are responsible for their capture, coalescence, aggregation, detachment, and redispersion. These forces are called external forces and include: the force caused by the Brownian motion, hydrodynamic forces, friction forces etc. [10–15].

Coalescence at the liquid-liquid interface

The coalescence of droplets at the liquid–liquid interface consists of the following: the droplet transport from bulk liquid to the interface, the continuous phase film formation between the droplets and its established phase, the rupture, film breakage, drainage and coalescence of droplets into the surface of continuous phase. The developed mathematical models for the droplet coalescence at the liquid–liquid interface allow monitoring the kinetics of the film drainage trapped between the droplets and the liquid–liquid interface. The time to reach the film thickness for its rupture is given in some mathematical relations [16–23].

Coalescence at the liquid–liquid interface can be performed with or without deformation [3,5,16–24]. The coalescence without deformation is shown in Figure 1a where a rigid droplet and the rigid interface exist. This form of coalescence is generally efficient, as it provides effective rupture and drainage of the film. Droplet and phase interface interact in only one point at which the film has the minimum thickness. In that way the film breaks up more efficient.

Deformation of the droplet can be single or double. The deformation can appear only on the liquid interface but the droplet remains rigid, Figure 1b, or droplet deformation could occur leaving the liquid-liquid interface unchanged, Figure 1c. Also the droplet may be further deformed due to its own weight, Figure 1d. The double deformation includes both the liquid interface deformation, as well as droplet contact surface deformation. The proper deformation of both surfaces forms a radial shaped film, Figure 1e, or a corrugated surface of droplets, Figure 1f.

The mentioned deformations are present and possible, either in the dispersed oil in water, or dispersed water in oil.

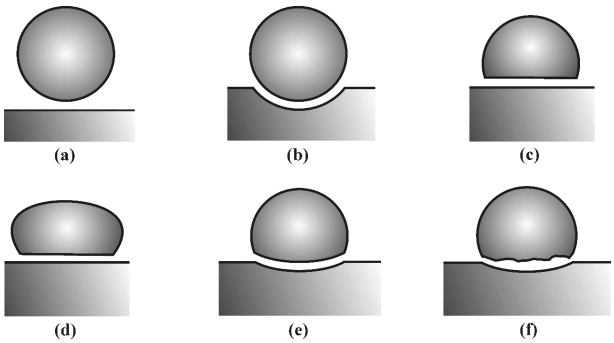

Figure 1. The coalescence models in the phase interface: a) without deformation, b) rigid sphere, c) rigid interface, d) droplet deformation due to own weight, e) proper deformation of both surfaces forms film with shape of bow, f) deformation of corrugated surface of the droplets.

Coalescence of the adjacent droplets

Coalescence of the adjacent droplets comprises of the following steps: mutual approach of droplets, formation of the continuous phase film between droplets, film rupture, drainage of the film, droplet–droplet coalescence and formation of enlarged droplets. Coalescence of the adjacent droplets may be complete or partial. Partial coalescence involves in addition to large droplet formation, the formation of a smaller droplet, secondary droplet, so-called the “daughter” [3,16].

Many authors acknowledge various forms of coalescence of the adjacent droplets and only a few will be specified: coalescence of the same size droplets, coalescence of different size droplets, the coalescence between large or coalescence of small droplets, as well as the coalescence without or with droplets deformation [3,5,16–24].

Ivanov *et al*. [16–24] investigated the interaction between two droplets of radius *a* having a narrow gap (thin film) between them. In this system the hydrodynamic and intermolecular forces are present. The hydrodynamic forces exist due to the viscous friction and they are usually in a rather long range. The interaction between two droplets in the emulsion favours the role of the following intermolecular forces: van der Waals, repulsive electrostatic double-layer forces, steric, etc. The authors claim that depending on the resultant of all the forces when two droplets collide, it may lead to droplet rebound, aggregation and coalescence. Aggregation is a process of the formation of droplet packets, aggregates, of several droplets that do not lose their individuality. If the resultant of all the forces is suffi-

cient to maintain the droplets in a small equilibrium distance, the aggregation will occur. These processes can take place through a number of mechanisms depending on the droplet size and the surfactant properties. The authors also state that the total coalescence time, being the drop lifetime; depend on the time required for the mutual approach of two droplets and rupture of the film.

During the droplet–droplet coalescence, the droplets can retain the spherical shape, initiating the coalescence without deformation having the model of rigid spheres, Figure 2a. This coalescence model can be attributed to droplets with small diameters. In other cases, during the coalescence between two droplets, deformations primarily occur in both droplets forming a film of different shapes: planar film, Figure 2b, and film model of large/small droplets, Figure 2c. Truncated droplets and the planar film can be formed in the zone of contact during the coalescence of large droplets. In the dispersed systems, where the emulsifier is present, a planar thin film is formed between the droplets. The formation of a thin film between the two droplets greatly enhances the role of surface forces and opposes the film drainage [3,16–24]. The emulsifier concentration in the deformed surface is non-uniform, and therefore the interaction forces are not of uniform intensity. The surfactants do not only affect the intermolecular interactions across the film, but, at the same time, favour the formation of the gradient of interfacial tension. Various surfactants amounts bond on the surface of droplets in a monolayer consequently forming the gradient of interfacial tension. This phenomenon occurs due to the surface non-uniformity of the droplet and is called the Marangoni effect. In this case the surfactant presence opposes the film drainage and reduces the velocity rate of the droplet approach.

Coalescence of irregularly shaped or crescent-shaped droplets, Figure 2e, is also considered to be one of the types of coalescence having significantly different interaction between these mentioned droplets. During the deformation process, two droplets can come into contact. In these circumstances, multipoint surfaces of the droplets participate in the interaction. When smaller drops are present, considering that the interaction is at only one point, then the deformation does not occur and therefore the effect of surface non-uniformity is not dominant.

Due to the van der Waals attractive forces, droplet deformation could occur in the zone of their contact. Ivanov et al. [16–24] concluded that if the droplets diameter is larger than 80μm due to the action of the hydrodynamic pressure they twist towards the inside, leading to the formation of a flat film.

When the droplet diameter is less than 80 μm a different type of strain occurs. If the distance between the drops is $h = h_P$ the formation of bulges occurs. The bulge formation mechanism was suggested by Yanitsios and Davis [25] during the investigation of modeling the behavior of pure liquid emulsions without the presence of surfactants. Cristini *et al*. [26] found in their research on systems in the presence of surfactants, that effective and rapid coalescence takes place at a distance of $h < h_P$. The cause of the bulge formation is due to the disjoining pressure that rises faster than the hydrodynamic pressure when the distance reduction, *h,* occurs. At a distance of $h < h_P$ the bulges spontaneously grow until the drop contact and the coalescence starts. Modern techniques of high-speed video camera recorded this scenario of the bulge formation during coalescence between two droplets [27–30].

Danov *et al*. [16,20,21] investigated coalescence of different size droplets, with radius, R_1 and R_2 ($R_1 < R_2$). The film that was formed in these circumstances, in the zone of contact was curved with uniform thickness. The film length is *R* and thickness *h*. The given situation can be analyzed either thermodynamically and/or kinetically. In the thermodynamic approach due to the interaction between the droplets over the film, additional disjoining pressure occurs within the film. The disjoining pressure depends on the thickness of the film. Posi-

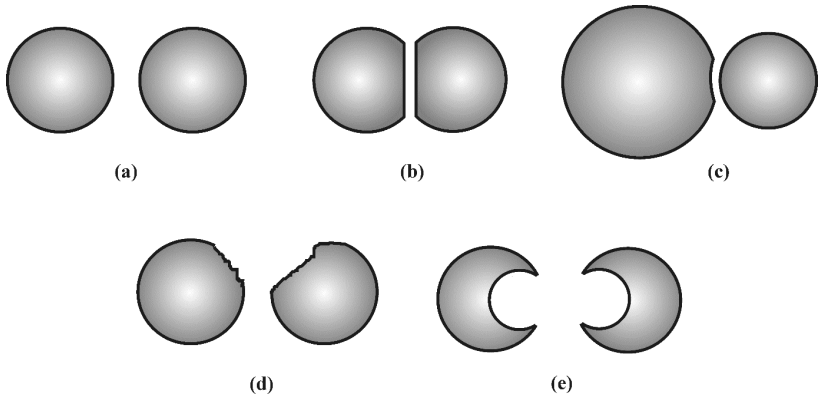

Figure 2. The droplet models when in mutual contact: a) model of rigid spheres, b) model of planar film, c) model of large/small droplets, d) irregular deformation, e) model of crescent-shaped droplets.

tive values of the pressure correspond to the repulsion of two droplets, while the negative values of the pressure indicate that the attractive forces are dominant. As a consequence of the disjoining pressure influence, the difference increases between the surface tension of the continuous phase, and interfacial tension of both liquids.

The film length increases with the increase of the contact angle. When the contact angle is zero, the equilibrium length of the film is also zero, and in such situation there is no possibility of the formation of equilibrium doublets, aggregates or coalescence. The disjoining pressure is the dominant thermodynamic factor that stabilizes the droplets and hinders coalescence. In addition to the mentioned thermodynamic factors, kinetic factors in the system may also occur. In this case, the effect of hydrodynamic forces must be taken into account. If the intensity is high enough, the hydrodynamic forces can cause film rupture before it reaches the thermodynamic equilibrium. During the contact of two droplets, with any disorder, including hydrodynamic, a capillary wave is generated on the surfaces of droplets. The resulting wave is usually formed in the upper and lower part of the film. If the amplitude of one or both waves becomes equal to the film thickness in any region, the film ruptures and the coalescence occurs [16,20,21].

The effect of hydrodynamic force can be reduced by the effect of kinetic stability. The most significant kinetic stabilization factors are: Gibbs surface elasticity, surface viscosity and surfactant adsorption relaxation time [20,21].

Gibbs surface elasticity tends to eliminate the gradient of the surface tension and suppress the fluctuations of the capillary waves. Surfactant and electrolyte concentration influence the mentioned elasticity. With the increase in their concentration the elasticity increases, which obstructs the coalescence. It should be noted that the electrolyte presence, may have a double effect on coalescence. An increase in electrolyte concentration may trigger an increase or decrease in the electrostatic barrier. This barrier increase may be caused by the increase of the film elasticity that hinders the coalescence. However, the barrier reduction may be the consequence of the reduction of electrical double-layer thickness that is more compact at higher concentration of ions, and therefore is less influential, which promotes the coalescence.

The film viscosity is often different from the viscosity of the continuous phase due to the local impacts, such as the capillary phenomenon and the surface roughness of the capillary wall. Therefore, the film viscosity is called the surface viscosity. Due to the dominant influence of the viscosity force in the capillaries, the behaviour of the fluid flow is different than in the free volume of the liquid. Consequently, an increase in surface viscosity slows the drainage of the film down. If the surfactants are present and if there is film thickness deformation due to delamination, then there is an additional effect on the surface viscosity [20,21].

Mechanisms of film rupture

There are a number of mechanisms and models of film rupture. Most of the models are based on the assumption that the film is planar. Models that simulate the film drainage of the continuous phase starts from two droplets submerged in an incompressible viscous fluid.

Danov *et al*. claim that the film rupture can unfold through four main mechanisms: capillary-wave, film rupture by nucleation of pores, the solute transport across the film and the barrier mechanism [3,24]. Derjaguin published that Vries with his research group first proposed the capillary-wave mechanism [31,32]. This mechanism explains the rupture of the film under the influence of attractive forces. Since the space between the two droplets is narrow, it corresponds to the dimensions of the capillaries. The upper and lower capillary film surfaces oscillate as sinusoidal phase-shift. The capillary waves are generated due to the kinetic energy of the molecules. The mentioned phenomenon accelerates and facilitates the rupture of the film in several ways. The reduction of the film thickness is achieved due to the presence of capillary waves and disjoining pressure. The disjoining pressure enhances the oscillation amplitude. Increasing the oscillating amplitude of the capillary waves can lead to the film rupture when the critical thickness is reached.

The mechanisms of the film rupture by nucleation of pores have been investigated by Derjaguin [31,32]. The pores are created by breakage of the film due to the departure of the ruptured parts of the film. The resulting empty space between the ruptured parts the authors called pores. The liquid film is thereby torn into two parts being the left and right wall of the pores that could be also called the pore edges of the pore periphery. Ivanov is of the opinion that not every rupture will lead to the pore formation [16]. Pore formation is favoured by the decrease in surface energy, but it is opposed by the edge energy obtained during the formation.

Edge energy of the pores can be explained macroscopically and microscopically [16–21]. Macroscopic approach describes the edge energy of the pore as a line tension that has the tendency to reassemble the two parts of the film. The microscopic approach defines the edge energy as an effect of the spontaneous curvature and bending elasticity of the wall that does not have uniform distribution of surfactants that are present in the monolayer. This is defined as the Marangoni effect. For small ruptures or cracks of the film, the edge

energy is predominant, while for the larger ruptures the surface energy is dominant. Therefore, larger pores cause the rupture of the film enabling the spontaneous pore formation, while smaller pores shrink and disappear. Regarding the mechanism of film rupture due to the formation of numerous pores, the film can rupture triggering droplet formation. Due to the development of bulges from the dispersed droplets in the pore space, the newly formed droplets of the continuous phase are trapped and cannot be drained. In this way, the double emulsion can be formed.

Ivanov *et al*. [16–21] have investigated the rupture mechanism due the solute transport across the film. The solute transport across the film amplifies the Marangoni effect, and therefore the chemical entropy increases. Marangoni effect is favoured by simultaneous mass and heat transport.

The mechanism of the barriers results from the explanation of the equilibrium states of film thickness h_1. When the pressure is increased to the value higher than the barriers, then the film rupture can be caused, initiating coalescence or the transition to another stable state with defined film thickness h_2. The increase of the adsorbed surfactant stabilizes the secondary films. During the pressure increase, the accumulated mechanical energy is released overcoming the barrier. The lower the barrier energy is, the less chance of film rupture is present. If the barrier is not too high, the film rupture might not occur. Overcoming the barriers is usually achieved by reducing the film thickness in several places, rather than by a sudden decrease of the whole film thickness [16–21].

Droplet coalescence in the porous bed

As already mentioned, a number of forces coexist in the solid matrix. From the resultant of the dominating forces in the system, the drop can be either captured or detached. The hydrodynamic forces are present due to the fluid flow. Depending on the interstitial velocity, these forces can predominantly be viscous or inertial. If the hydrodynamic forces are low intensity then the retaining, capturing and agglomeration of the droplets in the porous bed primarily occur. On the contrary, when the intensity of hydrodynamic forces is higher, then the dispersed phase leaves the porous bed, and the droplets detachment or even re-dispersion could happen.

Mechanisms of drop capture can be classified into two main groups: transport mechanisms and mechanisms of attraction [33,34]. The transport mechanisms include: screening effect, interception, sedimentation, inertia, diffusion, hydrodynamic forces and motion due to temperature gradients. Mechanisms of attraction forces include electrostatic interactions, van der Waals forces, adhesion and mutual adsorption.

Hubbe, Ryan and Elimelech with coworkers [35–41] investigated the detachment of colloidal particles/ /droplets from solid surfaces influenced by shear stress, Figure 3. It should be emphasized that the particles/droplets are exposed to the adhesive force and the hydrodynamic forces. Hydrodynamic forces consist of two components, horizontal and vertical. The horizontal component is the viscous force acting parallel to the surface where colloidal particles are situated, while the vertical component is the lifting force. Usually the intensity of the horizontal component is greater than of the lifting force. The horizontal component has a significant impact on the moment when colloidal particle/ /droplet will detach from the solid surface. The rotation and rolling of the drops appear due to the influence of the torque force. Hubbe claims that the drop detachment predominantly depends on its size and shear stress.

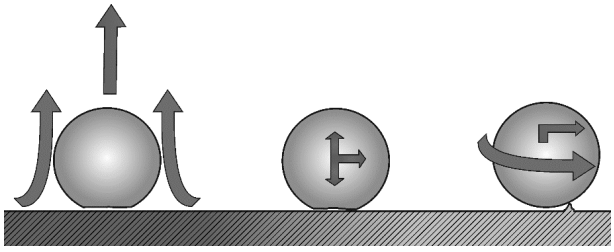

Figure 3. Schematic view of forces that influence the droplet trapped on a solid surface.

According to Spielman, there are three forms of the dispersed phase in the pores of the bed: capillary-conducted phase, globules and small droplets [42–46]. Capillary-conducted phase is formed quickly in the bed. Only this form of the dispersed phase influences the pressure drop during the flow of both phases through the bed. The amount of capillary-conducted phase in the pores of the bed is predominantly determined by its geometry, the volume of interconnected pores and the intensity of hydrodynamic and adhesion forces. Emulsion separation by bed coalescence can occur in two conditions: unsteady-state and steady-state conditions. The flow of relatively unstable emulsions through the bed initiates increasing filling of the pores in the bed by the dispersed liquid phase, resulting in a permanent rise of the pressure drop with time. Due to the accumulation of the dispersed phase in the pores of the bed, there is a cross-section reduction of flow capillaries, causing an actual increase of the fluid velocity and the flow resistance, by which the bed permeability reduction is achieved. In the case of deep bed filtration the amount of capillary-conducted phase changes in the pore volume, increasing quantity of the disperse phase. This regime is unsteady-state due to the change of pressure drop with time [47]. The filter cycle in the case of deep bed filtration ends when reaching the

maximum allowable pressure drop or when penetration of the dispersed phase through the bed is achieved. The filtration ends when the bed cannot accumulate any new amount of the dispersed phase and at this point the washing could begin. During the bed washing additional oily wastewater is formed due to which this regime seem unfavourable for the liquid–liquid separation. A more appealing application of the bed coalescence for the liquid-liquid separation is the steady-state regime [2,3]. Fluid velocity determines the intensity of the hydrodynamic forces, and the quantity of a capillary-conducted phase in the pores of the bed. According to Spielman the maximum amount of this phase is 30% of the pore volume, while the coalescence on its surface already begins at the amount of 10% of the pore volume. Simultaneously, new droplets of the disperse phase enter the bed, while the other droplets/ /globules leave the porous bed. Depending on the achieved conditions of the resultant forces, larger or smaller droplets than the ones entering will leave the porous bed. If larger droplets leave the bed, then the goal is reached. These droplets will be separated by sedimentation behind the porous bed, in the settling section, Figure 4.

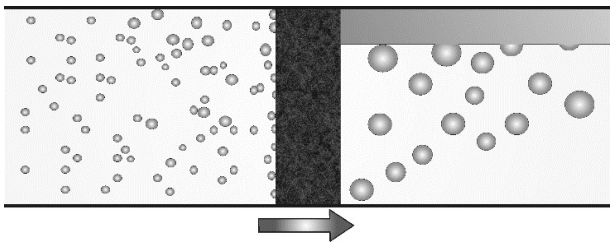

Figure 4. Operating scheme of bed coalescer.

The steady-state regime is achieved when the constant pressure drop is established, meaning that the pressure drop does not change with time anymore. Steady-state regime exists in an indefinite period of time. The steady-state regime eliminates filter cycle and bed washing requirements. Coalescence of droplets that enter into the bed occurs on the surface of the capillary-conducted phase, leading to their detachment and emerging from the bed as enlarged droplets.

Three coalescence mechanisms can occur in the porous bed: coalescence of the droplets on the fibre surface, coalescence of the adjacent droplets in the pore space and coalescence of the droplets on the surface of the capillary-conducted disperse phase, saturated liquid [3,42–46]. With the coalescence of droplets on the surface of the solid material the formation of capillary-conducted phase in pores is obtained. Coalescence in the capillary-conducted phase is similar to coalescence at the liquid–liquid interface. All previous discussion about the droplet–droplet coalescence also applies to their mutual coalescence in the volume of the pores. Mutual drop coalescence in the pores may be enhanced by the bed properties that influence the distance between drops and hence favouring this type of coalescence [3,5,9,48–54].

DESIGN VARIABLES OF BED COALESCER

The porous bed that exists in the practice may have drastically different properties [3,5,46–49,55]. The two bed properties that mostly differ are: bed porosity and bed length. The bed porosity can be from close to zero to up 98%. Such a wide range of bed porosity inevitably influences different behaviours of disperse and continuous phase flows and droplets coalescence. Granular bed has a porosity interval of up to around 50%, while the fibre beds are able to form a high-porosity bed [47].

The bed length also can be found in two extreme situations, being the finite and infinite bed length. The finite bed length can be defined as expressively low bed length ranging from a few millimetres to a few centimetres, which corresponds to the membrane, while high bed length can range from half meter to several meters. The porous bed with infinite length is the petroleum reservoir. Taking into account that gas, oil and water are exploited from the earth depth, the phenomena for this porous bed are extremely important because it significantly influences the global economy [3].

Bed can be formed from natural or artificial materials, inorganic or organic. When the bed is formed out of polymeric fibres, it has the ability of such a compression that the bed can have completely different properties, although formed out of the same polymer fibres [48,49,55,56].

Selection of the filter media, as well as its packing conditions is essential for design of bed coalescer. When designing the steady-state bed coalescer it is necessary to determine the ratio of droplet size to pore size. If it is possible, the conditions should be chosen in such a way that the pore size is greater than the size of droplets. In most cases, the mentioned relation is usually achieved. In these circumstances the basic preconditions are provided, enabling the formation of the capillary-conducted phase in the pores of the bed where the coalescence of the newly arrived droplets is realized.

Šećerov Sokolović *et al*. published several papers on the subject of the design of steady-state bed coalescer [2,48,56–65]. Common design targets were small unit with low energy spending. For high working velocity, size of coalescer is small, but at the same time consumption of energy increases. Energy consumption and pressure drop can be modified with variations in bed properties. By reducing the size of the coalescer, its weight is also reduced. Therefore, less structural material for the coalescer production, less material for foundation, as well as less space for its accommodation

are needed. These specifics are of particular importance on ships and oil platforms where the carrying capacity and space are drastically limited.

Bed coalescers can be installed in the industry to perform separation of oil from water in two different situations. One is to separate same oil during its lifetime, and the other with the task to separate different oils during time [65]. The same oil is separated by the coalescer in the oil fields and on ships. These coalescers can be designed on the basis of experiments on the model emulsion of this oil and optimal working conditions can be selected. In petroleum refineries and petrochemical industry coalescers, as part of a central facility for wastewater treatment, are able to separate oils of different quality over time. The coalescer design for such circumstances is the most complex.

Many factors affect steady-state bed coalescence and separation efficiency: fluid velocity, bed properties, fibre properties, properties of liquids, surface phenomena, set-up of the unit and interdependences of many variables.

Fluid velocity

Numerous authors have investigated the role and importance of the fluid velocity related to the coalescence and the flow of heterogeneous systems through the porous media [42–46,66–77]. Very early in the investigation the scientists observed that there is a limit value of the fluid velocity at which the behaviour of the system changes. According to available literature, this velocity, was first mentioned by Voyutskii *et al.* and was called the critical velocity [66]. Evidently, the interpretation of the critical velocity depends on whether the researchers focused on unsteady-state or the steady-state regime. In the first one the critical velocity is the velocity below which a complete retention of the dispersed phase in the pores of the bed is achieved.

Sareen *et al*. defined the critical velocity as the velocity at which the re-dispersion of the dispersed phase in the bed occurs. Therefore the droplets leaving the bed have smaller diameters than the droplets that enter the bed and cannot be separated by settling. For fluid velocity below the critical, the complete coalescence is achieved of large output droplets that can be easily separated. It is more than obvious that the coalescence in this case is in the steady-state regime [67].

Spielman studied the effect of the fluid velocity on the flow of two immiscible fluids through the porous bed [42–46]. The investigation of fluid velocity focused on the filtration coefficient, the total pressure drop and the amount of the capillary-conducted phase in the bed. His experiments covered a region of critical velocity, but the author did not mention, nor analyse or define this value.

Rosenfeld gave numerical values of critical velocity for Spellman's experiments [68]. He defined the critical velocity as the velocity at which the filtration coefficient begins to rapidly decrease, Figure 5. According to Rosenfeld, the critical velocity is the velocity at which the hydrodynamic forces become dominant compared to the other forces, leading to the detachment of a part of the dispersed phase. Rosenfeld studied the flow through the interior of reservoirs and the following phenomenon was observed. The flow of the fluid carries the dispersed phase further through the bed causing the clogging of pore channels and the decrease of bed permeability. Additional increase of the velocity leads to the increase of the dispersed phase amount that is detached moving in the direction of the liquid flow. In contrast, if the bed length is low, then the detached dispersed phase emerges from the bed, increasing the bed permeability due to the decrease of the capillary-conducted phase amount in the pores.

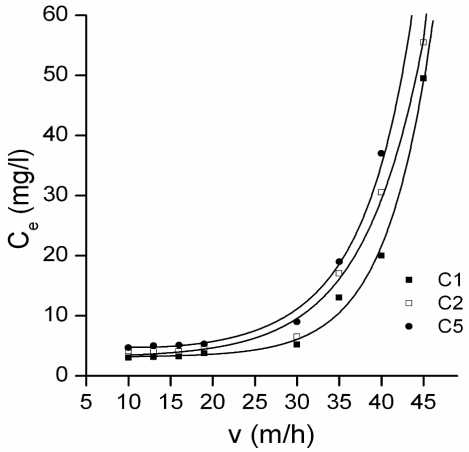

Figure 5. Illustration of the existence of the critical velocity.

One of the key information essential for investigation is whether the fluid velocity below or above the critical value. Considering that this information is not provided in numerous cases, incorrect interpretations could occur by comparing the dependencies that exist above and below the critical velocity. Sometimes, the working conditions that are selected provide an extremely low critical velocity, leading to a misconception that the investigated area cannot be above the critical velocity.

Grilc, Golob and Modić published a series of papers on the effect of fluid velocity on coalescence and investigated the critical velocity as the phenomena [69–72]. These authors studied both water-in-oil and oil-in-water emulsions and the influence of following parameters: bed length, interfacial tension and pH on the critical velocity and modified Spielman adhesive number. Authors modified the Spielman equation for dimensionless filtration coefficient and adhesive num-

ber by introducing the critical velocity. Furthermore, the critical velocity was defined as the velocity at which the effluent concentration of the dispersed phase is no longer constant and begins to rise exponentially.

Soo and Radke studied the influence of the fluid velocity on the flow of the oil-in-water emulsion through bed of sand, simulating the conditions in the underground collectors. Unlike other authors, their research focused on the events that take place in the bed for diluted, stable emulsions with the dominant retention mechanisms, such as filtration and interception [73––76]. During the flow of a stable emulsion through the bed, each single drop is captured on the surface of the filter media, but there is no coalescence between the droplets, or formation of capillary-conducted disperse phase that was reported by Spielman. These authors define the critical velocity as the velocity above which the capturing possibility of the droplets is zero, meaning that there is no capturing of new drops, initiating the detachment of the previously "captured" ones.

Maini *et al*. emphasized the importance of the fluid velocity during the investigation of suspended particles migration in the oil fields [77]. In the case of the suspension flow the term critical velocity also occurs. They noted that the permeability decrease due to the particle migration occurs only when the fluid velocity becomes higher than the critical velocity. Low velocity initiates the flow of a small number of particles, which move towards the collector, one by one. At high fluid velocity a larger number of particles are torn from the surface of the reservoir rock, and collide with each other, interact and migrate in another way.

Ryan and Elimelech studying the transport of colloids in the groundwater also accepted the concept of critical velocity [37]. In theory, the mobilization of colloids by physical disturbance is based on the torque moment, which affects the particles that are stored on a solid surface, and is the result of fluid flow that initiates the particle detachment. The torque moment, which influences the detached particles, includes the adhesive force operating normal to the solid surface, the drag force operating tangential to the surface, and lift force operating normal to the solid surface.

Šećerov Sokolović *et al.* studied the importance of the influent concentration, bed length and fluid velocity on the effluent concentration for the system of oil-in-water emulsion and polyurethane bed [57]. In this paper the importance of the critical velocity as a boundary of behaviour of the system was underlined. The effect of the influent concentration and bed length in the observed range on the effluent concentration is negligible for the fluid velocity below the critical; while for the velocity above the critical this effect is significant. According to these authors, critical velocity is a key variable for designing the coalescers, by which the capacity and dimensions of the bed coalescer are determined. The fluid velocity need to be high, but below the critical value for the given system. The critical velocity can be determined from the experimental data concerning the dependence of the effluent concentration on the fluid velocity. The authors proposed that the critical fluid velocity should be the velocity at which the effluent oil concentration reaches a value of 15 mg/l, which is often the recommended limit of oil concentration in wastewater, Figure 6.

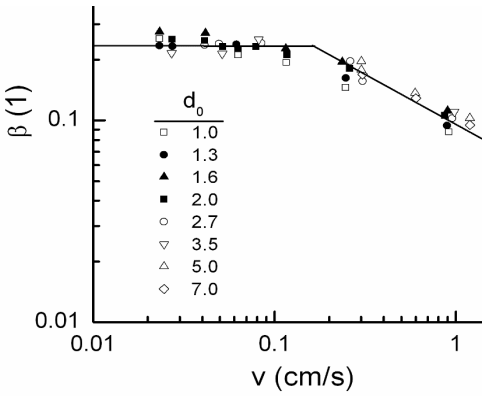

Figure 6. Dependence of effluent concentration on fluid velocity for polyurethane bed length 15 cm over influent oil concentration: C_1 = 500 mg/l, C_2 = 800 mg/l andC_5 = 2000 mg/l.

Šećerov Sokolović *et al.* in all of their later published work applied the critical velocity as a key variable for the investigation of the influence of many factors.

Researchers are still investigating the influence of fluid velocity using other parameters, such as efficiency, quality factors and etc. They also concluded that over lower flow velocity droplet separation performance is better than over higher flow velocity in all investigated circumstances [78,79].

Fluid flow orientation-flow mode

Fluid flow orientation can be horizontal (H), vertical down (VD) and vertical up (VG). Most frequent type of fluid flow mode for liquid-liquid separation is vertical down that has probably been taken from deep bed filtration. Investigation of fibre bed coalescence phenomenon often neglects fluid flow orientation. However, in term of coalescence efficiency the fluid flow mode in relation with the fibre bed coalescence has additional significance [3,59,60,78,79].

Šećerov Sokolović *et al*. in earlier stages of their research spotted the importance of the flow mode on the coalescence efficiency [59,60]. In their comprehensive research, as well as in their equipment development activities, they investigated the possibilities for increasing the coalescence efficiency.

Šećerov Sokolović *et al*. experimentally determined that the separation efficiency of steady-state bed coalescer is highly influenced by the flow mode. The flow of the dispersion in through the filter media and coalescence efficiency are conditioned by the balance of acting forces. This balance is mainly determined by the density of the dispersed phase, and fluid flow mode. The dominant forces that are of influence in the porous bed are: gravity, F_g, hydrodynamic forces, F_h, buoyant force, F_p, and adhesion, F_a. The adhesion is present in the pore space in all directions equally, having a short radius of action, and for this investigation can be ignored when the same filter media is used.

For H fluid flow mode the forces act at two planes, in the direction of *x*- and *z*-axis. Under these circumstances, it is defined as a two-dimensional system. The gravity force, F_g, and the buoyant force, F_p, act opposite to each other in the direction of the *z*-axis. Their resulting force of the higher density dispersed phase than the continuous phase will be directed downward, whereas lower density dispersed phase will be directed upwards. The hydrodynamic force, F_h, is oriented in the direction of the *x*-axis, and is at an angle of 90° when compared to the resultant force of F_p and F_g. The resulting force of these three forces is the diagonal of a parallelogram with the direction determined by the density ratio of existing liquids. Such orientation of the resulting force promotes settling of droplets leaving the bed, which is desirable.

The fluid flow mode VD and VG differ to each other in direction and intensity of the observed resulting force. If the dispersed phase has lower density than the continuous phase in case of VD flow mode, the hydrodynamic and gravity forces are added, and the buoyant force reduces this total. For VG flow mode, the hydrodynamic force is added to the buoyant force and the gravity force reduces the intensity of resulting force.

As previously emphasized, the critical velocity should be regarded as the maximum possible fluid velocity of the device. In the experiments of Šećerov Sokolović *et al*. the highest critical velocity was realized in the H flow mode, for all observed bed lengths and bed permeability. The value of the critical velocity varies up to 100% for different conditions.

Šećerov Sokolović *et al*. analyzed the separation efficiency of two commercial coalescers with different geometry marked as "04" and "H" [60]. Experiments were carried out over a wide range of oil properties and fluid velocities. Operation of coalescer "04" was characterized by an extremely low working velocity. This coalescer involved both vertical flow modes (VG and VD), while coalescer "H" had a horizontal flow mode.

This phenomenon can be explained by the amount of the capillary-conducted phase in the bed for the steady-state operating conditions of the coalescer. For the H flow mode the amount of the capillary-conducted phase was the highest in relation to the other two flow modes. In the H flow mode high amounts of the dispersed phase retained in the bed, since only the hydrodynamic force tends to drain out the part of dispersed phase pushing it outside the bed. The other two forces, being vertically oriented, tend to retain the dispersed phase in the bed.

The most unfavourable situation is when vertical up, VG, flow mode existed. In these circumstances, the hydrodynamic force tends to push the dispersed phase from the bed. When the dispersed oil is less dense than water, quantity of the saturated oil in the pores is low and the contact time is insufficient for the efficient coalescence. Published results confirmed that separation efficiency is the lowest for vertical up flow mode [59].

The study of Vigneaux *et al*. observed the flow of the emulsion through inclined pipes and presented the distribution of the dispersed phase through the cross-section of the pipe, confirming the above explanation, Figure 7 [80]. Based on the mentioned analysis it can also be pointed out that the amount of the capillary-conducted phase in the bed with the H flow mode is not uniform over the cross-section of the pipes. When the dispersed phase is of lower density than the continuous phase, then the upper parts of the bed is enriched by it. On the contrary, when the dispersed phase has higher density than the continuous phase, then higher amounts of the capillary-conducted phase is present in the lower part of the bed. It could be concluded that the amount of dispersed liquid phase, as well as the uniformity of its distribution in the bed volume, is a function of the flow mode.

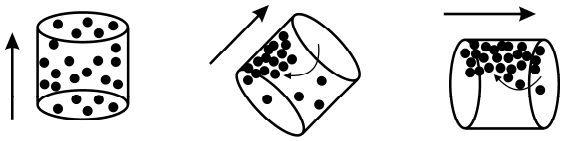

Figure 7. Distribution of the dispersed oil in pipes with different orientations: a) vertical pipe, b) slightly tilted pipe and c) considerably tilted pipe.

The literature search shows that only one research group have addressed the problem of fluid flow mode. Burganos *et al*. investigated this problem but in the domain of deep bed filtration for a solid-liquid system. On the basis of their simulation, the importance of the flow mode in this operation was explicitly pointed out [81].

The fibre bed geometry

The fibre bed geometry is defined by two sets of properties: fibre properties and bed properties. The

fibre properties are considered to be: the fibre diameter, fibre length, shape of cross-section, tortuosity, interconnected fibre structure and surface roughness. The bed properties are: porosity, bed permeability, bed length, shape and tortuosity of pores, pore size, the fibre orientation, active surface area and the packing density of fibres.

The fundamental problem for defining the bed geometry is the absence of a representative characteristic that give the overall description. Although this is an important feature, most authors do not give enough data on the bed geometry and thereby the bed properties for the conducted investigation are not precise. The authors usually give the bed length, sometimes the fibre diameter, but very rarely bed permeability and/or bed porosity. The most investigated effects in the literature were the fibre diameter and the bed length. Most authors who have studied the influence of the bed length claim that reducing the fibre diameter increases the separation efficiency [82–85], while Dalquist and Setterwall noted that with the reduction in the fibre diameter the bed length could be reduces [86]. Golob *et al*. pointed out that the required fibre diameter is determined by the droplet size of the dispersed phase and that these two values should be close to each other [72].

Investigation of fibre diameter effect is usually irregular because there is no report whether the changes in fibre diameter in the same time initiated the variation of the solid phase ratio. The bed which Hazlett used in the study consisted of several segments of glass fibres with different diameters [82–84]. The author used glass fibres of smaller diameter (0.75 and 1 μm) and glass fibres with larger diameter (2.8 and 4.6 μm). Fluid flow mode was vertically down, VD. The bed was formed in such a way that on the top were usually segments of thinner fibre, followed by the segments of thick fibres. The author detected that the stacking order of the segments with different fibre thickness affects the coalescence efficiency. The fibre diameter at the bed exit has a predominant influence on the dimensions of detached droplets. The fibres of smaller diameters at the bed exit may reduce the coalescence efficiency, and therefore thicker fibres are suggested to be on the bed exit. If the fibre diameter of the last segment is not well defined, all the positive effects of the droplet capture and their aggregation can be annulled.

Daiminger *et al*. introduced a microporous membrane of nano fibres with low thickness in front of the polypropylene bed, having vertically upward, VG, fluid flow mode, in order to enable enlargement of the smallest droplets, and thus improve the separation of the dispersed oil and allow higher fluid velocity [87].

Šećerov Sokolović *et al*. [56] reported that the porosity dependence on the bed permeability and fibre diameter completely determined the fibre bed geometry. In addition, the authors indicated that the existence of the critical bed permeability, below which the system becomes unstable. Authors have pointed out that the operation range in terms of the permeability is suggested to be above the critical value, Figure 8. The authors also claimed that it is necessary to maintain the same bed geometry when investigating other effects such as: bed length, the droplet size, the properties of the filter media, the properties of the dispersed phase, and etc. The authors noted that only comparable results are those that have been realized in the same fluid flow mode and the same bed permeability higher than the critical one.

Bed length

Bed length is one of the most important design variables in bed coalescence. Sareen and Hazlett both investigated bed coalescence of water-in-oil emulsion

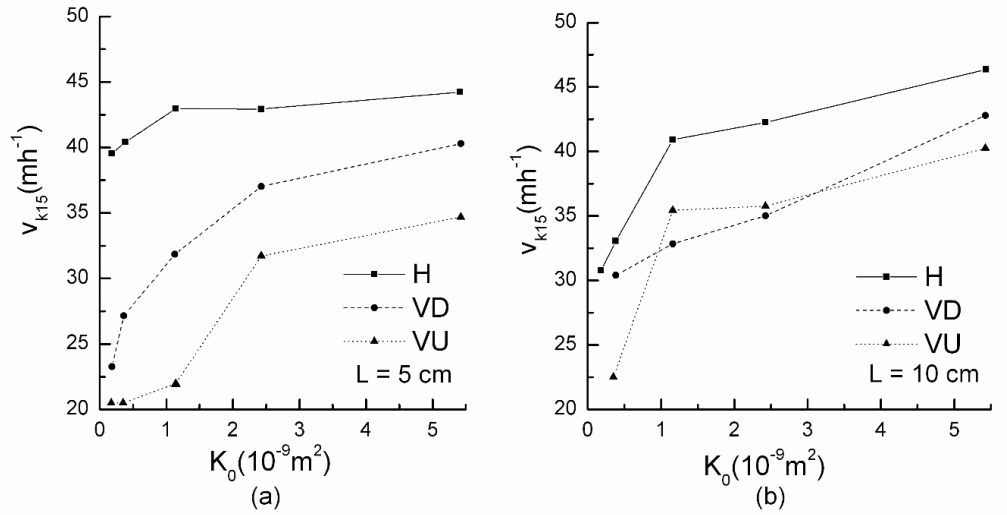

Figure 8. Dependence of critical velocity on bed permeability for all flow modes for the bed length of: a) 5 and b) 10 cm.

[67,82–84]. In connection with bed length Sareen concluded that there is an optimal bed length which enables maximal value of the critical velocity [67]. Hazlett thought that the bed length, above the minimal value, has no influence on coalescence efficiency [82––84]. It is important to point out that investigations of both researchers were conducted in a very narrow range of bed length around its minimal value, between 0.5 and 3.2 cm.

Fahim and Akbar investigated the effect of a wide range of bed lengths, from 10 to 40 cm, on separation efficiency of oil from wastewater, over a wide range of fluid velocity, using high surface energy fibre materials at vertical up flow mode [88]. They concluded that separation efficiency is very high for all bed lengths. The authors observed that drop diameter decreases with increase in fibre bed length. At higher velocity and relatively high bed lengths, the droplets enlarged by coalescence can be re-dispersed while passing through the fibre bed.

Deshamps *et al*. [89] explored the possibility of separation of dispersed vegetable oil from water. The bed was formed out of cotton fibres and the bed length was varied from 9 to 12 cm. The authors claimed that with the increase of the bed length, the coalescence efficiency also increases.

In general, it could be concluded that with the increase of the bed length the coalescence efficiency increases. Magiera and Blass compared experimental data with the simulation data and they also concluded that longer fibre beds have better separation efficiency [85]. High and low surface energy fibre materials and three bed lengths over two fluid velocities were included in this investigation.

Šećerov Sokolović *et al*. established that the effect of bed length on the bed coalescence is dominantly determined by the applied range of fluid velocity over the investigated bed length (3–15 cm). The effect of the bed length on the separation efficiency is negligible for the fluid velocity below critical. When the fluid velocity exceeds the critical value, the bed length exhibits an unexpected effect on effluent oil concentration [61,65].

Shin and Chase, on the basis of two glass micro-nanofibre bed length (3 and 5 mm), over horizontal flow mode concluded that the capture efficiency and quality factor were higher for the 5mm bed, but the overall coalescence efficiency decreased with the increase in the bed length applied [89,90].

Šećerov Sokolović *et al.* explained all aforementioned observations analyzing interdependences between the bed lengths, flow mode and bed permeability [61]. The effect of the bed length on the critical velocity was monitored. Critical velocity increases with the increase in bed length, ranging from 3 to 10 cm, over all three flow modes (H, VD and VG). These results were obtained at the maximal bed permeability, 5.39×10^{-9} mm^2. This dependence under the applied circumstances is expected, because at high bed permeability and the maximum bed length, highest pore size, pore volume and contact time were obtained. Corresponding to this, the amount of the capillary-conducted phase is maximal, and the droplet coalescence on its surface is optimal. Dependence of the critical velocity on bed length is similar over all three flow modes, but numerical values are very different as a consequence of resulting forces which are acting in the system, Figure 9.

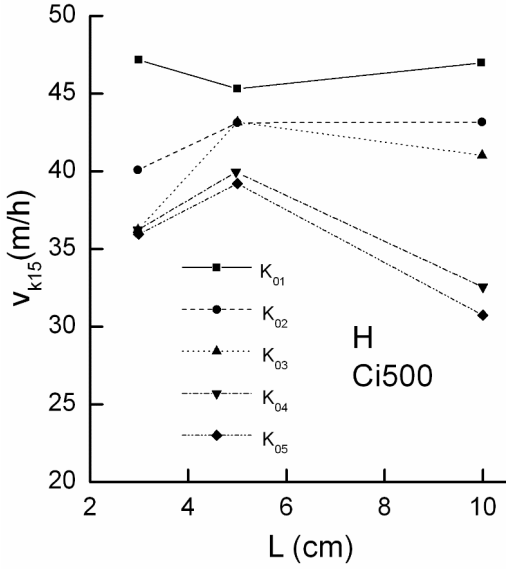

Figure 9. Illustration of existence of the optimal bed length.

Šećerov Sokolović *et al.* also recognized the presence of the minimal bed length in the steady-state bed coalescence [61]. This property could be defined as the critical bed length. The effect of the bed length above the critical value on steady-state bed coalescence is dominantly determined by bed permeability and influent oil concentration, independent on the flow mode. At low bed permeability and with H and VD flow mode, the authors detected the existence of the optimal bed length. Under the applied experimental conditions this optimal value of the bed length was 5 cm for polyurethane fibre bed.

DISCUSSION AND OUTLOOK

Up till now, there has been no systematic approach to the problem of the complex bed coalescence phenomena. Experimental conditions differ from study to study over different bed properties and fluid flow orientations. Very often, the chosen conditions do not allow studying the desired phenomenon because of the simultaneous influence of several variables. In these

circumstances it is difficult to set up any general conclusions. On the other hand, the existing knowledge of coalescence mechanisms, mechanisms of film rupture and flow of two immiscible liquids through porous bed is still not adequately connected to each other. Limitation of current experience about phenomena on the liquid–liquid–solid interface also prevents further progress of fibre bed coalescer design.

Acknowledgment

The work was supported by the Ministry of Education, Science and Technological Development of the Republic of Serbia, Grant number 172022.

REFERENCES

[1] S. Sokolović, R. Šećerov-Sokolović, S. Šević, Two-stage coalescer for oil-water separation, Water Sci. Technol. **26** (1992) 2073-2076.

[2] R. Šećerov Sokolović, S. Sokolović, S. Šević, Oily Water Treatment Using a New Steady-State Fibre-Bed Coalescer, J. Hazard. Mater. **162** (2009) 410−415.

[3] D. Govedarica, D.D. Sokolović, Separacija emulzija koalescencijom u sloju vlakana, Fakultet tehničkih nauka, Univerzitet u Novom Sadu, Novi Sad, edicija Monografije, 2014, pp. 1–22, 91–100.

[4] R. Šećerov Sokolović, S. Sokolović, B. Galešev, New Technology for Wastewater Treatment, Water Sci. Technol. **26** (1992) 2507−2509.

[5] D. Govedarica, Koalescencija mineralnih ulja u vlaknastom sloju, Doktorska disertacija, Tehnološki fakultet, Novi Sad, April 2011.

[6] B.V. Derjaguin, L.D. Landau, Theory of the Stability of Strongly Charged Lyophobic Soils and of the Adhesion of Strongly Charged Particles in Solution of Electrolytes, Acta Physicochim. **14** (1941) 633−662.

[7] E.J. Verwey, J.G. Overbeek, Theory of the Stability of Lyophobic Colloids, Elsevier, Amsterdam, 1948, pp. 98––104.

[8] M. Elimelech, C.R. O'Melia, Kinetics of Deposition of Colloidal Particles in Porous Media, Environ. Sci. Technol. **24** (1990) 1528−1536.

[9] M. Elimelech, Kinetics of Capture of Colloid Particles in Packed Beds under Attractive Double Layer Interactions, J. Colloid Interface Sci. **146** (1991) 337−352.

[10] L.A. Spielman, S.L. Goren, Capture of Small Particles by London Forces from Low-Speed Liquid Flows, Environ. Sci. Technol. **4** (1970) 135−140.

[11] L.A. Spielman, J.A. Fitzpatrick, Theory for Particle Collection under London and Gravity Forces, J. Colloid Interface Sci. **42** (1973) 607−623.

[12] L.A. Spielman, P.M. Cukor, Deposition of Non-Brownian Particles under Colloidal Forces, J. Colloid Interface Sci. **43** (1973) 51−65.

[13] L.A. Spielman, S.K. Friedlander, Role of the Electrical Double Layer in Particle Deposition by Convective Diffusion, J. Colloid Interface Sci. **46** (1974) 22−31.

[14] R. Rajagopalan, Probing Interaction Forces in Colloidal Fluids through Static Structural Data: the Inverse Problem, Langmuir. **8** (1992) 2898−2906.

[15] Y. Wang, R. Rajagopalan, W.L. Mattice, Kinetics of Detachment of Homopolymers from a Solid Surface, Phys. Rev. Lett. **74** (1995) 2503−2506.

[16] I.B. Ivanov, Thin liquid films, Fundamentals and applications, Marcel Dekker, Inc., New York, 1988, pp. 382––385, 392–394, 435–442.

[17] K.D. Danov, N.D. Denkov, D.N Petsev, I.B. Ivanov, R. Borwankar, Coalescence Dynamics of Deformable Brownian Emulsion Droplets, Langmuir **9** (1993) 731––740.

[18] K.D. Danov, I.B. Ivanov, T.D. Gurkov, R.P. Borwankar, Kinetic Model for the Simultaneous Processes of Flocculation and Coalescence in Emulsion Systems, J. Colloid Interface Sci. **167** (1994) 8−17.

[19] A. Hadjiiski, R. Dimova, N.D. Denkov, I.B. Ivanov, R. Borwankar, Film Trapping Technique: Precise Method for Three-Phase Contact Angle Determination of Solid and Fluid Particles of Micrometer Size, Langmuir **12** (1996) 6665−6675.

[20] S.D. Stoyanov, V.N. Paunov, E.S. Basheva, I.B. Ivanov, A. Mehreteab, G. Broze, Motion of the Front between Thick and Thin Film: Hydrodynamic Theory and Experiment with Vertical Foam Films, Langmuir **13** (1997) 1400−1407.

[21] I.B. Ivanov, K.D. Danov, P.A. Kralchevsky, Flocculation and Coalescence of Micron-Size Emulsion Droplets, Colloids Surfaces, A **152** (1999) 161−182.

[22] D.S. Valkovska, I.B. Ivanov, Effect of Surfactants on the Film Drainage J. Colloid Interface Sci. **211** (1999) 291−303.

[23] N. Alexandrov, K.G. Marinova, K.D. Danov, I.B. Ivanov, Surface Dilatational Rheology Measurements for Oil/Water Systems with Viscous Oils, J. Colloid Interface Sci. **339** (2009) 545−550.

[24] K.D. Danov, S.D. Stoyanov, N.K. Vitanov, I.B. Ivanov, Role of Surfactants on the Approaching Velocity of Two Small Emulsion Drops, J. Colloid Interface Sci. **368** (2012) 342−355.

[25] S.G. Yiantsios, R.H. Davis, Close Approach and Deformation of Two Viscous Drops due to Gravity and van der Waals Forces, J. Colloid Interface Sci. **144** (1991) 412−433.

[26] V. Cristini, J. Blawzdziewicz, M. Loewenberg, Near--Contact Motion of Surfactant-Covered Spherical Drops, J. Fluid Mech. **366** (1998) 259−287.

[27] H.Q. Sun, L. Zhang, S. Zhao, J. Yu, Interfacial Dilational Properties of Acidic Model Oil and Chemical Flooding Systems, J. Dispersion Sci. Technol. **32** (2011) 389−394.

[28] C.W. Angle, Y. Hua, Dilational Interfacial Rheology for Increasingly Deasphalted Bitumens and n-C5 Asphaltenes in Toluene/$NaHCO_3$ Solution, Energy Fuels. **26** (2012) 6228−6239.

[29] K.L. Thompson, E.C. Giakoumatos, S. Ata,G.B. Webber, S.P. Armes, E.J. Wanless, Direct Observation of Giant Pickering Emulsion and Colloidosome Droplet Interaction and Stability, Langmuir **28** (2012) 16501−16511.

[30] J.Y. Won, J. Krägel, A.V. Makievski, A. Javadi, G. Gochev, G. Loglio, P. Pandolfini, M.E. Leser, C. Gehin-Delval, R. Miller, Drop and Bubble Micro Manipulator (DBMM)-A Unique Tool for Mimicking Processes in Foams and Emulsions, Colloids Surfaces, A **441** (2014) 807−814.

[31] B.V. Derjaguin, Summarizing Remarks, Colloid Stability, Discuss. Faraday Soc. **42** (1966) 317−321.

[32] B.V. Derjaguin, Effect of Lyophile Surfaces on the Properties of Boundary Liquid Films, Discuss. Faraday Soc. **42** (1966) 109−119.

[33] K.J. Ives, Rapid Filtration. Water Res. **4** (1970) 201−223.

[34] K.J. Ives, C.S.B. Fitzpatrick, Detachment of Deposits from Sand Grains, Colloids Surfaces, **39** (1989) 239−253.

[35] M.A. Hubbe, Theory of Detachment of Colloidal Particles from Flat Surfaces Exposed to Flow, Colloids Surfaces. **12** (1984) 151−178.

[36] M.A. Hubbe, Detachment of Colloidal Hydrous Oxide Spheres from Flat Solids Exposed to Flow 1. Experimental system, Colloids Surfaces **16** (1985) 227−248.

[37] J.N. Ryan, M. Elimelech, Colloid Mobilization and Transport in Groundwater, Colloids Surfaces, A **107** (1996) 1−56.

[38] M. Elimelech, Predicting Collision Efficiencies of Colloidal Particles in Porous Media, Water Res. **26** (1992) 1−8.

[39] P.R. Johnson, M. Elimelech, Dynamics of Colloid Deposition in Porous Media: Blocking Based on Random Sequential Adsorption, Langmuir **11** (1993) 801−812.

[40] M. Elimelech, J. Gregory, X. Jia, R.A. Williams. Particle Deposition and Aggregation: Measurement, Modeling and Simulation, Butterworth-Heinemann, Woburn, 1998, pp. 113−401.

[41] N. Tufenkji, M. Elimelech, Correlation Equation for Predicting Single-Collector Efficiency in Physicochemical Filtration in Saturated Porous Media. Environ. Sci. Technol. **38** (2004) 529−536.

[42] L.A. Spielman, S.L. Goren, Theory of Coalescence by Flow through Porous Media, Ind. Eng. Chem. Fundam. **11** (1972) 66−72.

[43] L.A. Spielman, S.L. Goren, Experiments in Coalescence by Flow through Fibrous Mats, Ind. Eng. Chem. Fundam. **11** (1972) 73−83.

[44] L.A. Spielman, S.L. Goren, Progress in Induced Coalescence and a New Theoretical Framework for Coalescence by Porous Media, Ind. Eng. Chem. **62** (1970) 10−24.

[45] L.A. Spielman, Y.P. Su, Coalescence of Oil-in-Water Suspensions by Flow through Porous Media, Ind. Eng. Chem. Fundam. **16** (1977) 272−282.

[46] R.M. Šećerov-Sokolović, S.M. Sokolović, Višefazni sistemi i porozni sloj. Hem. Ind. **58** (2004) 49−54.

[47] R. Šećerov Sokolović, S. Sokolović, D. Govedarica, Performance of expanded polystyrene particles in deep bed filtration, Sep. Purif. Technol. **68** (2009) 267–272.

[48] D.D. Govedarica, R.M. Šećerov-Sokolović, A.I. Kiralj, O.M. Govedarica, D.S. Sokolović, M.S. Hadnađev-Kostić, Separation of Mineral Oil Droplets using Polypropylene Fibre Bed Coalescence, Hem.Ind. **69** (2014) 339–345.

[49] R. Šećerov Sokolovic, D. Govedarica, D. Sokolović, S. Sokolović, Separacija dispergovanog ulja primenom koalescera sa vlaknastim slojem, Zaštita materijala **55** (2014) 259–263.

[50] C. Shen, F. Wang, B. Li, Y. Jin, L. Wang, Y. Huang, Y. Application of DLVO Energy Map To Evaluate Interactions between Spherical Colloids and Rough Surfaces, Langmuir **28** (2012) 14681−14692.

[51] C. Shen, V. Lazouskaya, H. Zhang, B. Li, Y. Jin, Y. Huang, Influence of Surface Chemical Heterogeneity on Attachment and Detachment of Microparticles, Colloids Surfaces, A **433** (2013) 14−29.

[52] C. Shen, Y. Jin, B. Li, W. Zheng, Y. Huang, Facilitated Attachment of Nanoparticles at Primary Minima by Nanoscale Roughness is Susceptible to Hydrodynamic Drag under Unfavourable Chemical Conditions, Sci. Total Environ. **466**–**467** (2014), 1094−1102.

[53] M.B. Seymour, G. Chen, C. Su, Y. Li, Transport and Retention of Colloids in Porous Media: Does Shape Really Matter? Environ. Sci. Technol. **47** (2013) 8391−8398.

[54] S.A. Bradford, S. Torkzaban, A. Shapiro, A Theoretical Analysis of Colloid Attachment and Straining in Chemically Heterogeneous Porous Media, Langmuir **29** (2013) 6944−6952.

[55] R.M. Šećerov-Sokolović, O.P. Stanimirović, S.M. Sokolović, Uticaj promene nasipne gustine na osobine sloja, Hem. Ind. **57** (2003) 335−340.

[56] R.M. Šećerov Sokolović, T.J. Vulić, S.M. Sokolović, R.P. Marinković Nedučin, Effect of Fibrous Bed Permeability on Steady-State Coalescence, Ind. Eng. Chem. Res. **42** (2003) 3098−3102.

[57] R.M. Šećerov Sokolović, S.M. Sokolović, B.D. Đoković, Effect of Working Conditions on Bed Coalescence of an Oil-in-Water Emulsion using a Polyurethane Foam Bed, Ind. Eng. Chem. Res. **361** (1997) 4949−4953.

[58] R.M. Šećerov Sokolović, S.M. Sokolović, Effect of the Nature of Different Polymeric Fibres on Steady-State Bed Coalescence of an Oil-in-Water Emulsion, Ind. Eng. Chem. Res. **43** (2004) 6490−6495.

[59] R.M. Šećerov Sokolović, T.J. Vulić, S.M. Sokolović, Effect of Fluid Flow Orientation on the Coalescence of Oil Droplets in Steady-State Bed Coalescers, Ind. Eng. Chem. Res. **45** (2006) 3891−3895.

[60] R.M. Šećerov Sokolović, D.D. Govedarica, D.S. Sokolović, Separation of Oil-In-Water Emulsion using Two Coalescers of Different Geometry, J. Hazard. Mater. **175** (2010) 1001−1006.

[61] R.M. Šećerov Sokolović, T.J. Vulić, S.M. Sokolović, Effect of Bed Length on Steady-State Coalescence of Oil-in--Water Emulsion, Sep. Purif. Technol. **56** (2007) 79−84.

[62] D.D. Govedarica, R.M. Šećerov Sokolović, D.S. Sokolović, S.M. Sokolović, Evaluation of the Separation of Liquid––Liquid Dispersions by Flow through Fibre Beds, Ind. Eng. Chem. Res. **51** (2012) 16085−16091.

[63] D.S. Sokolović, R.M. Šećerov Sokolović, S.M. Sokolović, Proučavanje reoloških osobina nestabilnih emulzija mineralnog porekla, Hem. Ind. **67** (2013) 293−301.

[64] D.D. Govedarica, R.M. Šećerov Sokolović, D.S. Sokolović, S.M. Sokolović, A Novel Approach for the Estimation of

the Efficiency of Steady-State Fibre Bed Coalescence, Sep. Purif. Technol. **104** (2013) 268−275.

[65] R.M. Šećerov, Sokolovic, D.D. Govedarica, D.S. Sokolović, Selection of Filter Media for Steady-State Bed Coalescers, Ind. Eng. Chem. Res. **53** (2014) 2484−2490.

[66] S.S. Voyutskii,, K.A. Aklyanova, R. Panich, N. Fodiman, Mechanism of Separation of the Disperse Phase of Emulsions during Filtration, Dokl. Akad. Nauk SSSR **91** (1953) 1155−1158.

[67] S.S. Sareen, P.M. Rose, R.C. Gudesen, R.C. Kintner, Coalescence in Fibrous Beds, AIChE J. **12** (1966) 1045−1050.

[68] J.I. Rosenfeld, D.T. Wasan, Coalescence of Drops in a Liquid-Liquid Dispersion by Passage through a Fibrous Bed, Can. J. Chem. Eng. **52** (1974) 3−10.

[69] J. Golob, R. Modic, Coalescence of Liquid/Liquid Dispersions in Gravity Settlers, Trans. IChemE **55** (1977) 207−211.

[70] J. Golob, R. Grilc, R. Modic, Separation of Secondary Droplets on Fibrous Beds, Advance in Separation Science, Trieste, 1978.

[71] J. Golob, R. Grilc, R. Modic, Drop Coalescence in Liquid/Liquid Dispersions by Flow through Glass Fibre Beds, Chem. Eng. Res. Des. **62** (1984) 48−52.

[72] J. Golob, R. Grilc, R. Modic, Drop Coalescence in Liquid/Liquid Dispersions by Flow through Glass Fibre Beds. Part II, Chem. Eng. Res. Des. **64** (1986) 67−70.

[73] H. Soo, C. Radke, The Flow Mechanism of Dilute, Stable Emulsions in Porous Media, Ind. Eng. Chem. Fundam. **23** (1984) 342−347.

[74] H. Soo, C. Radke, Velocity Effects in Emulsion Flow through Porous Media, J. Colloid Interface Sci. **102** (1984) 462−476.

[75] H. Soo, C. Radke, Flow of Dilute, Stable Liquid and Solid Dispersions in Underground Porous Media, AIChE J. **31** (1985) 1926−1928.

[76] H. Soo, C. Radke, Filtration Model for the Flow of Dilute, Stable Emulsions in Porous Media-I. Theory, Chem. Eng. Sci. **41** (1986) 263−272.

[77] B. Maini, F. Wassmuth, L.L. Schramm, Fines Migration in Petroleum Reservoirs, Adv. Chem. Ser. **251** (1996) 369−373.

[78] S. Agarwal, V. Von Arnim, T. Stegmaier, H. Planck, A. Agarwal, Effect of Fibrous Coalescer Geometry and Operating Conditions on Emulsion Separation, Ind. Eng. Chem. Res. **52** (2013) 13164−13170.

[79] Y. Du, C. Shen, H. Zhang, Y. Huang, Effects of Flow Velocity and Nonionic Surfactant on Colloid Straining in Saturated Porous Media Under Unfavourable Conditions, Transp. Porous Media **98** (2013) 193−208.

[80] P. Vigneaux, P. Chenais, J. Hulin, Liquid-Liquid Flows in an Inclined Pipe, AIChE J. **34** (1988) 781−789.

[81] V.N. Burganos, C.A. Paraskeva, A.C. Payatakes, Monte Carlo Network Simulation of Horizontal, Upflow and Downflow Depth Filtration, AIChE J. **41** (1995) 272−285.

[82] R.N. Hazlett, Fibrous Bed Coalescence of Water: Steps in the Coalescence Process, Ind. Eng. Chem. Fundam. **8** (1969) 625−632.

[83] R.N. Hazlett, Fibrous Bed Coalescence of Water: Role of a Sulfonate Surfactant in the Coalescence Process, Ind. Eng. Chem. Fundam. **8** (1969) 633−640.

[84] R.N. Hazlett, H.W. Carhart, Removal of Water from Fuel using a Fibrous Bed, Filtr. Sep. **9** (1972) 456−462.

[85] R. Magiera, E. Blass, Separation of Liquid–Liquid Dispersions by Flow through Fibre Beds, Filtr. Sep. **34** (1997) 369−376.

[86] E. Dahlquist, F. Setterwall, Study on the Importance of Fibre Properties and Filter Structure on the Efficiency of Coalescence Filters, in Proceedings of FILTECH Conference, Utrecht, The Netherlands, Sep. 23−25, 1987, pp. 36−43.

[87] U. Daiminger, W. Nitsch, P. Plucinski, S. Hoffmann, Novel Techniques for Oil-Water Separation, J. Membr. Sci. **99** (1995) 197−203.

[88] M.A. Fahim, A.M. Akbar, Removal of Fine Oily Hazes from Wastewater using Deep Fibrous Bed Coalescer, J. Environ. Sci. Health. Environ. Sci. Eng. **19** (1984) 299−319.

[89] G. Deschamps, H. Caruel, M. Borredon, C. Albasi, J. Riba, C. Bonnin, C. Vignoles, Oil Removal from Water by Sorption on Hydrophobic Cotton Fibres. 2. Study of Sorption Properties in Dynamic Mode, Environ. Sci. Technol. **37** (2003) 5034−5039.

[90] C. Shin, G.Chase, Separation of Liquid Drops from Air by Glass Fibre Filters Augmented with Polystyrene Nanofibres. J. Dispersion Sci. Technol. **27** (2006) 5−9.

[91] C. Shin, G. Chase, Separation of Water-in-Oil Emulsions using Glass Fibre Media Augmented with Polymer Nanofibres, J. Dispersion Sci. Technol. **27** (2006) 517−522.

IZVOD

Separacija tečno–tečno primenom koalescentnog filtera u stacionarnom stanju

Radmila M. Šećerov Sokolović[1], Dunja S. Sokolović[2], Dragan D. Govedarica[1]

[1]*Tehnološki fakultet, Univerzitet u Novom Sadu, Bulevar cara Lazara 1, 21000 Novi Sad, Srbija*
[2]*Fakultet tehničkih nauka, Univerzitet u Novom Sadu, Trg Dositeja Obradovica 6, 21000 Novi Sad, Srbija*

(Pregledni rad)

Ovaj rad daje literturni pregled postojećeg znanja i razumevanja separacije tečno–tečno, koja je izuzetno rasprostranjena u praksi, ističući da je koalescer koji radi u stacionarnom stanju odlično rešenje za ovakvu separaciju. Koalescentna filtracija je metoda koja se pokazala kao izizetno efikasna separaciona tehnika u industriji. Zauljene vode zastupljene su u čitavoj procesnoj industriji. Voda je često rashladni fluid. U izmenjivačima toplote može da dođe do proboja organske faze koja se hladi i da voda bude kontaminirana. Sve pumpe i kompresori koriste ulja za podmazivanje. Zbog lošek zaptivanja, hlađenjem, pranjem i održavanjem kako te opreme tako i prostora gde je ona smeštena nastaju zauljene vode. Održavanje vozila i teških mašina takođe uzrokuju formiranje značajnih količina zauljenih otpadnih voda. Posebne operacije koje koriste ulja ili druge organske rastvarače kao što su solventna ekstrakcija, kaljenje, i slično izvor su nastajanja zauljenih otpadnih voda. Kod proizvodnje nafte postoji potreba separacije sistema tečno-tečno i to kako vode od nafte tako i nafte od ležišne vode. U procesima naftno-petrohemijske industrije koalescer sa slojem se sve češće primenjuje ne samo za tretpan otpadnih tokova nego i u procesima proizvodnje. Zbog složenosti fenomena koji se odigravaju tokom ove separacije projektovanje koalescera još uvek zahteva eksperimente. Ovaj literaturni pregled oslikava ključne fenomene koji uslovljavaju efikasnu separaciju kapi dispergovane faze kao što su koalescencija na granici faza, koalescencija između kapi, koalescencija u poroznom sloju, kao i proticanje emulzije kroz porozni sloj. Pored toga dat je pregled postojećeg znanja projektovanja koalescera. Opisane su najvažnije projektne veličine: brzina fluida, geometrija sloja, debljina sloja i orijentacija toka fluida kao do sada proučavane veličine. Zbog mogućih međusobnih zavisnosti i interakcja, površinskih pojava koje se događaju na granici faza tečno-tečno-čvrsto i dalje su neophodni eksperimenti za dimenzionisanje uređaja, odabiranje materijala za sloj i usvajanje radnih uslova.

Ključne reči: Separacija emulzija • Koalescencija kapi • Vlaknasti sloj • Koalescer

Sorption of rare-earth erbium from aqueous solution onto sol–gel-derived zirconia

Nafisa A. Salem[1], Sobhy M. Yakout[2,3]

[1]*Egyptian ministry of education, Cairo, Egypt*
[2]*Biochemistry Department, College of Science, King Saud University, Riyadh, Kingdom of Saudi Arabia*
[3]*Hot Laboratories Center, Atomic Energy Authority, Cairo, Egypt*

Abstract

Zirconia powder was synthesized via sol gel method and used for erbium sorption. The adsorption is strongly dependent on pH of the medium where the removal efficiency increases as the pH turns to alkaline range. The process was very fast initially and maximum adsorption was attained within 60 min of contact. Pseudo-second-order model and homogeneous particle diffusion model (HPDM) was found to be the best to correlate the diffusion of erbium into zirconia particles. Adsorption thermodynamic parameters were calculated. Erbium adsorption is an endothermic ($\Delta H > 0$) and good affinity of erbium ions towards the zirconia ($\Delta S > 0$).

Keywords: erbium, zirconia, sol–gel; kinetics; thermodynamics.

Available online at the Journal website: http://www.ache.org.rs/HI/

SCIENTIFIC PAPER

UDC 66:544.3:546.666:546.831

Hem. Ind. **70** (4) 383–390 (2016)

doi: 10.2298/HEMIND150911040S

Rare earth elements (REE) are gaining increasing importance, both in terms of research activity, and in terms of commercial products. The REE elements are being widely used in industry due to their metallurgical, optical and electronic properties. They are used in glass additives, fluorescent materials, catalysts, ceramics, lighters, supra-conductors and magnets or condensers [1]. They are also reported to be used as diagnosis reagents of magnetic resonance imaging (MRI) in medicine and some fertilizers in agriculture [2]. Among REE, erbium is used as a neutron-absorbing control rods. It is commonly used as a photographic filter, and due to its resilience it is useful as a metallurgical additive and in nuclear technology as nuclear poison, as neutron-absorbing control rods [3]. Anthropogenic activities may thus end up with REE metals in the hydrosphere and eventually in the food cycle and biosystem [4]. Therefore, the isolation of these elements from the environment is an important preventive measure against harmful exposure.

A good deal of interest has grown in the last decades in the application of inorganic ion-exchangers in nuclear technology due to their high mechanical, chemical and radiation stabilities, granulometric properties suitable for column operation and high ion-exchange capacity and adsorption efficiency [5]. Among these materials, metal oxides are a group of inorganic ion exchangers that has been investigated extensively in the treatment of radioactive waste [6]. Preparation method affects the crystallinity of the metal oxides and its ion exchange properties [7–14]. Sol–gel process is an attractive alternative to other methods for synthesis of inorganic ion-exchangers for many reasons: for example, low temperature synthesis, simple equipment that is used, thin film formability and so on. Adsorbent powders of metal oxide origin, synthesized by the sol-gel process in this work, have not previously been used in removing erbium from aqueous solutions.

In the present study, zirconia was successfully prepared by a sol–gel technique and used as an adsorbent for the removal of erbium ions from aqueous solution. Adsorption kinetics and thermodynamics of erbium adsorption by sol–gel-derived zirconia from aqueous solutions were studied.

METHODOLOGY

Chemicals and reagents

All chemicals used were of analytical reagent grade. An accurately weighed quantity of the erbium nitrate (purchased from Merck Company) was dissolved in deionized water to prepare a stock solution. Experimental solutions of the desired concentrations were obtained by successive dilutions. All sample bottles and glassware were cleaned; rinsed with deionized water and oven dried at 60 °C.

Preparation and characterization of zirconia

In the present work, the synthesis of zirconia was carried out using sol–gel polymeric route. Briefly polymerization reaction between urea and formaldehyde was carried out at 70–80 °C with stirring for 1 h in an alkaline medium (pH 8–9) to form the respective resin. Zirconium nitrate was added during the resin form-

Correspondence: N.A. Salem, Egyptian ministry of education, Cairo, Egypt.
E-mail: nasalem2015@yahoo.com
Paper received: 11 September, 2014
Paper accepted: 15 July, 2015

ation. Ethylene glycol was used to terminate the polymerization reaction. The produced gel was slowly dried at 120 °C and then calcined at 900 °C for 2 h to produce the zirconia powder [15].

The X-ray powder diffraction patterns of the prepared material were recorded on film at room temperature in a Philips XRG3100 X-ray diffractometer using CuKα X-ray operated at 30 kV and 30 mA with a fixed slit. FTIR analysis was investigated by a Fourier transform infrared spectrometer (IRPrestige-21, Japan). The thermogravimetric analysis (TGA) was carried out using Shimadzu TGA-50 analyzer, Japan.

Sorption studies

100 mg of zirconia powder in 25 ml conical flasks containing 10 ml of erbium solution (10^{-2} M) were mixed. The conical flasks then covered with aluminum foil and were then placed in a thermostatic shaker at room temperature for different time intervals. The adsorbent was finally removed by filtration, erbium concentration was determined radiometrically, using a NaI crystal using a pulse height multi-channel analyzer (McA) model 800 obtained from USA. Influence of solution pH on the sorption of erbium (30 ppm) was studied in the pH range of 2.0 to 10.0 under similar experimental conditions. Before each experiment, the solution pH was initially adjusted using HCl and/or NaOH depending on the required pH value. The thermodynamic studies were investigated by carrying out batch study at different temperatures. The temperatures chosen for study were 298, 313 and 333 K. The temperature of the erbium solution was adjusted using a thermostatic water bath (Memmert WB29 Model). The erbium uptake *qt* (mg/g) at any time *t* was calculated from the mass balance as follows:

$$q_t = [(A_o - A_t) / A_o] c_o \frac{V}{m} \quad (1)$$

where A_o and A_t are the initial and time interval activities of metal ion in solution, V is the volume of the solution (L) and m is the weight of the adsorbent (g) and c_o is the initial concentration (mmol/l) of the metal ion used.

RESULTS AND DISCUSSION

X-ray diffraction (XRD) analysis

X-ray diffraction is one of the techniques commonly used for the structural characterization of inorganic ion-exchangers. The X-ray diffraction (XRD) patterns using CuKα of sol–gel-derived zirconia are shown in Fig. 1. By analyzing the XRD patterns of the synthesized materials, it was observed that X-ray pattern showed the monoclinic zirconium phase at 900 °C. It was observed that the three strongest peaks ($2\theta \approx 30$, 50 and 60°) could be assigned to zirconia [16]. The peak at 2θ 28° is considered due to the monoclinic phase. The sharp peak at 2θ 30° corresponds to tetragonal phase [17].

FTIR characterization

Infrared spectra of the prepared zirconia were carried out in the range of 200–4000 cm^{-1} and shown in Fig. 2. The broad absorption band in the range 3396––2950 cm^{-1} is due to the stretching vibrations of the water molecule OH groups [18], whereas the absorption band which appears at 1624.5 cm^{-1} is characteristic of the bending vibration of water molecules. It is uncertain whether the water observed in these spectra reflects the composition of the surface resulting from the heating process, or water which had rapidly reached to the surface during cooling. The peaks at 1124.8 and 800 cm^{-1} are due to the bending vibration of hydroxyl groups bound to zirconia.

Effect of pH

It is known that pH is important factor for the adsorption of metal ions on the adsorbents. Specifically it affects the solution chemistry of the solute as well as the functional groups present in the sorbent**.** Results of the effect of solution pH on adsorption of erbium ions on the zirconia are shown in Fig. 3. The plot shows a

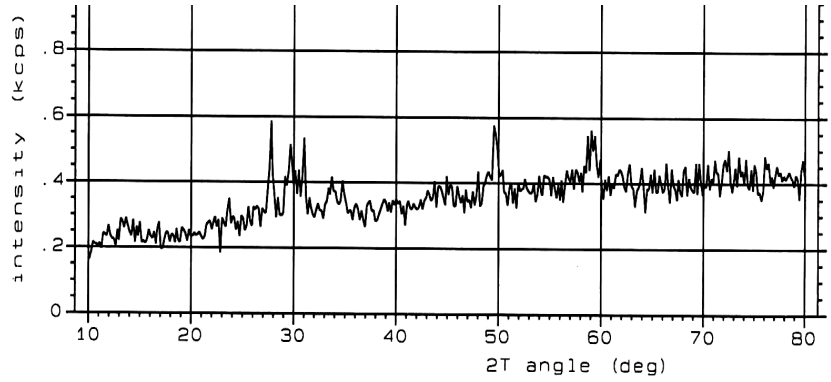

Figure 1. X-ray diffraction pattern of prepared zirconia at 900 °C.

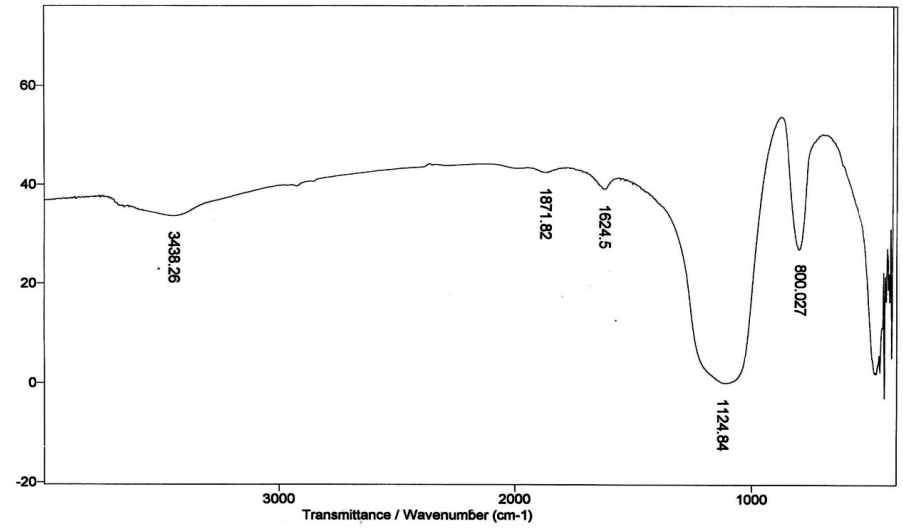

Figure 2. IR spectrum of prepared zirconia.

marked influence with a gradual rise in the uptake with increase in pH from 2 to 5 and thereafter it remained constant. The variation in the removal of the erbium with respect to pH can be elucidated by considering the functional groups present on the surface of the zirconia and the nature of the physicochemical interaction of the species in solution. Zirconia contains hydroxyl groups which can act good role in ion-exchange reaction through the substitution of its protons by erbium ion, according to the following reactions [19]:

$$M^{n+} + m(^{-}OH) \rightleftarrows M(OOC^{-})_{m}^{n-m} + mH^{+} \quad (2)$$

Where M^{n+}= metal ion with n+ charge, $^{-}$OH = hydroxyl group, and mH^{+} = number of protons released. In such a system, for low pH, because of the high concentration of H^{+}, there is competition of excess H^{+} with erbium ions for binding onto the biomass surface. Then Eq. (2) lies to the left. At the same time the predominant charges on Zirconia are positive, which results in the lower uptake of positively charged erbium ions on Zirconia. By increased pH, active sorption sites available for erbium ions increase as results of deprotonating of ion exchange sites and then negative charge on the sorbent increases. Therefore, electrostatic attraction between the negatively charged sorbent surface and the positively charged erbium ions will occur. This means that Eq. (2) precedes further to the right and metal ion removal is increased. Within this pH range, the ion exchange process is the major mechanism for removal of metal ion from solution. In the subsequent studies, experiments were performed in the solution pH value of 5 to avoid any possible hydroxide precipitation. Further, a decrease in the solution pH was observed after equilibration as compared to the initial solution pH. The drop in equilibrium pH suggests that H^{+} ions are liberated from the solid surface into the aqueous phase as a result of the exchange with metal cations.

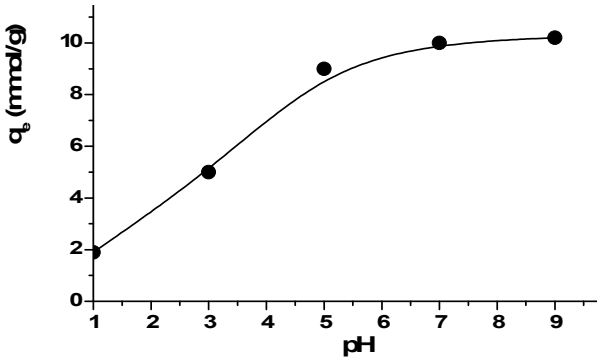

Figure 3. Effect of solution pH on uptake of erbium by zirconia.

Effect of contact time and temperature

The adsorption profile of erbium uptake with time at different temperature is shown in Fig. 4. The removal curves are single, smooth and continuous leading to saturation, suggesting possible monolayer coverage of erbium ions on the surface of the zirconia and typically 80–90 % adsorption of the equilibrium value for each ion occurred within 30 min. Erbium removal increases with time and attained equilibrium at 60 min. Short equilibrium time is one of the important considerations for economical wastewater treatment applications. The initial rapid adsorption of erbium ions on zirconia is due to the availability of larger number of vacant adsorption sites for the erbium of the bulk solution. The subsequent slower adsorption is likely because of the competition among the erbium ions for the limited number of vacant adsorption sites. Thus the driving concentration gradient between the bulk sol-

ution and the solid surface is the main factor controlling the kinetics of the system.

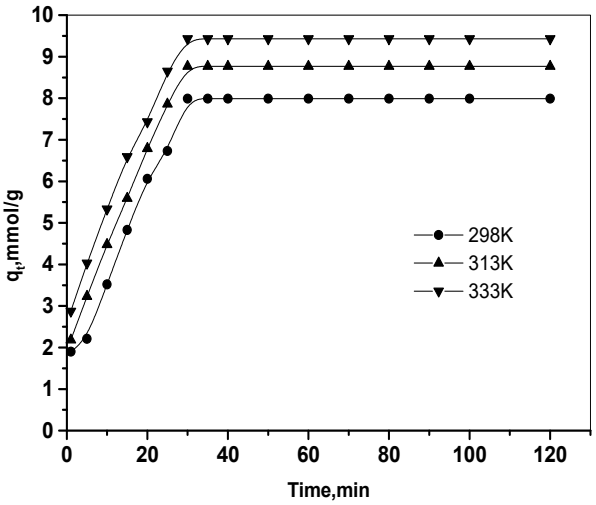

Figure 4. Effect of contact time on erbium ions adsorption onto prepared zirconia at 298, 313 and 333 K.

The equilibrium sorption capacity of erbium onto zirconia was found to increase with increasing temperature, increasing indicating that the erbium ion sorption on the adsorbent was favored at higher temperatures. The sorption of erbium is endothermic, thus the extent of sorption increased with increasing temperature. The sorption of erbium by zirconia involves not only physical, but also chemical sorption. At high temperature, ions are readily dehydrated, and therefore their sorption becomes more favorable.

Kinetic study

Analysis of experimental date at various time make possible to calculate the kinetic parameters, and take some information for designing and modeling the adsorption processes. To understand the adsorption mechanism of zirconia for erbium, the adsorption kinetics was investigated using pseudo first order [20] and pseudo second order [21], with Eq. (3) and Eq. (4) respectively:

$$\log(q_e - q_t) = \log q_e - \frac{k_1}{2.303} t \text{ , pseudo-first order} \quad (3)$$

$$\frac{t}{q_t} = \frac{1}{k_2 q_e^2} + \frac{1}{q_e} t \text{ , pseudo second order} \quad (4)$$

where q_t and q_e are the amount adsorbed (mmol g^{-1}) at time t and at equilibrium time, respectively and K_1 and K_2 are the first and second rate adsorption constants, respectively. By testing the two plots of $\log(q_e - q_t)$ *versus* t (Fig. 5), and (t/q_t) *versus* t (Fig. 6), the rate constants, k_1 and k_2, can be calculated. The conformity between experimental data and each model predicted values was expressed by the correlation coefficient (R^2) in Table 1.

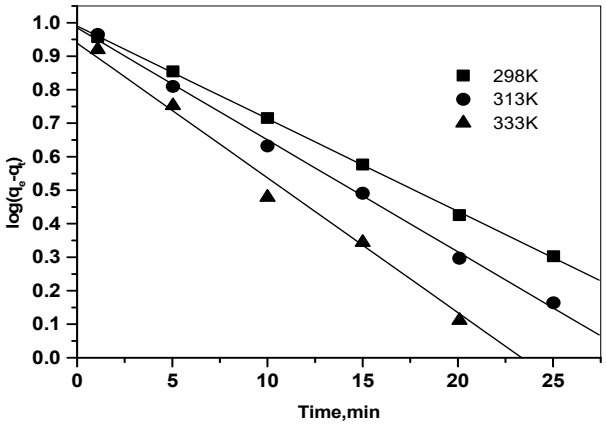

Figure 5. Pseudo first order plots for the sorption of erbium ions onto prepared zirconia at 298 313 and 333 K.

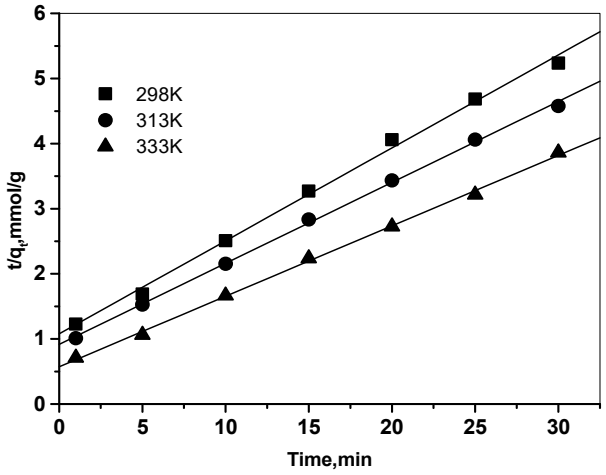

Figure 6. Pseudo second order plots for the sorption of erbium ions onto prepared zirconia at 298, 313 and 333 K.

Table 1. The calculated parameters of the pseudo-second order kinetic model; R^2 = 0.999

Temperature K	q_e mmol/g	h mmol/(g min)	K_2 g/(mmol min)
298	8.8	2.5	0.03
313	9.9	4.3	0.04
333	11.9	10.7	0.08

The result indicates that the pseudo-second-order model (R^2 = 0.98) is more suitable than the pseudo-first-order kinetic model (R^2 = 0.92) for erbium adsorption on zirconia, and that the adsorption complies with the pseudo-second-order reaction. The calculated q_e values obtained from the first-order kinetic model do not give responsible values, which are too low compared with experimental q_e values. Estimated q_e values of pseudo-second-order model accurately predict the

adsorption kinetics over the entire working times and temperatures. Therefore, this model has enough sufficiency for acceptable accurate prediction of the kinetics of erbium adsorption onto zirconia. This suggested the overall rate of the adsorption process is most likely to be controlled by the chemisorption process [22] and rate of reaction is directly proportional to the number of active sites on the surface of adsorbent. From Table 1, it can be shown that the values of the initial sorption rate ($h = k_2 q_e^2$) increased with the increase in temperature. According to pseudo second order model, the adsorption rate dq_t/dt is proportional to the second order of q_e–q_t. Since zirconia has relatively high equilibrium adsorption density q_e, the adsorption rates become very fast and the equilibrium times are short. Such short equilibrium times coupled with high adsorption capacity indicate high degree of affinity between adsorbate molecules and carbon surface [23]. These results explain that the pseudo second order sorption mechanism is predominant and that the overall rate constant of each ion exchange process appears to be controlled by the chemical sorption process [24–26].

One of the most widely models describe the kinetic of ion exchange data and can predict the actual slowest step is the homogeneous particle diffusion model (HPDM). In this model, the rate-determining step of sorption normally involves two mainly steps of film diffusion that involve diffusion of ions through the liquid film surrounding the adsorbent and/or particle diffusion that involve diffusion of ions into the adsorbent beads. If film diffusion is rate-determining step, the following expression can be utilized to calculate the diffusion coefficient:

$$-\ln(1-X) = \frac{3Dc}{r_o \delta c_r} t \quad (5)$$

where c and c_r are the equilibrium concentrations of the ion in solution and solid phases, respectively, D is the diffusion coefficient in the liquid phase, X is the fraction attainment of equilibrium or extent of adsorbent conversion, r_o is the radius of the adsorbent particle, δ is the thickness of the liquid film. If film diffusion was involved in erbium adsorption, then the plot of −ln(1 − X) *vs*. time would be the straight line through the origin.

If the diffusion of erbium ions through the adsorbent beads is the slowest step, the particle diffusion will be the rate determining step and the particle diffusion model can be apply to calculate the diffusion coefficients. Then, the rate equation is expressed as:

$$-\ln(1-X^2) = \frac{2D_r \pi^2}{r_o^2} t \quad (6)$$

where D_r is the particle diffusion coefficient. If particle diffusion was involved in erbium adsorption, then the plot of −ln(1 − X^2) *vs*. time would be the straight line through the origin.

The kinetic rate data of erbium ions sorbed onto zirconia powder were tested using Eqs. (4) and (5). The kinetic plots of ln(1 − X) *vs*. time exhibit straight lines that do not pass through the origin for all studied temperatures. This indicating that the film diffusion model does not control the rate of the sorption processes. When adsorption starts, reacted layer thickness is still very small and film resistance to erbium ions diffusion is therefore comparable to adsorbent outer shell resistance. Moreover, ln (1 − X^2) *vs. t* plots is given in Fig. 7. Straight line with zero intercept would suggest erbium adsorption to be controlled by its diffusion within the particles of zirconia.

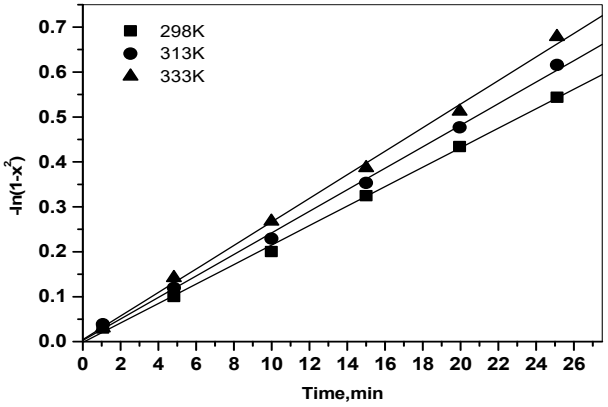

Figure 7. Plots of –ln(1 – X^2) as a function of time for the diffusion of erbium ions onto prepared zirconia at 298, 313 and 333 K.

Thermodynamic studies

In any sorption process, both energy and entropy considerations must be taken into account in order to determine what process will occur spontaneously. Values of thermodynamic parameters are the actual indicators for practical application of a process. Diffusion coefficient of erbium sorption is expressed as a function of temperature by the following Arrhenius type relationship:

$$\ln D_r = \ln D_0 - (E_a / RT) \quad (7)$$

where D_0 is a pre-exponential constant analogous to Arrhenius frequency factor.

A plot of ln D_r *vs*. 1/T was found to be linear (Fig. 8). The E_a value calculated from the slope of the plot is equal to 9.95 kJ mol^{-1}. The relatively low activation energy (less than 42 kJ/mol) suggested that erbium sorption is a diffusion-controlled process [27].

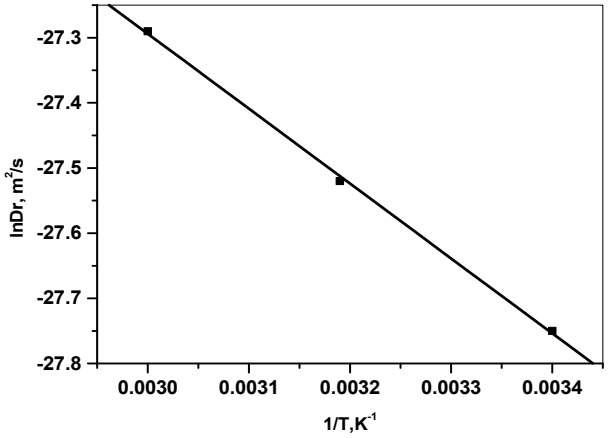

Figure 8. Arrhenius plot for the sorption of erbium ions onto zirconia.

The other thermodynamic parameters, change in the free energy (ΔG), enthalpy (ΔH) and entropy (ΔS), were determined by using following equations [28,29]:

$$D_0 = 2.72(kTd^2 / h)\exp(\Delta S / R) \quad (8)$$

$$\Delta G = \Delta H - T\Delta S = E_a - RT - T\Delta S \quad (9)$$

where k is the Boltzmann constant, h is the Plank constant, d is the average distance between two successive positions, R is the gas constant and T is the absolute temperature. Assuming that the value of d is equal to 5×10^{-8} cm [30], the values of thermodynamic parameters were calculated and presented in Table 2. The positive values ΔH indicate the presence of an energy barrier in the sorption and endothermic process [31]. The positive value of entropy change reflects good affinity of erbium ions towards the sorbent and the increasing randomness at the solid-solution interface during the sorption process [32]. The positive ΔG values suggest the existence of an energy barrier and that the reaction is non-spontaneous process [33].

Table 2. Thermodynamic parameters of the sorption of erbium ions onto zirconia; R^2 = 0.999

T	$D_x\times10^{11}$	$D_o\times10^{12}$	E_a	ΔS	ΔG	ΔH
K	m^2/s	m^2/s	KJ/mol	J/mol K	KJ/mol	KJ/mol
298	11.1	8.9	9.95	439.0	127.1	7.3
313		44,9				
333		49.8				

CONCLUSIONS

Using of zirconia for erbium ion removal from aqueous solution was studied. The highest removal efficiency of zirconia for erbium ion was obtained at pH 5.0. The adsorption can be explained as ion exchange mechanism between erbium ion and hydroxyl groups. The kinetics studies showed that most of the erbium ion uptake rapidly occurred in the first 30 min, and the adsorption equilibrium was obtained within one hour. The adsorption kinetics was well described by pseudo--second-order and homogeneous particle diffusion models implied that chemisorption is a predominant mechanism and particle diffusion control erbium adsorption. Based on the values obtained from some adsorption thermodynamic parameters such as ΔH, ΔS and ΔG, it was found that erbium adsorption on zirconia is an endothermic and good affinity of erbium ions towards the sorbent.

Acknowledgments

This project was supported by King Saud University, Deanship of Scientific Research, College of science Research Centre.

REFERENCES

[1] T.G. Goonan, Rare Earth Elements — End Use and Recyclability, U.S. Geological Survey Scientific Investigations Report, 2011 (http://pubs.usgs.gov/sir/2011/5094/pdf/sir2011-5094.pdf).

[2] P. Liang, Y. Liu, L. Guo, Determination of trace rare earth elements by inductively coupled plasma atomic emission spectrometry after preconcentration with multi-walled carbon nanotubes, Spectrochim. Acta, B **60** (2005) 125–129.

[3] N.S. Awwad, H.M. Gad, M.I. Ahmad, H.F. Aly, Sorption of lanthanum and erbium from aqueous solution by activated carbon prepared from rice husk, Colloids Surfaces, B **81** (2010) 593–599.

[4] S.U. Yesiller, A.E. Eroğlu, T. Shahwan, Removal of aqueous rare earth elements (REEs) using nano-iron based materials, J. Ind. Eng. Chem. **19** (2013) 898–907.

[5] S.A. Nabi, M. Naushad, Inamuddin, Synthesis and characterization of a new inorganic cation-exchanger – Zr(IV) tungstomolybdate: analytical applications for metal content determination in real sample and synthetic mixture, J. Hazard. Mater. **142** (2007) 404–411.

[6] A. Ruvarac, Inorganic Ion Exchange Materials, 1982.

[7] K.M. El-Rahman, A.M. El-Kamash, M.R. El-Sourogy, N.M. Abdel- Moniem, Thermodynamic modeling for the removal of Cs^+, Sr^{2+}, Ca^{2+} and Mg^{2+} ions from aqueous waste solutions using zeolite A, J. Radioanl. Nucl. Chem. **288** (2006) 221–230.

[8] A.M. El-Kamash, A.A. Zaki, M. Abdel-Geleel, Modeling batch kinetics and thermodynamics of zinc and cadmium ions removal from waste solutions using synthetic zeolite A, J. Hazard. Mater. **127** (2005) 211–220.

[9] P.K. Sinha, K.B. Lal, P.K. Panicker, V. Krishnasamy, A comparative-study on indigenously available synthetic zeolites for removal of strontium from solutions by ion-exchange, Radiochem. Acta **73** (1996) 157–163.

[10] E.S. Zakaria, I.M. Ali, I.M. El-Nagger, Thermodynamics and ion exchange equilibria of Gd^{3+}, Eu^{3+} and Ce^{3+} ions on H^+ form of titanium(IV) antimonate, Colloids Surfaces, A **210** (2002) 33–40.

[11] M.M. Abou-Mesalam, I.M. El-Nagger, Diffusion mechanism of Cs^{+}, Zn^{2+} and Eu^{3+} ions in the particles of zirconium titanate ion exchanger using radioactive tracers, Colloids Surfaces, A **215** (2003) 205–211.

[12] I.M. Ismail, M.R. El-Sourogy, N.M. abdel- Moniem, H. Aly, Equilibrium and Kinetic Studies of the Sorption of Caesium by Potassium Nickel Hexacyanoferrate Complex, J. Radioanal. Nucl. Chem. **240** (1999) 59–67.

[13] I.M. Ismail, M.R. El-Sourogy, N.M. Abdel- Moniem, H.F. Aly, Characterization, and Utilization of Potassium Nickel Hexacyanoferrate for the Separation of Caesium and Cobalt from Contaminated Waste Water, J. Radioanal. Nucl. Chem. **237** (1998) 97–102.

[14] T. Moller, R. Harjula, A. Dye, J. Newton, E. Tusa, S. Amin, M. Webb, A. Araya, Uptake of ^{85}Sr, ^{134}Cs and ^{57}Co by antimony silicates doped with Ti^{4+}, Nb^{5+}, Mo^{6+} and W^{6+}, J. Mater. Chem. **11** (2001) 1526–1532.

[15] H.S. Hassan, Ph.D. Thesis, Faculty of Science, Mansoura University, 2004.

[16] H. Liu, X. Sun, C. Yin, C. Hu, Removal of phosphate by mesoporous ZrO_2, J. Hazard. Mat. **151** (2008) 616–622.

[17] G. Negrón, C.X. Hernández, D. Angeles, L. Lomas, E. Gónzalez, J. Méndez, Comparative study of regioselective synthesis of beta-aminoalcohols under solventless conditions catalyzed by sulfated zirconia and SZ/MCM-41, Molecules **12** (2007) 2515–2532.

[18] D.R. Uhlmann, B.J. Zelinski, C.E. Wsek, The ceramist as chemist. Opportunities for New Materials in Better Ceramics through Chemistry, C.I. Brinker, D.E. Clark, D.R. Ulrich (Eds.), Cambridge University Press, Cambridge, 1984.

[19] N. Khalid, S. Ahmad, A. Toheed, J. Ahmed, Potential of rice husks for antimony removal, Appl. Radiat. Isotopes **52** (2000) 31–38.

[20] S. Lagergren, About the theory of so-called adsorption of soluble substances, Kungl. Svenska Vetenskaps akademien Handlingar Band **24** (1898) 1–39.

[21] Y.S. Ho, G. McKay, The kinetics of sorption of basic dyes from aqueous solution by Sphagnum moss peat, Can. J. Chem. Eng. **76** (1998) 822–827.

[22] B. Singha, S.K. Das, Adsorptive removal of Cu(II) from aqueous solution and industrial effluent using natural/agricultural wastes, Colloids Surfaces, B **107** (2013) 97–106.

[23] M.S. Chiou, H.Y. Li, Equilibrium and kinetic modeling of adsorption of reactive dye on cross-linked chitosan beads, J. Hazard. Mat. **93** (2002) 233–248.

[24] M.S. Chiou, Y.S. Ho, H.Y. Li, Adsorption Behavior of Dye AAVN and RB4 in Acid Solutions on Chemically Cross-Linked Chitosan Beads, J. Chin. Chem. Eng. **34** (2003) 625–634.

[25] G. McKay, Y.S. Ho, Pseudo-second order model for sorption processes, J. Process Biochem. **34** (1999) 451–465.

[26] D. Nibou, H. Mekatel, S. Amokrane, M. Barkat, M. Trari, Adsorption of Zn^{2+} ions onto NaA and NaX zeolites: Kinetic, equilibrium and thermodynamic studies, J. Hazard. Mater. **73** (2010) 637–646.

[27] K.G. Scheckel, D.L. Sparks, Temperature Effects on Nickel Sorption Kinetics at the Mineral–Water Interface, J. Soil Sci. Soc. Am. **65** (2001) 719–728.

[28] A. Dyer, M. Pillinger, R. Harjula, S. Amin, Sorption characteristics of radionuclides on synthetic birnessite-type layered manganese oxides, J. Mater. Chem. **10** (2000) 1867–1874.

[29] F. Helfferich, Ion Exchange, McGraw-Hill, New York, 1962.

[30] Y.S. Ho, G. McKay, A comparison of chemisorption kinetic models applied to pollutant removal on various sorbents, Process Saf. Environ. Prot. **76** (1998) 332–340.

[31] B.H. Hameed, A.A. Ahmad, N. Aziz, Isotherms, kinetics and thermodynamics of acid dye adsorption on activated palm ash, Chem. Eng. J. **133** (2007) 195–203.

[32] N. Yeddou Mezenner, A. Bensmaili, Kinetics and thermodynamic study of phosphate adsorption on iron hydroxide-eggshell waste, Chem. Eng. J. **147** (2009) 87–96.

[33] G. Atun, B. Bilgin, A. Kilislioglu, Kinetic of isotopic exchange between strontium polymolybdate and strontium ions in aqueous solution, Appl. Radiat. Isot. **56** (2002) 797–803.

IZVOD

SORPCIJA ERBIJUMA IZ VODENIH RASTVORA NA SOL–GEL DOBIJENOM CIRKONIJUM-OKSIDU

Nafisa A. Salem[1], Sobhy M. Yakout[2,3]

[1]*Egyptian ministry of education, Cairo, Egypt*
[2]*Biochemistry Department, College of Science, King Saud University, Riyadh, Kingdom of Saudi Arabia*
[3]*Hot Laboratories Center, Atomic Energy Authority, Cairo, Egypt*

(Naučni rad)

Prah cirkonijum-oksida je sintetisan sol–gel postupkom i korišćen za sorpciju erbijuma. Adsorpcija uveliko zavisi od pH vrednosti medijuma gde efikasnost otklanjanja raste u odnosu povratka pH u alkalni spektar. Proces je prvobitno veoma brz i maksimalna adsorpcija je postignuta u 60 min nakon kontakta. model Pseudo-drugi reda reakcije i model difuzije homogenih čestica (HPDM) su najbolji u korelaciji difuzije erbijuma na čestice cirkonijuma. Izračunata je adsorpcija termodinamičkih parametara. Adsorpcija erbijuma je endotermička ($\Delta H > 0$) i dobrog je afiniteta erbijumovih jona u odnosu na cirkonijum ($\Delta S > 0$).

Ključne reči: Erbijum • Cirkonijum • Sol–gel • Kinetika • Termodinamika

Ultrasound-assisted extraction of polyphenols from *Thymus serpyllum* and its antioxidant activity

Aleksandra A. Jovanović[1], Verica Đorđević[1], Gordana M. Zdunić[2], Katarina P. Šavikin[2], Dejan Pljevljakušić[2], Branko M. Bugarski[1]

[1]*Faculty of Technology and Metallurgy, Department of Chemical Engineering, University of Belgrade, Belgrade, Serbia*
[2]*Institute for Medicinal Plant Research "Dr Josif Pančić", Belgrade, Serbia*

Abstract

The present study was designed to establish and optimize a method for extracting natural bioactive compounds from *Thymus serpyllum* which possess antioxidant, antimicrobial, antispasmodic and stimulant properties. Ultrasound-assisted extraction (UAE) is a well-established method in the processing of plant material, particularly for extraction of bioactive substances such as polyphenols. The influential factors including extraction time (3, 7 and 10 min), solid:solvent ratio (1:10, 1:20 and 1:30) and particle size (0.3, 0.7 and 1.5 mm), have been studied to optimize the extraction process, while using 30% ethanol as an extraction medium and amplitude set to 65%. The yield of UAE was expressed *via* total phenol content and antioxidant activity of the obtained extracts. The optimum process parameters were found to be: extraction time, 3 min; solid:solvent ratio, 1:30; particle size, 0.3 mm. Under these conditions, the yield of total polyphenols was raised up to 23.03 mg/L GA and the highest antioxidant activity was recorded (10.32 mmol/mg Trolox and IC_{50} of 3.00 mg/ml).

Keywords: *Thymus serpyllum*, ultrasound-assisted extraction, polyphenols, antioxidant activity.

Available online at the Journal website: http://www.ache.org.rs/HI/

SCIENTIFIC PAPER

UDC 635.71:66.061:615:54

Hem. Ind. **70** (4) 391–398 (2016)

doi: 10.2298/HEMIND150629044J

Lamiaceae family represents an important component of Mediterranean shrub vegetation, especially in dry and arid environments. *Thymus* species grow wild in the Mediterranean environment and there are several ecotypes which are different in morphology and highly chemically polymorphic [1,2]. The number of species within this genus is depending on taxonomical point of view and usually assumed to be larger than 200 [3]. The diversity of biological activities of these plants may be a consequence of their rich chemical diversity. *Thymus serpyllum*, well-known as wild thyme is perennial, herbaceous plant of genus *Thymus* and possesses aromatic, antiseptic, analgesic, diuretic, diaphoretic, carminative, antioxidant, spasmolytic, anti-inflammatory and stimulant properties. Also, it has been used in mouth washes and gargles and against cough and cold because of antimicrobial activities of its extracts [4]. The main components of *T. serpyllum* are essential oils (44.4% carvacrol, 14% *o*-cymene, 6.47% α-terpineol, 6.06% α-pinene and 5.25% β-caryophyllene), phenolic acids (mainly rosmarinic, caffeic and chlorogenic acid) and flavonoids (naringenin, dihydroquercetin, apigenin, eriodictyol, quercetin and rutin). These secondary metabolites play important biological roles and possess pharmacological effects including antioxidant and anticarcinogenic activities, protection against coronary diseases (prevention of atherosclerosis, antiarrhythmic and antihypertensive effect), lipid lowering activity, effect on central nervous system, antimicrobial, anti-inflammatory and analgesic activities [4–6]. Content of polyphenolics and their structure (the number and position of the hydroxyl groups in a molecule) significantly influence the pharmacological properties of medicinal plants. Water, methanol and ethanol are the most frequently used solvents for extraction of polyphenolics from plant material. One of the frequently applied techniques for extraction of active compounds is extraction in the Soxhlet apparatus. Due to the relatively long extraction time and to the considerable amounts of the samples and consumed solvents, this technique tends to be replaced by more modern extraction methods [7]. In this study, dry flowering aerial part of *T. serpyllum* (*Serpylli herba*) was evaluated as a source of polyphenolic compounds, which are extracted by the application of ultrasound probe instead of the traditional ways of extraction (maceration, percolation, Soxhlet). Ultrasound extraction has become a good alternative extraction method when compared to classical methods due to its high efficiency, low energy, shortening of extraction time and solvent consumption. Ultrasound assisted extraction is a well-established method in the processing of

Correspondence: A.A. Jovanović, Faculty of Technology and Metallurgy, Department of Chemical Engineering, University of Belgrade, Karnegijeva 4, Belgrade, Serbia.
E-mail: cancarevica@tmf.bg.ac.rs
Paper received: 29 June, 2015
Paper accepted: 24 July, 2015

plant material, particularly for extraction of bioactive substances such as polyphenols [8]. The ultrasound waves in the extraction medium induce mechanical, cavitation and thermal effects that can lead to the disruption of cell walls, without causing significant changes in the structural and functional properties of the most target compounds [9]. Optimization of the extraction has been carried out through varying time of extraction, solid:solvent ratio and particle size.

In this paper, the extraction conditions for extracting polyphenols from *Serpylli herba* by using ultrasonic probe have been studied and optimum conditions for ultrasound-assisted extraction were established. Extraction efficiency was expressed *via* total polyphenols content (Folin–Ciocalteu method) and antioxidant activity (ABTS and DPPH methods) of the obtained extracts.

MATERIALS AND METHODS

Plant materials and reagents

In order to optimize the extraction method, air-dried herbs of wild thyme (*T. serpyllum*) were commercially purchased from the Institute for Medicinal Plant Research "Dr Josif Pančić", Belgrade, Serbia. These commercial samples differ in particle size (0.3, 0.7 and 1.5 mm).

The following reagents of the analytical purity grade were used: ethanol (Fisher Science, UK), Folin–Ciocalteu reagent (Merck, Darmstadt, Germany), sodium carbonate (Fisher Science, UK), gallic acid (Merck, Darmstadt, Germany), 2,2'-azino-bis(3-ethylbenzothiazoline-6-sulphonic acid) or ABTS (Sigma–Aldrich, St. Louis, MO, USA), potassium persulfate (Centrohem, Belgrade, Serbia), 6-hydroxy-2,5,7,8-tetramethylchroman-2-carboxylic acid or Trolox (Sigma–Aldrich, St. Louis, MO, USA) and 2,2-diphenyl-1-picrylhydrazyl or DPPH (Sigma-Aldrich, St. Louis, MO, USA).

Ultrasound-assisted extraction

Ultrasound-assisted extractions were performed by using ultrasound probe (Bandelin, Ultrasonic Homogenizer HD 2200, processor of 200 W output with a 20 kHz converter and a solid titanium probe of 13 mm). Amplitude applied for the extraction was set to 65%. Samples for ultrasound probe treatment were placed in 250 mL beaker and mixed with appropriate solvent (30% ethanol) in different solid:solvent ratio (1:10, 1:20 and 1:30). Larger volume of extraction mixture was applied because of technical properties of the probe. Samples were treated for 3, 7 and 10 min with power ultrasound, high intensity and low frequency at room temperature. After extraction, the obtained extracts were filtered through a 0.45 μm cellulose filter and reconstituted filtrates were properly diluted up to a required concentration for further analysis.

Determination of total polyphenolic content

Total polyphenolic content in ethanol extracts was determined by the Folin–Ciocalteu (FC) procedure. A volume of 6 mL water and 100 μL properly diluted sample was mixed with 500 μL of FC reagent previously diluted with distilled water in a 1:2 ratio. After that, 1.5 mL of 20% sodium carbonate solution was added and the volume was made up to 10 mL. The samples were shaken and left in the dark for 2 h to react. Then the absorbance of blue coloration was measured at 765 nm against a blank using the Shimadzu UV spectrophotometer UV-1800. The blank contained water, 30% ethanol, FC reagent and sodium carbonate solution in the same ratio as in the samples. All samples were done in triplicate. The same procedure was done with gallic acid standard (concentrations of 100, 200, 300, 400, 500, 600 and 700 mg/L) and a calibration curve was calculated. The total polyphenolic content (TPC) was expressed as milligram per litre of gallic acid equivalents (mg/L GAE) [10].

Determination of free radical-scavenging ability

ABTS method

The $ABTS^{\bullet+}$ scavenging assay was based on the procedure described by Re *et al*. with a slight modification [11]. $ABTS^{\bullet+}$ was produced by mixing 5 ml of ABTS water stock solution (7 mM) with 88 μL of potassium persulfate (140 mM). Before use, the mixture was incubated in a fridge in the dark for 16–20 h to prepare ABTS radical cation ($ABTS^{\bullet+}$). Freshly-prepared $ABTS^{\bullet+}$ working solution ($ABTS^{\bullet+}$ stock solution diluted with ethanol to achieve an absorbance of 0.70±0.02 at 734 nm) was used. To a volume of 2 ml of $ABTS^{\bullet+}$ working solution, 20 μL of diluted extract were added (100 μL of ethanol extract and 900 μL of solvent) and, after 6 min of incubation in the dark, the absorbance was measured at 734 nm. The blank contained 2 mL of ethanol and 20 μL of solvent. The scavenging capacity was calculated as $\Delta A = A_0 - A_x$ (where A_0 refers to the absorbance of 2 mL $ABTS^{\bullet+}$ working solution and 20 μL of solvent; A_x is the absorbance of sample). All measurements were performed in triplicate. The same procedure was done with Trolox standard (concentrations of 0.2, 0.4, 0.6, 0.8 and 1 mM), and a calibration curve was calculated. The antioxidant activity was expressed as mmol per mg of Trolox (mmol/mg Trolox).

DPPH method

This method is based on the reduction of stable DPPH radical by antioxidants present in tested extracts. In the presence of antioxidants purple color of the DPPH radical solution changes to a bright yellow and the intensity of this change can be monitored spectro-

photometrically [12]. Briefly, DPPH was diluted in ethanol to achieve an absorbance of 0.8 at 517 nm. Ethanol extracts were further diluted in ethanol to obtain concentration 5–160 μL/mL. After that, 200 μL of diluted extract was added to 2.8 mL of DPPH solution. The mixture was kept in dark for 20 min and the absorbance at 517 was measured. The blank contained 2.8 mL of ethanol and 200 μL of solvent. The scavenging IC_{50} = = $100(A_0 - A_x)/A_0$ capacity was calculated as (where A_0 refers to the absorbance of 2.8 mL DPPH working solution and 200 μL of solvent; A_x is the absorbance of sample). All determinations were performed in triplicate. Values of IC_{50} were calculated from the regression equation, prepared from the concentration of samples and percentage inhibition of DPPH. Results were expressed as IC_{50} (mg/mL), defined as the concentration of extract required to scavenge 50% of free radicals.

Statistical analysis

All data were subjected to analysis of variance (ANOVA), significant differences among mean values from triplicate analysis ($p < 0.05$) were determined by Duncan's multiple range tests with data analysis statistical tool of Statistica 7.0.

RESULTS

In order to study the effects of different extraction conditions of ultrasound-assisted extraction, three different particle size (0.3, 0.7 and 1.5 mm) were tested in this study in combination with different extraction time (3, 7 and 10 min) and solid:solvent ratio (1:10, 1:20 and 1:30). The obtained extracts were first tested for total polyphenols content by means of spectrophotometric analysis.

The highest content of polyphenols (23.03 mg/L GAE) was determined in the extract obtained at a particle size of 0.3 mm and solid:solvent ratio 1:30 after 3 min of extraction. The lowest total polyphenols content was detected in extracts obtained with a particle size of 1.5 mm and at solid:solvent ratio 1:10, after 3 and 10 min of the extraction (12.07–12.10 mg/L GAE). Statistical analysis by means of analysis of variance (ANOVA) confirmed a significant influence of solid:solvent ratio on the content of extracted phenolic compounds ($p < 0.05$). The influence of the particle size and extraction time did not prove to be statistically significant. The effects of extraction time and solid:solvent ratio on total polyphenols content is illustrated in 3D surface plot (Figure 1). As seen in Figure 1, TPC increases with increase in solid:solvent ratio, regardless extraction time. Figure 2 shows the effects of extraction time and particle size on TP and reveals the best conditions of extraction: particle size 0.2–0.4 mm and extraction time 2–4 min. In Figure 3, the surface plot shows the effect of solid:solvent ratio and particle size on TP. In the region of solid:solvent ratio 1:28–1:32 and particle size between 0.2 and 0.6 mm, the highest values of total polyphenols are recorded. As seen in Figure 3, there is no significant difference between the different particle sizes in total polyphenols content.

In the Tables 1 and 2 the results of two antioxidant activity assays (ABTS and DPPH method) are presented. Since these two assays are based on different reactions ($ABTS^{\bullet+}$ + any reducing agent *X* and DPPH + any molecule with a weak *X*–H bond), it is possible to obtain different results for the antioxidant capacity of the same samples and a better insight in their properties. The main limitations of these tests are that the probes are chemically very different from the radicals respon-

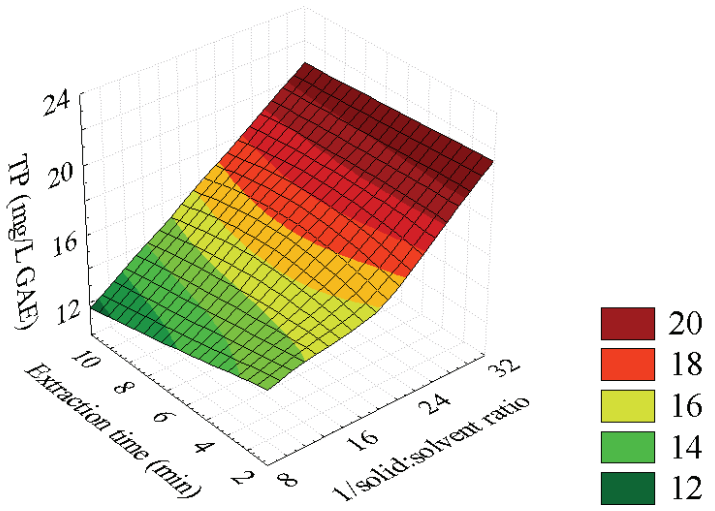

Figure 1. Effect of extraction time and solid:solvent ratio on total polyphenols content (mg/L GAE) of T.serpyllum. The value of the missing independent variable in the plot was kept at the centre point.

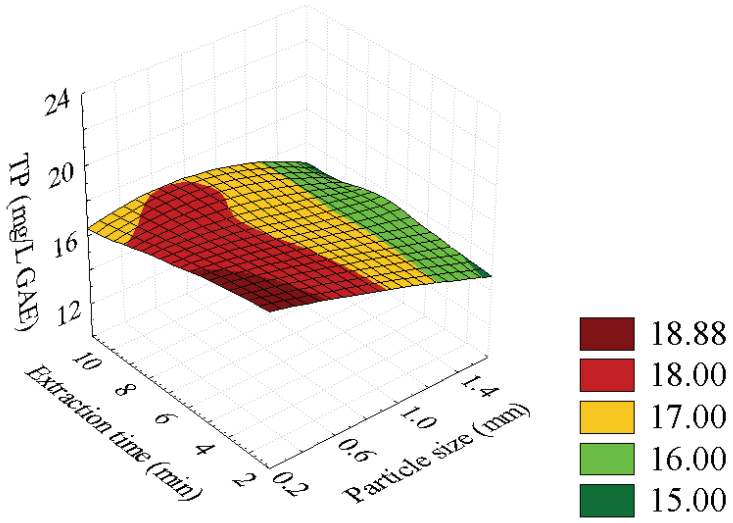

Figure 2. Effect of extraction time and particle size on total polyphenols content (mg/L GAE) of T.serpyllum. The value of the missing independent variable in the plot was kept at the centre point.

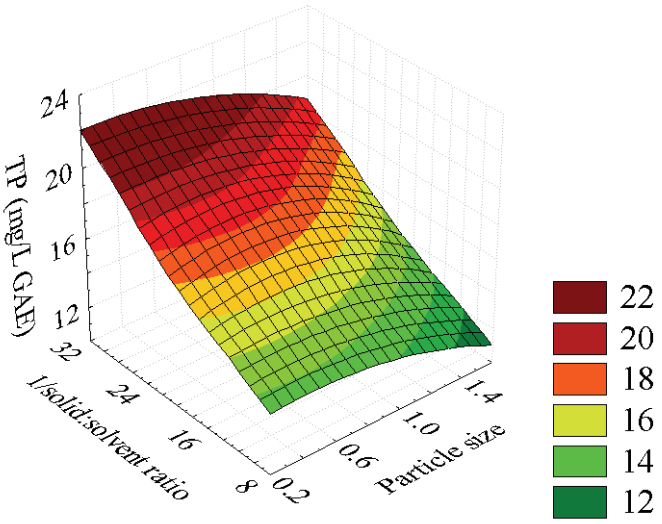

Figure 3. Effect of solid:solvent ratio and particle size on total polyphenols content (mg/L GAE) of T. serpyllum. The value of the missing independent variable in the plot was kept at the centre point.

Table 1. Antioxidant activity of T.serpyllum ethanol extracts – ABTS method (mmol/mg Trolox)

Particle size, mm	Extraction time, min	Solid:solvent ratio		
		1:10	1:20	1:30
0.3	3	7.53±0.04	8.47±0.88	10.32±0.12
	7	6.22±0.04	9.51±0.53	10.05±0.36
	10	5.72±0.03	9.88±0.27	9.19±0.32
0.7	3	7.92±0.39	8.74±0.56	9.56±0.56
	7	6.28±0.27	9.00±0.23	9.93±0.24
	10	5.83±0.05	7.76±0.08	9.11±0.72
1.5	3	7.43±0.85	8.39±0.11	10.00±0.40
	7	6.20±0.05	8.74±1.23	9.94±0.01
	10	6.39±0.25	8.57±0.03	9.22±0.02

Table 2. Antioxidant activity of T.serpyllum ethanol extracts – DPPH method (IC_{50} / mg mL^{-1})

Particle size, mm	Extraction time, min	Solid:solvent ratio		
		1:10	1:20	1:30
0.3	3	3.37±0.04	3.05±0.01	3.00±0.02
	7	3.67±0.07	3.04±0.00	3.17±0.06
	10	4.53±0.13	3.11±0.07	3.17±0.01
0.7	3	3.71±0.19	3.51±0.16	3.40±0.14
	7	4.70±0.12	3.39±0.13	3.22±0.01
	10	4.66±0.17	3.68±0.18	3.05±0.02
1.5	3	4.78±0.55	3.55±0.11	3.3±00.10
	7	4.71±0.25	3.78±0.23	3.44±0.11
	10	4.62±0.16	3.66±0.03	3.32±0.08

sible for the oxidation in *in vivo* conditions. These results indicate a "radical trapping power" rather than true antioxidant activity. This means that molecules able to scavenge these synthetic radicals are not necessarily able to stop the oxidative chain. However, due to the similar electronic configuration between DPPH and peroxyl radicals, the significance of this method could be greatly improved under appropriate settings, particularly by monitoring the entire time evolution of the reaction, instead of performing single-point measurements [13,14].

The highest value of antioxidant capacity in the ABTS assay was recorded after 3 min of extraction, with particle size of 0.3 mm and at solid:solvent ratio 1:30, whereas the lowest antioxidant activities were detected after 10 min of extraction with solid:solvent ratio 1:10 (10.32 mmol/mg Trolox and 5.72–5.83 mmol/mg Trolox, respectively). The best results of antioxidant capacity in DPPH assay (the lowest values of IC_{50}) were determined in extracts obtained with a particle size of 0.3 mm and solid:solvent ratio 1:20 and 1:30 (IC_{50} 3.00––3.17 mg/mL). Therefore, the lowest values of antioxidant activity (very high values of IC_{50}) were detected with solid:solvent ratio 1:10 and particle size of 1.5 mm (IC_{50} 4.62–4.78 mg/mL).

DISCUSSION

Effect of extraction time

Fick's second law predicts how diffusion causes the concentration to change with time and prolonged time of extraction is expected to increase the content of soluble polyphenols in the extracts. Furthermore, the duration of the extraction is a function of the molecular weight of the active substances and the molecular weight of ballast substances. If the molecular weight of the active substances is smaller than molecular weight of ballast material, extraction process will last shorter, since the active ingredients diffuse rapidly [15]. However, in this paper, the effect of time was not statistically significant and an excessive time was not useful for better extraction of polyphenols. A possible explanation lies behind sensitivity of phenolic compounds especially at higher temperatures [16]. Similarly, extraction time did not prove to be statistically significant in case of ultrasound-assisted extraction of polyphenols from *Urtica dioica* [17], neither from *Lawsonia inermis* [18].

Polyphenols are widely seen as very unstable and highly susceptible to degradation. The stability of polyphenols under different conditions is a very important aspect which has to be taken into account to ensure that polyphenolic compounds have the desired properties and maintain their activity and structure during the different stages of processing, which can involve high temperature, light, oxygen, solvents, the presence of enzymes, proteins and metallic ions [19]. Therefore, shorter extraction time (3 min) is more acceptable both in terms of yield of bioactive compounds and energy efficiency.

In addition, antioxidant activity slightly decreased with prolonged extraction time and this could be explained by sensitivity of natural antioxidant compounds to heat released by the ultrasound probe and at air exposure. Also, ultrasound is known to generate free radicals, which can degrade natural antioxidants and cause decrease of the antioxidant capacity [20]. Similarly, in case of ethanol extracts of *Yellow tea*, prolonged extraction time caused a slight decrease in antioxidant capacity [21]. The overall conclusion is that shorter time of extraction is more appropriate for *T. serpyllum* extraction too, because of better protection of antioxidants present in the extract and because of energy efficiency.

Effect of the solid:solvent ratio

In general, by extending the extraction time and increasing of solid:solvent ratio, the amount of extractive substances is increased because of higher concentration gradient. Moreover, a larger solvent volume can dissolve constituents more effectively, which leads to

an enhancement of the extraction yield of polyphenols [15,22]. In this study, solid:solvent ratio influenced significantly TP content and the extraction yield of polyphenols increased of the solid:solvent ratio (Figures 1 and 3). This result is consistent with literature data on ultrasound-assisted extraction of rutin and quercetin from *Eunymus alatus* [22]. This could be explained by the better performance of acoustic cavitation in the dilute solution (1:30) than in the more viscous one (1:10). Besides that, the diffusion rate is inversely proportional to the viscosity of the medium and the molecular weight of the active substances [23]. In addition, both assays showed that antioxidant activity significantly decreased with the decreasing ratio drug:solvent, especially when this ratio was 1:10.

Effect of particle size

The transition of active compounds from plant material in the extraction medium is directly proportional to the diffusion coefficient, the contact surface between drug and solvent and concentration gradient. In general, the extraction in a shorter time of a drug which has a higher degree of fragmentation, more effectively recover of the target compounds can be achieved [15]. This can be explained by increase in exchange surface and decrease in path length necessary for the solute to reach the surface, both help to reduce the extraction time. On the other hand, the use of very small particles may lead to technical difficulties (for example, during the filtration) [24]. According to our results (Figures 2 and 3), the values of total polyphenols decreased with increasing fragmentation degree, but these differences were not statistically significant, as determined by analysis of variance (ANOVA). The highest yield was recorded with the smallest particle size (0.3 mm), which confirmed that the convective mass transfer had the dominant influence. The similar results were obtained in case of extraction conditions of *Ginkgo biloba* [25]. This could be explained by the mechanism of ultrasound extraction, which involves the disruption of the cell walls, reduction of the particle size and the intensification of the mass transfer of the cell content to the extraction medium and easier access of the solvent to the plant cells, caused by the collapse of the bubbles produced by cavitation, regardless of the initial particle size. If this collapse is within a biological material, ultrasound can affect these biological materials and tissues on micro- and a macro-scale [26]. For instance, SEM micrograph analysis in the study of ultrasound-assisted extraction of *E. alatus* revealed a large number of ruptures on the surface of plant caused by ultrasonic waves [22]. As reflected in Tables 1 and 2, particle size did not influence significantly antioxidant capacity tested in ABTS and DPPH assays.

CONCLUSION

The study represents optimization of ultrasound-assisted extraction of *T. serpyllum* with 30% ethanol, and amplitude applied for extraction was set to 65% at room temperature. The optimal conditions (extraction time, solid:solvent ratio and particle size) for the UAE were developed by quantitative analysis of the polyphenols by using Folin–Ciocalteu method and antioxidant activity assays, ABTS and DPPH. The best extraction performance was achieved with a particle size of 0.3 mm and solid:solvent ratio 1:30 after 3 min of extraction. Also, analysis of variance (ANOVA) confirmed a significant influence of solid:solvent ratio on the content of extracted phenolic compounds (1:30 > 1:20 > > 1:10), whereas time of extraction and particle size had no statistical significant effect on TP.

Acknowledgements

The authors acknowledge their gratitude to the Ministry of Education, Science and Technological Development of Serbia, project numbers 46010 and 46013.

REFERENCES

[1] L. Lorens, J.A. Llorens-Molina, S. Agnelo, H. Boira, Geographical and environment-related variations of essential oils in isolated populations of *Thymus richardii* Pers. in the Mediterranean basin, Biochem. System. Ecol. **56** (2014) 246–254.

[2] A.D. Lisi, L. Tedone, V. Montesano, G. Sarli, D. Negro, Chemical characterization of *Thymus* populations belonging from Southern Italy, Food Chem. **125** (2011) 1284–1286.

[3] R. Morales, The genus *Thymus*, 1st ed., Taylor and Francis, London, 2002.

[4] S. Aziz, Studies on the Chemical Constituents of *Thymus serpyllum*, Turk. J. Chem. **32** (2008) 605–614.

[5] A.I. Hussain, F. Anwar, S.A.S. Chatha, S. Latif, S.T.H. Sherazi, A. Ahmad, J. Worthington, S.D. Sarker, Chemical composition and bioactivity studies of the essential oils from two *Thymus* species from the Pakistani flora, LWT – Food Sci. Technol. **50** (2013) 185–192.

[6] B. Boros, S. Jakabova, A. Dornyei, G. Horvath, Z. Pluhar, F. Kilar, A. Felinger, Determination of polyphenolic compounds by liquid chromatography-mass spectrometry in *Thymus* species, J. Chromatog. A **1217** (2010) 7972–7980.

[7] M. Orlowska, I. Stanimirova, D. Staszek, M. Sajewicz, T. Kowalska, M. Waksmundzka-Hajnos, Optimization of Extraction based on the Thin-Layer Chromatographic Fingerprints of Common Thyme, J. AOAC Inter. **97** (2014) 1274–1281.

[8] S. Rodrigues, G.A.S. Pinto, Ultrasound extraction of phenolic compounds from coconut (*Cocos nucifera*) shell powder, J. Food Eng. **80** (2007) 869–872.

[9] M. Rostagno, J. Prado, Natural Product Extraction, Principles and Applications, The Royal Society of Chemistry Green Chemistry No. 21, 2013.

[10] E. Skotti, A. Anastasaki, G. Kanellou, M. Polissiou, Total phenolic content, antioxidant activity and toxicity of aqueous extracts from selected Greek medicinal and aromatic plants, Ind. Crop. Prod. **53** (2014) 46–54.

[11] R. Re, N. Pellegrini, A. Proteggente, A. Pannala, M. Yang, C. Rice-Evans, Antioxidant activity applying an improved ABTS radical cation decolorization assay, Free Radic. Biol Med. **26** (1999) 1231–1237.

[12] D. Horžić, D. Komes, A. Belščak, K. Kovačević-Ganić, D. Iveković, D. Karlović, The composition of polyphenols and methylxanthines in teas and herbal infusions, Food Chem. **115** (2009) 441–448.

[13] K.M. Schaich, X. Tian, J. Xie, Reprint of "Hurdles and pitfalls in measuring antioxidant efficacy: A critical evaluation of ABTS, DPPH and ORAC assays", J. Funct. Food 2015, doi: 10.1016/j.jff.2015.05.024.

[14] R. Amorati, M.C. Foti, L. Valgimigli, Antioxidant Activity of Essential oils, J. Agric. Food Chem. **61** (2013) 10835––10847.

[15] G. Vuleta, J. Milić, S. Savić, Farmaceutska tehnologija, Farmaceutski fakultet Univerziteta u Beogradu, Beograd, 2012.

[16] M. Friedman, S.-Y. Kim, S.-J. Lee, G.-P. Han, J.-S. Han, K.-R. Lee, N. Kozuke, Distribution of catechins, theaflavins, caffeine, and theobromine in 77 teas consumed in the United States. J.Food Sci.**70** (2005) 550–559.

[17] U.-J. Vajić, J. Grujić-Milanović, J. Živković, K. Šavikin, D. Gođevac, Z. Miloradović, B. Bugarski, N. Mihailović-Stanojević, Optimization of extraction of stinging nettle leaf of phenolic compounds using response surface methodology, Ind. Crop.Prod. **74** (2015) 912–917.

[18] D.B. Uma, C.W. Ho, W.M.W. Aida, Optimization of Extraction Parameters of Total Phenolic Compounds from Hena (*Lawsonia intermis*) Leaves, Sains Malaysiana **39** (2010) 119–128.

[19] A. Castaneda-Ovando, M.L. Pacheco-Hernandez, M.E. Paez-Hernandez, J.A. Rodrigez, C.A. Galan-Vidal, Chemical studies of anthocyanins: A review, Food Chem. **113** (2009) 859–871.

[20] O. Potterat, Antioxidants and free radical scavengers of natural origin, Curr, Organic Chem. **1** (1997) 415–440.

[21] D. Horžić, A. Režek Jambrak, A. Belščak-Cvitanović, D. Komes, V. Lelas, Comparison of Conventional and Ultrasound Assisted Extraction Techniques of Yellow Tea and Bioactive Composition of Obtained Extracts, Food Bioprocess. Technol. **5** (2012) 2858–2870

[22] Y. Yang, F. Zhang, Ultrasound-assisted extraction of rutin and quercetin from *Eunymus alatus*, Ultrason. Sonochem. **15** (2008) 308–313.

[23] M.H. Entezari, S. H. Nazary, M.H.H. Khodaparast, The direct effect of ultrasound on the extraction of date syrup and its micro-organisms, Ultrason. Sonochem. **11** (2004) 379–384.

[24] E.M. Silva, H. Rodrigez, Y. Larondelle, Optimization of extraction of phenolics from *Inga edulis* leaves using response surface methodology, Sep. Purif. Tech. **55** (2007) 381–387.

[25] S.G. Milošević, Ž.D. Lepojević, Z.P. Zeković, S.S. Vidović, Determination of extraction conditions of *Ginkgo biloba* L. leaves by supercritical CO_2 using response surface methodology, Hem. Ind. **65** (2011) 147–157.

[26] A.D. Alarcon-Rojo, H. Janacua, J.C. Rodrigez, L. Paniwnyk, T.J. Mason, Power ultrasound in meat processing, Meat Sci. **107** (2015) 86–93.

IZVOD

ULTRAZVUČNA EKSTRAKCIJA POLIFENOLA IZ *Thymus serpyllum* I NJEGOVA ANTIOKSIDATIVNA AKTIVNOST

Aleksandra A. Jovanović[1], Verica Đorđević[1], Gordana M. Zdunić[2], Katarina P. Šavikin[2], Dejan Pljevljakušić[2], Branko M. Bugarski[1]

[1]*Tehnološko-metalurški fakultet, Katedra za hemijsko inženjerstvo, Univerzitet u Beogradu, Karnegijeva 4, Beograd, Srbija*

[2]*Institut za proučavanje lekovitog bilja „Dr Josif Pančić", Tadeuša Košćuška 1, Beograd, Srbija*

(Naučni rad)

U ovom radu je predstavljena i optimizovana metoda za ekstrakciju prirodnih-biološki aktivnih jedinjenja iz *T. serpyllum*, koja poseduju antioksidativnu, antimikrobnu, spazmolitičnu, antiinflamatornu i stimulativnu aktivnost. Ultrazvučna ekstrakcija se sve više koristi u procesu izolovanja aktivnih principa iz biljnog materijala, posebno u ekstrakciji bioaktivnih supstanci poput polifenola. Osnovne prednosti ultrazvučne ekstrakcije nad klasičnim metodama su visoka efikasnost, kraće vreme ekstrakcije i ušteda rastvarača. Ultrazvučni talasi u medijumu indukuju mehaničke, kavitacione i termalne efekte, koji uzrokuju degradaciju ćelijskog zida, bez promena u strukturnim i funkcionalnim karakteristikama ciljanih jedinjenja. Optimizacija procesa ekstrakcije je vršena kroz variranje vremena ekstrakcije (3, 7 i 10 min), odnosa droga:rastvarač (1:10, 1:20 i 1:30) i stepena usitnjenosti (0,3, 0,7 i 1,5 mm), pri čemu je kao rastvarač korišćen 30% etanol i primenjena je amplituda od 65%. Optimalni uslovi su ispitani korišćenjem kvantitativne spektrofotometrijske metode sa Folin-Ciocalteu reagensom. Osim toga, efikasnost ekstrakcije je izražena preko antioksidativne aktivnosti određene u ABTS i DPPH metodama. Utvrđeno je da su najbolji uslovi za ekstrakciju stepen usitnjenosti 0,3 mm, vreme ekstrakcije 3 min i odnos droga:rastvarač 1:30. Pod ovim uslovima prinos ukupnih polifenola je iznosio 23,03 mg/L GA, dok je zabeležena antioksidativna aktivnost bila 10,32 mmol/mg Trolox i IC_{50} 3,00 mg/mL. Nakon statističke analize pokazano je da odnos droga:rastvarač statistički značajno utiče na sadržaj ukupnih polifenola (1:30 > 1:20 > 1:10), dok vreme ekstrakcije i stepen usitnjenosti ne pokazuju statistički značajan uticaj na vrednost ukupnih polifenola. Može se zaključiti da je ekstrakcija ultrazvučnom sondom metod izbora za ekstrakciju polifenola iz *Serpylli herba*, jer je potrebno kraće ekstrakciono vreme, kao i zbog uštede energije, visoke efikasnosti i visokog prinosa ekstrakcije.

Ključne reči: *Thymus serpyllum* • Ultrazvučna ekstrakcija • Polifenoli • Antioksidativna aktivnost

Uticaj stepena kristaličnosti, sadržaja aluminijum-oksida i natrijum-oksida na kapacitet sorpcije vode NaY zeolitom

Dragana M. Kešelj[1], Dragica Z. Lazić[1], Živan D. Živković[2], Branko T. Škundrić[3], Jelena V. Penavin-Škundrić[4], Slavica G. Sladojević[4]

[1]*Univerzitet u Istočnom Sarajevu, Tehnološki fakultet Zvornik, Republika Srpska, BiH*
[2]*Univerzitet u Beogradu, Tehnički fakultet u Boru, Srbija*
[3]*Akademija nauka i umjetnosti Republike Srpske, Republika Srpska, BiH*
[4]*Univerzitet u Banjoj Luci, Tehnološki fakultet, Republika Srpska, BiH*

Izvod

U radu su prezentovani matematički modeli koji opisuju zavisnost kapaciteta sorpcije vode od stepena kristalizacije, sadržaja Na_2O i Al_2O_3 u NaY zeolitu. Pri različitim uslovima kristalizacije, sintetisan je NaY zeolit iz natrijum-aluminatnog rastvora, vodenog stakla i sumporne kiseline. Dobijeni zeolitski prahovi okarakterisani su na sledeće parametre: Na_2O, Al_2O_3, kapacitet sorpcije vode (*WSC*) i stepen kristaličnosti (*SK*). Regresionom analizom uzoraka zeolitskih prahova, u kojima su se vrednosti kretale za: sadržaj Na_2O u intervalu 13,81 do 16,14%, Al_2O_3 od 21,58 do 27,17%, *SK* od 58,70 do 114,00% i *WSC* od 21,32 do 36,59%, došlo se do zaključka da postoji značajna korelacija između kapaciteta sorpcije vode i stepena kristaličnosti, za razliku od sadržaja Na_2O i sadržaja Al_2O_3 u zeolitskom prahu, čija se korelacija sa kapacitetom sorpcije vode, može zanemariti. Matematički model dobijen linearnom regresionom analizom imao je visok R^2 = 0,796, dok je bolji matematički model dobijen nelinearnom regresionom analizom R^2 = 0,912, kojom je kapacitet sorpcije vode iskazan preko kvadratnog modela.

Ključne reči: regresiona analiza, kapacitet sorpcije vode, stepen kristaličnosti.

Dostupno na Internetu sa adrese časopisa: http://www.ache.org.rs/HI/

NAUČNI RAD

UDK 66.065.5:51:549.67:66.081

Hem. Ind. **70** (4) 399–407 (2016)

doi: 10.2298/HEMIND150126046K

Zeoliti su materijali koji su izgrađeni od sistema pora, čije veličine i oblik zavise od samog tipa zeolita tj. od izgleda njegove osnovne izgrađivačke ćelije. Jedan od najznačajnijih sintetičkih zeolita , koji ima strukturu prirodnog fožezita, je NaY zeolit [1–3]. Ima kubnu jediničnu ćeliju, veoma velikih dimenzija, koja se kreće od 24,61–24,85 Å u zavisnosti od sadržaja aluminijuma u jediničnoj ćeliji, katjona i stepena hidratacije. Ćelija je izgrađena od ukupno 192 tetraedra SiO_4 i AlO_4 [4]. Kod fožezitnog tipa zeolita jedinična ćelija predstavlja 9 kubooktaerdara (sodalitnih jedinica), međusobno povezanih preko heksagonalnih prizmi. Ovakva struktura ima veoma razvijen sistem pora. Centar elementarne ćelije ima oblik 26-edra sa četiri prozora u obliku dvanaestočlanog prstena slobodnog dijametra od 0,74 nm (često nazivan superkavez). Sodalitna jedinica (β-kavez) ima unutrašnji prečnik od 6,6 Å i ulaz maksimalnog otvora preko šestočlanih prstenova prečnika 2,6 Å. Dakle, strukturu Y zeolita čine sodalitna jedinica, superkavez i heksagonalna prizma, sa maksimalnim „prozorima“ 2,6; 7,4 i 2,6 Å, i prečnicima 6,6; 11,8 i 2,6 Å. Gustina skeleta fožezitnih zeolita je 12,7 T atoma/Å i ima najveću centralnu šupljinu. Smatra se da ovaj tip zeolita može da primi 235 molekula vode[5–8].

Voda u zeolitu može biti hemisorbovana i fizisorbovana [8]. Fizisorbovana voda je posledica slobodnog kretanja molekula vode kroz postojeće pore u zeolitu, dok se hemisorbovana voda javlja kao posledica interakcije dipol molekula vode sa katjonima u strukturi zeolita, pre svega sa jonima natrijuma i aluminijuma. Tako na primer prve adsorbovane molekule vode na najpristupačnijim katjonima NaY zeolita, čine sodalitnu jedinicu dostupnu za vodu. Kompletno punjenje superkaveza i sodalitnog kaveza je dostupno za migraciju nestrukturnih katjona i vode, preko dvostrukog šestočlanog prstena prizme [8–10]. U strukturi zeolita manjka pozitivnog naboja, jer su atomi silicijuma zamenjeni atomima aluminijuma, usled čega se višak negativnog naboja nastoji uravnotežiti sa jednovalentnim katjonima, kao što je Na^+. Samo to nastojanje da se uravnoteži naelektrisanje sa većim brojm atoma aluminijuma u strukturi, dovodi do veće hidrofilnosi zeolita. Kako jedinična ćelija kod Y zeolita može da ima 48 do 76 atoma Al, to će i njegovo prisustvo znatno uticati i na adsorpciju vode kod ovog tipa zeolita [2,8].

Difrakcijom X-zraka na prahu se dobija informacija o strukturi zeolita. Položaj svih refleksija u difraktogramu određuju tip zeolita, a poznavajući strukturu moguće je na osnovu refleksija odrediti veličinu jedinične ćelije [11,12]. Fožezitni tip zeolita ima kubnu jediničnu ćeliju,

Prepiska: D. Kešelj, Tehnološki fakultet Zvornik, Karakaj bb, 75400 Zvornik, Republika Srpska, BiH.
E-pošta: draganakeselj@yahoo.com
Rad primljen: 26. januar, 2015
Rad prihvaćen: 19. jun, 2015

pa se veličina jedinične ćelije (a) jednostavno može izračunati na osnovu Milerovih indeksa (h,k,l), rastojanje između reflektovanih paralenih ravni koje imaju Milerov indeks h,k,l ($d_{(h,k,l)}$) i talasne dužine upadnih X-zraka (λ), koja je 1,54178 Å za CuKα. Jednačina po kojoj se računa veličina jedinične ćelije je:

$$a = d_{(h,k,l)}\sqrt{(h^2 + k^2 + l^2} \quad (1)$$

gde je:

$$ad_{(h,k,l)} = \frac{\lambda}{\sin\theta} \quad (2)$$

a ϑ ugao refleksije X-zraka.

Poznavajući veličinu ćelije moguće je pomoću relacije naučnika Breck-Flanigeni saradnici odrediti molarni odnos Si/Al [7]. Intenzitet pika je direktno vezan za stepen kristalizacije. Često se stepen kristaličnosti računa - SK [12]:

$$SK(\%) = 100\sum\text{Integralni intenzitet pikova uzorka zeolita}/\sum\text{Integralni intenzitet pikova referentnog uzorka zeolita} \quad (3)$$

Širina pika je u vezi sa veličinom kristalita, tj. ona može indicirati na kvalitet kristalita, dok ravnija osnovna linija ukazuje na veću kristalizaciju.

Jedna od važnijh osobina zeolita jeste i reverzibilna dehidratacija, tj. sposobnost zeolita da dehidratiše, a da pri tom ne dođe do narušavanja njegove structure, i nakon toga da ponovo adsorbuje vodu. Veličina kojom se iskazuje ova osobina je kapacitet sorpcije vode.

Ispitivanjem adsorpcionih izotermi vode na zeolite različitih molskih odnosa Si/Al, pri visokim stepenima kristaličnosti, utvrđeno je da sa rastom molskog odnosa raste kapacitet sorpcije vode, što se objašnjava jakom vezom sa veličinom i arhitekturom pora [13–18]. Mehanizam adsorpcije različitih jona korišćenjem Monte Karlo simulacije bio je predmet brojnih istraživanja [19––21], ali avaj pristup ne daje kvantifikaciju jačine uticaja pojedinih parametara na ishod procesa adsorpcije. Strukturnu interpretaciju adsorpcionih izotermi vode na 3A zeolitu u cilju statističke generalizacije termodinamike adsorpcionog modela definisali su Restzrepo i Mosquera [21].

Novija istraživanja sve su više usmerena ka definisanju matematičkih modela primenom linearne i nelinearne regresione analize, kojim se nastoji putem odgovarjućih matematičkih modela iskazati veza između pojedinih varijabli, koje su značajne za posmatrane procese [22,23]. Cilj ovog rada je da utvrdi vezu između kapaciteta sorpcije vode (kao zavisne varijable) i stepena kristaličnosti, sadržaja Al_2O_3 i Na_2O (kao nezavisnih varijabli) i izrazi preko odgovarajućeg matematičkog modela. Izabrani modeli statisatičke obrade dobijenih rezultata : linearna i nelinerana regresiona analiza daju mogućnosti realne procene jačine uticaja pojedinih parametara na ishode proučavanog procesa sorpcije vode u NaY zeolitu, kao i vrednosti koeficijenata determinacije, kao pouzdanih ocena validnosti definisanih matematičkih modela [23].

EKSPERIMENTALNI DEO

Za eksperimentalna istraživanja, čiji su rezultati prezentovani u ovom radu, korišteni su aluminijum-hidroksid, natrijum-hidroksid, vodeno staklo, natrijum-aluminatni rastvor (sintetički i iz procesa proizvodnje glinice po Bayer tehnologiji) i H_2SO_4 kiselina (Tabela 1).

Aluminijum-hidroksid i natrijum-hidroksid su korišteni kao sirovine za dobijanje sintetičkog aluminata. Sintetički aluminat dobijen je rastvaranjem aluminijum-hidroksida sa natrijum-hidroksidom na temperaturi ključanja rastvora i imao je koncentraciju Na_2O = 395,6 g/dm^3 i Al_2O_3 = 81,9 g/dm^3.

Za poređenje dobijenih rezultata tokom sinteze u ovom radu korišćen je komercijalni zeolit CBV 100.

Eksperimentalni dio ovog rada izveden je u laboratoriji Fabrike glinice "Alumina“ u Zvorniku i laboratorijama Tehnološkog fakulteta Zvornik. Za izvođenje sinteza zeolita NaY korišćena je:

– aparatura za dobijanje hidrogela, koja se sastojala od: termostatiranih bireta za doziranje sirovina, reakcione posude i stubne mešalice,

– reaktor od polipropilena zapremine 500 cm^3, koji je služio za kristalizaciju,

Tabela 1. Hemijski sastav sirovina korištenih u sintezama NaY zeolita
Table 1. The chemical compositon of raw materials used in sythesis of NaY zeolite

Red. br.	Sirovina	Karakteristike
1.	Aluminijum-hidroksid	Sadržaj: Al_2O_3 = 64,83%; SiO_2 = 0,009%; Fe_2O_3 = 0,012%; Na_2O_{uk} = 0,22%; CaO = 0,017%; gubitak žarenjem na 1000 °C: 34,89%
2.	Natrijum-hidroksid	48,78%, ρ = 1,514 g/cm^3
3.	Vodeno staklo	Sadržaj: Na_2O=159,3 g/dm^3; SiO_2=380,4 g/ dm^3; ρ=1,430 g/ cm^3
4.	Aluminatni rastvor iz procesa proizvodnje glinice po Bayer tehnologiji	Sadržaj: Na_2O_k = 155 g/dm^3; Al_2O_3 = 161,2 g/dm^3; ρ = 1,310 g/cm^3
5.	H_2SO_4	96%, ρ = 1,840 g/ cm^3

– vazdušni termostat, za obezbeđivanje temperature kristalizacije.

Sve sinteze su izvedene hidrotermalnim putem, uz dodatak „klica“ (seed gel) u cilju skraćenja vremena kristalizacije. Klice su mešane sa vodom, odgovarajućom količinom vodenog stakla, aluminatnog rastvora i sumpornom kiselinom, do odgovarajućih molskih odnosa. Molski odnosi sinteza su bili:

$2Na_2O:Al_2O_3:6\ SiO_2:96H_2O$

$2Na_2O:Al_2O_3:6\ SiO_2:120H_2O$

$2Na_2O:Al_2O_3:6{,}5SiO_2:120H_2O$

$2{,}5Na_2O:Al_2O_3:6SiO_2:120H_2O$

$3Na_2O:Al_2O_3:6SiO_2:120H_2O$

U cilju dobijanja zeolitskih prahova različitog stepena kristaličnosti, sve sinteze su izvođene na temperaturi od 105 °C, ali su imale različita vremena kristalizacije (12, 20 i 24 h). Kao rezultat sinteza, dobijani su prahovi zeolita NaY različitog hemijskog sastava i stepena kristalizacije. Dobijenom zeolitskom prahu, rađena je hemijska anliza, rendgenska difrakciona analiza i apsorpcija vode. Hemijskom analizom, u dobijenom prahu, određivan je:

- Sadržaj Na_2O (%), metodom atomsko-apsorpcionom spektroskopijom na aparatu Perkin-Elmer 4000.
- Sadržaj Al_2O_3 (%), potenciometrijskom titracijom na aparatu tipa "Titripol".

Mineraloška analiza dobijenog praha je rađena difrakcionom analizom X-zraka na difraktometaru Philips, PW1710, uz upotrebu Cu antikatoda (40 V, 50 mA, Kα = 0,15405 μm). Na osnovu dobijenih difraktograma dalje je određivan stepen kristaličnosti. Priprema uzoraka i odabir pikova za računanje stepena kristaličnosti rađen je prema standardu ASTM D 3906-03.

Kapacitet sorpcije vode (*water sorption capacity)* zeolita određivan je na uzorku, koji je predhodno dehidratisan žarenjem na 500 °C. Pritisak u aparaturi je bio 24±1 mbar, dok je temperatura na kojoj se određivao kapacitet sorpcije bila 20±1 °C . Na tim uslovima uzorak je sorbovao vodu tokom 5 sati.

Kapacitet sorpcije vode se računao po izrazu:

$$WSC = 100\frac{m_v - m_0}{m_0} \quad (4)$$

WSC – kapacitet sorpcije vode (%), m_0 – masa suvog (g), m_v – masa uzorka nakon sorpcije vode (g).

REZULTATI I DISKUSIJA

U ovom radu predstavljeni su matematički modeli, koji opisuju zavisnost kapaciteta sorpcije vode od stepena kristalizacije i sadržaja Na_2O i Al_2O_3 u NaY zeolitu. Sinteze su rađene sa natrijum-aluminatnim rastvorom iz Bayer procesa proizvodnje glinice, vode-

Tabela 2. Stepen kristaličnosti (X_1), hemijski sastav (Na_2O- X_2, Al_2O_3-X_3) i sorpcija vode (Y) prahova NaY zeolita dobijenih na temperaturi kristalizacije 100°C, pri različitim molskim odnosima i vremenima kristalizacije
Table 2. The degree of crystallinity(X_1), chemical composition (Na_2O- X_2, Al_2O_3-X_3) and water sorption capacity (Y) of the powders NaY zeolite, obtained at temperature of crystallization 100°C, different molar ratios and time of crystallization

Red. br.	Molski odnos	Vreme kristalizacije, h	X_1	X_2	X_3	Y
1.	$2Na_2O{\cdot}Al_2O_3{\cdot}6SiO_2{\cdot}96H_2O$	20	104,00	14,29	22,60	33,56
2.		12	98,00	14,43	23,22	35,11
3.		24	113,00	14,23	22,04	36,59
4.		12	58,70	15,35	22,36	22,24
5.		24	98,00	14,99	23,98	34,33
6.		24	88,00	14,85	22,84	33,79
7.		24	97,00	15,36	23,78	34,16
8.		12	68,00	14,74	22,62	21,32
9.		24	91,00	14,69	23,00	29,22
10.	$2Na_2O{\cdot}Al_2O_3{\cdot}6\ SiO_2{\cdot}120H_2O$	24	86,00	14,70	23,53	29,40
11.		12	61,00	14,80	22,02	21,60
12.		24	107,00	15,24	23,51	34,11
13.		24	114,00	15,59	23,38	33,47
14.		24	110,00	15,56	23,67	33,18
15.		24	114,00	14,71	23,15	34,27
16.		24	111,00	14,44	23,66	32,06
17.	$3Na_2O{\cdot}Al_2O_3{\cdot}6SiO_2{\cdot}120H_2O$	24	95,00	16,14	27,17	35,14
18.	$2{,}5Na_2O{\cdot}Al_2O_3{\cdot}6SiO_2{\cdot}120H_2O$	24	102,00	15,43	25,47	34,52
19.		24	93,00	15,55	25,48	34,25
20.	$2Na_2O{\cdot}Al_2O_3{\cdot}6{,}5SiO_2{\cdot}120H_2O$	24	114,00	13,97	21,97	31,62
21.		24	113,00	13,81	21,58	32,81

nog stakla i H_2SO_4 kiseline, pri različitim molskim odnosima i vremenima kristalizacije (tabela 2). U cilju dobijanja zavisnosti između kapaciteta sorpcije vode i varijabli koje utiču na njega, u daljem tekstu uvedene su oznake:

Y – kapacitet sorpcije vode, *WSC* (%),
X_1 – stepen kristaličnosti (%),
X_2 – sadržaj Na_2O (%) i
X_3 – sadržaj Al_2O_3 (%).

Stepen kristaličnosti je određivan rendgenskom difrakcijonom analizom, poređenjem intenziteta osam karakterističnih refleksija („integralni intenzitet“) sintetisanih zeolita (slika 1b–g) sa osam karakterističnih reflefsija (prema ASTM D 3906-03 standardu) komercijalnog uzorka CBV 100 (slika 1a) i računato po izrazu (3). Prema standardu ASTM D 3906-03 karakteristični difrakcioni uglovi 2θ na kojima su uzimani integralni intenziteti pikova su: 15,7±0,2; 18,7±0,2; 20,4±0,3; 23,7±0,4; 27,1±0,5; 30,8±0,5; 31,5±0,5 i 34,2±0,6.

Dobijeni rezultati su prikazani u tabeli 2.

Stepen kristaličnosti za posmatrane uzorke zeolita kretao se u intervalu od 58,70 do 114,00% (slika 1. b-58,70%, c-88,00%, d-97,00%, e-68,00%, f-107,00%, g-114,00%), jer je za računanje kao referentni uzorak uzet komercijalni zeolit NaY CBV 100, čiji je stepen kristaličnosti prema deklaraciji proizvoda bio veći od 90%.

Statistička obrada dobijenih rezultata

U cilju utvrđivanja analitičke zavisnosti WSC-Y od varijabli stepena kristaličnosti (X_1), sadržaja Na_2O (X_2) i sadržaja Al_2O_3 (X_3), izvršena je statistička obrada dobijenih rezultata korištenjem linearne regresione analize (LRA) i kvadratne nelinearne regresione analize (KNRA).

Rezultati deskriptivne statistike dobijenih eksperimentalnih rezultata iz tabele 2 prikazani su u tabeli 3, a međusobni korelacioni odnos zavisne varijable (*Y*) i nezavisnih varijabli (X_1–X_3) prikazani su u tabeli 4.

Tabela 3. Deskriptivna statistika za ulazne (X_1–X_3) i izlazne (Y) vrednosti prahova NaY zeolita dobijenih pri različitim molskim odnosima i vremenima kristalizacije, broj sinteza zeolite: 21; minimum – minimalna vrednost varijabli X_1, X_2, X_3, Y u posmatranom broju sinteza N, maksimum – maksimalna vrednost varijabli X_1, X_2, X_3, Y u posmatranom broju sinteza N
Table 3. Descriptive statistics for the input (X_1–X_3) and the output (Y) values of the powders NaY zeolite obtained under different molar ratios and time of crystallization

Promenljiva	Minimum	Maksimum	Srednja vrednost	Standardna devijacija
X_1	58,7	114,0	96,938	17,0027
X_2	13,81	16,14	14,8986	0,59813
X_3	21,58	27,17	23,3824	1,33188
Y	21,32	36,59	31,7500	4,54072

Rezultati korelacione analize, prikazani u tabeli 4, ukazuju na zanačajan nivo korelacije između *Y* – *WSC* i X_1 – *SK* (Pearson korelacija, *PC* = 0,830 i statistička značajnost, *p* = 0,000) i X_2 (Na_2O) i X_3 (Al_2O_3) (*PC* = 0,763 i *p* = 0,000). Ostale korelacije, *Y*–X_2 (*PC*=0,061 i *p* = = 0,794), *Y*–X_3(*PC* = 0,392 i *p* = 0,079) i X_1–X_2 (*PC* = 0,079 i *p* = 0,733) imaju vrlo niske vrednosti za *PC* bez sta-

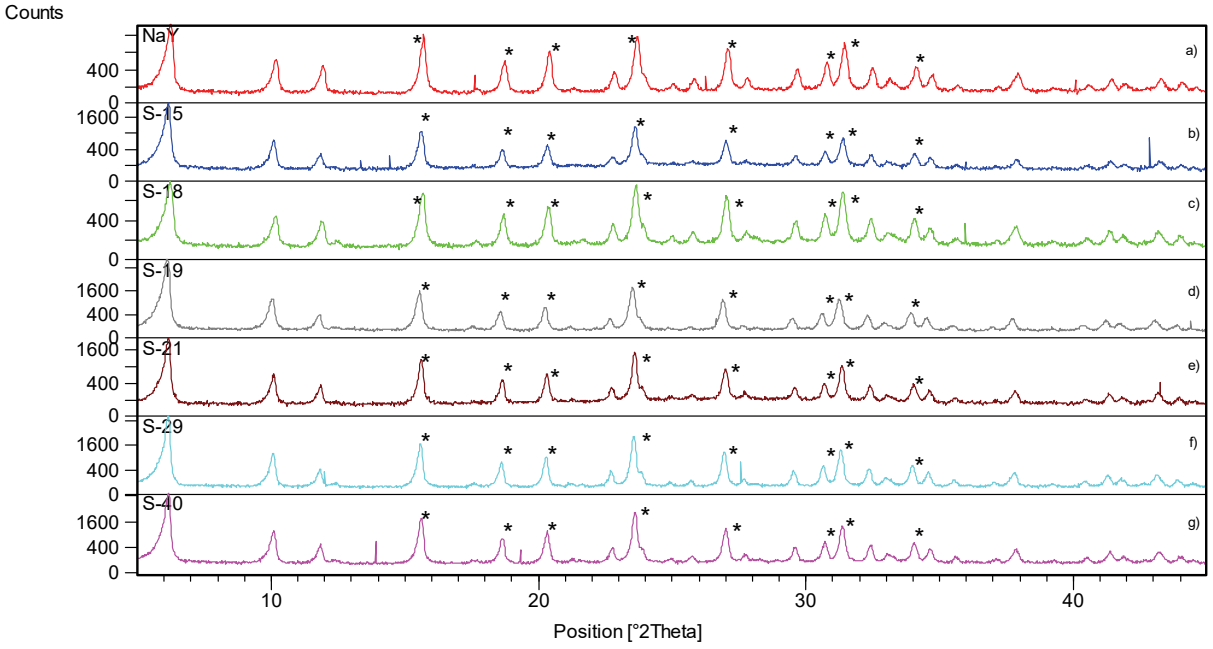

Slika 1. Difraktogrami uzoraka zeolita (a – CBV100; b – SK = 58,7%; c – SK = 88%; d – SK = 97%; e – SK = 68%; f – SK = 107%; g – SK = 114%).
Figure 1. Diffractogram of the samples of NaY zeolite(a – CBV100; b – SK = 58.7%; c – SK = 88%; d – SK = 97%; e – SK = 68%; f – SK = 107%; g – SK = 114%).

tističke značajnosti. Dobijeni rezultati ukazuju da *SK* u značajnoj meri utiče na *WSC*, kao i sadržaj Na_2O i Al_2O_3 u NaY zeolitu. Obradom dobijenih rezultata metodom LRA, definisane su analitičke zavisnosti $Y = f(X_1)$; $Y = f(X_2)$; $Y = f(X_3)$; $Y = f(X_1,X_2)$; $Y = f(X_1,X_3)$; $Y = f(X_2,X_3)$ i $Y = f(X_1,X_2,X_3)$, koje imaju sledeće oblike:

$$Y = 10{,}268 + 0{,}222X_1,\ R^2 = 0{,}689 \quad (5)$$

$$Y = 24{,}825 + 0{,}460X_2,\ R^2 = 0{,}004 \quad (6)$$

$$Y = 0{,}506 + 1{,}336X_3,\ R^2 = 0{,}154 \quad (7)$$

$$Y = -18{,}487 + 0{,}235X_1 + 1{,}843X_2,\ R^2 = 0{,}745 \quad (8)$$

$$Y = -15.226 + 0.215X_1 + 1.119X_3,\ R^2 = 0{,}746 \quad (9)$$

$$Y = -30{,}351 - 4{,}335X_2 + 2{,}822X_3,\ R^2 = 0{,}290 \quad (10)$$

$$Y = -11{,}309 + 0{,}210X_1 - 0{,}517X_2 + 1{,}301X_3,\ R^2 = 0{,}797 \quad (11)$$

Tabela 4. Korelaciona analiza za ulazne (X_1–X_3) i izlazne (Y) vrednosti prahova NaY zeolita dobijenih pri različitim molskim odnosima i vremenima kristalizacije
Table 4. Correlation analysis for the input (X_1–X_3) and the output (Y) values of the powders NaY zeolite obtained under different molar ratios and time of crystallization

Parametri		*Y*	X_1	X_2	X_3
Y	Pearson korelacija (*PC*)	1	**0,830****	0,061	0,392
	Statistička značajnost	–	0,000	0,794	0,079
X_1	Pearson korelacija (*PC*)	–	1	–0,207	0,079
	Statistička značajnost	–	–	0,368	0,733
X_2	Pearson korelacija (*PC*)	–	–	1	**0,763****
	Statistička značajnost	–	–	–	0,000
X_3	Pearson korelacija (*PC*)	–	–	–	1
	Statistička značajnost	–	–	–	–

Dobijeni rezultati metodom LRA ukazuju na to da zavisnosti date jednačinama (5)–(10) sa niskim vrednostima R^2 predviđaju zanemarljiv uticaj X_2 i X_3 pojedinačno ili zajedno nemaju direktnu korelaciju sa *Y – WSC*.

Imajući u vidu vrednosti *PC* i *p* iz tabele 4, očigledno je da na *SK* dominantan uticaj ima odnos X_2/X_3 (Na_2O/Al_2O_3) koji direktno utiče na X_1(*SK*), a od *SK* zavisi *Y – WSC*.

U cilju definisanja zavisnosti sa većim vrednostima R^2 i pouzdanijim predikcijama *WSC* od navedenih varijabli, izvršena je kvadratna nelinearna regresiona analiza (KNRA) dobijenih eksperimentalnih podataka, a dobijeni eksperimentalni podaci pokazani su u tabeli 5.

Analitički oblici, dobijeni metodom KNRA, zavisnosti $Y = f(X_1)$; $Y = f(X_2)$; $Y = f(X_3)$; $Y = f(X_1,X_2)$; $Y = f(X_1,X_3)$; $Y = f(X_2,X_3)$ i $Y = f(X_1,X_2,X_3)$, i $X_1 = f(X_2,X_3)$ imaju sledeće oblike:

$$Y = -35{,}643 + 1{,}309X_1 - 0{,}006X_1^2,\ R^2 = 0{,}845 \quad (12)$$

$$Y = 806{,}385 - 104{,}438X_2 + 3{,}515X_2^2,\ R^2 = 0{,}102 \quad (13)$$

$$Y = -123{,}626 + 11{,}641X_3 - 0{,}213X_3^2,\ R^2 = 0{,}166 \quad (14)$$

$$Y = -527{,}064 + 3{,}579X_1 + 48{,}909X_2 - 0{,}149X_1X_2 - 0{,}006X_1^2 - 1{,}084X_2^2,\ R^2 = 0{,}896 \quad (15)$$

$$Y = 66{,}571 + 0{,}932X_1 - 7{,}501X_3 + 0{,}012X_1X_3 - 0{,}005X_1^2 - 0{,}141X_3^2,\ R^2 = 0{,}864 \quad (16)$$

$$Y = 1265{,}849 - 239{,}603X_2 + 44{,}492X_3 + 7{,}579X_2X_3 + 2{,}056X_2^2 - 3.294X_3^2,\ R^2 = 0{,}621 \quad (17)$$

$$Y = -1056{,}378 + 2{,}712X_1 + 177{,}048X_2 - 37{,}782X_3 - 0{,}004X_1X_2X_3 - 0{,}006X_1^2 - 5{,}527X_2^2 + 0{,}897X_3^2,\ R^2 = 0{,}912 \quad (18)$$

$$X_1 = 7168{,}633 - 1416{,}256X_2 + 290{,}363X_3 - 37{,}782X_3 - 21{,}512X_2X_3 + 30{,}411X_2^2 - 12{,}814X_3^2,\ R^2 = 0{,}719 \quad (19)$$

Dobijene vrednosti R^2 korišćenjem KNRA (jednačine (10)–(16)) u odnosu LRA pokazuje bolje fitovanje u slučaju korištenja KNRA.

Zavisnosti dobijene pomoću KNRA pokazuju zadovoljavajući nivo pouzdanosti za predikciju *Y – WSC* od karakteristika Y zeolita, X_1 – *SK*, (X_1 – *SK* i X_2 – $\%Na_2O$), (X_1 – *SK* i X_3 – $\%Al_2O_3$) i (X_1, X_2, X_3). Grafički prikaz ovih zavisnosti dat je na slikama 2–7.

Takođe, koeficijent determinacije za zavisnost X_1 – *SK* od sadržaja X_2 – $\%Na_2O$ i X_3 – $\%Al_2O_3$, ima zadovoljavajuću vrednost $R^2 = 0{,}719$.

Dobijeni koeficijenti determinacije imaju opadajući niz:

$R^2_{18}(0{,}912) > R^2_{15}(0{,}896) > R^2_{16}(0{,}864) > R^2_{12}(0{,}845) > R^2_{17}(0{,}621) > R^2_{14}(0{,}166) > R^2_{13}(0{,}102)$, što ukazuje na opadajući niz nivoa fitovanja zavisnoasti (18) → (15) → (16) → (12) → (17) → (14) → (13). Očigledno je da X_1 – *SK* i odnos Na_2O/Al_2O_3 (X_2/X_3) ima najbolju predikciju *WSC*.

Dobijena zavisnost $Y = (X_1,X_2,X_3)$ sa $R^2 = 0{,}912$ pokazuje veliki stepen fitovanja primenom analitičkog oblika zavisnosti, koji je prikazan jednačinom (18), koja predstavlja pogodan oblik za predikciju *WSC* od sastava NaY zeolita ($\%Na_2O$ i $\%Al_2O_3$) i njegove kristaličnosti. Najveći koeficijent determinacije ($R^2 = 0{,}912$, slika 6) je dobijen u modelu kvadratne zavisnosti kapaciteta sorpcije od stepena kristaličnosti, sadržaja Na_2O i sadržaja Al_2O_3. Dobijeni model se može posmatrati kao dopunjeni linearni model gde se vidi da pozitivan uticaj na kapacitet sorpcije vode imaju X_1 i X_2, prvog eksponenta, i X_3 na drugi eksponent, dok negativan uticaj ima X_3, prvog eksponenta, X_1 i X_2 na drugi eksponent.

Dobijeni rezultati ukazuju da sa porastom *SK* raste *WSC*, slika 2. Stepen kristaličnosti zavisi od sadržaja Al_2O_3 i Na_2O, što na indirektan način utiče na *WSC*. Optimalan sastav NaY zeolita, kada se postižu maksimalne vrednosti *SK* od (100–114%), je pri sadržaju Na_2O: 13–14% i sadržaju Al_2O_3: 21–23%, koji obezbeđuju *WSC* u granicama 34–36%.

Tabela 5. Kvadratni modeli sorpcije vode (Y) u zavisnosti od stepena kristaličnosti (X_1), sadržaja Na_2O (X_2) i Al_2O_3 (X_3)
Table 5. The square models of water sorption capacity (Y) depending on the degree of crystallinity (X_1) and contents of Na_2O (X_2) and Al_2O_3 (X_3)

Model	Varijable	Parametri		Standardna greška	Interval poverenja, 95%	
					Donja granica	Gornja granica
1.	X_1	*A*	–35,643	11,025	–58,805	–12,480
		B	1,309	0,256	0,772	1,847
		C	–0,006	0,001	–0,009	–0,003
2.	X_2	*A*	806,385	557,165	–364,175	1976,945
		B	–104,438	74,729	–261,439	52,563
		C	3,515	2,503	–1,744	8,774
3.	X_3	*A*	–123,626	237,600	–622,806	375,553
		B	11,641	19,687	–29,720	53,003
		C	–0,213	0,407	–1,067	0,641
4.	X_1	*A*	–527,064	354,996	–1283,720	229,592
	X_2	*B*	3,579	1,160	1,107	6,051
		C	48,909	41,861	–40,315	138,134
		D	–0,149	0,072	–0,301	0,004
		E	–0,006	0,001	–0,009	–0,003
		F	–1,084	1,243	–3,734	1,565
5.	X_1	*A*	66,571	272,354	–513,938	647,081
	X_3	*B*	0,932	1,203	–1,631	3,495
		C	–7,501	18,614	–47,175	32,174
		D	0,012	0,067	–0,131	0,154
		E	–0,005	0,003	–0,011	0,000
		F	0,141	0,272	–0,439	0,720
6.	X_2	*A*	1265,849	505,227	188,985	2342,714
	X_3	*B*	–239,603	97,508	–447,438	–31,769
		C	44,492	30,264	–20,013	108,998
		D	7,579	4,203	–1,381	16,538
		E	2,056	5,135	–8,888	13,001
		F	–3,294	1,097	–5,631	–0,956
7.	X_1	*A*	–1056,378	482,925	–2099,675	–13,082
	X_2	*B*	2,712	0,756	1,078	4,346
	X_3	*C*	177,048	83,076	–2,427	356,523
		D	–37,782	20,288	–81,611	6,048
		E	–0,004	0,002	–0,008	0,001
		F	–0,006	0,002	–0,010	–0,002
		G	–5,527	2,711	–11,383	0,329
		H	0,897	0,422	–0,015	1,810
8.	X_1 – zavisna varijabla	*A*	7168,633	1628,194	3698,220	10639,047
		B	–1416,256	314,239	–2086,041	–746,471
	X_2	*C*	290,363	97,530	82,482	498,244
	X_3	*D*	21,512	13,547	–7,362	50,386
		E	30,411	16,548	–4,861	65,682
		F	–12,814	3,534	–20,348	–5,281

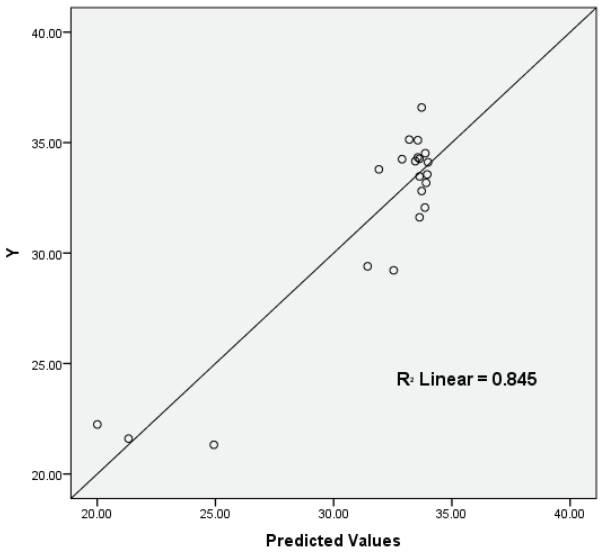

Slika 2. Zavisnost između eksperimentalno određenih i izračunatih vrednosti kapaciteta sorpcije vode prahova NaY zeolita datih jednačinom (12).
Figure 2. The relationship between the experimentally determined and calculated values of water sorption capacity of the powders NaY zeolite given by the equation (12).

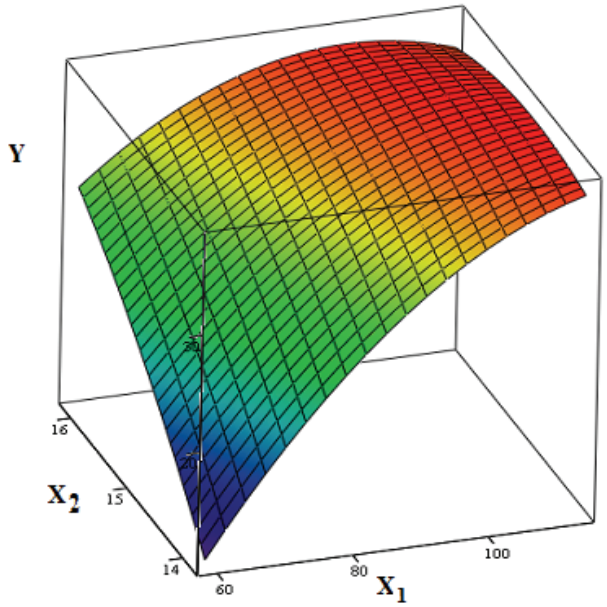

Slika 3. Zavisnost između eksperimentalno određenih i izračunatih vrednosti kapaciteta sorpcije vode prahova NaY zeolita datih jednačinom (15).
Figure 3. The relationship between the experimentally determined and calculated values of water sorption capacity of the powders NaY zeolite given by the equation (15).

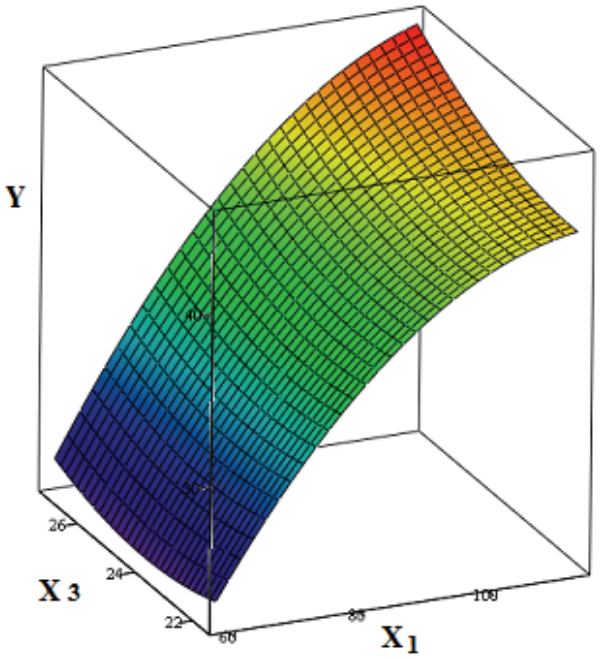

Slika 4. Zavisnost između eksperimentalno određenih i izračunatih vrednosti kapaciteta sorpcije vode prahova NaY zeolita datih jednačinom (16).
Figure 4. The relationship between the experimentally determined and calculated values of water sorption capacity of the powders NaY zeolite given by the equation (16).

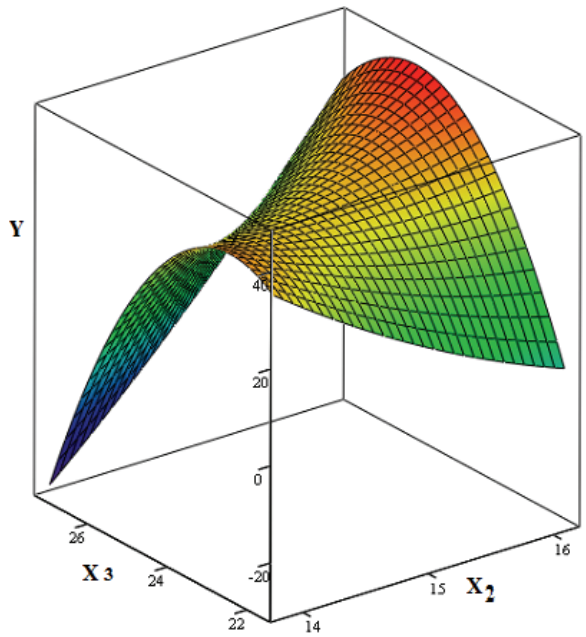

Slika 5. Zavisnost između eksperimentalno određenih i izračunatih vrednosti kapaciteta sorpcije vode prahova NaY zeolita datih jednačinom (17).
Figure 5. The relationship between the experimentally determined and calculated values of water sorption capacity of the powders NaY zeolite given by the equation (17).

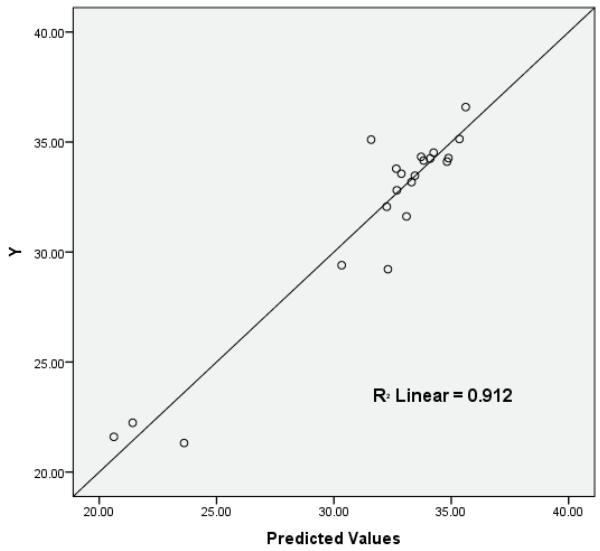

Slika 6. Zavisnost između eksperimentalno određenih i izračunatih vrednosti kapaciteta sorpcije vode prahova NaY zeolita datih jednačinom (18).
Figure 6. The relationship between the experimentally determined and calculated values of water sorption capacity of the powders NaY zeolite given by the equation (18).

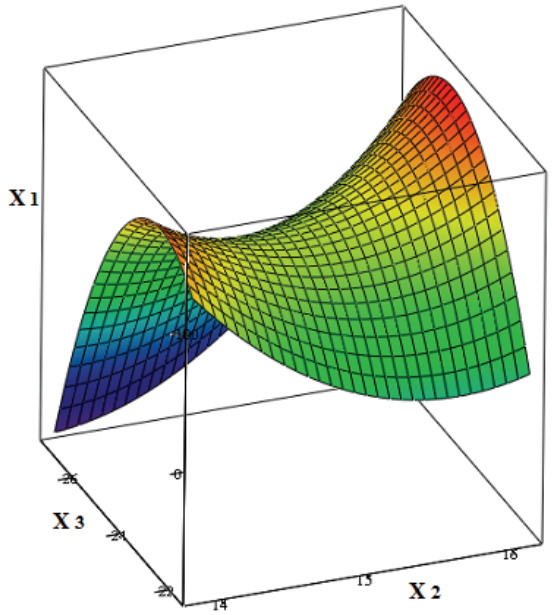

Slika 7. Zavisnost između eksperimentalno određenih i izračunatih vrednosti kapaciteta sorpcije vode prahova NaY zeolita datih jednačinom (19).
Figure 7. The relationship between the experimentally determined and calculated values of water sorption capacity of the powders NaY zeolite given by the equation (19).

ZAKLJUČAK

Izvedena ispitivanaja uticaja sastava NaY zeolita (%Na_2O i %Al_2O_3) kao i *SK* na *WSC*, ukazuju da dominantan uticaj na *WSC* ima *SK* (*PC* = 0,830 i *p* = 0,000) i sadražaj Al_2O_3 (*PC* = 0,763 i *p* = 0,000). Optimalani sastav NaY zeolita sa Na_2O : 13–14% i sadržaju Al_2O_3: 21––23%, uz stepen kristaličnosti 100–114%, obezbeđuje maksimalne vrednosti *WSC* u granicama od 34–36%. Dobijena zavisnost $Y = f(X_1,X_2,X_3)$, u obliku kvadratne funkcije (KNRA), obezbeđuje pouzdanu predikciju *WSC* od *SK* i sadržaja Na_2O i Al_2O_3 sa vrednošću R^2 = 0,912, iako je broj uzoraka bio ograničen.

LITERATURA

[1] M.M. Rahman, M.B. Awang, A.M. Yusof, Preparation, Characterization and Application of Zeolite-Y (Na-Y) for Water Filtration, Aust. J. Basic Appl. Sci. **6** (2012) 50–54.
[2] D. Milić, D. Opsenica, B. Adnađević, B. Šolaja, NaY Zeolite: A Useful Catalyst for Nitrile Hydrolysis, Molecules **5** (2000) 118–126.
[3] J. Weitkamp, L. Puppe. Catalysis and Zeolites: Fundamentals and Applications, Springer, New York, 1999.
[4] R. Xu, W. Pang, J. Yu, Q. Huo, J. Chen, Chemistry of Zeolites and Related Porous Materials: Synthesis and Structure, John Wiley & Sons, New York, 2009.
[5] http://www.iza-structure.org/
[6] J.A. Kaduk, J. Faber, Crystal Structure of Zeolite Y as a Function of Ion Exchange, Rigaku J. **2** (1995) 14–34.
[7] H.V. Bekkum, E.M. Flanigen, P.A. Jacobs, J.C. Jansen. Introduction to Zeolite Science and Practice, 2nd ed., Elsevier, Amsterdam, 2001.
[8] K. Byrappa, M. Yoshimura, Hand Book of hydrothermal Technology: A Technology for Crystal Growth and Materials Processing, William Andrew Inc, Norwich, 2001.
[9] J.P. Bellat, C. Paulin, M. Jeffroy, A. Boutin, J.L. Paillaud, J. Patarin, A. Di Lella, A. Fuchs, Unusual Hysteresis Loop in the Adsorption−Desorption of Water in NaY Zeolite at Very Low Pressure, J. Phys. Chem., C **113** (2009) 8287––8295.
[10] A.W. Chester, E.G. Derouane, Eds., Zeolite Characterization and Catalysis, A Tutorial, Springer, New York, 2009.
[11] ASTM Standard Test Method: D 3942-03 TM for Determination of the Unit Cell Dimension of a Faujasite-Type Zeolite, ASTM Standard Test Method: D 3906-03 TM for Determination of Relative Zeolite Diffraction Intensities of a Faujasite-Type Zeolite.
[12] A. Gola, B. Rebours, E. Milazzo, J. Lynch, E. Benazzi, S. Lacombe, L.Delevoye and C. Fernandez, Effect of Leaching Agent in the Dealumination of Stabilized Y Zeolites, Micropour. Mesopour. Mater. **40** (2000) 73–83.
[13] K. Ojha, N.C. Pradhan, A.N. Samanta, Zeolite from Fly Ash: synthesis and Characterization, Bull. Mater. Sci. **27** (2004) 555–564.
[14] Y. Iwai, T. Yamanishi, Influence of Framework Silica-to-Alumina Ratio on the Tritiated Water Adsorption and Desorption Characteristics of NaX and NaY Zeolites, J. Nucl. Sci. Technol. **45** (2008) 532–540.
[15] K. Tsutsumi, K. Mizoe, Heat of adsorption of water on hydrophobic zeolite, Colloids Surfaces **37** (1989) 29–38.
[16] W. Lutz, C.H. Rüscher, Th.M. Gesing, M. Stöcker, S. Vasenkov, D.Freude, R. Gläser, C. Berger, Investigations

of the Mechanism of Dealumination of Zeolite Y by Steam: Tuned Mesopore Formation *versus* The Si/Al ratio, Proceedings of the 14th International Zeolite Conference, Cape Town, South Africa, 2004, pp. 1411––1417.

[17] A. Shalhbazi, R.G. Olmos, F.D. Kopinke, P.Z. Poor, A. Georgi, Natural and sythetic zeolites in adsorption/oxidation process to remove surfactant molecules from water, Sep. Purif. Technol. **127** (2014) 1–9.

[18] L. Nasrasimhan, B. Kuchta, O. Scheaf, P. Brunet, P. Boulet, Mechanism of adsorption of p-cresol uremic toxin into faujasite zeolite in presence of water andsodium cations-A Monte Carlo study, Micropour. Mesopour. Mat. **173** (2013) 70–77.

[19] M. Rahmati, H. Modarress, Grand canonical Monte Carlo simulation of isotherm for hydrogen adsorption on nanopouros siliceous zeolites at room temperature, App. Surf. Sci. **255** (2009) 4773–4778.

[20] M.L. Restrepo, M.A.Mosquera, Accurate correlation, thermochemistry, andstructural interpretation of equilibrium adsorption isotherms of water vapor in zeolite 3A by means of a generalized statistical thermodynamic adsorption model, Fluid Phase Equilib. **283** (2009) 73–88.

[21] Ž. Živković, I. Mihajlović, Dj. Nikolić, Artificial neural network method applied of the nonlinear multivariante problems, Serb. J. Manag. **4** (2009) 137–149.

[22] P. Đorđević, I. Mihajlović, Ž. Živković, Comparasion of linear and nonlinear ststistics methods applied in industrial process modeling procedure, Serb. J. Manage. **5** (2010) 189.

SUMMARY

EFFECT OF DEGREE OF CRYSTALLINITY AND THE CONTENTS OF ALUMINIUM OXIDE AND SODIUM OXIDE ON WATER SORPTION CAPACITY IN NaY ZEOLITE

Dragana M. Kešelj[1], Dragica Z. Lazić[1], Živan D. Živković[2], Branko T. Škundrić[3], Jelena V. Penavin-Škundrić[4], Slavica G. Sladojević[4]

[1]*University of East Sarajevo, Facluty of Technology Zvornik, Republic of Srpska*
[2]*University of Belgrade, Techical facuty in Bor, Republic of Serbia*
[3]*Academy of Sciences and Arts of the Republic of Srpska, Republic of Srpska, Bosnia and Hercegovina*
[4]*University of Banja Luka, Faculty of Technology Republic of Srpska, Bosnia and Hercegovina*

(Scientific paper)

The paper presents mathematical models which describe the dependence between water sorption capacity, on one hand, and the degree of crystallinity and the content of Na_2O and Al_2O_3 in NaY zeolite, on the other. NaY was synthesized from sodium aluminate solution, water glass and sulfuric acid under different conditions of crystallization. The obtained zeolite powders underwent chemical analysis (Na_2O and Al_2O_3), water sorption capacity (*WSC*), as well as diffraction analysis which served to determine the degree of crystallinity (*CD*). Zeolite powder samples had the following values: for the content of Na_2O from 13.81 to 16.14%, for Al_2O_3 from 21.58 to 27.17%, degree of crystallinity from 58.70 to 114.00 and *WSC* from 21.32 to 36.59%, and regression analysis lead to the conclusion that there is a significant correlation between water sorption capacity and the degree of crystallinity, unlike the contents of Na_2O and Al_2O_3 in the zeolite powder, whose correlation with water sorption capacity was neglibile. The mathematical model obtained by linear regression analysis had a high R^2 = 0.796, where as non-linear regressional analysis produced a better mathematical model R^2 = 0.912, where water sorption capacity was expressed through a quadratic model.

Keywords: Regression analysis • Water sorption capacity • Degree of crystallinity

Development of a new ultra-high performance liquid chromatography––tandem mass spectrometry method for determination of ambroxol hydrochloride in serum with pharmacokinetic application

Maja M. Vujović[1,2], Milan Jokanović[1], Goran M. Nikolić[1]

[1]*Faculty of Medicine, University of Niš, Serbia*
[2]*Institute of Forensic Medicine, Toxicology Laboratory, Niš, Serbia*

Abstract

Ambroxol hydrochloride is an expectorant agent, successfully applied in mucolytic therapy for acute and chronic bronchopulmonary diseases. The drug regulates not only mucus secretion but also showed antioxidant, anti-inflammatory and local anesthetic properties. To supplement the pharmacokinetic and toxicological studies of ambroxol, a rapid ultra-high performance liquid chromatography–tandem mass spectrometry method for the quantitation of ambroxol in rabbit serum was developed. A validation of the method was performed as per the ICH guidelines for the validation of bioanalytical methods. The chromatographic separation was achieved in a submicron Kinetex RP-C_{18} column (2.1 mm×50 mm, 1.3 μm) using the no buffer mobile phase. The ESI mass spectrometry in the MRM mode was used with a typical transitions *m/z* 378.9→263.8 for ambroxol and *m/z* 455.2→165.0 for IS. Linearity was determined with an average coefficient of determination >0.999 over the dynamic range from 0.5–200 ng/mL with *LOD* and *LOQ* of 0.25 and 0.5 ng/mL, respectively. The results of the intra- and inter-day precision and accuracy determined in different days were all found to be within the acceptable limits ±15%. The present method was successfully applied to pharmacokinetic study in the rabbits after a single oral dose administration.

Keywords: ambroxol hydrochloride, UHPLC–MS/MS, serum, pharmacokinetics.

Available online at the Journal website: http://www.ache.org.rs/HI/

SCIENTIFIC PAPER

UDC 543.544.5:616.15–092.9:615

Hem. Ind. **70** (4) 409–418 (2016)

doi: 10.2298/HEMIND150625048V

During the last three decades, the ambroxol hydrochloride has been widely used as a mucoregulatory agent in different pharmaceutical formulations. Ambroxol is the drug that is used as a mucolytic agent alone and in combination with antibiotics. The pharmacology of ambroxol is apparently complicated considering that it is known several mechanisms of its action. In addition to the well-known expulsion of the mucus and clearance facilitation, the ambroxol also facilitates productive cough and had shown antioxidant, anti-inflammatory, analgesic, local anesthetic, antiviral and antibacterial effects [1–5]. Ambroxol is applied in mucolytic therapy of acute and chronic diseases associated with increased production and disruption of the formation and transportation of mucus (mucociliary clearance). The increase in the fluid secretion and mucociliary clearance facilitate the expectoration [6]. Local anesthetic effect of ambroxol observed in the rabbit eye model is interpreted as the ability to block sodium channels [7]. *In vitro* studies have shown that ambroxol blocks the cloned neuronal sodium channel, and this binding was reversible and concentration-dependent [8]. It has been shown that the ambroxol *in vitro* also significantly reduces the release of the cytokines from the blood, as well as the mononuclear and polymorphonuclear cells associated with the tissue [9]. These pharmacological properties are consistent with the accompanying observations in the clinical trials for efficacy of the ambroxol treatment of upper respiratory tract symptoms, which leads to the relief of pain and discomfort associated with pain in the region of the ear-nose-trachea [10]. Ambroxol is often combined with antibiotics (amoxicillin, doxycycline and erythromycin), even in a single tablet or syrup, because it increases the concentration of antibiotics in bronchopulmonary secretions and sputum [11].

Pharmacokinetics of the ambroxol in humans is well documented. After oral administration, the ambroxol is rapidly and completely absorbed, and the maximum plasma concentration (c_{max}) is reached within two hours after administration of immediate-release tablets. Distribution of the ambroxol is rapid, with the largest concentration achieved in the lungs. It is highly bound to binds to the plasma proteins (70–80%) [12]. Approximately 30% of a given oral dose is eliminated by the first-pass metabolism. The ambroxol is metabolized mostly in the liver by glucuronidation and decomposition of the dibromantranilic acid in the pre-

Correspondence: M.M. Vujović, Faculty of Medicine, University of Niš, Bul. Dr. Zorana Đinđića 81, 18000 Niš, Serbia.
E-mail: majavujovic1@gmail.com
Paper received: 25 June, 2015
Paper accepted: 28 August, 2015

sence of CYP3A4. The ambroxol is eliminated with a half-life of 10 h [13].

Several chromatographic and non-chromatographic methods have been developed for the determination of the ambroxol in different pharmaceutical formulations (syrup, tablets, lozenges) and biological samples. Using electrochemical properties of the ambroxol, non-chromatographic methods such as amperometric with carbon film resistor electrodes [14] and cyclic voltammetry with boron-doped diamond electrode method [15] were reported, both used in the pharmaceutical research and development. The capillary gas-liquid chromatography [16], capillary zone electrophoresis and fluorescent detection [17,18] with reached limit of detection of 2 and 8 ng/ml, were successfully applied for the quantification of ambroxol in human plasma. The most employed chromatographic method for this purpose is a high-performance LC with UV/Vis spectrophotometric [19,20] and photodiode array detection [21]. The separation LC chromatographic methods are usually used for the ambroxol determination in the pharmaceuticals as well as in human, rat or dog plasma [22–26]. Using a high mobile phase flow rate (>1 mL/ /min, except EC 0.2 mL/min), long chromatographic run time (>15 min) and large sample injection volume (>50 mL) to reach a low quantification limits (>10 ng/ml), make this methods unsuitable for extensive and sensitive validation procedures. To analyze ambroxol in the biological specimens several highly sensitive and precise LC–MS and LC–MS/MS methods have also been reported. The achieved limits of detection were in the range of 0.2–1.0 ng/mL with a sample volume of 0.5–1 mL [27–30]. The presented MS methods have already enabled pharmacokinetic studies of ambroxol in the human volunteers [31,32].

The purpose of this study was to develop an ultra--high performance liquid chromatography–tandem mass spectrometry (UHPLC–MS/MS) method for the simple determination of the ambroxol in rabbit serum. Further method application should contribute to a new pharmaceutical and pharmacokinetic studies of the ambroxol in animals and humans.

The experimental procedure included evaluation of the optimal parameters for sample preparation, chromatographic conditions and MS/MS detection. Through the validation process, several significant advances were achieved: 1) a chromatographic separation with a shorter run time in 1.3 µm submicron column, 2) a high sensitivity with a very small amount of sample and injection volume and 3) a high purity of the sample extracts obtained with a solid-phase extraction procedure which has provided the MS/MS measurements without the interferences. The developed UHPLC––MS/MS method was successfully implemented in a pharmacokinetic study of the ambroxol in rabbits.

MATERIAL AND METHODS

Chemicals and reagents

Ambroxol hydrochloride, standard and verapamil hydrochloride, internal standard (IS) were provided by Fluka (Dorset, UK). Methanol (MeOH), acetonitrile (ACN), formic acid (gradient grade for LCMS) were purchased from Promochem (Wesel, Germany), while ammonium hydroxide (NH_4OH), hydrochloric acid (HCl) and potassium hydrogen phosphate (analytical grade) were purchased from Sigma–Aldrich (Dorset, UK). Ultra-pure Optima™ LC/MS water was obtained from Fisher Chemical (Waltham, MA, USA). Strata^{TM}-X-C polymeric strong cation exchange solid phase extraction cartridges (30 mg, 1 mL) were obtained from Phenomenex (Torrance, CA, USA).

Instrumentation and chromatographic conditions

The data were collected with a liquid chromatography–tandem quadrupole Shimadzu LCMS-8030 mass spectrometer equipped with the atmospheric pressure chemical ionization (APCI), the electrospray ionization (ESI) and the dual ion source (DUIS) mode. The MS detection was carried out in a positive (+) electrospray ionization mode with the multiple reaction monitoring (MRM) of the transitions for each compound. An automated wizard was used to perform the MRM optimization and determination of the optimum ion optics voltages and collision energies, as well as the highest intensity of the product ions. The desolvation line (DL) and heater block (HB) temperatures were 270 and 400 °C, respectively. Argon was used as collision gas (230 kPa) and nitrogen as the nebulizer and dry gas at flow rates of 3 and 15 L/min. The selected MRM transitions were: m/z 378.9→263.8 for the ambroxol and m/z 455.2→165.0 for the internal standard (verapamil). The compounds were identified by matching the retention times and mass spectral data with those of the calibration standards while the method of internal standard was used for the quantification of ambroxol in all samples.

The Shimadzu UHPLC system with binary pumps (LC-30AD, Nexera), column oven (CTO-30A, Nexera), degasser (DGU-20A, Prominence), communication interface (CBM-20A, Prominence) and autosampler (SIL-30AC, Nexera) were used. Optimal chromatographic efficiency was achieved at reversed-phase column Kinetex^{TM} C_{18}-column (2.1 mm×50 mm, 1.3 µm, Phenomenex, USA) with an isocratic mobile phase methanol––0.01% formic acid aqueous solution (90:10, *V*/*V*) at a flow rate of 0.3 ml/min. Before the use, the mobile phase was filtered through 0.22 µm membrane filter paper. The operating temperature of the column was set to 40 °C and the cooler of autosampler at 15 °C. The

measured signal was monitored and processed using Lab Solution software.

Preparation of stock and standard solutions

Stock solutions of the ambroxol and internal standard were prepared at a concentration of 1 mg/mL in methanol and were serially diluted to get working standard solutions for the preparation of calibration curves. The stock solutions were stored at –20 °C and used up to three weeks for preparation while working dilutions were freshly made when needed.

For the preparation of calibrators (CCs) and quality control samples (QC_S), the standard solutions of ambroxol and internal standard (20 ng/mL) were spiked to 250 µl of blank serum in 10 ml glass tube, within calibration limit. Calibrators for this method were prepared at the following concentrations: 0.5, 2, 5, 10, 20, 50, 100, 150 and 200 ng/mL and the quality control samples at levels of lower limit of quantitation (*LLOQ*): 0.5 ng/mL, low (*LQC):* 20 ng/mL, medium (*MQC*): 100 ng/mL and high (*HQC*): 200 ng/mL. All samples were stored at 4 °C and analyzed during the same day.

Sample preparation

All calibrators (CCs), quality controls (QC_S), and serum samples were prepared in the same manner using polymeric strong cation exchange solid phase extraction cartridges (Strata™-X-C). Summarily, after stirring with the vortex mixer, the 250 µl diluted, pH adjusted (1:1 phosphate buffer, pH 6.7/25 °C) and added IS (20 ng/mL) samples were loaded onto cartridges. The cartridges were previously conditioned and equilibrate with 1 ml of methanol and 1 ml of 0.1 M HCl. Washing step was also performed using 1 ml of 0.1 M HCl. The SPE tubes were then dried under full vacuum for 5 min and eluted with 2×500 µl 90:10 MeOH/ACN containing 5% of concentrated NH_4OH solution applying a light vacuum. The residue was evaporated to dryness under a stream of nitrogen at 40 °C and dissolved in 250 µl of the mobile phase. After filtration (0.22 µm syringe filter), 2 µl was injected into the UHPLC–MS/MS system.

Method validation

The validation of the UHPLC–MS/MS method for the determination of ambroxol in rabbit serum was performed in accordance with ICH Q2A/Q2B guidelines [33] and included the following parameters: sensitivity, linearity, accuracy and precision, specificity, stability tests, carry-over and matrix effects.

Extraction recovery

The absolute recovery of ambroxol from serum by SPE was determined for three different standard concentrations by spiking the analyte into the blank serum. The extraction recovery was calculated by comparing the peak areas extracted from spiked samples with those of the same quantities added to the mobile phase. The recovery of three QCs (20, 100 and 200 ng/mL) concentrations in serum was repeated six times.

Animal experiment

Male *Oryctolagus cuniculus* rabbits (3.0–3.5 kg) were bred and housed in the Laboratory Animal Services Centre. All experiments were conducted to comply with the Good Laboratory Practice (GLP, 40 CFR Part 160: U.S. EPA) regulations [34] and approved by the Animal Research Ethics Committee. The animals were housed with free access to food and water in a temperature controlled room (23±2 °C) with a 12 h light-dark cycle. In the animal study, rabbits were fasted overnight with free access to the water before administration of the ambroxol. After administration of a single tablet containing 30 mg of ambroxol directly to each rabbit's stomach, 1 ml of the blood samples were collected from the auricular marginal vein at 0.25, 0.5, 1, 2, 4, 6 and 24 h time-points. Serums were separated by the centrifugation 7000×*g* for 10 min at room temperature and then stored at –70 °C prior to analysis. Aliquots of 0.25 ml serum samples were processed with defined SPE method and analyzed for the ambroxol content.

Pharmacokinetic and statistical analysis

Statistical analyzes of the validation parameters were performed by using Microsoft Office Excell 2013. Each value was expressed as the mean ±*SD* and the *RSD* (%). The pharmacokinetic parameters for ambroxol were calculated using a non-compartmental model of the Thermo Scientific™ Kinetica software for PK/PD data analysis (version 5.0, Thermo Electron Corporation, USA).

RESULTS AND DISCUSSION

Method development

Chromatographic parameters

All the LC chromatographic conditions were optimized to achieve the symmetric peak shapes, good resolution and short run time. Three types of the columns C-18 (1.3, 1.7 and 2.6 µm) were tested and finally a reversed-phase Kinetex RP-C-18 column (2.1 mm×50 mm; 1.3 µm, Phenomenex, USA) with security guard C-8 column (Kinetex, Phenomenex, USA) was applied. The stationary UHPLC phase with 1.3 µm particle size, which use has not been recorded in the literature data so far, enabled the separation of the analytes with high sensitivity in a very short chromatographic run time. Using data from published works, the various concentrations of formic buffer solutions in the methanol and acetonitrile were tested as a mobile phase

[27,28,31,32]. Finally, the modified bicomponent mixture of 90% methanol and 10% formic acid solution in water (0.01%), was found as appropriate for the chromatographic separation. The retention times of the ambroxol and IS (verapamil) were 0.79 and 0.91 min, respectively, with the total chromatographic run time of 1.5 min.

Spectrometric parameters

The electrospray MS detection was performed in the full-scan and the multiple reaction ion monitoring mode (MRM). First, the full tuning of tandem quadrupole control parameters was performed to obtain the accurate ion mass calibration and the measurement of mass spectrums with high sensitivity and resolution. Then, the *m*/*z* values of the precursor (Q1 quadrupole) ions, product (Q3 quadrupole) ions and the voltages of collision energies were input into the MRM event table and auto-optimized for the each compound. The MS detecting conditions were operated according to the MS signal response of the target compound. The full--scan mode results showed that the positive mode of ionization was much more sensitive than the negative mode with a typical protonated MS ion mass spectra $[M+H]^+$; *m*/*z* 378.9 for ambroxol and IS *m*/*z* 455.2 at 100 mg/L. Furthermore, the MRM mode was used for the quantification of analytes with the appropriate transitions and run time segments; *m*/*z* 378.9→263.8 (0.4–1.2 min) and *m*/*z* 455.2→165.0 (0.5–1.5 min) for ambroxol and IS, respectively, as present Figure 1. All applied transitions were according to the literature data [30]. The total run time was 1.5 min with a dwell/ /pause time of 200/1 and 100/2 ms for each compound. The MRM ion chromatograms of a blank, zero, ambroxol standard at 20 ng/mL and rabbit serum sample were presented in Figure 2. Other optimized MS conditions were as follow: interface voltage: 4.5 kV; conversion dynode voltage: 6 kV; detector: –1.92 kV and exit lens: –4.0 V. The collision energy was optimized and applied to –20 and –25 V; Q1 precursor bias/Q3 product bias: –28/–18 and –11/–10 V for AMB and IS, respectively.

Sample preparation

Sample preparation with the high recovery and purity without matrix interferences is the key to successful MS/MS determination. The most common problems faced in the extraction of an analyte from biological matrices are solubility and natural organic substances in the samples that reduce extraction efficiency and hinder detection [35]. The MS/MS analysis of low purity biological samples can cause ion suppression, elevated background, and other negative matrix effects. Results may significantly influence on the lack of selectivity. Moreover, the use of columns with submicron particles (<2 μm) which leads to very high back pressures require very pure solvents and sample extracts. The residual matrix components also limit the lifespan of these columns much more than they limit the lifespan of conventional columns.

According the literature data, extraction techniques published for this purpose are protein precipitation (PPE) and liquid–liquid extraction (LLE) with the extraction recovery 70–90% [27–32]. In order to achieve better extracts purity and recovery with a smaller sample volume, in this study was developed a four-step solid phase extraction (SPE) procedure. Considering the solubility and pK_a values of ambroxol and verapamil (IS), the strong cation exchange cartridges (Strata^{TM} – X-C) showed the satisfactory results and therefore used in further proceedings of the sample preparations. The relative extraction efficiency (*RE*) was determined by comparing peak areas obtained from extracted serum samples with those found by extracting blank matrices through the extraction procedure and spiking with a known amount of the ambroxol. The examined extract

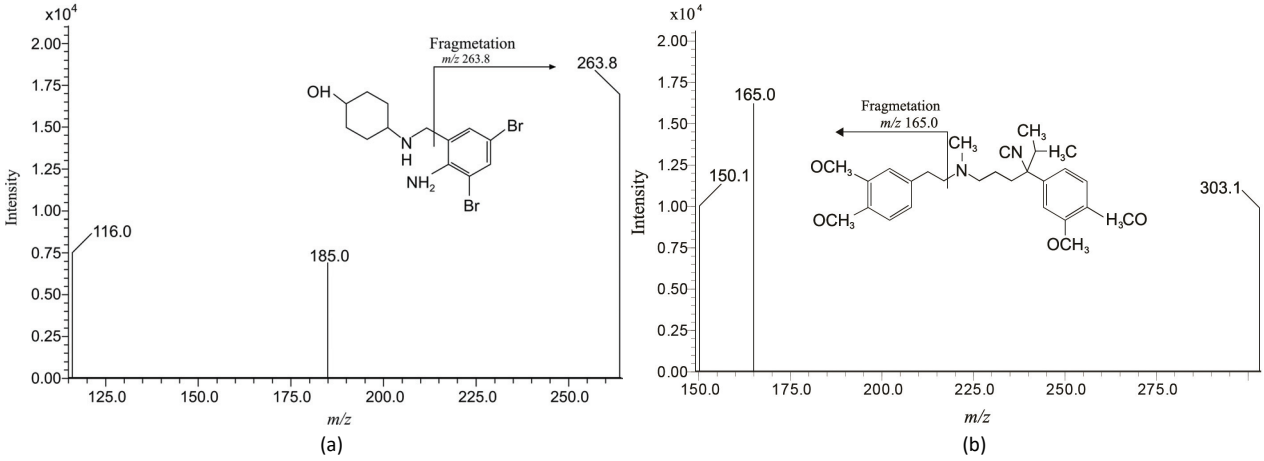

Figure 1. Typical product MS ion mass spectra of the protonated $[M+H]^+$ for: a) ambroxol, m/z 378.9→263.8, and b) internal standard (verapamil), m/z 455.2→165.0, in MRM mode with structural fragmentation.

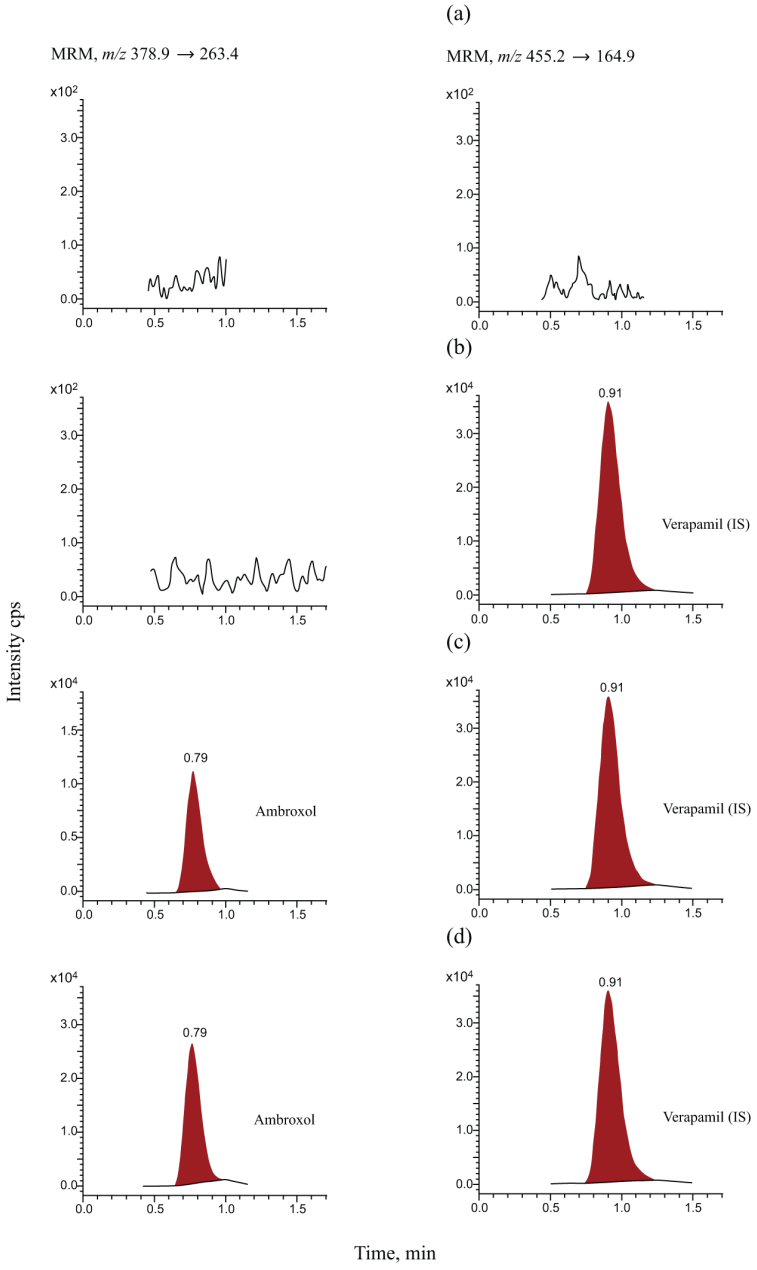

Figure 2. MRM ion chromatogram of: a) sample without internal standard (blank), b) sample with internal standard (zero), c) ambroxol at 20 ng/mL (m/z 378.9→263.8) and d) rabbit serum at 4 h after administration of 30 mg single oral dose of ambroxol.

efficiency was evaluated over three concentration levels, 20, 100 and 200 ng/mL, with the mean relative recovery of 85.96±9.05%.

Method validation

Linearity-calibration curve

Linearity was assessed by three calibration curves over nine-point calibration with a concentration range from 0.5–200 ng/mL, without zero points. The calibration samples were injected six times (n = 6) on three different days. The high correlation coefficients (r^2 > > 0.99) for all calibration curves indicated good correlations. The corresponding average regression line was: $y = (0.0125\pm0.0003)x - (0.0013\pm0.0008)$, where y is the peak ratio of ambroxol/IS and x the concentration of the ambroxol. A least square regression model was fitted to each standard curve with the mean value of the correlation coefficient (r^2) of 0.9995 and standard deviation of 0.00045. Under certain assumptions required for valid linear regression, reliable results were obtained, and suitable prediction function was defined. First, the linear relationship between the concentrations and the peak areas is evident from the corresponding scatter plots. No significant "outliers" were noticed. Further, homoscedasticity of the error terms was established using Hartley's test, and the

independence of the residuals was proved by using the Durbin-Watson autocorrelation test. Also, the normality of the error terms of the regression line was not violated as Shapiro–Wilk test showed. The "lack of the fit" test was also performed and showed the high coefficients of the correlation ($r > 0.999$) between the two variables. The value of $p < 0.001$ indicated that the regression model statistically significantly predicts the outcome variable, *i.e.*, is a good fit for the data.

Sensitivity

The lowest standard on the calibration curves, 0.5 ng/mL was accepted as the *LLOQ* with accuracy criteria within ±20% of the signal to noise ratio $S/N \geq 1:10$. The accepted quantitation limit showed the satisfactory levels of the published LC–MS/MS methods for determination of ambroxol in human plasma [30]. The accuracy of the other CC samples at all concentration levels were within the acceptable RSD range of 1.63–10.72%. The *LOD*s were set at three times the noise level of the baseline in the chromatogram ($S/N \geq 1:3$) and the concentration of 0.25 ng/mL was confirmed as a limit of detection for the method.

Accuracy and precision (repeatability)

To evaluate accuracy and precision of the method, the six replicates at four concentration levels (*LLOQ*: 0.5 ng/mL; low: 20 ng/mL, medium: 100 ng/mL and high: 200 ng/mL) were obtained with one batch for intra-day and over the 3 days for inter-day. Acceptance criteria were *RSD* ≤ 20% for *LLOQ* and low concentrations and ≤ 15% for medium and high concentrations. The mean intra-day *RSD* (%) was 3.38% (range 0.69––5.74%) and the corresponding value for inter-day was 5.43% (range 3.18–7.77%). The mean intra-day accuracy was 107.6% (range 100.3–118.6%) and corresponding value for inter-day was 106.7% (range 99.9––110.1%). The satisfactory measured results indicated that the established method is high reproducible and repeatable, as listed in Table 1.

Matrix effect and selectivity

For completely bioanalytical method validation, the influence of matrix effect was evaluated according the Matuszewski *at al*. (2003). The matrix factors for the ambroxol and IS, was calculated as the ratio between the areas in the presence (A) and absence (B) of the matrix. The calculated matrix factors ($A/B > 0.9$) indicates that no statistically significant ion suppression occurred. Furthermore, the assay selectivity was assessed by extracts from the free lots of serums by different untreated rabbits. The endogenous and exogenous peaks at the retention times of analytes were not observed in any of the evaluated blank serum lots as showed Figure 2a. In addition, to prove absence of a cross interferences between MS/MS channels used for the ambroxol and IS monitoring, it was separately injected each of the compound at a high concentration (200 ng/ml) and monitored in opposite channel. No cross-talk effect was observed.

Carryover effect

The carryover effects were studied by analysis of the three replicates of the blank sample, which was injected immediately after the sample at concentration 1.5 higher than HQC (300 ng/mL). The response of the blank at a retention time of ambroxol has not been exceeded 20% of the average responses of the analyte at *LLOQ* concentration level.

Stability tests

The stock solution stability test was evaluated at one concentration (20 ng/mL, $n = 3$). The average area of stored standard solution (5 h/room temperature) compared with the freshly prepared standard solution showed no significant static difference (not higher than 5%). Aqueous work standards solutions of the ambroxol were stable for at least 20 days stored at the fridge temperature (4 °C). The short-term, long-term and on the instrument stability test of QC samples were evaluated at two concentration levels, low (20 ng/mL) and high (200 ng/mL). Six replicates of each level were achieved at the initial time point and after a period of

Table 1. Intra- and inter-day precision and accuracy (n = 6); SD, standard deviation; RSD, relative standard deviation

Solution stability	Nominal concentration, ng/mL	Precision		Accuracy, %
		Mean±*SD*	*RSD* / %	
Intra-day	0.5	0.59±0.03	5.74	118.59
	20	20.92±1.16	5.52	104.58
	100	106.87±1.69	1.59	106.87
	200	200.63±4.71	0.69	100.32
Inter-day (3 days)	0.5	0.55±0.04	7.77	110.10
	20	21.35±1.07	5.01	106.78
	100	109.92±3.50	3.18	109.92
	200	199.72±11.53	5.77	99.86

storage (1 h) at a room temperature for short-term, at –20 °C/10 days for long-term, and after 24 h sample standing on an autosampler stability test. The same concentrations and replicates were applied for analysis freeze/thaw stability after three cycles. Concentrations of sample stability were back-calculated against freshly prepared calibration curve. The evaluated relative standard deviations were obtained in acceptable ranges between ±15% at a high levels and ±20% at a low level, as showed in Table 2. All of the applied stability tests did not show significant degradation level, which indicates the constant stability of ambroxol in serum under different conditions at least ten days.

ention times.

The ruggedness of the method was studied by comparison of calibrators and QC samples at low and high concentrations with two analysts on different days. The calculated relative standard deviation values less than 5% indicate the ruggedness of the proposed method with no statistically significant differences in measurement.

Pharmacokinetic study

Analytical applicability of the developed UHPLC––MS/MS method was tested in the pharmacokinetic study in rabbits. After single oral dose administration of

Table 2. Stability of quality controls in serum (n = 6), mean ± standard deviation, %

Conditions	c / ng mL^{-1}	
	20	200
Short-term stability (1 h)	111.79±2.58	104.88±1.41
Long-term stability (–20 °C/10 days)	113.42±4.35	112.72±1.10
Autosampler stability (24 h)	96.94±3.49	96.22±1.18
Three freeze/thaw cycles	99.66±8.07	93.71±17.08

Robustness and ruggedness

According to the validation guideline, the robustness of an analytical procedure represent its capacity to remain unaffected by small variations of critical chromatographic parameters [33]. In present work, effects of minor variations of a flow rate, organic percentage share of the mobile phase and column oven temperature were examined around the parameters set in the validated method to demonstrated reliability during normal usage. Chromatographic parameters were changed through the values; 90±0.5% of methanol, 0.3±0.05 mL/min and 40±5 °C for mobile phase organic strength, flow rate, and column oven temperature, respectively. The measurements were performed in three replicate injections (n = 3) with one parameter changing at a time. The obtained results, as represented in Table 3, indicated no significant difference between the results and confirmed the robustness of the developed method, with less variability in the ret-

30 mg ambroxol tablets per rabbit, the serum concentrations were determined over a period of 24 h after administration. The maximum serum concentration (c_{max}), time to reach c_{max} (T_{max}) and the area under the plasma concentration–time curve (AUC) were calculated for each animal and as a mean values. The AUC from time zero to the last quantifiable time point, 24 h ($AUC_{0–24}$) and from time zero to infinity ($AUC_{0–\infty}$) were calculated by the log-linear trapezoidal rule. The elimination half-life ($t_{1/2}$) as 0.693/λz, where λz is the elimination rate constant, was derived from the terminal linear portion of the log plasma concentration–time profile. All above pharmacokinetic parameters, as well as volume of distribution based on the terminal phase (V_d) and total body clearance (Cl), were directly obtained from the experimental data processed by the Kinetica Software, version 5.0. The main pharmacokinetic parameters of ambroxol in rabbit serums are presented in Table 4 and the average concentration–time

Table 3. Robustness evaluation of UHPLC–MS/MS method at concentration of ambroxol standard 20 and 200 ng/mL (n = 3)

Parameter	Value	Mean accuracy[a], %	Precision (*RSD* / %)	Mean accuracy[a], %	Precision (*RSD* / %)
		20 ng /mL		200 ng/ mL	
Column oven emperature (40±5 °C)	–5 °C	101.45	1.24	99.14	1.31
	5 °C	100.25	1.75	96.46	0.41
Mobile phase organic strength (90±5% methanol)	–5% methanol	111.25	0.12	107.91	0.55
	5% methanol	97.83	1.07	94.89	0.44
Flow rate (0.30±0.05 ml/min)	–0.05 ml/min	111.58	1.96	106.72	0.71
	0.05 ml/min	97.29	1.27	89.43	0.89

[a]Mean accuracy at evaluated parameter was calculated by comparison with mean value at validated condition

profile is showed in Figure 3. The average c_{max} and T_{max} of ambroxol in rabbits were 185.52±3.25 ng/mL and 1.61±0.35 h.

Table 4. Mean pharmacokinetic parameters of ambroxol for rabbits following administration of a single oral dose of 30 mg (n = 3)

Parameter	Mean value ± *SD*
c_{max} / ng mL^{-1}	185.52±3.25
AUC0-24, h ng/mL	536.39±67.16
AUC0-inf, h ng/mL	538.74±66.85
T_{max} / h	1.61±0.35
MRT / h	3.15±0.21
$T_{1/2}$ / h	3.53±0.18
K_{el} / h^{-1}	0.19±0.01
Cl, mg h / ng mL^{-1}	0.06±0.01
Vd, mg / ng mL^{-1}	0.29±0.05
Vss, mg / ng mL^{-1}	0.18±0.03

without employing buffer solutions as a component of the mobile phase. The lower limit of detection was achieved at 0.5 ng/mL with only 2 µl of injection volume and 250 µl of sample volume. Repeatability of all concentration levels was high precise with *RSD* less than 5.5% and accuracy greater than 100%. The reported UHPLC–MS/MS method was proved to be reliable and highly sensitive for the determinations of ambroxol in short analysis run time for an only minute and a half. Consequently, the method is enabled a hundred of injections per day which makes the validation process faster and more efficient. The method was also successfully applied to the analysis of ambroxol levels in rabbit serum and determination of pharmacokinetic parameters after dosing a single 30 mg of ambroxol tablet to rabbits.

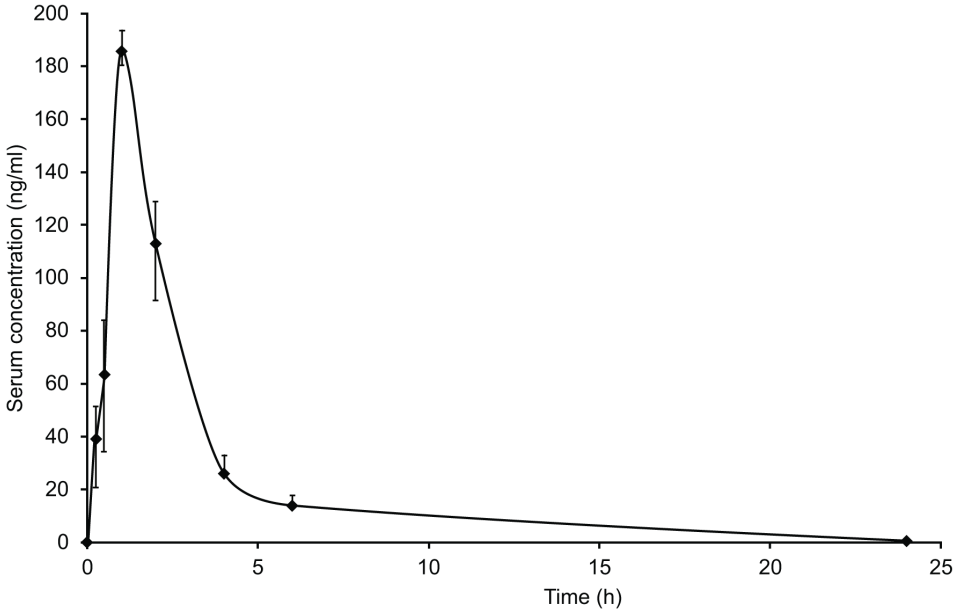

Figure 3. Mean serum concentration-time curve of ambroxol after single oral administration of 30 mg tablet formulation to rabbits at seven time-points (0.25, 0.5, 1, 2, 4, 6 and 24 h).

CONCLUSION

In this study, the determination of ambroxol by UHPLC–MS/MS method in serum after SPE extraction have been established and validated. The validation of the method was performed according the ICH Q2A/ /Q2B guidelines for the validation of bioanalytical methods. Linearity, precision, extraction recovery, carryover, and stability test of the spiked serums stored under different conditions satisfy the acceptance criteria. The presented method was found to be appropriate for all validation parameters. The method was developed in novel 1.3 µm submicron C-18 column

Acknowledgements

This work was supported by Ministry of Education, Science and Technological Development of the Republic Serbia (project 175045). MV is grateful to Ivana Ilić for statistical analysis.

REFERENCES

[1] V. Štětinová, V. Herout, J. Květina, In vitro and in vivo antioxidant activity of ambroxol, Clin. Exp. Med. **4** (2004) 152–158.

[2] K.M. Beeh, J. Beier, A. Esperester, L.D. Paul, Antiinflammatory properties of ambroxol, Eur. J. Med. Res. **13** (2008) 557–562.

[3] W. Gaida, K. Klinder, K. Arndt, T. Weiser, Ambroxol, a Nav1.8-preferring Na(+) channel blocker, effectively suppresses pain symptoms in animal models of chronic, neuropathic and inflammatory pain, Neuropharmacology **49** (2005) 1220-1227.

[4] A. Leffler, J. Reckzeh, C. Nau, Block of sensory neuronal Na+ channels by the secreolytic ambroxol is associated with an interaction with local anesthetic binding sites, Eur. J. Pharmacol. **630** (2010) 19–28.

[5] B. Yang, D.F. Yao, M. Ohuchi, M. Ide, M. Yano, Y. Okumura, H. Kido, Ambroxol suppresses influenza-virus proliferation in the mouse airway by increasing antiviral factor levels, Eur. Respir. J. **19** (2002) 952–958.

[6] M. Malerba, B. Ragnoli, Ambroxol in the 21st century: pharmacological and clinical update, Expert Opin. Drug Metab. Toxicol. **4** (2008) 1119–1129.

[7] Boehringer Ingelheim Ltd Consumer Healthcare, Summary of Product Characteristics last updated on medicines.ie: 31/07/2014, Lysopadol Mint 20 mg Lozenges, (http://www.medicines.ie/printfriendlydocument.aspx?documentid=15167&companyid=2470)

[8] T. Weiser, Comparison of the effects of four Na+ channel analgesics on TTX-resistant Na+ currents in rat sensory neurons and recombinant Nav1.2 channels, Neurosci. Lett. **395** (2006) 179–184.

[9] B.F. Gibbs, W. Schmutzler, I.B. Vollrath, P. Brosthardt, U. Braam, H.H. Wolff, G. Zwadlo-Klarwasser, Ambroxol inhibits the release of histamine, leukotrienes and cytokines from human leukocytes and mast cells, Inflamm. Res. **48** (1999) 86–93.

[10] C. De Mey, H. Peil, S. Kölsch, J. Bubeck, J.Vix, Efficacy and safety of ambroxol Lozenges in the treatment of acute uncomplicated sore throat, Arzneimittel-Forsch. **58** (2008) 557–568.

[11] F. Fraschini, F. Scaglione, G. Scarpazza, F. Marchi, M. Calzavara, Effects of a mucolytic agent on the bioavailability of antibiotics in patients with chronic respiratory diseases, Curr. Ther. Res. **43** (1988) 734–742.

[12] H.J. Lee, S.K. Joung, Y.G. Kim, J.Y. Yoo, S.B. Hana, Bioequivalence assessment of ambroxol tablet after a single oral dose administration to healthy male volunteers, Pharmacol. Res. **49** (2004) 93–98.

[13] N. Ishiguro, C. Senda, W. Kishimoto, Y. Sakai, K. Funaeoe, T. Igarashi, Identification of CYP3A4 as the predominant isoform responsible for the metabolism of ambroxol in human liver microsomes, Xenobiotica **30** (2000) 71–80.

[14] F.S. Felix, C.M.A. Brett, L. Angnes, Flow injection analysis using carbon film resistor electrodes for amperometric determination of ambroxol, Talanta **76** (2008) 128–133.

[15] A. Levent, Y. Yardım, Z. Sentürk, Electrochemical performance of boron-doped diamond electrode in surfactant-containing media for ambroxol determination, Sensors Actuators, B: Chem. **203** (2014) 517–526.

[16] J. Schmid, Assay of ambroxol in biological fluids by capillary gas-liquid chromatography, J. Chromatogr., B **414** (1987) 65–75.

[17] J. Li, Y. Bi, L. Wang, F. Sun, Z. Chen, G. Xu, G. Fan, β-Cyclodextrin enhanced on-line organic solvent field-amplified sample stacking in capillary zone electrophoresis for analysis of ambroxol in human plasma, following liquid–liquid extraction in the 96-well format, J. Pharm. Biomed. Anal. **66** (2012) 218– 224.

[18] T. Perez-Ruiz, C. Martınez-Lozano, A. Sanz, E. Bravo, Sensitive method for the determination of ambroxol in body fluids by capillary electrophoresis and fluorescence detection, J. Chromatogr., B **742** (2000) 205–210.

[19] E. Satana, H. Basan, N.G. Goger, Determination of ambroxol hydrochloride in tablets using flow-Injection UV spectrophotometry and HPLC, J. Ana.l Chem. **63** (2008) 451–454.

[20] G.M. Hadad, A. El-Gindy, W.M.M Mahmoud, HPLC and chemometrics-assisted UV spectroscopy methods for the simultaneous determination of ambroxol and doxycycline in capsule, Spectrochim. Acta, A **70** (2008) 655––663.

[21] K.L. Narasimha Rao, Ch. Krishnaiah, K.S. Babu, K.P. Reddy, Development and validation of a stability-indicating LC method for simultaneous determination of related compounds of guaifenesin, terbutaline sulfate and ambroxol HCl in cough syrup formulation, J. Saudi Chem. Soc. **18** (2014) 593–600.

[22] B.D. Kiss, K.B. Nemes, I. Ürmös, J. Szúnyog, I. Klebovich, Determination of ambroxol in dog plasma by high-performance liquid chromatography and UV detection, Chromatographia **51** (2000) S217–220.

[23] R. Rupali, K.S. Dhot, K.B. Ilango, S. Shabbeer, Pharmacokinetic of ambroxol hydrochloride microspheres in rats after oral administration, IJRPC **2** (2012) 280–288.

[24] J. Dharumana, M. Vasudhevanc, T. Ajithlal, High performance liquid chromatographic method for the determination of cetirizine and ambroxol in human plasma and urine - a boxcar approach, J. Chromatogr., B **879** (2011) 2624–2631.

[25] F.F. Belal, M.K. Sharaf El-Din, N.M. El-Enany, S. Saad, Micellar Liquid chromatographic method for the simultaneous determination of levofloxacin and ambroxol in combined tablets: Application to biological fluids, Chem. Cent. J. **7** (2013) 162.

[26] S. Emara, M. Kamal, M.A. Kawi, On-line sample cleanup and enrichment chromatographic technique for the determination of ambroxol in human serum, J. Chromatogr. Sci. **50** (2012) 91–96.

[27] F. Su, F. Wang, W. Gao, H. Li, Determination of ambroxol in human plasma by high-performance liquid chromatography–electrospray ionization mass spectrometry (HPLC–MS/ESI), J. Chromatogr., B **853** (2007) 364–368.

[28] H. Kim, J.Y. Yoo, S.B. Han, H.J. Lee, K.R. Lee, Determination of ambroxol in human plasma using LC–MS/MS, J. Pharm. Biomed. Anal. **32** (2003) 209–216.

[29] W. Hu, Y. Xu, F. Liu, A. Liu, Q. Guo, Rapid and sensitive liquid chromatography tandem mass spectrometry

method for the quantification of ambroxol in human plasma, Biomed. Chromatogr. **22** (2008) 1108–1114.

[30] X. Dong, L. Ding, X. Cao, L. Jiang, S. Zhong, A sensitive LC-MS/MS method for the simultaneous determination of amoxicillin and ambroxol in human plasma with segmental monitoring, Biomed. Chromatogr. **27** (2013) 520–526.

[31] T. Hang, M. Zhang, M. Song, J. Shen, Y. Zhang, Simultaneous determination and pharmacokinetic study of roxithromycin and ambroxol hydrochloride in human plasma by LC–MS/MS, Clin. Chim. Acta **382** (2007) 20––24.

[32] A. Wen, T. Hang, S. Chen, Z. Wang, L. Ding, Y. Tian, M. Zhang, X. Xu, Simultaneous determination of amoxicillin and ambroxol in human plasma by LC–MS/MS: Validation and application to pharmacokinetic study, J. Pharm. Biomed. Anal. **48** (2008) 829–834.

[33] International Harmonized Tripartite Guideline (ICH)/ /World Health Organization (WHO), Validation of Analytical Procedures: Text and Methodology, Q2(R1), current step 4 version, parent guidelines on methodology dated November 6, 1996, incorporated in November 2005.

[34] US Environmental Protection Agency (EPA, 1989a) 40 CFR Part 160: Good Laboratory Practice Standards, FIFRA and FFDCA (1989) and its subsequent revisions.

[35] M. Vogeserand, C. Seger, Pitfalls associated with the use of liquid chromatography–tandem mass spectrometry in the clinical laboratory, Clin. Chem. **56** (2010) 1234––1244.

[36] B.K. Matuszewski, M.L. Constanzer, C.M. Chavez, Strategies for the assessment of matrix effect in quantitative bioanalytical methods based on HPLC–MS/MS," Eng. Anal. Chem. **75** (2003) 3019–3030.

IZVOD

RAZVOJ NOVE ANALITIČKE METODE ULTRA-BRZE TEČNE HROMATOGRAFIJE SA TANDEM MASENIM DETEKTOROM ZA ODREĐEVANJE AMBROKSOL-HIDROHLORIDA U SERUMU I FARMAKOKINETIČKA PRIMENA

Maja M. Vujović[1,2], Milan Jokanović[1], Goran M. Nikolić[1]

[1]Medicinski fakultet, Univerzitet u Nišu, Bulevar Dr Zorana Djindjića 81, 18000 Niš, Srbija
[2]Zavod za sudsku medicinu u Nišu, Toksikološko-hemijska laboratorija, Bulevar Dr Zorana Djindjića 81, 18000 Niš, Srbija

(Naučni rad)

Ambroksol-hidrohlorid je ekspektorans koji se uspešno primenjuje u mukolitičkoj terapiji više od trideset godina. Lek reguluše sekreciju mukoze ali pokazuje i antioksidativno, antiinflamatorno, analgetičko, lokalno anestetičko, antivirusno i antibakterijsko dejstvo. Primenjuje se u mukolitičkoj terapiji kod akutnih i hroničnih bronhopulmonalnih bolesti povezanih sa povećanim stvaranjem i poremećajem formiranja i transporta mukusa. Cilj ovog naučnog istraživanja je razvoj nove analitičke metode za određivanje ambroksola u serumu primenom ultra-brze tečne hromatografije sa tandem masenim detektorom (UHPLC–MS/MS) i njena farmakokinetička primena. Validacija analitičke metode sprovedena je u skladu sa priručnikom Internacionalne Komisije za harmonizaciju i validaciju bioanalitčkih metoda ICH (1996). Hromatografsko razdvajanje ambroksola i verapamila (IS) izvršeno je na submikrometarskoj koloni Phenomenex Kinetex^{TM} RP - C_{18} (2.1 mm×50 mm, 1.3 μm), sa mobilnom fazom metanol – 0.01% mravlja kiselina u vodi (90:10, *V*/*V*) pri brzini protoka od 0.3 ml/min. Za MS detekciju primenjena je elektrosprej pozitivna jonizacija (ESI) masenog spektrometra u multi-reakcionom monitoring modu (MRM) sa tipičnim jonskim tranzicijama *m*/*z* 378,9→263,8 za ambroksol i *m*/*z* 455,2→165,0 za IS pri kolizionim energijama od –20 i –25 V. Električni naponi na interfejsu i detektoru bili su 4,5 i –1,92 kV. Linearnost metode je utvrdjena sa srednjim koeficijentom korelacije (r > 0,999) u koncentracionom opsegu 0.5–200 ng/mL sa limitom detekcije (*LOD*) od 0.25 ng/mL i donjim limitom kvantifikacije (*LLOQ*) 0,5 ng/mL. Rezultati intra- i inter-dnevne preciznosti i tačnosti izmerene u tri različita dana pokazali su prihvatljive vrednosti od ±15%. Razvijena metoda je uspešno primenjena za određivanje farmakokinetičkih parametara u serumu kunića nakon primene jednokratke oralne doze ambroksol-hidrohlorida od 30 mg.

Ključne reči: Ambroksol-hidrohlorid • UHPLC–MS/MS • Serum kunića • Farmakokinetika

Improvement of antioxidant properties of egg white protein enzymatic hydrolysates by membrane ultrafiltration

Jelena R. Jovanović[1], Andrea B. Stefanović[1], Milena G. Žuža[1], Sonja M. Jakovetić[1], Nataša Ž. Šekuljica[3], Branko M. Bugarski[2], Zorica D. Knežević-Jugović[1]

[1]*Department of Biochemical Engineering and Biotechnology, Faculty of Technology and Metallurgy, University of Belgrade, Belgrade, Serbia*
[2]*Department of Chemical Engineering, Faculty of Technology and Metallurgy, University of Belgrade, Belgrade, Serbia*
[3]*Innovation Center, Faculty of Technology and Metallurgy, University of Belgrade, Belgrade, Serbia*

Abstract

The production of bioactive peptides from egg white proteins (EWPs) and their separation are emerging areas with many new applications. The objective of this study was to compare antioxidant activity of three distinct EWP hydrolysates and their peptide fractions prepared by membrane ultrafiltration using membranes with 30, 10 and 1 kDa molecular weight cut-off. The hydrolysates were obtained by thermal and ultrasound pretreated EWPs hydrolyzed with a bacterial protease, Alcalase. It appeared that the pretreatment significantly affected peptide profiles and antioxidant activity of the hydrolysates measured by ABTS, DPPH and FRAP methods. The hydrolysate prepared using alcalase and ultrasound pretreatment at 40 kHz – 15 min has shown to be the most effective in scavenging both DPPH and ABTS radicals (28.10±1.38 and 79.44±2.31%, respectively). It has been noticed that this hydrolysate had a nutritionally more adequate peptide profile than the other hydrolysates with a much lower amount of peptides <1 kDa (11.19±0.53%) and the greatest content of the peptide fraction in the molecular weight (MW) range of 1–10 kDa (28.80±0.07%). This peptide fraction has shown the highest DPPH and ABTS antioxidant activity compared to all other fractions having a potential to be used as a functional food ingredient.

Keywords: antioxidant derived egg white peptides, membrane ultrafiltration, ultrasound pretreatment, hydrolysis, alcalase.

Available online at the Journal website: http://www.ache.org.rs/HI/

SCIENTIFIC PAPER

UDC 637.413.045:66:66.094.941

Hem. Ind. **70** (4) 419–428 (2016)

doi: 10.2298/HEMIND150506047J

The importance of oxidation processes in the body and foodstuffs has been widely recognized. It is well known that the formation of free radicals and other reactive oxygen species (ROS), which can induce oxidative damage, is a consequence of the oxidation metabolism which is indispensable for the survival of cells [1]. An important role in the preservation of human health has inhibition of oxidative reaction and scavenging of free radicals which take place under the influence of antioxidants. Synthetic antioxidants like butylated hydroxytoluene (BHT) and butylated hydroxyanisole (BHA) which were ordinarily applied for radical scavenging in biological systems pose a risk for human health. Accordingly, the contribution of many studies was aimed to isolate natural antioxidants such as tocopherols, catechin, phenolic compounds and peptides [2–5].

Correspondence: Z.D. Knežević-Jugović, Faculty of Technology and Metallurgy, University of Belgrade, Karnegijeva 4, 11000 Belgrade, Republic of Serbia.
E-mail: zknez@tmf.bg.ac.rs
Paper received: 6 May, 2015
Paper accepted: 10 July, 2015

The bioactive peptides derived from food proteins with low molecular weight and useful bioactivities which are easily absorbed have attracted more attention, because they are safer and healthier than synthetic ones [6]. The evaluation and characterization of bioactive peptides, released after enzymatic hydrolysis, have been widely investigated demonstrating that besides its nutritional value, they might have pharmacological activities. These bioactive peptides, obtained from animal and plant proteins have indicated antioxidant, antitumoral, antithrombic, antihypertensitive or antimicrobial activities opening the opportunity of having therapeutically functional food [7]. In the last decade, a number of studies have dealt with the isolation of bioactive peptides with high antioxidant activity. These peptides have been produced by enzymatic hydrolysis of different protein from plant and animal sources like rice bran [8], peanut [9], sunflower [10], corn gluten meal [11], casein [12], yam [13], milk-kefir and soymilk-kefir [14], mackerel [15], curry leaves [16], egg-yolk [17], cotton leaf worm [18] and several others.

Due to its nutritional quality, egg white proteins (EWPs) are suitable choice for the production of bioactive peptides intended for human consumption. Enzymatic hydrolysis is frequently used to improve and

upgrade the functional and nutritional properties of EWPs and obtain value-added egg products. EWP hydrolysates provide a number of benefits as a protein source in human nutrition in regard to the native EWPs and they also have a positive impact on body functions or conditions and may ultimately influence health. Furthermore, enzymatic hydrolysis of EWPs is considered to be one of the possibilities to exceed problem with allergenicity and high viscosity of the native proteins, since these are the main constraints for more extensive usage of EWPs in food formulations [19].

Many recently published studies attempt to fractionate proteins, protein hydrolysates and peptides with membrane separation processes and isolate the fractions with the most antioxidant active peptides with the aim of enhancing their biological and/or functional properties. The separation processes are based upon selective permeability of one or more of the liquid constituents through the membrane according to the pressure difference. The ultrafiltration membrane system separates the protein hydrolysates into defined molecular weight ranges and represents the best technology available for the enrichment of peptides with a specific molecular weight range [20]. In particular, fractions with a molecular weight between 0.1–0.5 kDa and 1–3.5 kDa would be the most interesting bioactive peptides for nutritional and pharmaceutical uses. The extraction and recovery of these fractions from the hydrolysate are the key issues. Compared to other bioseparation methods such as gel chromatography, membrane technology offers several advantages such as higher productivity, lower capital investment, high throughput of products and while maintaining product purity under ambient conditions, ease of translation to large-scale commercial production and easy equipment cleaning [5].

We recently reported on the impact of ultrasound pretreatment on the enzymatic hydrolysis of EWPs with a range of commercially available proteases and on the functionalities of the resultant hydrolysates [21]. In the present study, the antioxidant activities of the above mentioned EWP hydrolysates obtained with Alcalase and of the fractionated hydrolysates prepared using membrane ultrafiltration were investigated by multiple assays, including the ability of the scavenging effect on free radicals and the ferric reducing ability. Hence, the aim was to identify the most antioxidant peptide fractions hydrolysate for application as a functional ingredient in food products production.

EXPERIMENTAL

Materials

Chicken egg white obtained from a local supermarket was separated from the yolk and gently stirred without foam formation to provide homogeneous mixture. Alcalase 2.4L (protease from *Bacillus licheniformis*) was obtained from Sigma Aldrich (St Louis, MO, USA). The enzyme activity was ≥2.4 U/g Anson units, where one Anson unit is defined as the amount of enzyme which, under specified conditions, digests urea-denatured hemoglobin at an initial rate such that there is liberated an amount of TCA-soluble product per min, giving the same color with Folin–Ciocalteu phenol reagent as one milliequivalent of tyrosine at 25 °C and at pH 7.50. The chemicals, bovine serum albumin (BSA), 2,2′-diphenyl-1-picrylhydrazyl (DPPH), 2,2′--azinobis(3-ethylbenzothiazoline-6-sulphonic acid) diammonium salt (ABTS) and complex ferric ion-TPTZ (2,4,6--tri(2-pyridyl)-*s*-triazine) were purchased from Sigma––Aldrich. All other chemicals used in this research were of analytical grade.

Ultrasound and thermal protein denaturation

Prior to the enzymatic hydrolysis, a series of 10 mass% egg white solution samples was exposed to ultrasonic waves in ultrasonic water bath with a frequency of 40 kHz (EI-NIS-RO-VEP, Serbia) and 35 kHz (Bendelin electronic, sonorex digitec, DT 102 H, Germany) during 15 and 30 min, respectively. At the same time, the samples were subjected to the thermal pretreatment at high temperature (75 °C) for half an hour. The samples were prepared in a beaker of 600 cm^3 capacity where the working volume (~360 cm^3) was kept constant for all pretreatments. For the ultrasound control, 10 mass% egg white solution was left in the ultrasonic bath at a frequency of 0 kHz at the same time and thermal control was kept out at the ambient temperature for half an hour. Each treatment was conducted in triplicate.

Preparation of protein hydrolysates

Before the enzymatic reaction catalyzed by alcalase, egg white solution samples were pre-incubated in a glass reactor at optimum conditions for protease (50 °C and pH 8.0) during 20 min. The hydrolysis reaction was initiated by adding the enzyme in the amount of 2 mass% with stirring at 240 rpm. During the course of the reaction, pH was kept at a constant value by adding 0.2 M NaOH, using pH-stat method with automatic dosage of the base. The reaction was stopped by heating the mixture at 90 °C for 15 min to inactivate the enzyme. The hydrolysate obtained was cooled down to room temperature and centrifuged at 12,000×*g* for 10 min. The supernatant was finally collected as the hydrolysate and stored at 4 °C for subsequent studies.

Fractionation of protein hydrolysates using membrane ultrafiltration

The hydrolysates obtained after ultrasound and thermal pretreatments were subjected to ultrafiltration

using membranes with 30, 10 and 1 kDa molecular weight cut-off (MWCO), sequentially. The ultrafiltration was performed using a Millipore ultrafiltration stirred cell unit (model 8050 1 unit, Millipore Corporation, Bedford, MA, USA) through cellulose membranes. During the ultrafiltration process, the pressure was applied with nitrogen, as indicated by the manufacturer of the membranes. The experimental setup and diagram of the ultrafiltration system for separation of antioxidant peptides from EWP hydrolysate using membranes with various molecular weights cut-off are presented in Scheme 1.

A sample of 50 cm^3 hydrolysates was first ultrafiltered through a 30 kDa membrane to obtain two fractions: retentate (Fraction 1, representing hydrolysates >30 kDa) and permeate (MW <30 kDa). The permeate fraction was further ultrafiltered through a 10 kDa membrane to yield the second retentate (fraction 2, representing hydrolysates between 10 and 30 kDa) and the second permeate (MW <10 kDa). Permeate was also further subjected to ultrafiltration through an 1 kDa membrane to obtain the third retentante (fraction 3, representing hydrolysates between 1 and 10 kDa) and permeate (fraction 4, representing hydrolysates <1 kDa). Each retentate or permeate was collected and stored in the freezer. After ultrafiltration, protein content was determined by Lowry method [22].

Determination of antioxidant properties

DPPH radical scavenging activity

The scavenging activity of egg white protein hydrolysate and its fractions against the DPPH radical was determined based on the method described previously [23] with only slight protocol modification. Briefly, a 0.5 cm^3 aliquot of each obtained hydrolysate was mixed with 0.5 cm^3 of 0.15 mM DPPH solution in methanol. After mixing vigorously for 2 min, the mixture was allowed to stand at room temperature in the dark and after 30 min absorbance was measured at 517 nm using UV–Vis spectrophotometer (Ultrospec 3300 pro, Amerscham Bioscience). DPPH radical scavenging activity (*RSA*, %), expressed as the percentage of inhibition, was calculated according next equation:

$$RSA = 100\left[1 - \frac{A_s - A_b}{A_c}\right] \quad (1)$$

where A_s is the absorbance of the tested egg white hydrolysate (EWH), A_b is the absorbance of the EWH in methanol and A_c is the absorbance of the DPPH solution without the sample. All experiments were carried out in triplicate.

ABTS radical scavenging activity

The ABTS radical scavenging activity of prepared hydrolysates and their fractions was measured using the decolorization assay [24]. This method is based on the ability of antioxidant molecules to quench the stable bisradical cation, $ABTS^{\bullet+}$, a blue-green chromophore with characteristic absorption at 734 nm. In this research, the $ABTS^{\bullet+}$ solution was prepared by reaction of 5 cm^3 of a 7 mM aqueous ABTS solution and 0.088 cm^3 of a 140 mM (2.45 mM final concentration) potassium-persulfate solution. After storage in the dark for 16 h, the radical cation solution was further diluted with 5 mM phosphate-buffered saline (PBS, pH 7.4) until the initial absorbance value of 0.7±0.05 at 734 nm was reached. Solutions of each sample under study were prepared in water so that their final concentration after the addition of 0.01 cm^3 the radical solution (2 cm^3) was 0–15 μM and a 20–80% decrease in the initial absorbance of the reaction solution was achieved. Absorbance was measured at 734 nm after 5 min and ABTS radical scavenging activity (%) was calculated using following equation:

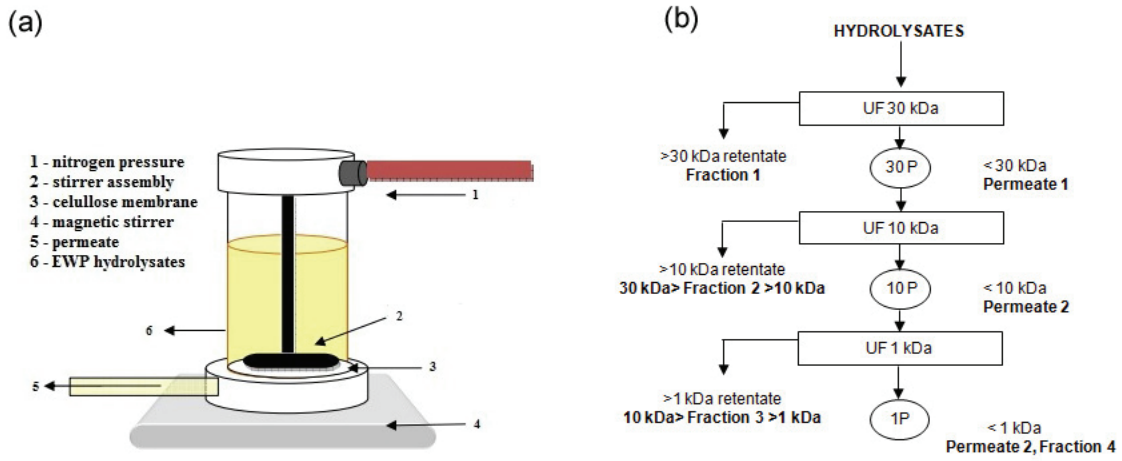

Scheme 1. a) Experimental set-up unit; b) diagram of the ultrafiltration system applied for separation antioxidant peptides from EWP hydrolysate using membranes with various molecular weights cut-off.

$$ABTS = 100\frac{A_s - A_b}{A_c} \quad (2)$$

where A_s represents the absorbance of the sample solution in the presence of the $ABTS^{\bullet+}$, A_b is the absorbance of the sample solution without $ABTS^{\bullet+}$ and A_c is the absorbance of the control solution with $ABTS^{\bullet+}$. The assay was standardized using Trolox and ascorbic acid, a synthetic and a natural antioxidant, respectively, and results were expressed as Trolox equivalent (Trolox equivalent antioxidant capacity, *TEAC*) as well as ascorbic acid equivalent (ascorbic equivalent antioxidant capacity, *AEAC*). All experiments were carried out in triplicate.

Ferric reducing antioxidant power (FRAP) assay

The reducing ability of peptide fractions from EWH was determined by FRAP assay of Benzie and Strain with slight modifications [25]. FRAP assay measures the change in absorbance at 593 nm due to the formation of a blue Fe (II)–TPTZ compound from colorless oxidized Fe(III) form by the action of electron donating antioxidants. The working FRAP reagent was prepared by mixing 10 volumes 0.3 M acetate buffer pH 3.6, with 1 volume 10 mM TPTZ (2,4,6-tri(2-pyridyl)-*s*-triazine) in 40 mM hydrochloric acid and with 1 volume 20 mM ferric chloride. A 0.15 cm^3 EWH was added to 4.5 cm^3 freshly prepared FRAP reagent and mixed thoroughly and reading taken at 593 nm. Absorbance readings were taken after 30 min. The aqueous solutions of known Fe(II) concentration, in the range of 0.1–1.0 mM $FeSO_4 \times 7H_2O$ were used for calibration. All solutions were used on the day of preparation. In the FRAP assay, the reducing ability of the hydrolysates under the test was calculated with reference to the reaction signal given by a Fe(II) solution of known concentration. The values were expressed as micromole of Fe(II) equivalents per mg of proteins. All measurements were done in tree repetitions for each EWH.

Statistical analysis

All experiments were performed in triplicate and the data are presented in average of triplicates and standard deviation (*SD*). Statistical differences between antioxidant activity of enzymatic hydrolysates and their respective ultrafiltration fractions were determined by one-way analysis of variance (ANOVA). A Tukey test was applied as a test a posteriori with a level of significance of 95%. All the tests were considered statistically significantly at $p < 0.05$. Statistical analyses were performed using the Origin Pro 8 software package.

RESULTS AND DISCUSSION

Effect of pretreatments on the antioxidant activity of EWPs

Heat pretreated and ultrasound pretreated EWPs were hydrolyzed in the batch reactor using an endopeptidase, namely alcalase. This endopeptidase was chosen as the biocatalyst for the EWP hydrolysis on the basis of preliminary results and literature survey [21,26]. The *in vitro* antioxidant activities of the obtained hydrolysates were measured by ABTS, DPPH and FRAP methods since each assay reflected a different aspect of the antioxidant behavior of the hydrolysates. Namely, when discussing the antioxidant activity of a food product, it is strongly recommended to use at least two methods due to the differences between the test systems [27]. The results of antioxidant activity of hydrolysates obtained after different pretreatments and measured by three methods are presented in Table 1.

It seemed that the pretreatment significantly affected the antioxidant properties of the hydrolysates ($p < 0.05$). The DPPH and ABTS activity of the hydrolysates generally decreased in the order: ultrasound pretreated at 40 kHz – 15 min > ultrasound pretreated at 35 kHz – 30 min > thermal pretreated at 75 °C – 30 min. It is worth noting that all hydrolysates had better antioxidant properties than the native EWP solution, which is in agreement with similar studies [28,29].

As a result of the enzymatic hydrolysis, a complex mixture of peptides and amino acids produced in which individual effect of each molecule in the subsequent fractionation process is difficult to reveal and quantify. Molecular weight is an important parameter reflecting the hydrolysis of proteins, which further correlates with the bioactivity of protein hydrolysates. Thus, it is attempted in this study to design of an efficient fractionation methodology for peptides separation with the aim of enhancing their antioxidant properties.

Table 1. Antioxidant activities and total protein content of EWP hydrolysates prepared by ultrasound and thermal pretreatment; m_p – total protein content determined by Lowry method. DPPH and ABTS radical scavenging activities of untreated egg white were 15.8±2.04 and 7.69±1.59 %, respectively. Concentration of reducing Fe^{2+} for untreated egg white was 0.062±0.01 μM mg^{-1} proteins

Parameter	Ultrasound pretreatment		Thermal pretreatment
	40 kHz – 15 min	35 kHz – 30 min	75 °C – 30 min
m_p / mg	591.7±3.67	578.6±3.02	574.9±6.02
DPPH / %	28.10±1.38	25.20±1.75	23.50±1.12
ABTS / %	79.44±2.31	77.34±2.46	76.17±2.59
Fe^{2+}, mM mg^{-1} proteins	0.097±0.01	0.109±0.009	0.064±0.01

Therefore, the obtained hydrolysates have been separated into four fractions depending on their molecular size by successive UF using membranes with molecular cut off sizes of 30, 10 and 1 kDa. The values of the separated fraction (< 1, 1–10, 10–30 and >30 kDa) and its impact on the peptidic population in terms of molecular weight were presented in Figure 1.

Significant differences concerning the content and the molecular weight distribution profiles of obtained peptides occurred among pretreatments. It was apparent that the hydrolysis after thermal pretreatment generated more peptides <1 kDa (19.04±1.02%) than ultrasound pretreatment did (11.90±0.53%), whereas the proportion of peptides <10 kDa was higher in the second case (28.80±0.07 *vs.* 20.46±0.39%). Different pretreatments seemed to influence the protein folding leading to different molecular weight distribution profile after hydrolysis which could influence the antioxidant activities of the hydrolysate fractions. Although the mechanism of ultrasound-induced protein unfolding is not completely understood, important differences in protein unfolding have been suggested for egg white proteins caused after heat or ultrasound pretreatments [30].

DPPH radical scavenging activity

The antioxidant properties of different EWPs hydrolysates fractions have been chosen as the most relevant criteria to choose the most appropriate hydrolysates for the food application. The DPPH radical scavenging activity assay is one of the *in vitro* methods for the measurement of the capacity of an antioxidant to reduce free radicals. The degree of color changes appears to be correlated with the sample antioxidant activity. The obtained ultrafiltration fractions from Alcalase hydrolysates were tested for DPPH radical scavenging activity, and results are depicted in Figure 2.

The results showed that enzymatic hydrolysis and ultrasound pretreatment enhanced antioxidant properties of hydrolysates and fractions. The highest DPPH scavenging activities were achieved for fraction 3 induced by both ultrasound and thermal pretreated hydrolysates which outcomes have been statistically significant ($p < 0.05$) and values were 33.57±0.07, 21.17±2.01 and 30.30±2.65 %, respectively. These results indicated that the ultrasound pretreatment could improve inhibition of DPPH radical of EWP hydrolysates compared with conventional thermal pretreatment. Consequently, it can be deduced that ultrasound released peptides and isolated fractions, especially fraction 3, possibly contained peptides which acts as electron donors and could react with free radicals to. Unhydrolysed EWPs showed a rather low DPPH radical scavenging activity (15.8±2.04%) and the values increased significantly with the course of hydrolysis for both pretreatments. The antioxidant activity of all obtained Fractions 3 varied significantly between the different pretreatment used ($p < 0.05$). The appropriated EWPs pretreatment prior to hydrolysis has resulted in different alterations in the protein's tertiary structure affecting profile of produced peptides and consequently their DPPH radical scavenging activity. The results of this research are in agreement with results obtained by several authors who reported that the antioxidant activity of the defatted soybean meal was improved after sonication [31]. It can be noticed that the frequency of

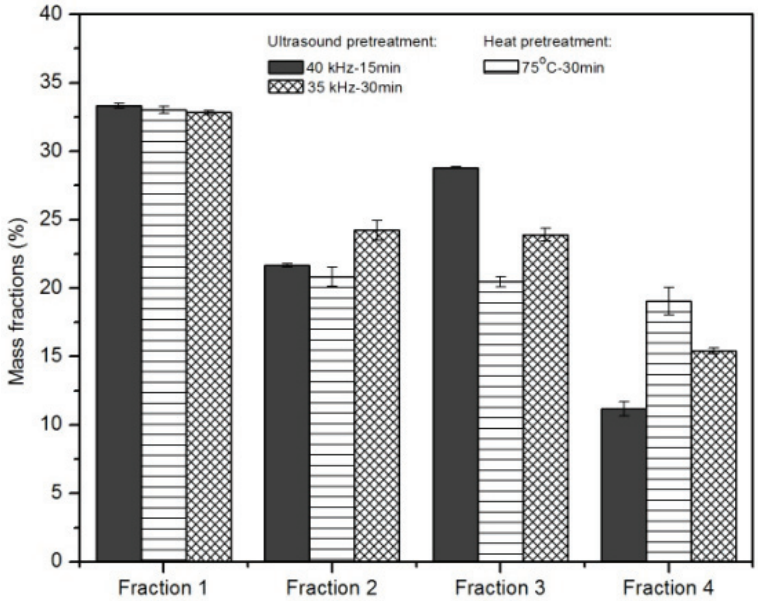

Figure 1. The molecular weight distribution profile of EWP hydrolysates and their ultrafiltered fractions obtained by thermal and ultrasound pretreatment (Hydrolysis conditions were as follows: 50 ℃, pH 8.0; 2.12 U of alcalase, 10 mass% aqueous solution of egg white (E/S mass ratio 0.02)).

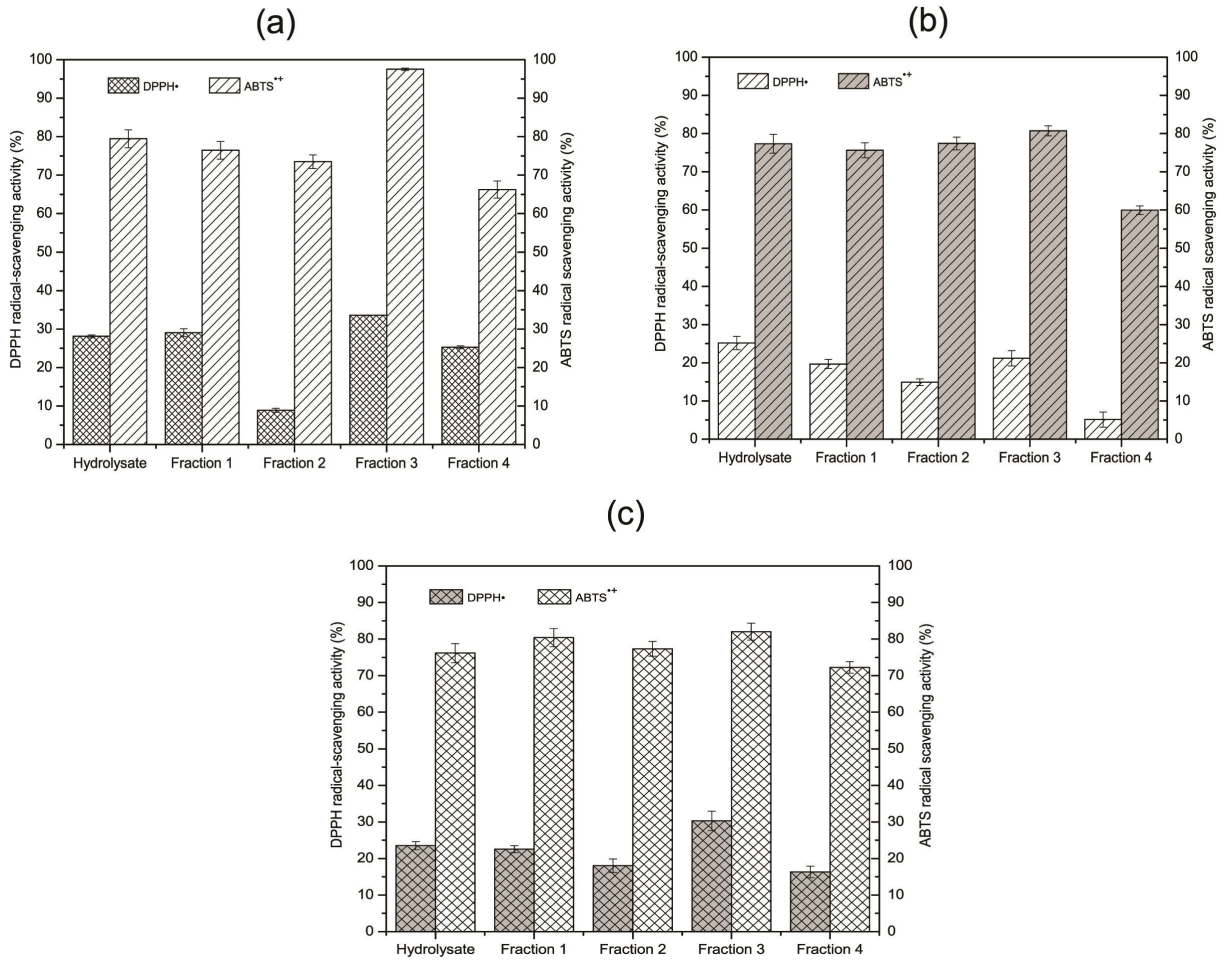

Figure 2. DPPH and ABTS radical scavenging activity of EWP hydrolysates and their ultrafiltered fractions: a) ultrasound pretreatment at 40 kHz during 15 min, b) ultrasound pretreatment at 35 kHz during 30 min and c) thermal pretreatment at 75 ℃ during 30 min.

ultrasound did not significantly affect ($p > 0.05$) on the DPPH scavenging activities, but it is evident the results disclose the presence of antioxidant peptides in all isolated ultrasound pretreated fractions and the fraction 3 was the most abundant with the highest DPPH values for both pretreatments. Very little attention in the literature was devoted to the influence of ultrasound on the isolation of antioxidant peptides from EWPs but some researches were investigated antioxidant activity of EWPs hydrolysates. Thus, Chenand and colleagues [28] have been separately hydrolysed EWPs with several commercially available proteases and it has been noted that antioxidant activity increased with the increasing time of hydrolysis. Also, they reported that papain hydrolysate had the scavenging activity of DPPH and hydroxyl radicals more effective than superoxide anion radical ($p < 0.05$) and a greater DPPH radical scavenging activity (78.74% at 5 mg/ml) was noted with low molecular-weight peptides (<3 kDa). Other authors showed that alcalase EWPs hydrolysates possessed the strong antioxidant ability compared with the other hydrolysates (pepsin and tripsin), particularly for the fraction with peptides <1 kDa [29].

ABTS radical scavenging activity

ABTS radical is relatively stable but readily reduced by antioxidants. The scavenging activity against cationic ABTS radical indicates the ability of peptide fractions to act as electron donors or hydrogen donors in free radical reactions [32]. To assay the ABTS radical scavenging of peptide fractions, cationic ABTS radical decolorization was carried out. The results obtained from this experimental set are presented in Figure 2. Taking into account these results it has been shown that fraction 3 with MW between 1 to 10 kDa revealed the highest scavenging activity. Hence, ABTS scavenging activity induced by ultrasound (35 kHz – 30 min) and thermal pretreated hydrolysates of fraction 3 have not been statistically significant ($p > 0.05$) and values were 80.72±1.32 and 82.01±2.29%, respectively. However, fraction 3 obtained by membrane ultrafiltration of ultrasound pretreated hydrolysate (40 kHz – 15 min) has shown a significantly higher ABTS radical scav-

enging assay of 97.54±0.3%. The ABTS scavenging activity of eleven amaranth peptide fractions has been reported, and among them, two fractions exhibited higher antioxidant activity than the other fractions. Their activities were 66.8 and 83% (both at 310 μg cm^{-3}), but the other fractions (at concentration lower than 200 μg cm^{-3}) registered less than 37% [33].

For easy comparison with literature data, results of ABTS radical scavenging activity were expressed as Trolox and ascorbic acid equivalents antioxidant capacity and presented in Figure 3.

Between hydrolysates and their fractions, except for the fraction 3 obtained after ultrasound pretreatment (40 kHz – 15 min), no substantial difference in the values of Trolox and ascorbic acid equivalents. The fraction 3 has shown the notably values for both Trolox and ascorbic acid equivalents: 1.569±0.007 and 1.852±0.008 μmol g^{-1} peptides, respectively. As well, the ABTS radical scavenging activity for fraction 3 was approximately two times lower than the peptide fraction with small peptides (fraction 4, < 1 kDa). Generally, the results showed that fraction with a small molecular weight exerted better ABTS inhibition ability.

It was found that hen egg white lysozyme (HEWL) hydrolysate possessed ABTS radical inhibition assay 1.91±0.13, 2.57±0.19 and 2.82±0.14 μmol trolox equivalents (TE) mg^{-1} protein for trypsin, papain and trypsin–papain hydrolysates, respectively [34]. For HEWL hydrolysate obtained by alcalase, TEAC value was 1.69 μmol trolox equivalents (TE) $mg^{-1}$of protein [35].

Ferric reducing antioxidant activity (FRAP)

The FRAP is often used to evaluate the ability of an antioxidant to donate an electron or hydrogen, and some researchers have indicated that there is a direct correlation between antioxidant activities and reducing power of peptide [36]. The FRAP activity of protein/ /peptide components in enzymatic hydrolysates and their ultrafiltration fractions are represented in Figure 4.

Hydrolysates prepared after ultrasound pretreatment frequency 40 and 35 kHz and with thermal pretreatment had no detectable activity and/or the values were not statistically significant. Therefore, the FRAP activity of the EWP hydrolysates was concentrated in the peptides with 1–10 kDa and <30 kDa size for thermal and ultrasound pretreatment, respectively, meanwhile presence of the other peptides (>10 and >30 kDa) could be responsible for the lack of the activity. On the basis of this antioxidant assay, the concentration of reduced iron was 3.79±0.60 μM per milligram of proteins for Fraction 3 obtained by hydrolysate prepared after thermal treatment. The fractions 1, for both ultrasound pretreatment 35 and 40 kHz, had a significantly lower value of Fe (II) concentration amounted 1.79±0.13 and 2.05±0.34 μM per milligram of proteins, respectively. According to the available literature data, it can be said that protein hydrolysates from plant source possess higher ferric reducing antioxidant activity than hydrolysates acquired from animal proteins. The researchers found that the phenolic and indolic groups of tyrosine and tryptophan play important roles as hydrogen donors in redox systems [37].

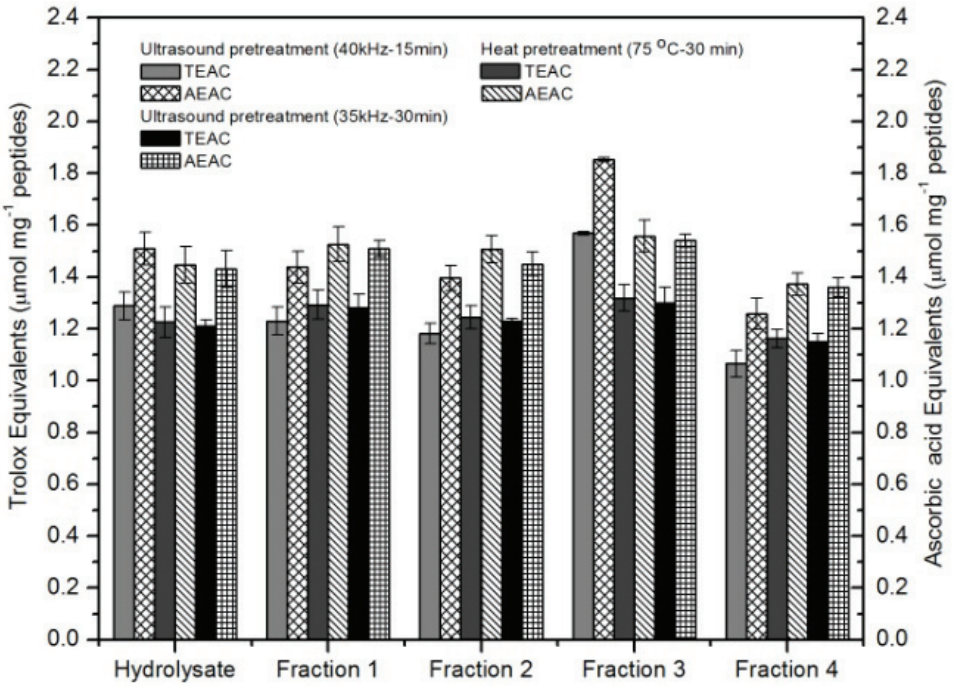

Figure 3. ABTS scavenging activity for EWP hydrolysates and their ultrafiltrated fractions obtained with ultrasound and thermal pretreatments expressed in Trolox and ascorbic acid equivalents per gram of dry proteins.

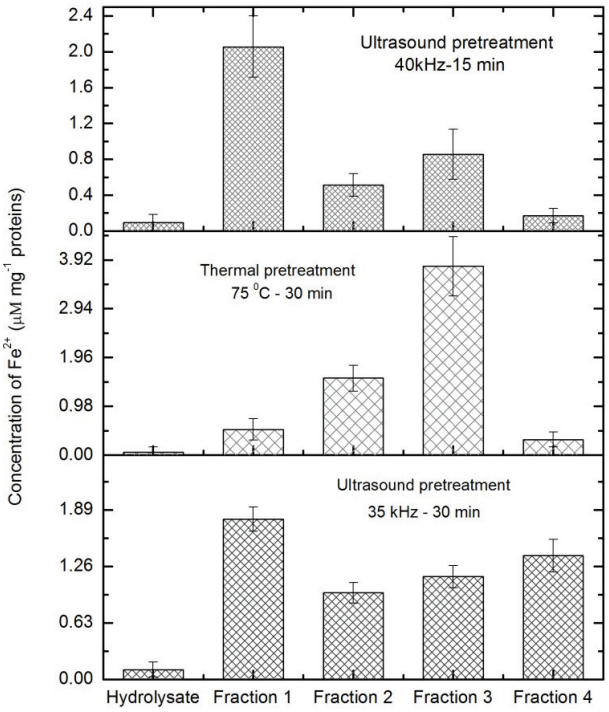

Figure 4. Ferric reducing power assay of EWP hydrolysates and their ultrafiltered fractions expressed as concentration of Fe(II).

Generally, based on the all represented results, fraction 3 with low molecular weight peptides possessed relevant antioxidant activity and these results are in agreement with literature data which indicates that antioxidant peptides from food proteins contain 5–16 amino acid residues. Namely, the 1–10 kDa fractions was the most abundant after membrane ultrafiltration of the protein hydrolysates after ultrasound pretreatment which suggests that the protease alcalase and ultrasound pretreatment (40 kHz – 15 min) were efficient in reducing the native egg white proteins into low molecular weight peptides.

CONCLUSION

The impact of ultrasound and thermal pretreatments of EWPs on enzymatic hydrolysis and antioxidant properties of the obtained hydrolysates and their fractions was assessed. The hydrolysate prepared using Alcalase and ultrasound pretreatment at 40 kHz – 15 min has shown to be most effective in scavenging both DPPH and ABTS radicals (28.10±1.38 and 79.44±2.31 %, respectively). The release of bioactive peptides from intact proteins has been shown to be significantly affected by the pretreatment type. The fraction produced from the ultrasound pretreated EWPs by enzymatic hydrolysis and ultrafiltration containing antioxidant peptides of MW ranging from 1 to 10 kDa showed the highest DPPH and ABTS radicals quenching capability compared to other fractions. The outcomes showed that this fraction possibly contained some effective antioxidant peptides, which could convert free radicals to more stable products and force out the radical chain reaction. These findings suggest that Alcalase hydrolysis of ultrasound pretreated egg white protein hydrolysates combined to ultrafiltration fractionation of hydrolysate could provide new opportunities for the development of health-promoting ingredients.

Acknowledgement

This work was supported by Innovative project "Production of new dietary formulations based on natural protein with antioxidant and antitumor effect" and III46010 from the Ministry of Education, Science and Technological Development of the Republic of Serbia.

REFERENCES

[1] K. Cui, X. Luo, K. Xu, M.R. Murthy, Role of oxidative stress in neurodegeneration: recent developments in assay methods for oxidative stress and nutraceutical antioxidants, Prog. Neuro-psychoph. **28** (2004) 771–799.

[2] B. Hernandez-Ledesma A. Davalos, B. Bartolome, L. Amigo, Preparation of antioxidant enzymatic hydrolysates from alpha-lactalbumin and beta-actoglobulin. Identification of active peptides by HPLC–MS/MS, J. Agric. Food Chem. **53** (2005) 588–593.

[3] J.T. Hancock, R. Desikan, S.J. Neill, Role of reactive oxygen species in cell signaling pathways, Biochem. Soc. Trans. **29** (2001) 345–50.

[4] B. Halliwell, Free radicals, antioxidants, and human disease: curiosity, cause, or consequence, Lancet **344** (1994) 721–724.

[5] S. Saidi, A. Deratani, M.P. Belleville, R.B. Amar, Antioxidant properties of peptide fractions from tuna dark muscle protein by-product hydrolysate produced by membrane fractionation process, Food Res. Int. (2014), doi: 10.1016/j.foodres.2014.09.023.

[6] B.H. Sarmadi, A. Ismail, Antioxidative peptides from food proteins: A review, Peptides **31** (2010) 1949–1956.

[7] N.P. Moller, K.E. Scholz-Ahrens, N. Roos, J. Schrezenmeir, Bioactive peptides and proteins from foods: indication for health effects, Eur. J. Nutr. **47** (2008) 171–182.

[8] E. Revilla, C.S. Maria, E. Miramontes, J. Bautista, A. Garcia-Martinez, O. Cremades, R.Cert, J. Parrado, Nutraceutical composition, antioxidant activity and hypocholesterolemic effect of a water-soluble enzymatic extract from rice bran, Food Res. Int. **42** (2009) 387–393.

[9] G.T. Chen, L. Zhao, L.Y. Zhao, T. Cong, S.F. Bao, In vitro study on antioxidant activities of peanut protein hydrolysate, J. Sci. Food Agric. **87** (2007) 357–362.

[10] C. Megias, J. Pedroche, M.M. Yust, J. Giron-Calle, M. Alaiz, F. Millan, J. Vioque, Production of copper-chelating peptides after hydrolysis of sunflower proteins with pepsin and pancreatin, Food Sci. Technol. **41** (2008) 1973–1977.

[11] X.X. Li, L.J. Han, L.J. Chen, In vitro antioxidant activity of protein hydrolysates prepared from corn gluten meal, J. Sci. Food Agric. **88** (2008) 1660–1666.

[12] K. Suetsuna, H. Ukeda, H. Ochi, Isolation and characterization of free radical scavenging activities peptides derived from casein, J. Nutr. Biochem. **11** (2000) 128––131.

[13] T. Nagai, N. Suzuk, Y. Tanoue, N. Kai, T. Nagashima, Antioxidant and antihypertensive activities of autolysate and enzymatic hydrolysates from yam (*Dioscorea opposita* Thunb.) ichyoimo tubers, J. Food Agric. Environ. **5** (2007) 64–68.

[14] J.R. Liu, M.J. Chen, C.W. Lin, Antimutagenic and antioxidant properties of milk-kefir and soymilk-kefir, J. Agric. Food Chem. **53** (2005) 2467–2474.

[15] C.H. Wu, H.M. Chen, C.Y. Shiau, Free amino acids and peptides as related to antioxidant properties in protein hydrolysates of mackerel (*Scomber austriasicus*), Food Res. Int. **36** (2003) 949–957.

[16] M. Ningappa, L. Srinivas, Purification and characterization of ~35 kDa antioxidant protein from curry leaves (*Murraya koenigii* L.), Toxicol. In Vitro. **22** (2008) 699––709.

[17] S. Sakanaka, Y. Tachibana, Active oxygen scavenging activity of egg-yolk protein hydrolysates and their effects on lipid oxidation in beef and tuna homogenates, Food Chem. **95** (2006) 243–249.

[18] L. Vercruysse, G. Smagghe, T. Beckers, J. Van Camp, Antioxidative and ACE inhibitory activities in enzymatic hydrolysates of the cotton leafworm, Spodoptera littoralis, Food Chem. **114** (2009) 38–43.

[19] G. Martos, R. López-Fandiño, E. Molina, Immunoreactivity of hen egg allergens: Influence on in vitro gastrointestinal digestion of the presence of other egg white proteins and of egg yolk, Food Chem. **136** (2013) 775––781.

[20] L. Najafian, M. Jafarzade, M. Said, A.S. Babji, Biochemical properties and antioxidant activity of myofibrillar protein hydrolysates obtained from patin *(Pangasius sutchi)*, Int. J. Food Sci. Tech. **48** (2013) 2014–2022.

[21] A.B. Stefanović, J.R. Jovanović, S.Ž. Grbavčić, N.Ž. Šekuljica, V.B. Manojlović, B.M. Bugarski, Z.D. Knežević-Jugović, Impact of ultrasound on egg white proteins as a pretreatment for functional hydrolysates production, Eur. Food Res. Technol. 239 (2014) 979–993.

[22] O.H. Lowry, N.J. Rosebrough, A.L. Farr, R.J. Randall, Protein measurement with the Folin phenol reagent, J. Biol. Chem. **193** (1951) 265–275.

[23] S. Jakovetić, B. Jugović, M. Gvozdenović, D. Bezbradica, M. Antov, D. Mijin, Z. Knežević-Jugović, Synthesis of aliphatic esters of cinnamic acid as potential lipophilic antioxidants catalyzed by lipase b from *Candida antarctica*, Appl. Biochem. Biotehnol. **170** (2013) 1560––1573.

[24] R. Re, N. Pellegrini, A. Proteggente, A. Pannala, M. Yang, C. Rice-Evans, Antioxidant activity applying an improved ABTS radical cation decolorization assay, Free Radic. Biol. Med. **26** (1999) 1231–1237.

[25] I.F. Benzie, J.J. Strain,The ferric reducing ability of plasma (FRAP) as a measure of bantioxidant power Q the FRAP assay, Anal. Biochem. **239** (1996) 70-76.

[26] S. Jakovetić, N. Luković, B. Jugović, M. Gvozdenović, S. Grbavčić, S.J. Jovanović, Z. Knežević-Jugović, Production of Antioxidant Egg White Hydrolysates in a Continuous Stirred Tank Enzyme Reactor Coupled with Membrane Separation Unit, Food Bioprocess Technol. **8** (2015) 287–300.

[27] K. Schlesier, M. Harwat, V. Bohm, R. Bitsch, Assessment of antioxidant activity by using different in vitro methods, Free Radical Res. **36** (2002) 177–187.

[28] J. Xu, Q. Zhao, Y. Qu, F. Ye, Free radical scavenging activity of peptide fractions from defatted soybean meal hydrolysates evaluated by electron spin resonance, Food Sci. Technol. Int. **19** (2013) 557–566.

[29] C. Chen, Y. Chi, M. Zhao, L. Lv, Purification and identification of antioxidant peptides from egg white protein hydrolysate, Amino Acids **43** (2012) 457–466.

[30] İ. Gülseren,D. Güzey, B.D. Bruce, J. Weiss, Structural and functional changes in ultrasonicated bovine serum albumin solutions, Ultrason. Sonochem.**14** (2007) 173–183.

[31] S. Lin, Y. Jin, M. Liu, Y. Yang, M. Zhang, Y. Guo, G. Jones, J. Liu, Y. Yin, Research on the preparation of antioxidant peptides derived from egg white with assisting of high-intensity pulsed electric field, Food Chem. **139** (2013) 300–306.

[32] R.L. Prior, X. Wu, K. Schaich, Standardized methods for the determination of antioxidant capacity and phenolics in foods and dietary supplements, J. Agric. Food Chem. **53** (2005) 4290–4302.

[33] V.A. Tironi, M.C. Añón, Amaranth proteins as a source of antioxidant peptides: Effect of proteolysis. Food Res. Int. **43** (2010) 315–322.

[34] M. Memarpoor-Yazdi, A. Asoodeh, J.K. Chamani, A novel antioxidant and antimicrobial peptide from hen egg white lysozyme hydrolysates, J. Funct. Foods **4** (2012) 278–286.

[35] S.J. You, C.C. Udenigwe, R.E. Aluko, J.P. Wu, Multifunctional peptides from egg white lysozyme, Food Res. Int. **43** (2010) 848–855.

[36] X. Tang, Q.P. Wu, G.W. Le, J. Wang, K.J. Yin, Y.H. Shi, Structural and antioxidant modification of wheat peptides modified by the heat and lipid peroxidation product malondialdehyde, J. Food Sci. **77** (2012) 16–22.

[37] Y. Xia, F. Bamdad, M. Gänzle, L. Chen, Fractionation and characterization of antioxidant peptidesderived from barley glutelin by enzymatic hydrolysis, Food Chem. **134** (2012) 1509–1518.

IZVOD

BIOLOŠKI AKTIVNI PEPTIDI SA POBOLJŠANOM ANTIOKSIDATIVNOM AKTIVNOŠĆU DOBIJENI ULTRAFILTRACIONOM SEPARACIJOM HIDROLIZATA PROTEINA BELANCETA

Jelena R. Jovanović[1], Andrea B. Stefanović[1], Milena G. Žuža[1], Sonja M. Jakovetić[1], Nataša Ž. Šekuljica[3], Branko M. Bugarski[2], Zorica D. Knežević-Jugović[1]

[1]*Katedra za biohemijsko inženjerstvo i biotehnologiju, Tehnološko–metalurški fakultet, Univerzitet u Beogradu, Karnegijeva 4, 11000 Beograd, Srbija*
[2]*Katedra za hemijsko inženjerstvo, Tehnološko–metalurški fakultet, Univerzitet u Beogradu, Karnegijeva 4, 11000 Beograd, Srbija*
[3]*Inovacioni centar, Tehnološko–metalurški fakultet, Univerzitet u Beogradu, Karnegijeva 4, 11000 Beograd, Srbija*

(Naučni rad)

U ovom radu određena je antioksidativna aktivnost utrafiltracionih frakcija hidrolizata proteina belanceta ispitivanjem sposobnosti neutralizacije 2,2'-difenil--1-pikrilhidrazil (DPPH) i 2,2'-azinobis(3-etilbenzotiazolin-6-sulfonska kiselina)--diamonijum so (ABTS) radikala, kao i sposobnost redukcije 2,4,6-tri(2-piridil)-*s*--triazina (TPTZ). Proteini belanceta, korišćeni kao supstrat, neposredno pre enzimske hidrolize pretretirani su ultrazvučnim talasima frekvencije 35 i 40 kHz ili termički na 75 °C kako bi se postigla delimična denaturacija nativnih proteina i time omogućila olakšana dostupnostproteaze unutrašnjim peptidnim vezama u molekulu. Bakterijska endopeptidaza izolovana iz *Bacillus lichenoformis*, komercijalnog naziva alkalaza, korišćena je kao biokatalizator u reakciji hidrolize. Radi lakšeg literaturnog poređenja sa konvencionalnim termičkim postupkom, osim prethodno navedenim ultrazvučnim talasima visoke frekvencije, proteini belanceta su termički tretirani 30 min na 75 °C. Ultrafiltracionim frakcionisanjem dobijenih hidrolizata, korišćenjem celuloznih membrana različitih veličina pora, izolovane su četiri frakcije (>30, 10–30, 1–10 i <1 kDa) koje su okarakterisane sa aspekta sadržaja proteina i antioksidativne aktivnosti u cilju dobijanja bioaktivnih peptida. Dokazano je da je frakcija 3, koja sadrži peptide molekulske mase 1–10 kDa, u poređenju sa ostalim frakcijama svih pretretmana, imala najveće vrednosti za sva tri ispitivana antioksidativna testa. Značajno je istaći da je najveći doprinos izolovanju peptida sa visokom antioksidativnom aktivnošću dao ultrazvučni pretretman frekvencije 40 kHz. Naime, stepen inhibicije DPPH i ABTS radikala iznosio je 28,10±1,38 and 79,44±2,31%, redom. Na osnovu dobijenih rezultata, može se zaključiti da se ultrazvučnim pretretmanom i enzimskom hidrolizom proteina belanceta uspešno mogu izolovati bioaktivni peptidi, čija primena u prehrambenoj industriji kao dodataka ishrani predstavalja izuzetan doprinos.

Ključne reči: Antioksidativni peptidi belanceta • Membranska ultrafiltracija • Ultrazvučni pretretman • Enzimska hidroliza • Alkalaza

Phenolic compounds and carotenoids in pumpkin fruit and related traditional products

Gordana M. Zdunić[1], Nebojša R. Menković[1], Milka B. Jadranin[2], Miroslav M. Novaković[2], Katarina P. Šavikin[1], Jelena Č. Živković[1]

[1]*Institute for Medicinal Plants Research "Dr Josif Pančić", Belgrade, Serbia*
[2]*Institute for Chemistry, Metallurgy and Technology, University of Belgrade, Belgrade, Serbia*

Abstract

Pumpkin fruit is used in a diet since ancient times especially in rural communities. The major contributory factors of nutritional and medicinal value of pumpkins are carotenoids, polysaccharides, vitamins, minerals, and phenolic compounds. Due to a very large fruit that it is not easy to consume a whole as well as short shelf-life of fresh-cut pumpkin, different ways of conserving and processing are performed. In our study, total carotenoids, total phenolics and individual phenolics in fresh pumpkin and pumpkin traditional products such as sweet in wine, jam and juice, which are typical for northern parts of Serbia, were studied. Total carotenoids ranged from 27.6 μg/g of pumpkin sweet in wine to86.3 μg/g of fresh fruit, while the amount of total phenolics varied between 93.0 μg GAE/g of pumpkin juice and 905.9 μg GAE/g of fresh fruit. Eight phenolic compounds were identified in the investigated samples and among them phenolic acids dominated. Among flavonoids, flavanon glycoside hesperidin was detected.

Keywords: *Cucurbita maxima*, jam, juice, sweet, phenols, carotenoids, LC/MS.

Available online at the Journal website: http://www.ache.org.rs/HI/

SCIENTIFIC PAPER

UDC 635.621:664:54

Hem. Ind. **70** (4) 429–433 (2016)

doi: 10.2298/HEMIND150219049Z

Pumpkin (*Cucurbita pepo*, *C. moschata*, *C. maxima* and *C. mixta*) is one of the vegetables used in healthy diets as well as in traditional medicine in many countries. Since ancient times, it has been essential in the diet of rural communities. Nowadays, it is cultivated both, for fruit and seeds that are used in a variety of ways. Fruit is regarded by consumers due to its sweet and mild taste as well as high nutritive value [1]. Also, pumpkin flesh is widely used as a component in a variety of products for children and adults [2]. Pumpkin seeds have also high nutritional and medicinal value. Cold pressed pumpkin seed oils are rich source of phytosterols, tocopherols and squalene [3].

The major contributory factors of nutritional and medicinal value of pumpkin fruit are high total content of carotenoids with >80% of β-carotene [4,5] as well as presence of pectin and non-pectin polysaccharides, minerals (potassium, phosphorus, magnesium, iron, and selenium), vitamins (C, E, K, thiamine (B1) and riboflavin (B2), piridoxine (B6)), dietary fiber, phenolic compounds (flavonoids, phenolic acids) and other substances beneficial to human health [1,6–8].

Due to such diverse chemical composition, a lot of biological activities are attributed to pumpkin. Jin *et al.* [9] showed that a pumpkin-rich diet could reduce blood glucose. Similar result was obtained by Zhao *et al*. [10] who showed increased levels of serum insulin, reduced blood glucose levels and improvement of glucose tolerance in mice by pumpkin polysaccharides. Also, hypocholesterolemic, antibacterial, antiinflammatory and antitumor activities were reported [11].

One of the problems with consuming pumpkin is that the fruits are big and it is not easy to consume a whole pumpkin in a day even by a whole family. On the other hand, shelf-life of fresh-cut pumpkin is very short, and it tends to deteriorate during storage. So, different ways of conserving and processing of pumpkin are reported among them processing into jams, puree, juice pickles and dried products and it is also used as a base for soups and desserts [12–14]. There are a few works about engineering of the pumpkin processing [15,16], but the results on the effects of processing on pumpkin phenolic compounds are limited [17].

The aim of this study was the analysis of total carotenoids, total phenolics and individual phenolic compounds in traditional products of pumpkin such as sweet in wine, jam and juice, which are typical for northern parts of Serbia, together with analyses in fresh pumpkin fruit. LC/MS analysis was used for qualitative analysis of individual phenolic compounds.

EXPERIMENTAL

Material

Traditional pumpkin products (sweet in wine, jam and juice) were obtained from household, family Stoja-

Correspondence: G. Zdunić, Institute for Medicinal Plants Research "Dr Josif Pančić", Tadeuša Košćuška 1, 11000 Belgrade, Serbia.
E-mail: gzdunic@mocbilja.rs
Paper received: 19 February, 2015
Paper accepted: 1 June, 2015

novic, Vojvodina, Serbia. These products are unique in wider area and they are prepared according to the old, traditional recipes and technology that has been handed down in the family for generations. Local variety of pumpkin (*Cucurbita maxima* L., Cucurbitaceae), which is grown in the household was used for products preparation. The pumpkins were washed with potable water, peeled and cut into small pieces. Prior further processing, average sample of fresh pumpkin fruit was used for chemical analysis. After processing, products were stored in cold, dry and dark place. Five samples of each type of traditional pumpkin products were randomly chosen, mixed and average sample was used further for analysis.

Total phenolics

Samples of fresh pumpkin fruit and sweet in wine were grained prior extraction and homogenized. A mass of 10 g of each sample was extracted with 20 mL of solvent mixture H_2O/MeOH (1:1) for 30 min using the ultrasonic bath. From those extracts 3 dilutions were made (depends of the sample, experimentally determined to be in a linear range $A = f(c)$) and used for obtaining total phenolics). Total phenolic content was determined using the method of Folin–Ciocalteu reagent (FCR) with slight modifications [18]. An aliquot (200 µL) of each extract was mixed with 1000 µL of 1:10 dilution of Folin-Ciocalteu reagent. After 6 min 800 µL of sodium carbonate (75 g/L) was added. After 2 h of incubation in the dark at room temperature, absorbance was measured at 740 nm. Gallic acid (0–100 mg/L) was used for the preparation of the calibration curve. Results are expressed as µg of gallic acid equivalents (GAE) per g of fresh fruit or product, or per mL of juice. Analyses were performed in triplicates and the results are expressed as mean ± standard deviation.

Total carotenoids

Samples of fresh pumpkin fruit and sweet in wine were grained prior extraction and homogenized. For all samples 1 g was extracted with 50 mL of methanol which was the solvent that gave the best results for the extraction of carotenoids [19]. Total carotenoids were determined using earlier developed method and were calculated and expressed in µg/g of the sample. Analyses were performed in triplicates and the results are expressed as mean ± standard deviation.

LC/MS analysis

Sample preparation for analysis: Each sample (100 g) was homogenized, diluted with water (100 mL), and then this solution was extracted three times with ethyl acetate (100 mL). The organic phases were combined and evaporated to dryness in a rotary vacuum evaporator. Obtained ethyl acetate extracts (10 mg) were dissolved in 1 mL of methanol, filtered (0.45 µm filter) and analyzed by LC/MS techniques. Apparatus: liquid chromatograph Agilent 1200 series, Agilent Technologies, with a degasser, a binary pump, an autosampler, a thermostated column compartment and a DAD detector, coupled with a 6210 time-of-flight LC/MS system (Agilent Technologies); column: Zorbax Eclipse Plus RR C-18, 150 mm×4.6 mm id., (1.8 µm); mobile phase: A – 0.5% formic acid in water and B – acetonitrile; combination of gradient and isocratic modes of elution: 0–20 min, 5–16% B, 20–28 min, 16–40% B, 28–40 min, 40–90% B, 40–45 min, 90% B, 45–46 min, 90–5% B, 46–51 min, 5% B; flow rate: 0.95 mL/min. The injection volume was 5 µL, and the column temperature 40 °C. DAD-MSD conditions: spectral data for all the signals were accumulated in the wavelength range of 190–450 nm, and chromatograms were recorded at wavelengths of 230, 260, 280 and 340 nm. The total ion chromatograms were recorded using the following parameters: ion source (ESI) polarity, negative; capillary voltage, 4000 V; gas temperature, 350 °C; drying gas, 12 L/min; nebulizer pressure, 45 psig (310.26 Pa); fragmentor voltage, 140 V, mass range 100–1500 *m*/*z*. A personal computer system running Mass Hunter Workstation software was used for data acquisition and processing. Identification: compounds were identified by comparing retention times (t_R), UV and MS spectra with those of the reference standards (protocatechuic acid, *p*-hydroxybenzoic acid, vanillin, *p*-coumaric acid and hesperidin), or on the basis of the exact mass measurement and literature data (salicylic acid, eriodictyol 7-neohesperidoside, and abscisic acid).

RESULTS AND DISCUSSION

Total carotenoids

Cucurbita species are known as a good source of carotenoids [4]. Total carotenoid content was analyzed in traditional products typically produced in north part of Serbia (Table 1). Fresh pumpkin fruit contained the highest amount of total carotenoids (86.3 µg/g FW), thus presenting a valuable source of this bioactive compounds. Murkovic *et al.* [20] investigated a carotenoid content in different varieties of three *Cucurbita* species grown in Austria (*C. pepo*, *C. maxima* and *C. moschata*)

Table 1. Total carotenoids and total phenolics in fresh pumpkin fruit and pumpkin traditional products; results are expressed on fresh mass basis as mean ± standard deviation of triplicate analysis

Sample	Total carotenoids µg/g	Total phenolics µg GAE/g
Pumpkin fruit	86.3±1.9	905.9±13.9
Pumpkin sweet in wine	27.6±0.8	227.2±8.0
Pumpkin jam	63.9±1.6	769.1±14.1
Pumpkin juice	28.6±1.1	93.0±6.0

and it was similar as in our sample. On the other hand, Provesi *et al*. [21] reported lower amounts of carotenoids in *C. moschata* and *C. maxima* from Brasil (*cca*. 40 and 30 μg/g, respectively). Total carotenoids content in pumpkin is known to be strongly influenced by the cultivar type as well as by the conditions of cultivation [22].

Processing affected the amount of total carotenoids, but the smallest decrease was noticed in jam in which about 70% of carotenoids content was preserved. Also, Provesi *et al*. [21] showed that decrease of carotenoids in pumpkin puree (similar product to jam) was less than 50%. On the other hand, decrease of total carotenoids in pumpkin sweet in wine as well as in pumpkin juice was more pronounced (for almost 70%). Total carotenoids content in pumpkin products are strongly influenced by the technological processes applied, specifically thermal processes [11,14]. The highest retention of carotenoids was obtained when vegetables were cooked almost without water and the lowest retention of carotenoids was associated with the use of a large amount of water during cooking [23]. Moreover, Provesi and Amante [14] stated that processing of pumpkin may cause oxidation and/or isomerization of carotenoids, which affect biological activity and colour. The most important factors that lead to this loss are temperature and contact with oxygen and light.

Total phenolics

Also, total phenolic content was determined in fresh pumpkin fruit as well as in pumpkin products. As it was previously shown for total carotenoids, pumpkin fruit was the most abundant in phenolics (Table 1). Obtained result was in accordance with literature data as Azizah *et al*. [24] detected similar amounts of total phenolics (90 mg GAE/100 g). However, Nawirska-Olsza *et al*. [25] detected lower amounts of total phenolics in pumpkin (24 mg/100 g FW). As it could be expected, in pumpkin products lower but still significant amounts of phenolics were determined and the registered reductions were probably due to the thermal processing. Pumpkin jam was the richest product in total phenols, pointed that this type of processing provides a product of high value. The lowest amount of total phenolics was detected in juice and it was almost 2.5 times lower than in jam. Content of total phenols is important parameter because it is usually correlated with antioxidant activity.

LC/MS analysis

Eight compounds were identified, and among them phenolic acids dominated (Table 2). Protocatechuic and chlorogenic acid are polyphenols which are widely distributed in variety of plant species known as the sources of potent antioxidants such as green tea. Also, Dragovic-Uzelac *et al.* [26] reported the presence of chlorogenic acid in *C. pepo*, *C. maxima* and *C. moschata*. Among flavonoids, hesperidin, glycoside of hesperetin, characteristic for citrus fruits was detected. Hesperidin shows different biological activities such as antioxidant, anti-inflammatory and anticancer activities [27,28]. Eriodictyol-7-neohesperidoside is also found in citrus fruits. It is strong antioxidant since it has catechol moiety in B ring and 5-OH group in A ring (capable for chelating metal cations with carbonyl group in position 3). Vanillin was noticed only in the pumpkin jam probably due to its addition according to the recipe.

Table 2. Compounds identified in pumpkin fruit and pumpkin traditional products by LC/MS

t_R in LC/ DAD, min	t_R in ESI ToF, min	Molecular formula	Exact mass	Compound
6.20	6.31	$C_7H_6O_4$	154.0266	Protocatechuic acid
6.42	6.58	$C_{16}H_{18}O_9$	354.0951	Chlorogenic acid
8.79	8.92	$C_7H_6O_3$	138.0317	Salicylic acid
9.21	9.36	$C_7H_6O_3$	138.0317	*p*-Hydroxibenzoic acid
16.58	16.75	$C_8H_8O_3$	152.0473	Vanillin[a]
17.21	17.46	$C_9H_8O_3$	164.0473	*p*-Coumaric acid
22.19	22.47	$C_{27}H_{32}O_{15}$	596.1741	Eriodictyol-7-neohesperidoside
25.34	25.64	$C_{28}H_{34}O_{15}$	610.1898	Hesperidin

[a]Detected only in pumpkin jam

CONCLUSION

Consumption of fruits and vegetables has been increased rapidly due to awareness regarding their health benefits for humans. Carotenoids and phenolics are among the phytochemicals, believed to reduce the risk of developing degenerative and chronic diseases. The results of our study indicated that tested pumpkin fruit as well as products made from pumpkin fruit, *i.e*., jam, sweets in wine, and juice, are a valuable source of carotenoids and phenolics. Although total carotenoids and total phenolic content in pumpkin products are strongly influenced by the applied technological pro-

cesses, specifically thermal processes, about 70% of carotenoids and 85% of total phenolics were preserved in pumpkin jam compared to fresh pumpkin fruit. Thus, obtained results pointed out possibilities for better utilization of such a nutritionally rich underutilized pumpkin products especially in the periods with the lack of fresh fruits.

Acknowledgements

The authors acknowledge their gratitude to the Ministry of Education, Science and Technological Development of Serbia for financial support, project number 46013.

REFERENCES

[1] S. Sharma, T.V.R. Rao, Nutritional quality characteristics of pumpkin fruit as revealed by its biochemical analysis, Int. Food Res. J. **20** (2013) 2309–2316.

[2] T. Rakcejeva, R. Galoburda, L. Cude, E. Strautniece, Use of dried pumpkins in wheat bread production, Proc. Food Sci. **1** (2011) 441–447.

[3] B.B. Rabrenovic, E.B. Dimic, M.M. Novakovic, V.V. Tesevic, Z.N. Basic, The most important bioactive components of cold pressed oil from different pumpkin (*Cucurbita pepo* L.) seeds, LWT - Food Sci Tech. **55** (2014) 521––527.

[4] C.H. Azevedo-Meleiro, D.B. Rodriguez-Amaya, Qualitative and quantitative differences in carotenoid composition among *Cucurbita moschata*, *Cucurbita maxima*, and *Cucurbita pepo*, J. Agric. Food Chem. **55** (2007) 4027–4033.

[5] C. Kurz, R. Carle, A. Schieber, HPLC-DAD-MS^n characterisation of carotenoids from apricots and pumpkins for the evaluation of fruit product authenticity, Food Chem. **110** (2008) 522–530.

[6] A. Nawirska-Olszanska, A. Biesiada, A. Sokol-Letowska, A. Z. Kucharska, Characteristics of organic acids in the fruit of different pumpkin species, Food Chem. **148** (2014) 415–419.

[7] C.L. Zhou, W. Liu, J. Zhao, C. Yuan, Y. Song, D. Chen, Y.Y. Ni, Q. H. Li, The effect of high hydrostatic pressure on the microbiological quality and physical–chemical characteristics of pumpkin (*Cucurbita maxima* Duch.) during refrigerated storage, Innov. Food Sci. Emerg. Technol. **21** (2014) 24–34.

[8] M.Y. Kim, E.J. Kim, Y.N. Kim, C. Choi, B.H. Lee, Comparison of the chemical compositions and nutritive values of various pumpkin (*Cucurbitaceae*) species and parts, Nutr. Res. Pract. **6** (2012) 21–27.

[9] H. Jin, Y.J. Zhang, J.X. Jiang, L.Y. Zhu, P. Chen, J. Li, H.Y. Yao, Studies on the extraction of pumpkin components and their biological effects on blood glucose of diabetic mice, J. Food Drug Anal. **21** (2013) 184–189.

[10] X.H. Zhaoa, L. Qianb, D.L. Yina, Y. Zhoua, Hypolipidemic effect of the polysaccharides extracted from pumpkin by cellulase-assisted method on mice, Int. J. Biol. Macromol. **64** (2014) 137–138.

[11] C. Fu, H. Shi, Q. Li, A review on pharmacological activities and utilization technologies of pumpkin, Plant Foods Hum. Nut. **61** (2006) 73−80.

[12] J.G. Provesi, C.O. Dias, R.D. de Mello Castanho Amboni, E.R. Amante, Characterisation and stability of quality indices on storage of pumpkin (*Cucurbita moschata* and *Cucurbita maxima*) purees, Int. J. Food Sci. Technol. **47** (2012) 67–74.

[13] M.T.M. Assous, E.M. Soheir Saad, A.S. Dyab, Enhancement of quality attributes of canned pumpkin and pineapple, Ann. Agric. Sci. **59** (2014) 9–15.

[14] J.G. Provesi, E.R. Amante, Carotenoids and Impact of Processing Treatments and Storage, in: V. Preedy (Ed.), Processing and Impact on Active Components in Food, Academic press, London, 2015, pp. 71–80.

[15] H.S. Phanindra-Kumar, K. Radhakrishna, P.K. Nagaraju, D. Vijaya-Rao, Effect of combination drying on the physico-chemical characteristics of carrot and pumpkin, J. Food Proc. Preserv. **25** (2001) 447–460.

[16] C.C. Garcia, M.A. Mauro, M. Kimura, Kinetics of osmotic dehydration and air-drying of pumpkins (*Cucurbita moschata*), J. Food Eng. **82** (2007) 284–291.

[17] R. Contador, F. González-Cebrino, J. García-Parra, M.L. R. Ramírez, Effect of hydrostatic high pressure and thermal treatments on two types of pumpkin purée and changes during refrigerated storage, J. Food Proc. Preserv. **38** (2014) 704–712.

[18] P. Waterman, S. Mole, Analysis of Phenolic Plant Metabolites, Blackwell Scientific Publication, Oxford, 1994.

[19] S. Dere, T. Gunes, R. Sivaci, Spectrophotometric determination of chlorophyll – A, B and total carotenoid contents of some algae species using different solvents, Tr. J. Bot. **22** (1998) 13–17.

[20] M. Murkovic, U. Mülleder, Carotenoid content in different varieties of pumpkin, J. Food Compos. Anal. **15** (2002) 633–638.

[21] J.G. Provesi, C.O. Dias, E.R. Amante, Changes in carotenoids during processing and storage of pumpkin puree, Food Chem. **128** (2011) 195–202.

[22] F.M. Oloyede, G.O. Agbaje, E.M. Obuotor, I.O. Obisesan, Nutritional and antioxidant profiles of pumpkin (*Cucurbita pepo* Linn.) immature and mature fruits as influenced by NPK fertilizer, Food Chem. **135** (2012) 460––463.

[23] E. Lešková, J. Kubíková, E. Kováčiková, M. Košická, J. Porubská, K. Holčíková, Vitamin losses: Retention during heat treatment and continual changes expressed by mathematical models, J. Food Compos. Anal. **19** (2006) 252–276.

[24] A. Azizah, K.C. Wee, O. Azizah, M. Azizah, Effect of boiling and stir frying on total phenolics, carotenoids and radical scavenging activity of pumpkin (*Cucurbita moschato*), Int. Food. Res. J. **16** (2009) 45–51.

[25] A. Nawirska-Olszanska, A. Biesiada, A. Sokol-Letowska, A.Z. Kucharska, Content of bioactive compounds and antioxidant capacity of pumpkin puree enriched with japanese quince, cornelian cherry, strawberry and apples, Acta Sci. Pol. Technol. Aliment. **10** (2011) 51–60.

[26] V. Dragovic-Uzelac, K. Delonga, B. Levaj, S. Djakovic, J. Pospisil, Phenolic profiles of raw apricots, pumpkins, and their purees in the evaluation of apricot nectar and jam authenticity, J. Agric. Food Chem. **53** (2005) 4836––4842.

[27] J.A. Manthey, K. Grohmann, N. Guthrie, Biological properties of citrus flavonoids pertaining to cancer and inflammation, Curr. Med. Chem. **8** (2001) 135–153.

[28] P.K. Wilmsen, D.S. Spada, M. Salvadar, Antioxidant activity of the flavonoid hesperidin in chemical and biological systems, J. Agric. Food. Chem. **53** (2005) 4757––4761.

ИЗВОД

ФЕНОЛНЕ КОМПОНЕНТЕ И КАРОТЕНОИДИ У ПЛОДУ ТИКВЕ И ТРАДИЦИОНАЛНИМ ПРОИЗВОДИМА ОД ТИКВЕ

Гордана М. Здунић[1], Небојша Р. Менковић[1], Милка Б. Јадранин[2], Мирослав М. Новаковић[2], Катарина П. Шавикин[1], Јелена Ч. Живковић[1]

[1]*Институт за проучавање лековитог биља „Др Јосиф Панчић”,Тадеуша Кошћушка 1, 11000 Београд*
[2]*Институт за хемију, технологију и металургију, Универзитет у Београду, Његошева 12, 11000 Београд*

(Научни рад)

Тиква се користи у исхрани од давнина, посебно у руралним срединама. Главни фактори који доприносе нутритивним и здравственим вредностима тикве су каротеноиди, полисахариди, витамини, минерали, и фенолна једињења. Због веома великих плодова као и кратког рока трајања свеже сечених кришки тикве, користе се различити начини чувања и прераде. У нашим истраживањима испитивали смо садржај укупних каротеноида и укупних фенола и присуство појединачних фенолних једињења у свежем плоду тикве, као и у традиционалним производима од тикве који су типични за северне делове Србије, као што су џем, слатко у вину и сок. Садржај укупних каротеноида се кретао од 27,6 μg/g слатка од тикве у вину до 86,3 μg/g свежег плода тикве, док се садржај укупних фенола кретао између 93,0 μg GAE/g сока тикве до 905,9 μg GAE/g свежег плода тикве. Што се тиче појединачних фенолних једињења у испитиваним узорцима, коришћењем LC/MS технике, идентификовано је осам једињења, међу којима доминирају фенолне киселине. Од флавоноида, детектован је флаванонски гликозид хесперидин.

Кључне речи: *Cucurbita maxima* • Џем • Сок • Слатко • Феноли • Каротеноиди • LC/MS

Mogućnosti, perspektive i ograničenja u proizvodnji mlečne kiseline na sporednim i otpadnim sirovinama

Dragana D. Mladenović[1], Aleksandra P. Djukić-Vuković[1], Jelena D. Pejin[2], Sunčica D. Kocić-Tanackov[2], Ljiljana V. Mojović[1]

[1]*Tehnološko–metalurški fakultet, Univerzitet u Beogradu, Beograd, Srbija*
[2]*Tehnološki fakultet, Univerzitet u Novom Sadu, Novi Sad, Srbija*

Izvod

U skladu sa ciljevima održivog razvoja i potrebama zaštite životne sredine danas se velika pažnja usmerava ka razvoju novih tehnologija u kojima se koriste sporedni i otpadni industrijski proizvodi. Otpadni proizvodi predstavljaju potencijalnu sirovinu za biotehnološku proizvodnju bioetanola, biogasa, biodizela, organskih kiselina, enzima, mikrobne biomase itd. Od prve industrijske proizvodnje do danas, mlečna kiselina (MK) je našla široku primenu u prehrambenoj, kozmetičkoj, farmaceutskoj i hemijskoj industriji, a poslednjih godina potražnja za MK je znatno povećana zbog njene uloge u proizvodnji biodegradabilnih laktidnih polimera. Ispitivanja mogućnosti fermentacione proizvodnje MK na otpadnim sirovinama su danas intenzivna kako zbog smanjenja ukupnih troškova proizvodnje MK, tako i zbog ekološkog problema odlaganja otpadnih materijala. U cilju unapređenja procesa, poboljšanja produktivnosti i dobijanja proizvoda visoke čistoće ispituju se novi proizvodni mikroorganizmi i fermentacioni postupci. U ovom radu je dat pregled nedavnih istraživanja proizvodnje MK na sporednim i otpadnim industrijskim sirovinama, kao i mogućnosti pojedinih tehnoloških postupaka u proizvodnji MK.

Ključne reči: mlečna kiselina, bakterije mlečne kiseline, otpadne sirovine, sporedne sirovine, fermentacija.

Dostupno na Internetu sa adrese časopisa: http://www.ache.org.rs/HI/

PREGLEDNI RAD

UDK 502/504:638.4.04:579.864

Hem. Ind. **70** (4) 435–449 (2016)

doi: 10.2298/HEMIND150403050M

Biorafinerijski koncept pored održive prerade biomase predviđa korišćenje sporednih i otpadnih proizvoda iz jednog proizvodnog procesa kao polaznih sirovina za dobijanje energije, goriva ili hemikalija. Trenutno se u svetu više od 80% energije i oko 90% organskih hemikalija proizvodi iz fosilnih izvora [1]. Zbog naglog porasta svetske populacije i poboljšanja životnog standarda potrošnja energije i hemikalija neprekidno raste (približno 7% godišnje) [1], što dovodi do sve veće zabrinutosti u pogledu snabdevanja kako energijom tako i sirovinama u budućnosti. Evropska komisija je 2012. godine usvojila strategiju pod nazivom „Inovativnost za održivi rast – bioekonomija za Evropu" čiji je cilj razvoj novih tehnologija i proizvodnja uz smanjenje štetne emisije, pretvaranje otpadnih proizvoda u bioproizvode, bioenergiju i biogorivo, kao i veća upotreba obnovljivih i održivih izvora [2]. U tom svetlu su ispitivani različiti supstrati za primenu u biotehnološkoj proizvodnji MK kao izuzetno tražene i široko primenjene supstance u hemijskoj, farmaceutskoj, kozmetičkoj, prehrambenoj i tekstilnoj industriji.

U novije vreme MK se intenzivno koristi za proizvodnju polimera-polilaktida. Zbog biorazgradivosti polilaktidi se mogu koristiti kao ekološki prihvatljiva alternativa za konvencionalne plastične materijale, a zbog biokompatibilnosti nalaze primenu u medicini i farmaciji kao materijali za fiksaciju fraktura, kontrolisano oslobađanje leka i sl. [3]. Prema procenama Global Industry Analyst Inc. očekuje se da će globalno tržište za MK dostići 367 300 tona do 2017. godine [4], a preko milion tona do 2020. godine [5]. Godišnji porast potražnje za MK od približno 20% se očekuje prvenstveno usled rastućeg trenda primene polilaktida [6]. Trenutno, 90% svetske proizvodnje MK se odvija mikrobnom fermentacijom ugljenih hidrata pomoću homofermentativnih mikroorganizama koji sintetišu MK kao glavni proizvod [7]. Izborom odgovarajućeg mikroorganizma koji proizvodi samo jedan od izomera (D- ili L-MK) se može dobiti optički čist proizvod, dok hemijska proizvodnja uvek daje racemsku smešu izomera MK [7]. Kao proizvodni mikroorganizmi najčešće se koriste bakterije mlečne kiseline (BMK), ali i predstavnici roda *Bacillus* i plesni roda *Rhizopus.* Svaka od navedenih grupa producenata MK ima određene prednosti i nedostatke usled različitih morfoloških, fizioloških i biohemijskih karakteristika, a najbolji uslovi za fermentaciju i postizanje visokih prinosa proizvoda nisu uvek najpovoljniji sa ekonomske tačke gledišta. Izbor mikroorganizma za proizvodnju MK prvenstveno zavisi od sposobnosti fermentacije ugljenih hidrata. Poželjna karakteristika proizvodnih mikroorganizama je sposobnost da

Prepiska: Lj. Mojović, Tehnološko–metalurški fakultet, Univerzitet u Beogradu, Karnegijeva 4, 11000 Beograd, Srbija.
E-pošta: lmojovic@tmf.bg.ac.rs
Rad primljen: 3. aprik, 2015
Rad prihvaćen: 2. septembar, 2015

daju visoke prinose D- ili L-MK fermentacijom jeftinih izvora ugljenika, sa minimalnom potrebom za obogaćivanjem medijuma izvorima azota i faktorima rasta.

Ovaj rad daje uvid u dosadašnja istraživanja vezana za fermentacionu proizvodnju MK na sporednim i otpadnim industrijskim sirovinama. Analizirani su izazovi u mlečno-kiselinskoj fermentaciji, kao i do sada ispitivane tehnologije na polju proizvodnje MK. U cilju postizanja boljih prinosa analizirana je upotreba mešanih kultura, različitih strategija dolivnog fermentacionog postupka, imobilisanih i bioreaktorskih sistema. Razmatrana je i mogućnost vođenja otvorenog (nesterilnog) fermentacionog postupka, kao jednog od načina za ekonomski održivu proizvodnju MK.

MIKROORGANIZMI PRODUCENTI MLEČNE KISELINE

Bakterije mlečne kiseline

BMK predstavljaju heterogenu grupu mikroorganizama čija je glavna karakteristika sposobnost sinteze MK kao glavnog, a ponekad i jedinog proizvoda fermentacije šećera. Grupa BMK uključuje sledeće rodove: *Carnobacterium, Enterococcus, Lactobacillus, Lactococcus, Leuconostoc, Oenococcus, Pediococcus, Streptococcus, Tetragenococcus, Vagococcus* i *Weissella* [8]. BMK su Gram-pozitivne, nesporogene, acidotolerantne, anaerobne do mikroaerofilne bakterije. Generalno se opisuju kao katalaza negativne, iako pojedine vrste roda *Lactobacillus* imaju pseudokatalazu [9]. BMK mogu selektivno da proizvode jedan specifičan stereoizomer MK ili njihovu mešavinu u različitim proporcijama. Glavni enzim odgovoran za stereospecifičnu proizvodnju MK je laktat dehidrogenaza (LDH) koji ima L i D formu, pa izomer proizvedene MK zavisi od toga koji je oblik enzima prisutan kod BMK [7]. BMK su auksotrofi i zbog ograničene sposobnosti da sintetišu faktore rasta zahtevaju podlogu bogatu aminokiselinama i vitaminima [7]. Pojedine vrste BMK imaju sposobnost produkcije ekstracelularnih amilolitičkih enzima, što ih čini pogodnim za direktnu proizvodnju MK iz različitih skrobnih sirovina [10]. Takođe, pojedine vrste BMK produkuju inulinazu i imaju sposobnost da fermentišu frukto-oligosaharide, pa se mogu koristiti za direktnu fermentacionu proizvodnju MK iz sirovina koje sadrže inulin [11,12]. U direktnoj fermentaciji na Jerusalimskoj artičoki sa *Lactobacillus paracasei* KCTC 13169 je postignuta koncentracija MK od 92,5 g L^{-1} [11], dok je pomoću *Lb. paracasei* DSM 23505 na brašnu cikorije postignuta koncentracija MK od 127,3 g L^{-1} [12]. Poslednjih godina istraživanje mogućnosti korišćenja lignocelulozno materijala za proizvodnju MK zahtevalo je pronalaženje mikroorganizama sposobnih za efikasnu konverziju pentoza (ksiloze i arabinoze) prisutnih u hemicelulozним frakcijama lignocelulozних sirovina. Na supstratima bogatim ksilozom su ispitivane sledeće vrste BMK: *Enterococcus mundtii* QU 25 [13], *Lb. pentosus* ATCC 8041 [14], *Leuconostoc lactis* [15] *i Lb. rhamnosus* ATCC 7469 [16].

Pored navedenih vrsta BMK od značaja za primenu u proizvodnji MK na otpadnim supstratima su i bakterije roda *Bacillus*, kao i plesni iz roda *Rhizopus*.

Bakterije roda *Bacillus*

Vrste iz roda *Bacillus* takođe imaju sposobnost proizvodnje MK, a na otpadnim supstratima je najviše ispitivana vrsta *Bacillus coagulans.* To su Gram-pozitivne, sporogene, aerobne do mikroaerofilne, termofilne bakterije koje mogu da rastu i proizvode optički čistu L-MK u temperaturnom intervalu od 50 do 60 °C [17–20]. Visoke optimalne temperature smanjuju rizik od kontaminacije mezofilnim vrstama mikroorganizama i omogućavaju otvorenu (nesterilnu) fermentaciju, što smanjuje ukupne troškove proizvodnje [19]. Sojevi *B. coagulans* fermentišu heksoze i pentoze i zbog toga su pogodni mikroorganizmi za proizvodnju MK na lignocelulozним sirovinama [20]. Za razliku od BMK ove bakterije mogu da rastu u jednostavnom medijumu, ne zahtevajući složene izvore azota. Michelson i sar. [21] su izvršili poređenje dva proizvodna mikroorganizma, *Lb. delbrueckii* DSM 20073 i *B. coagulans* SIM-7 u optimizovanom fermentacionom medijumu za oba soja. Koncentracija MK i produktivnost koju je postigao *B. coagulans* tokom 10 h fermentacije su bili 56 g L^{-1} i 5,5 g L^{-1} h^{-1}, dok su postignute vrednosti istih parametara fermentacije za *Lb. delbruecki* tokom 24 h fermentacije bile 52 g L^{-1} i 2,2 g L^{-1} h^{-1} [21]. Na osnovu postignute produktivnosti *B. coagulans* je pokazao sposobnost efikasnije konverzije supstrata pa se može smatrati pogodnijim za primenu u ispitivanom sistemu uz energetski i ekonomski niže zahteve.

Plesni roda *Rhizopus*

Pojedine vrste plesni koje pripadaju rodovima *Mucor, Monilia* i *Rhizopus* takođe proizvode MK, a *Rhizopus oryzae* je prva vrsta ispitivana za industrijsku proizvodnju MK [22]. *R. oryzae* i *R. arrhizus* proizvode amilolitičke enzime, pa mogu da fermentišu skrob do glukoze i dalje direktno do L-MK, bez prethodne saharifikacije [23,24]. *R. oryzae* ima sposobnost da metaboliše ksilozu, što ga čini atraktivnim za proizvodnju MK iz lignocelulozног materijala [25–27]. Filamentozni rast plesni olakšava njihovo odvajanje iz fermentacionog medijuma, a zaostala mikrobna biomasa predstavlja vredan sporedni proizvod fermentacije koji se može koristiti u ishrani životinja kao izvor proteina, za prečišćavanje otpadnih voda ili proizvodnju hitozana [23,27]. Plesni mogu da rastu u jednostavnom, neorganskom medijumu, bez dodatka skupih izvora azota [23], što je njihova osnovna prednost u odnosu na BMK. Međutim, na osnovu dosadašnjih rezultata može se zaključiti da fermentacija pomoću plesni još uvek

nije konkurentna bakterijskoj, a niži prinosi se pripisuju ograničenom prenosu mase kiseonika i hranljivih materija usled filamentoznog rasta, a delom i formiranju sporednih proizvoda kao što su etanol, CO_2, fumarna, jabučna i limunska kiselina [23,25].

METABOLIČKI PUTEVI BAKTERIJA MLEČNE KISELINE

BMK imaju sposobnost da fermentišu ugljene hidrate, heksoze i pentoze, različitim metaboličkim putevima i shodno tome daju različite produkte fermentacije, na osnovu čega se dele na homofermentativne i heterofermentativne. Na slici 1 su šematski prikazani različiti metabolički putevi proizvodnje MK. Glavni krajnji proizvod fermentacije kod homofermentativnih vrsta u anaerobnim uslovima je isključivo MK, dok heterofermentativni predstavnici metabolišu ugljene hidrate do acetate ili etanola, CO_2, MK i drugih metabolita. Homofermentativne BMK metabolišu heksoze Embden–Meyerhof–Parnas (EMP) putem, pri čemu nastaju 2 mola MK od svakog mola glukoze, sa teorijskim prinosom MK od 1 g g^{-1}. Budući da se mali procenat izvora ugljenika koristi za proizvodnju mikrobne biomase (0,07–0,22 g g^{-1}) eksperimentalni prinosi su obično niži (0,74–0,99 g g^{-1}) [28]. BMK koje koriste isključivo ovaj metabolički put su obligatno homofermentativne, a osim glukoze mogu da metabolišu i druge heksoze kao što su fruktoza, manoza ili galaktoza, ali nemaju sposobnost da fermentišu pentoze. Heterofermentativne BMK koriste alternativni pentozo-fosfatni (PF) put kojim heksoze konvertuju do pentoza i CO_2. Nastale pentoze dalje metabolišu fosfoketolaznim (FK) putem do laktata, etanola ili acetata. BMK koje metabolišu ugljene hidrate samo ovim putem su obligatno heterofermentativne. Heterofermentativne BMK iz jednog mola glukoze daju 1 mol MK, 1 mol CO_2 i 1 mol etanola ili acetata, pri čemu postižu maksimalni teorijski prinos MK od 0,5 g g^{-1} [28,29]. Mnoge heterofermentativne BMK metabolišu pentoze FK putem i pri tome postižu maksimalni prinos MK od 0,6 g g^{-1} [29]. Pored BMK koje su klasifikovane kao obligatno homofermentativne, odnosno obligatno heterofermentativne, pojedine vrste roda *Lactobacillus* su označene kao fakultativno heterofermentativne. Iako ove bakterije metabolišu heksoze preko EMP puta, takođe poseduju i enzim fosfoketolazu koja se može indukovati u prisustvu pentoza [30].

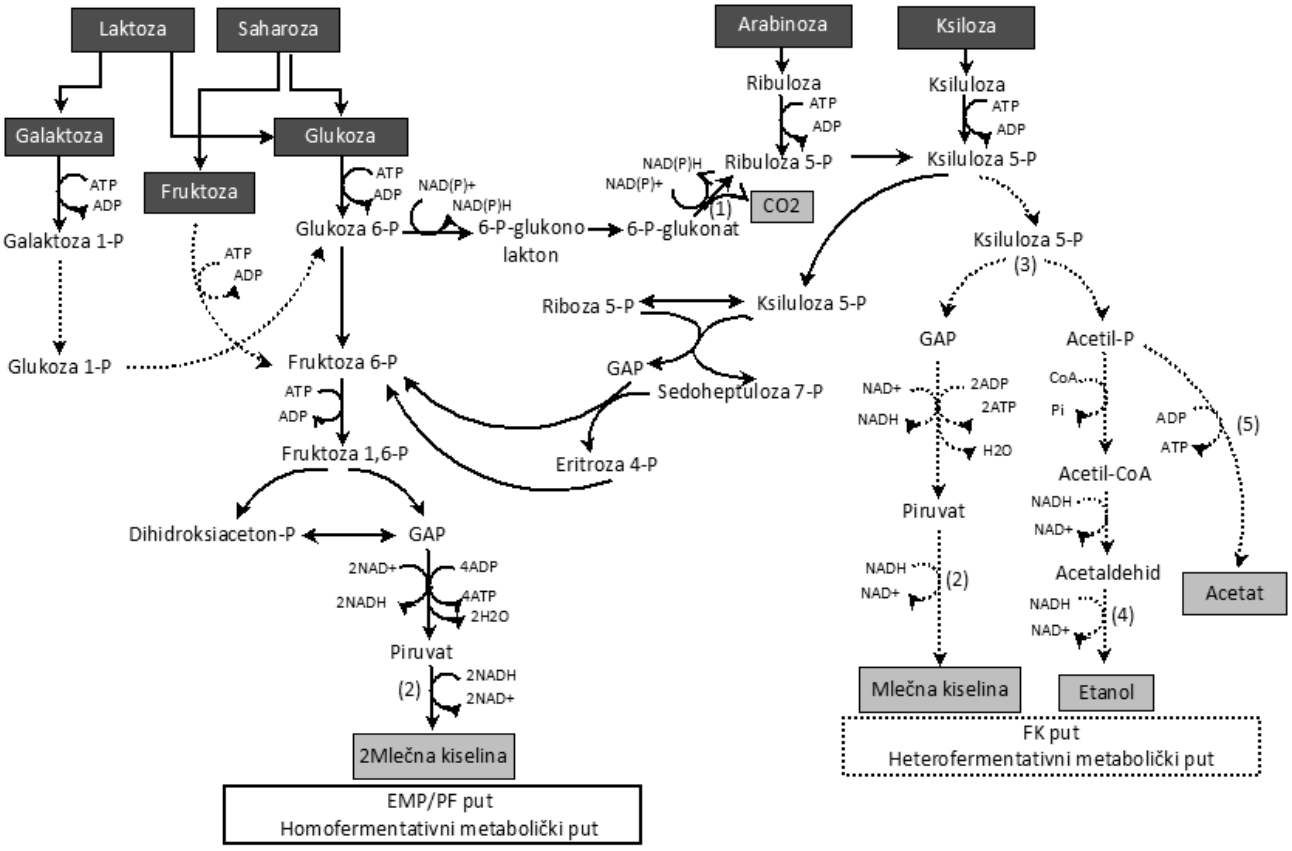

Slika 1. Metabolički putevi bakterija mlečne kiseline. Enzimi: (1) 6-fosfoglukonat dehidrogenaza; (2) laktat dehidrogenaza; (3) fosfoketolaza; (4) alkohol dehidrogenaza; (5) acetat kinaza.
Figure 1. Metabolic pathways in lactic acid bacteria. Enzymes: (1) 6-phosphogluconate dehydrogenase; (2) lactate dehydrogenase; (3) phosphoketolase; (4) alcohol dehydrogenase; (5) acetate kinase.

SPOREDNE I OTPADNE SIROVINE ZA PROIZVODNJU MLEČNE KISELINE

Za proizvodnju MK fermentacionim putem se mogu koristiti sirovine koje sadrže fermentabilne šećere ili polisaharide koji se mogu razgraditi do fermentabilnih šećera. Veliki broj istraživanja do nedavno je bio fokusiran na proizvodnju MK iz rafinisanih šećera i jestivih useva [7]. Međutim, ovakva proizvodnja je ekonomski nepovoljna, zato što su rafinisani šećeri skupi, a globalna potražnja za hranom je sve veća. Takođe, MK je prilično jeftin proizvod, trenutna tržišna cena MK za prehrambenu upotrebu iznosi 1400–1600 US$ po toni [31]. Zbog toga, u novije vreme se intenzivnije razmatra proizvodnja MK iz jeftinih sirovina, kao što su otpadne sirovine iz poljoprivrede, šumarstva i industrije.

Na slici 2 šematski su prikazani različiti postupci mlečno-kiselinske fermentacije u zavisnosti od korišćenog supstrata, dok su u tabeli 1 prikazane postignute vrednosti najvažnijih parametara mlečno-kiselinske fermentacije na različitim otpadnim supstratima.

Otpadne sirovine mogu imati veliki potencijal kao izvori fermentabilnih šećera, ali i mnogih drugih jedinjenja od značaja za rast mikroorganizama, kao što su proteini, mineralne materije i vitamini. Zbog složenosti njihovog sastava i varijacija u hemijskim i fizičkim karakteristikama potrebna su detaljna ispitivanja i optimizacija procesnih parametara za svaku od otpadnih sirovina kako bi se omogućila njihova upotreba u biotehnološkim procesima.

Surutka

Surutka je zeleno-žućkasta tečnost koja nastaje kao sporedni proizvod u procesu proizvodnje sira i kazeina. Žućkasta boja surutke je rezultat prisustva riboflavina (vitamina B_2) [32]. Iako surutku karakteriše nutritivno vredan sastav, a time i mogućnost njenog iskorišćavanja u različitim biotehnološkim procesima, čak 50% surutke se bez prethodne obrade ispušta u vodotokove [33]. Surutka ima visoko organsko opterećenje sa vrednostima hemijske i biološke potrošnje kiseonika u opsegu od 27–60 i 50–102 g L^{-1}, redom [32]. Takođe, proizvodnjom 1 kg sira nastaje 9 kg surutke [32], pa je jasno da surutka koja se ispušta u vodotokove predstavlja veliki ekološki problem. Prema prosečnom sastavu, surutka sadrži oko 93–94% vode i hranljive materije iz mleka, kao što su laktoza, rastvorljivi proteini, mineralne materije, MK i masti [32,34]. Međutim, i pored nutritivne vrednosti surutke BMK zahtevaju dodatno obogaćivanje aminokiselinama i peptidima [34]. U proizvodnji MK surutka se najčešće dopunjuje ekstraktom kvasca i proteinskim lizatima (peptonima) [34,35]. Obogaćivanje surutke se može izbeći ukoliko se supstrat prethodno tretira proteolitičkim enzimima ili proteolitičkim mikroorganizmima [34], kao što su vrste rodova *Pseudomonas* i *Bacillus.* Vasala i sar. [34] su

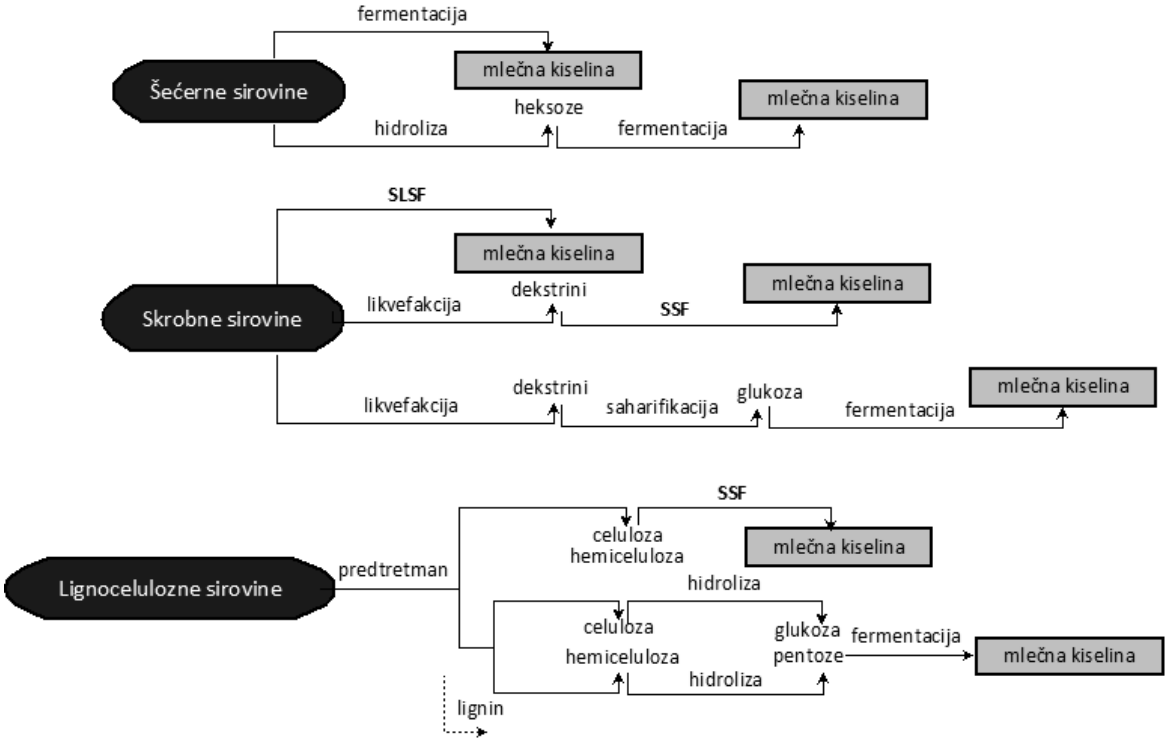

Slika 2. Shematski prikaz osnovnih faza proizvodnje mlečne kiseline na različitim supstratima. SSF – simultana saharifikacija i fermentacija; SLSF – simultana likvefakcija, saharifikacija i fermentacija.
Figure 2. Schematic overview of basic phases of lactic acid production on various materials. SSF – simultaneous saccharification and fermentation; SLSF – simultaneous liquefaction, saccharification and fermentation.

Tabela 1. Vrednosti najvažnijih parametara mlečno-kiselinske ferementacije na različitim otpadnim sirovinama; c – koncentracija MK, $Y_{p/š}$ – prinos (g MK/g početnog šećera), $Y_{p/uš}$ – koeficijent prinosa po supstratu (g MK/g utrošenog šećera), P – produktivnost
Table 1. Values of the most important parameters of lactic acid fermentation on different waste materials

Mikroorganizam	Soj	Tip otpadnog supstrata	Mlečna kiselina				Referenca
			c / g L^{-1}	$Y_{p/š}$ / g g^{-1}	$Y_{p/uš}$ / g g^{-1}	P / g L^{-1} h^{-1}	
Lactobacillus sp.	RKY2	Surutka	116,92	–	0,99	0,93	[99]
Lb. delbrueckii	NRRL B-445	Surutka	12–24,5	0,67–0,82	0,87–0,94	0,27–0,57	[100]
Lb. casei	NRRL B-441	Surutka	–	–	0,92–0,94	1,36–1,87	[101]
Lb. casei	LC1	Otpad iz proizvodnje rikota sira	14,4–30,6	–	0,86–0,92	0,72–1,53	[102]
Lb. delbrueckii	NCIMB 8130	Melasa šećerne repe	90,0	–	0,97	3,8	[42]
E. faecalis	RKY1	Melasa šećerne repe	65,1	–	0,98	4,3	[103]
Lb. delbrueckii	IFO 3202	Melasa šećerne repe	60,3	–	0,95	3,4	[104]
Lb. delbrueckii	C.E.C.T 286	Melasa šećerne repe	45,1	–	0,88	2,7	[105]
R. oryzae	NRRL 395	Melasa šećerne repe	37,0–49,0	–	–	–	[106]
Lb. delbrueckii	NCIM 2025	Melasa šećerne trske	64,86	–	–	2,7	[107]
Lb. delbrueckii	JCM 1148	Melasa šećerne trske	107	0,90	0,91	1,48	[108]
B. coagulans	H-1	Melasa šećerne trske	34,5	–	0,97	1,4	[109]
Lb. pentosus	NRRL B227	Sojina melasa	29,38	–	–	1,22	[49]
Lb. agilis	LPB 56	Sojina džibra	22,29	–	–	0,46	[49]
Lb. rhamnosus	ATCC 7469	Hlebna džibra	18,58	0,73	0,90	–	[46]
E. hawaiiensis	CICIM-CU B0114	Kukuruzna džibra	56,0	0,70	–	1,17	[110]
Lb. rhamnosus	LA-04-1	Hidrolizat pšeničnih mekinja	74,0–80,0	–	0,98–0,99	2,35–3,75	[111]
R. arrhizus	DAR 36017	Otpadni skrobni materijali	8,2–44,3	–	0,6–0,96	–	[112]
R. arrhizus	36017	Otpadna voda iz proizvodnje skroba	19,74	0,91	–	0,41	[24]
Lb. delbrueckii	JCM1106	Otpadni pirinač	63,3–79,0	0,65–0,81	–	1,40–3,59	[53]
Lb. rhamnosus	ATCC 7469	Otpad iz reciklaže papira	29,8–72,9	–	0,70–0,91	0,29–2,19	[16]
Lb. delbrueckii	UFV H2B20	Pivski trop	5,4	–	0,73	0,11	[113]
Bacillus sp.	XZL9	Otpad iz proizvodnje ksilitola	26,4	0,42	–	0,55	[114]

pokazali da tretiranje surutke pomoću *B. megaterium* može biti podjednako efikasno kao i tretiranje komercijalnim proteazama. Surutka koja je tretirana membranskim procesima kao što su ultrafiltracija i diafiltracija u cilju dobijanja koncentrata proteina je takođe ispitivana za proizvodnju MK [36].

Melasa

Melasa se zbog visokog sadržaja ugljenih hidrata, azotnih jedinjenja i slatkog ukusa, tradicionalno koristi za dobijanje vrednih proizvoda prehrambene i fermentacione industrije. U našoj zemlji veći deo melase se koristi za proizvodnju kvasca i etanola [37]. Danas se melasa više ne smatra otpadnim proizvodom već sekundarnom sirovinom, a na raspolaganju su ograničene količine koje su uslovljene proizvodnjom šećera zbog čega njena cena drastično raste. U industriji šećera pod melasom se smatra sirup dobijen na poslednjem stepenu kristalizacije u postupku proizvodnje rafinisanog šećera iz šećernih sirovina (šećerna repa i šećerna trska) [37]. Prinos melase zavisi od više faktora i razlikuje se od šarže do šarže, dok se hemijski sastav melase menja iz godine u godinu kako zbog promene kvaliteta osnovne sirovine, tako i zbog promena koje nastaju u toku njenog skladištenja i čuvanja. Smatra se da prinos melase šećerne repe iznosi oko 4% na repu, odnosno 25% na proizvedeni šećer [38].

Glavni deo melase šećerne repe čine ugljeni hidrati, pre svega saharoza, čiji je sadržaj u melasi oko 50%. Osim saharoze, melasa šećerne repe sadrži glukozu, fruktozu i rafinozu [37,38]. Najveći deo azotnih materija u melasi čini betain, a ostalo su aminokiseline, amidi i soli amonijaka [37,38]. Smatra se da je melasa koja ne sadrži dovoljnu količinu azotnih materija nekompletna sirovina za fermentacionu industriju. Jedan od kriterijuma za ocenu pogodnosti melase je sadržaj azota koji mikroorganizmi lako asimiluju, a od suštinske važnosti su aminokiseline, peptidi, amonijak, nitrati i nitriti [39]. Karakteristična tamnobraon boja melase najvećim delom potiče od melanoidina (proizvoda Majlardove reakcije), ali i od proizvoda karamelizacije i alkalne degradacije heksoza [37].

U pojedinim studijama je razmatrana prethodna obrada melase u cilju poboljšanja efikasnosti procesa (katjonske izmenjivačke smole, tretman sumpornom kiselinom, trikalcijum fosfatom, kalijum ferocijanidom,

aktivnim ugljem ili tretman etilen diamin tertasirćetnom kiselinom) jer bojene materije, 5-hidroksimetilfurfural i metali (Fe, Zn, Cu, Mn, Mg i Ca) koji se nalaze u melasi mogu da inhibiraju rast mikroorganizama [40––42] i inaktiviraju enzime biosintetičkog puta željenog proizvoda. Poređenjem pomenutuh postupaka predtretmana melase pokazano je da fermentacija na netretiranoj melasi daje najviše koncentracije MK [42], pa se može zaključiti da se ispitivanim predtretmanima neselektivno uklanjaju komponente melase koje su važne za efikasnu proizvodnju MK [42].

Destilerijska džibra

U postupku dobijanja bioetanola iz šećernih, skrobnih ili lignoceluloznih sirovina kao sporedni proizvod nastaje velika količina džibre. U proseku 8–15 L džibre nastaje proizvodnjom 1 L etanola [43]. Džibru karakterišu visoke vrednosti hemijske i biološke potrošnje kiseonika, niska pH vrednost, visok sadržaj organskih materija i zbog toga se ne sme ispuštati u okolinu bez prethodnog tretmana [43]. Visoki troškovi obrade džibre pre ispuštanja u vodotokove ozbiljno utiču na održivost i profitabilnost proizvodnje bioetanola, a njeno odlaganje predstavlja ozbiljan ekološki problem. Procesi koji koriste ovu otpadnu tečnost kao sirovinu za dalju proizvodnju imaju značajnu ulogu u kontroli i smanjenju zagađenja životne sredine, a takođe i povećavaju konkurentnost bioetanola kao alternativnog goriva. Neki od pravaca primene i iskorišćavanja džibre su recirkulacija u cilju ukomljavanja sirovine za proizvodnju etanola, njena upotreba kao visoko kvalitetne hrane za životinje, za fertigaciju biljaka i upotreba džibre kao supstrata u različitim fermentacionim tehnologijama [43,44]. Karakteristike džibre se razlikuju i zavise od načina izvođenja procesa proizvodnje etanola, kao i od karakteristika i obrade polazne sirovine. Nakon uklanjanja etanola destilacijom u džibri ostaju inaktivirane ćelija kvasca bogate vitaminima (naročito B kompleksa) zbog čega džibra može biti potencijalno dobar supstrat za dobijanje vrednih proizvoda. Takođe, u džibri se mogu naći zaostali fermentabilni šećeri koji su lako dostupni mikroorganizmima. Džibra je korišćena kao supstrat za proizvodnju kalijum acetata [45], MK [46], ali i drugih proizvoda kao što su hitozan, astaksantin, alternan, pululan [44].

Kao supstrat za mlečno-kiselinsku fermentaciju je ispitivana džibra iz proizvodnje bioetanola na otpadnom hlebu [46], kukuruzu [47], tritikaleu [48] i sojinoj melasi [49]. Ispitivanjem mogućnosti proizvodnje MK na džibri zaostaloj nakon proizvodnje bioetanola iz smeše otpadnog hleba i vode iz proizvodnje glutena postignuta je koncentracija MK od 50,18 g L^{-1} i produktivnost od 1,48 g L^{-1} h^{-1} [50]. Osim proizvodnje MK gde je ostvarena visoka produktivnost, ostaci nakon fermentacije i odvajanja tečne frakcije sa MK su analizirani sa aspekta primene u ishrani životinja čime je dokazana mogućnost paralelne proizvodnje kvalitetne stočne hrane zajedno sa MK [50]. Sojina melasa je sporedni proizvod koji zaostaje u proizvodnji proteinskog koncentrata sojine sačme, čijom daljom primenom u proizvodnji bioetanola zaostaje sojina džibra [49]. U studiji u kojoj je razmatrana mogućnost upotrebe sojine džibre i melase kao supstrata postignuta je koncentracija MK od 90,35 g L^{-1} sa produktivnošću od 1,88 g L^{-1} h^{-1} tokom 48 h fermentacije pomoću *Lb. agilis* LPB 56 koji je pokazao zadovoljavajuću sposobnost konverzije kompleksnih oligosaharida (stahioze i rafinoze) koji se nalaze u sojinoj melasi i džibri [49].

Skrobne otpadne sirovine

Među otpadnim skrobnim sirovinama za proizvodnju MK su ispitivani otpad iz prerade krompira [51] i kasave [52], otpadni pirinač [53], pšenične mekinje [54,55]. Ukoliko se ne koriste amilolitički proizvodni mikroorganizmi, ove sirovine zahtevaju izvesnu pripremu kojom se skrob i komponente skroba, amiloza i amilopektin, hidrolizuju do fermentabilnih šećera. Hidroliza skroba se izvodi kiselinama ili češće komercijalnim amilolitičkim enzimima (amilaze i glukoamilaze) [56]. Za hidrolizu skroba najviše se primenjuje α-amilaza dobijena iz *B. licheniformis* poznata pod komercijalnim nazivom Termamyl 120 L, kao i Termamyl SC, dok su najčešće korišćene glukoamilaze SAN extra L iz *Aspergillus niger* i AMG 300 L proizvedena iz genetski modifikovane *Aspergillus* vrste [56]. Konvencionalna fermentaciona proizvodnja MK iz skrobnih sirovina je višefazni proces koji uključuje likvefakciju (na temperaturi od 90–130 °C tokom 15 min), a zatim sledi saharifikacija kojim se skrob potpuno hidrolizuje do glukoze [57]. Najzad, mlečno-kiselinskom fermentacijom glukoza se konvertuje do MK (slika 2). Zbog uštede u vremenu i troškovima proizvodnje, kao i sprečavanja efekta inhibicije supstratom intenzivno se ispituje postupak simultane saharifikacije i fermentacije (SSF) kao i postupak simultane likvefakcije, saharifikacije i fermentacije (SLSF). Wang i sar. [58] su izvršili poređenje tri različita postupka fermentacije na brašnu kasave koristeći komercijalne amilolitičke enzime. U postupku SLSF pomoću *Lb. rhamnosus* je postignuta najveća koncentracija MK (187,2 g L^{-1}) sa produktivnošću od 1,6 g L^{-1} h^{-1}, dok je najmanja koncentracija MK zabeležena u postupku odvojene likvefakcije, saharifikacije i fermentacije (145,1 g L^{-1}) i produktivnost od svega 1 g L^{-1} h^{-1} [58]. Međutim, zbog visokih cena amilolitičkih enzima i složenosti postupka, sve veća pažnja se usmerava na proučavanje direktne fermentacije skrobnih sirovina pomoću mikroorganizama koji proizvode ekstracelularne amilolitičke enzime. Među BMK koje imaju amilolitičko dejstvo ispitivane su sledeće vrste: *Lb. manihotivorans, Lb. amylovorus, Lb. amilophilus, Lb. acidophilus, Lb. fermentum, Lb. plantarum, Lb. cellobiosus, Lb. amylolyticus* [10]. U direktnom postupku fermentacije po-

moću *Lb. amylophilus* GV6 na brašnu kasave i brašnu pirinča postignuta je koncentracija MK od 33,6 i 30,9 g L^{-1} sa produktivnošću od 0,36 i 0,32 g L^{-1} h^{-1}, redom [59], što je i dalje značajno manje od vrednosti postignutih u postupku SSF sa komercijalnim enzimima na istim supstratima [53,58].

Lignocelulozne otpadne sirovine

Lignocelulozni materijali su sastavljeni iz celuloze, hemiceluloze i lignina koji čine 90% suve materije, a ostatak su mineralne materije, ulja i druge komponente [60]. Procesom hidrolize, hemiceluloza i celuloza se moraju razložiti do monosaharida, odnosno fermentabilnih šećera. Hemiceluloza se razlaže do smeše šećera koju čine pentoze (ksiloza i arabinoza) i heksoze (galaktoza i manoza), dok se celuloza razlaže do glukoze. Različiti postupci mlečno-kiselinske fermentacije na lignicelulozним sirovinama su prikazani na slici 2. Upotreba lignocelulozne biomase u proizvodnji MK je ograničena zbog malog broja vrsta BMK sposobnih da fermentišu ksilozu i arabinozu i izraženog efekta kataboličke represije glukozom [60]. Pored toga, formiranje različitih sporednih proizvoda fermentacije (uglavnom sirćetne kiseline usled aktivacije enzima fosfoketolaze u prisustvu pentoza) smanjuje prinos MK i povećava troškove njenog prečišćavanja. Takođe, prisustvo lignina smanjuje dostupnost polisaharida hidrolitičkim enzimima, a time i efikasnost iskorišćenja lignocelulozne biomase [61], pa ga je neophodno ukloniti iz lignocelulozног materijala. Predtretman lignocelulozног materijala, osim uklanjanja lignina, ima za cilj i smanjenje stepena kristalne strukture celuloze [60,61]. Time se povećava unutrašnja poroznost materijala što dovodi do povećanja prinosa fermentabilnih šećera iz celuloze i hemiceluloze u fazi hidrolize, u prisustvu kiselina ili enzima. Kao postupci predtretmana primenjuju se određene fizičke, hemijske, fizičko-hemijske i biološke metode [60,61].

Među lignocelulozним otpadnim materijalima, za proizvodnju MK je ispitivan pivski trop, sporedni proizvod koji nastaje u procesu proizvodnje piva. Proizvodnjom 100 L piva nastaje oko 20 kg tropa, zbog čega je ova sirovina lako dostupna i jeftina [62]. Mussatto i sar. [63] su ispitivali proizvodnju MK iz hidrolizata pivskog tropa pomoću *Lb. delbrueckii*. Pivski trop je prvobitno podvrgnut hemijskom predtretmanu, a dobijena celulozna pulpa je potom tretirana komercijalnim celulaznim kompleksom u cilju saharifikacije [63]. U studiji u kojoj je tako dobijen hidrolizat korišćen u mlečno-kiselinskoj fermentaciji, uz kontrolu pH vrednosti i dodatak komponenata MRS bujona, postignuta je koncentracija MK od 35,54 g L^{-1} i produktivnost od 0,59 g L^{-1} h^{-1}. Pomoću *Lb. rhamnosus* na hidrolizatu pivskog tropa uz kontrolu pH vrednosti i dodatak kvašćevog ekstrakta postignuta je koncentracija MK od 12,48 g L^{-1} sa produktivnošću od 0,52 g L^{-1} h^{-1} [64].

IZAZOVI U FERMENTACIONOJ PROIZVODNJI MLEČNE KISELINE

Upotreba mešanih kultura

Osnovni cilj u proizvodnji MK na složenim, prirodnim supstratima je povećati efikasnost konverzije supstrata, zbog čega je u nekoliko studija proučavano korišćenje mešanih kultura. Upotrebom mešanih kultura se na osnovu sinergističkog delovanja različitih mikroorganizama može ostvariti bolja proizvodnja MK. Pomoću mešane kulture *Lb. casei* i *Lactococcus lactis* na ekstraktu urme je postignuta koncentracija MK od 60,3 g L^{-1}, dok su postignute koncentracije MK sa monokulturom *Lb. casei*, odnosno *Lc. lactis* bile 53 i 46 g L^{-1} [65]. Osim veće koncentracije MK, upotrebom mešane kulture je postignuta i efikasnija konverzija šećera (glukoze i fruktoze) u MK. Lee [66] je izvršio poređenje mono- i mešane kulture BMK na sintetskoj podlozi sa dodatkom koncentrovanog kukuruznog ekstrakta kao jedinog izvora azota. U fermentaciji sa mešanom kulturom pet sojeva roda *Lactobacillus* osim većeg prinosa MK, uočen je bolji rast ćelija i manja potrošnja proteina [66]. To ukazuje da mešane kulture zahvaljujući sinergističkom delovanju mogu lakše da prevaziđu nutritivna ograničenja i ostvare bolju produktivnost MK na siromašnijim supstratima. Mešana kultura *Lb. rhamnosus* i *Lb. brevis* je korišćena za SSF na kukuruznoj stočnoj hrani tretiranoj NaOH, pri čemu je postignuta koncentracija MK od 20,95 g L^{-1}, dok je postignuta koncentracija MK sa monokulturom *Lb. rhamnosus*, odnosno *Lb. brevis* bila manja za 15,5%, odnosno 20,2% [67]. Mešane kulture plesni i BMK su ispitivane za proizvodnju MK na sirovinama koje sadrže inulin, kao što je Jerusalimska artičoka [68]. Hidroliza inulina se odvija u prisustvu enzima inulinaze i invertaze. Sposobnost da proizvode ove enzime imaju pojedine bakterije i plesni, među kojima se često koriste vrste iz roda *Aspergillus* [68]. U SSF na Jerusalimskoj artičoki pomoću kulture *Aspergillus niger* SL-09 i *Lactobacillus* sp. G-02 je postignuta koncentracija MK od 120,5 g L^{-1} i prinos od 0, 95 g g^{-1} [68]. Nedostatak kompleksnih mešanih kultura se ogleda u njihovoj heterogenosti, pri čemu različiti sojevi mogu imati različit temperaturni i pH optimum, kao i različite potrebe za kiseonikom i nutrijentima, što otežava definisanje optimalnih i stabilnih uslova za takve kulture tokom fermentacije.

Otvorena (nesterilna) fermentacija

Za efikasnu proizvodnju MK neophodno je obezbediti sterilnost medijuma pre inokulisanja BMK, odnosno obezbediti uslove u kojima je proizvodnja MK dominantan proces u medijumu. Sa aspekta energetske efikasnosti kao i ekonomske pogodnosti i konkurentnosti fermentacione proizvodnje MK, otvorena (nesterilna) fermentacija ima sve veći značaj i u fokusu je

istraživanja poslednjih godina [19,69–71]. Otvorena fermentacija, pored toga što smanjuje potrošnju energije i pojednostavljuje postupak proizvodnje, sprečava Majlardovu reakciju, kao i formiranje furfurala tokom sterilizacije. U otvorenoj fermentaciji su uglavnom korišćene termofilne vrste roda *Bacillus*. U otvorenoj šaržnoj fermentaciji na lignoceluloznom hidrolizatu pomoću *Bacillus* sp. NL01 postignuta je koncentracija MK od 75 g L^{-1} i produktivnost 1,04 g L^{-1} h^{-1} [69]. Takođe, pomoću *B. coagulans* NBRC 12583 na skrobnom hidrolizatu kasave sa dodatkom otpadnog mulja kao nutrijenta je postignuta koncentracija MK od 98,1 g L^{-1} i produktivnost od 3,63 g L^{-1} h^{-1} [70]. Otvorena fermentacija je ispitivana i pomoću *E. mundtii* QU 25 na sintetskom supstratu [71]. Ponovljenim šaržnim postupkom sa recirkulacijom ćelija u toku petog ciklusa je postignuta koncentracija MK od 81,4 g L^{-1} i produktivnost od 12,3 g L^{-1} h^{-1} [71]. Očekivano je da se dalje razvijaju sistemi pogodni za otvorene fermentacije, što podrazumeva pronalaženje novih termofilnih mikroorganizama sposobnih za efikasnu proizvodnju MK na otpadnim sirovinama.

Uticaj izvora azota i značaj kontrole pH vrednosti

Zbog ograničene sposobnosti da sintetišu faktore rasta, BMK zahtevaju podlogu bogatu aminokiselinama, vitaminima, masnim kiselinama, purinima i pirimidinima [72]. U brojnim studijama u kojima je ispitivan sastav podloge za mlečno-kiselinsku fermentaciju zaključeno je da dodatak nutrijenata obezbeđuje bolju produktivnost procesa, kao i da među različitim izvorima azota kvaščev ekstrakt ima najveći uticaj na proizvodnju MK [7]. Tako je obogaćivanjem melase šećerne repe kvaščevim ekstraktom u fermentaciji sa *Lb. delbrueckii* postignuta značajno veća koncentracija MK u poređenju sa drugim izvorima azota (suvi pivski kvasac, proteini ekstrahovani iz pivskog kvasca, proteini surutke) [42]. Kako dodatak različitih izvora azota poput kvaščevog ekstrakta čini oko 38% ukupnih troškova proizvodnje [70], mnoga istraživanja se bave pronalaženjem jeftinih hranljivih materija koje bi mogle delimično ili potpuno da zamene kvaščev ekstrakt i ostale skupe nutrijente. Yu i sar. [73] su ispitivali pogodnost primene koncentrovanog kukuruznog ekstrakta kao alternative kvaščevom ekstraktu. Pomoću *Lb. rhamnosus* CGMCC 1466 na podlozi kojoj je dodat koncentrovani kukuruzni ekstrakt, glukoza, melasa, Tween 80 i Mn proizvedeno je 115,12 g L^{-1} MK [73]. U poređenju sa vrednostima dobijenim na supstratu sa kvaščevim ekstraktom, proizvodnja MK je bila veća za 30,4% [73]. Kao jeftini, alternativni izvori azota ispitivani su hidrolizat perja [74], otpadni mulj [70], sok japanske jabuke, hidrolizat pšeničnih mekinja [75] i hidrolizat soje [76].

Pored izvora azota, pH vrednost je još jedan faktor koji utiče na efikasnost procesa. S obzirom da optimalna pH za rast većine vrsta BMK i proizvodnju MK varira između 5–7, kiselost podloge povezana sa proizvodnjom MK inhibira dalju fermentaciju [16]. Upotrebom $CaCO_3$ i $Ca(OH)_2$ kao sredstva za neutralizaciju nakon izdvajanja i prečišćavanja MK zaostaje značajna količina gipsa ($CaSO_4$) koji je veoma štetan po životnu sredinu. U studiji u kojoj je testirano pet različitih jedinjenja za regulaciju pH vrednosti (NH_4OH, NaOH, dimetilamin, trimetilamin i $CaCO_3$), trimetilamin se pokazao najboljim neutrališućim agensom [77]. Zamena $CaCO_3$ drugim sredstvom za regulaciju pH vrednosti pored toga što sprečava nastanak velike količine gipsa, olakšava i izdvajanje MK. Upotreba genetski modifikovanih sojeva sposobnih da rastu pri niskoj pH vrednosti može biti alternativna strategija u prevazilaženju efekta inhibicije proizvodom. Stopa preživljavanja *Lb. delbrueckii* koji je podvrgnut mutagenezi indukovanom azotnom kiselinom je pri pH vrednosti 3.5 bila veća 1,3 puta u odnosu na roditeljski soj u istim uslovima [78]. Ye i sar. [79] su postupkom slučajne amplifikacije gena modifikovali *Lb. pentosus* koji je pri pH vrednosti 3.8 postigao prinos MK od 0,95 g g^{-1}, dok rast roditeljskog soja i proizvodnja MK pri istim uslovima nije uočena.

POSTUPCI IZVOĐENJA MLEČNO-KISELINSKE FERMENTACIJE

Šaržni i dolivni postupak u proizvodnji mlečne kiseline

Način na koji će se voditi fermentacioni proces zavisi od vrste i prirode polazne sirovine, vrste proizvodnog mikroorganizma, kao i karakteristika fermentacionog medijuma. Šaržni postupak je najjednostavniji i najčešće primenjivan tip fermentacionog procesa. Prednosti ovog postupka su manji rizik od kontaminacije i jednostavno upravljanje procesom, dok su nedostaci niska produktivnost usled izraženog efekta inhibicije supstratom i/ili proizvodom. U cilju prevazilaženja efekta inhibicije supstratom ili proizvodom kao moguća strategija je ispitivan dolivni postupak. U tabeli 2 je dato poređenje vrednosti osnovnih parametara fermentacije postignutih u šaržnom i dolivnom postupku na različitim supstratima. U dolivnom postupku svež supstrat se dodaje kontinualno ili povremeno, čime se koncentracija supstrata održava u optimalnim granicama i time povećava produktivnost procesa. Ispitivane su različite metode dolivanja supstrata, najčešće kontinualni, povremeni i eksponencijalni metod [80,81]. Kontinualnim dodavanjem glukoze hemijski definisanom medijumu pomoću *Lb. lactis* postignuta je koncentracija MK od 210 g L^{-1} i produktivnost od 2,2 g L^{-1} h^{-1}, a zaostala koncentracija glukoze u medijumu je bila manja od 0,5 g L^{-1} [82]. Ding i Tan [80] su ispitivali više metoda dolivanja supstrata, pri čemu se najefikasnijim pokazao eksponencijalni metod. U fermentaciji sa *Lb. casei* na hemijski definisanom medijumu obogaćenom glukozom i kvaščevim ekstraktom, postignuta je kon-

Tabela 2. Vrednosti najvažnijih parametara mlečno-kiselinske fermentacije u šaržnom i dolivnom postupku; c- – koncentracija MK, $Y_{p/uš}$ – koeficijent prinosa po supstratu (g MK/g utrošenog šećera), P – produktivnost
Table 2. Values of the most important parameters of lactic acid fermentation in batch and fed-batch mode of lactic acid production

Mikroorganizam	Supstrat	Fermentacioni postupak	Mlečna kiselina			Referenca
			c / g L^{-1}	$Y_{p/uš}$ / g g^{-1}	P / g L^{-1} h^{-1}	
Lb. lactis	Glukoza	Šaržni	150,2	–	1,34	[115]
BME5-18M		Kontinualni dolivni	161,2	–	2,02	
B. coagulans	Glukoza	Šaržni	103,6	0,93	0,72	[116]
36D1		Dolivni, dodatak šećera u 48 i 96 h	182,2	0,92	0,84	
B. coagulans	Ksiloza	Šaržni	102,3	0,86	0,71	[116]
36D1		Dolivni, dodatak šećera u 48 i 96 h	163,0	0,87	0,75	
Lb. lactis-11	Glukoza	Šaržni	82,7	0,92	1,7	[81]
		Dolivni, održavanje koncentracije šećera na 4–5 g L^{-1} u periodu od 18,5 do 49 h	96,3	0,99	1,9	
Lb. casei	Surutka	Šaržni	22,5	0,48	0,93	[117]
SU No 22		Kontinualni dolivni	46,0	0,77	1,91	
Lc. lactis						
WS 1042						
B. coagulans	Glukoza	Šaržni	91,5	0,97	9,7[a]	[21]
SIM-7		Dolivni, dodatak šećera 5 h nakon početka fermentacije	91,6	0,97	11,12[a]	

[a]Maksimalna produktivnost

centracija MK od 180 g L^{-1} i produktivnost od 2,14 g L^{-1} h^{-1} nakon 84 h fermentacije [80]. U dolivnom postupku koncentracija MK je bila za 56,5% veća od vrednosti dobijenih u šaržnoj fermentaciji, dok je produktivnost bila veća za 59,7% [80]. Istraživanja dolivnog postupka su uglavnom zasnovana na primeni hemijski definisanih supstrata, kojima su dodati faktori rasta poput kvaščevog ekstrakta, kao i mineralne materije, što dodatno utiče na efikasnost procesa. Može se primetiti da je znatno manje istraživanja u kojima je dolivni postupak ispitivan na otpadnim supstratima, pa ih je zbog toga teško porediti. U dolivnom postupku na hlebnoj džibri pomoću *Lb. rhamnosus* ATCC 7469 postignuta je maksimalna koncentracija MK od 97,1 g L^{-1} i produktivnost 1,80 g L^{-1} h^{-1} nakon 54 h fermentacije [82]. U poređenju sa šaržnim postupkom, primenom dolivnog postupka u ovom istraživanju koncentracija MK je povećana za 47,6%, a produktivnost za 17,2% [83].

Proizvodnja mlečne kiseline sa sistemima imobilisanih ćelija

Metode imobilizacije ćelija se, u novije vreme, sve više koriste u cilju povećanja koncentracije biomase u fermentorima što dovodi do povećanja produktivnosti procesa. Pored veće produktivnosti, imobilizacija omogućava ćelijsku i operativnu stabilnost, olakšava separaciju imobilisanih ćelija od fermentacionog medijuma i omogućava njihovo ponovno korišćenje. U tabeli 3 je dato poređenje vrednosti osnovnih parametara fermentacije postignutih u sistemima sa slobodnim i imobilisanim ćelijama. Imobilizacija u polimerne matrice gela je često korišćena tehnika imobilizacije BMK. Kao materijali za imobilizaciju korišćeni su prirodni polimeri, kao što su Ca-alginat [84,85], agar [86], κ-karagenan [87], a od sintetskih poliakrilamid [87,88] i polivinil alkohol [89]. Za imobilizaciju u polimerne matrice gela je karakteristična ograničena difuzija supstrata i proizvoda kroz polimernu matricu što smanjuje prinos MK. Osnovni nedostatak Ca-alginata za proizvodnju MK je gubitak mehaničke stabilnosti gela, tj. razmekšavanje čestica usled reakcije Ca sa MK. Pokazano je da oblaganje alginatnih čestica hitozanom u cilju povećanja stabilnosti može povećati produktivnost fermentacije [90].

Osim imobilizacije unutar čestica gela, ispitivana je i imobilizacija BMK adsorpcijom na površinu nosača, pri čemu se bakterije u vidu filma vezuju za različite prirodne ili sintetske nosače. Prednosti ove metode se ogledaju u njenom jednostavnom izvođenju, pri čemu je vijabilnost i aktivnost BMK očuvana. Takođe, zbog adsorpcije bakterija na površinu čvrstog nosača difuziona ograničenja su manje izražena i ostvaruje se bolji prenos mase. Nedostatak ove metode su relativno slabe veze ćelija i nosača, što može da dovede do njihovog spiranja sa površine nosača. Kao nosači za adsorpciju ispitivani su plastični kompozitni materijali [91], poliuretanska pena [92], zeolitni prah [93], lignocelulozni materijali [94,96] i čestice pšeničnog glutena [95].

U cilju povećanja produktivnosti procesa vršena su istraživanja proizvodnje MK pomoću imobilisane biomase u kontinualnim i bioreaktorima sa fibroznim pakovanim slojem. U kontinualnoj proizvodnji MK na hidrolizatu pirinčanih mekinja pomoću *Lb. rhamnosus*

Tabela 3. Vrednosti najvažnijih parametara mlečno-kiselinske fermentacije sa slobodnim i imobilisanim ćelijama; c- – koncentracija MK, $Y_{p/uš}$ – koeficijent prinosa po supstratu (g MK/g utrošenog šećera), P – produktivnost
Table 3. Values of the most important parameters of lactic acid fermentation with free and immobilized cells

Mikroorganizam	Tehnika imobilizacije i vrsta nosača/supstrat	Fermentacioni postupak	Mlečna kiselina			Referenca
			c / g L^{-1}	$Y_{p/uš}$ / g g^{-1}	P / g L^{-1} h^{-1}	
Lb. rhamnosus ATCC 7469	Adsorpcija na zeolit/hlebna džibra	Šaržni sa slobodnim ćelijama	34,7	0,81	0,66	[93]
		Ponovljeni šaržni sa imobilisanim ćelijama, 3. ciklus	42,2	0,99	1,22	
Lb. casei	Adsorpcija na čestice pšeničnog glutena/glukoza	Šaržni sa slobodnim ćelijama, fermentaciono vreme 18 h	41,4	–	2,3	[95]
		Šaržni sa imobilisanim ćelijama, fermentaciono vreme 12 h	42,2	–	3,51	
Lb. casei SU No 22	Koimobilizacija u čestice Ca alginata/deproteinizovana surutka	Kontinualni dolivni sa slobodnim ćelijama	46	0,77	1,91	[117]
Lc. lactis WS 1042		Kontinualni dolivni sa imobilisanim ćelijama	47	0,72	1,96	
Lb. delbrueckii IFO 3202	Zarobljavanje u čestice Ca-alginata/melasa šećerne repe	Šaržni sa slobodnim ćelijama	42,4	0,81	–	[118]
		Šaržni sa imobilisanim ćelijama	42,7	0,82	–	

koji je bio imobilisan na čestice kukuruzne stabljike ostvarena je produktivnost od 5,73–6,20 g L^{-1} h^{-1} [96]. Takođe, u šaržnoj fermentaciji surutke pomoću *Lb. bulgaricus* imobilisanog na porozne celulozne nosače postignuta je produktivnost od 6,78 g L^{-1} h^{-1} [94]. U dolivnom postupku sa *Lc. lactis* na hidrolizatu Jerusalimske artičoke u bioreaktoru sa fibroznim pakovanim slojem postignuta je koncentracija MK od 142 g L^{-1}, što je za 27,92% više u odnosu na fermentaciju sa slobodnim ćelijama [97]. Takođe, u dolivnom postupku pomoću *Sporolactobacillus inulinus* na hidrolizatu kukuruznog brašna u bioreaktoru sa fibroznim pakovanim slojem je postignuta koncentracija MK od 218,8 g L^{-1}, što je za 37,67% više u odnosu na fermentaciju sa slobodnim ćelijama [98]. Iako se u pomenutim bioreaktorima i imobilisanim sistemima na hemijski definisanim supstratima postiže daleko veća produktivnost, upotreba jeftinih i otpadnih materijala obezbeđuje ekonomsku i ekološku povoljnost procesa, dok dobijeni rezultati predstavljaju osnov za dalja istraživanja.

ZAKLJUČAK

Biorafinerijski procesi su u poslednjoj deceniji sve popularniji u proizvodnji energije, goriva, organskih hemikalija i polimera. S obzirom na trend stalnog porasta potrošnje MK biorafinerijski koncept bi mogao da doprinese smanjenju ukupnih troškova proizvodnje MK. Korišćenje sporednih i otpadnih sirovina u proizvodnji MK pored ekonomske održivosti procesa, nudi rešenje problema njihovog odlaganja. Otpadni industrijski proizvodi kao što su surutka, melasa, destilerijska džibra, različiti skrobni i lignocelulozni materijali mogu biti dobar izvor fermentabilnih šećera, ali i mnogih drugih jedinjenja od značaja za rast mikroorganizama, kao što su proteini, mineralne materije i vitamini. Zbog kompleksnog sastava, kao i varijacija u hemijskim i fizičkim karakteristikama otpadnih proizvoda potrebna su detaljna ispitivanja koja uključuju optimizaciju procesnih parametara kako bi se omogućila njihova upotreba u biotehnološkim procesima. Ekonomski održiva proizvodnja MK pored upotrebe otpadnih sirovina, uključuje i smanjenu potrošnju energije, zbog čega su ispitivanja otvorenih fermentacionih postupaka pomoću termofilnih mikroorganizama jedna od vodećih na polju proizvodnje MK. Razvojem novih tehnika genetičkog inženjerstva sve češće su modifikacije mikroorganizama u cilju poboljšanja produktivnosti procesa, čistoće proizvoda, sposobnosti iskorišćavanja različitih vrsta šećera ili otpornosti na niske pH vrednosti sredine. Dosadašnja ispitivanja mogućnosti proizvodnje MK na džibri zaostaloj iz proizvodnje etanola su dala zapažene rezultate, a očekivani porast potrošnje MK u narednim godinama navodi na pronalaženje novih sirovina i tehnoloških rešenja koja omogućavaju efikasnu i održivu proizvodnju.

Zahvalnica

Ovaj rad je deo projekta Tehnološkog razvoja (TR 31017) finansiranog od strane Ministarstva prosvete, nauke i tehnološkog razvoja Republike Srbije.

LITERATURA

[1] S.K. Maity, Opportunities, recent trends and challenges of integrated biorefinery: Part I, Renew. Sust. Energ. Rev. **43** (2015) 1427–1445.

[2] MEMO/12/97, Strategy for a sustainable bioeconomy to ensure smart green growth in Europe, 2012 (http://

//europa.eu/rapid/press-release_MEMO-12-97_en.htm?locale=en).

[3] K.M. Nampoothiri, N.R. Nair, R.P. John, An overview of the recent developments in polylactide (PLA) research, Bioresour. Technol. **101** (2010) 8493–8501.

[4] Global Industry Analysts, Inc., Lactic Acid: A Global Strategic Business Report, 2012 (http://www.prweb.com/releases/lactic_acid/polylactic_acid/prweb9369473.htm).

[5] Global Industry Analysts, Inc., Lactic Acid: A Global Strategic Business Report, 2014, (http://www.prweb.com/releases/lactic_acid/polylactic_acid/prweb12173291.htm).

[6] L.T. Sin, A.R. Rahmat, W.A.W.A. Rahman, Polylactic acid: PLA biopolymer technology and applications, Elsevier, Amsterdam, 2012, pp. 301–327.

[7] K. Hofvendahl, B. Hahn-Hägerdal, Factors affecting the fermentative lactic acid production from renewable resources, Enzyme Microb. Technol. **26** (2000) 87-107.

[8] M. Stiles, W. Holzapfel, Lactic acid bacteria of foods and their current taxonomy, Int. J. Food Microbiol. **36** (1997) 1–29.

[9] G. Felis, F. Dellaglio, Taxonomy of Lactobacilli and Bifidobacteria, Curr. Issues Intest. Microbiol. **8** (2007) 44–61.

[10] G. Reddy, M. Altaf, B.J. Naveena, M. Venkateshwar, E.V. Kumar, Amylolytic bacterial lactic acid fermentation – A review, Biotechnol. Adv. **26** (2008) 22–34.

[11] H-Y. Choi, H-K. Ryu, K-M. Park, E. G. Lee, H. Lee, S-W. Kim, E-S. Choi, Direct lactic acid fermentation of Jerusalem artichoke tuber extract using *Lactobacillus paracasei* without acidic or enzymatic inulin hydrolysis, Bioresour. Technol. **114** (2012) 745–747.

[12] P. Petrova, P. Velikova, L. Popova, K. Petrov, Direct conversion of chicory flour into L(+)-lactic acid by the highly effective inulinase producer *Lactobacillus paracasei* DSM 23505, Bioresour. Technol. **186** (2015) 329–333.

[13] M.A. Abdel-Rahman, Y. Xiao, Y. Tashiro, Y. Wang, T. Zendo, K. Sakai, K. Sonomoto, Fed-batch fermentation for enhanced lactic acid production from glucose/xylose, mixture without carbon catabolite repression, J. Biosci. Bioeng. **119** (2015) 153–158.

[14] Z.M. Zhu, Z.Z. Lee, R.T. Elander, Conversion of aqueous ammonia-treated corn stover to lactic acid by simultaneous saccharification and cofermentation. Appl. Biochem. Biotechnol. **136**–**140** (2007) 721–738.

[15] H. Ohara, M. Owaki, K. Sonomoto, Xylooligosaccharide fermentation with *Leuconostoc lactis*. J. Biosci. Bioeng. **101** (2006) 415–420.

[16] S. Marques, J.A.L. Santos, F.M. Gírio, J.C. Roseiro, Lactic acid production from recycled paper sludge by simultaneous saccharification and fermentation, Biochem. Eng. J. **41** (2008) 210–216.

[17] Q. Wang, X. Zhao, J. Chamu, K.T. Shanmugam, Isolation, characterization and evolution of a new thermophilic *Bacillus licheniformis* for lactic acid production in mineral salts medium, Bioresour. Technol. **102** (2011) 8152–8158.

[18] M.A. Patel, M.S. Ou, R. Harbrucker, H.C. Aldrich, M.L. Buszko, L.O. Ingram, K.T. Shanmugam, Isolation and Characterization of Acid-Tolerant, Thermophilic Bacteria for Effective Fermentation of Biomass-Derived Sugars to Lactic Acid, Appl. Environ. Microbiol. **72** (2006) 3228–3235.

[19] K. Ma, T. Maeda, H. You, Y. Shirai, Open fermentative production of L-lactic acid with high optical purity by thermophilic *Bacillus coagulans* using excess sludge as nutrient, Bioresour. Technol. **151** (2014) 28–35.

[20] L. Ye, X. Zhou, M.S.B. Hudari, Z. Li, J.Ch. Wu, Highly efficient production of L-lactic acid from xylose by newly isolated *Bacillus coagulans* C106, Bioresour. Technol. **132** (2013) 38–44.

[21] T. Michelson, K. Kask, E. Jõgi, E. Talpsep, I. Suitso, A. Nurka, L(+)-Lactic acid producer *Bacillus coagulans* SIM-7 DSM 14043 and its comparison with *Lactobacillus delbrueckii* ssp. *lactis* DSM 20073, Enzyme Microb. Technol. **39** (2006) 861–867.

[22] L.B. Lockwood, G.E. Ward, O.E. May, The physiology of *Rhizopus oryzae*, J. Agric. Res. **53** (1936) 849–857.

[23] Z.Y. Zhang, B. Jin, J.M. Kelly, Production of lactic acid from renewable materials by *Rhizopus* fungi, Biochem. Eng. J. **35** (2007) 251–263.

[24] L.P. Huang, B. Jin, P. Lanta, J. Zhou, Simultaneous saccharification and fermentation of potato starch wastewater to lactic acid by *Rhizopus oryzae* and *Rhizopus arrhizus,* Biochem. Eng. J. **23** (2005) 265–276.

[25] R.H.W. Maas, R.R. Bakker, G. Eggink, R.A. Weusthuis, Lactic acid production from xylose by the fungus *Rhizopus oryzae*, Appl. Microbiol. Biotechnol. **72** (2006) 861–868.

[26] R.H.W. Maas, J. Springer, G. Eggink, R.A. Weusthuis, Xylose metabolism in the fungus *Rhizopus oryzae*: effect of growth and respiration on L(+)-lactic acid production, J. Ind. Microbiol. Biotechnol. **35** (2008) 569–578.

[27] L. Zhang, X. Li, Q. Yong, S.T. Yang, J. Ouyang, S. Yu, Simultaneous saccharification and fermentation of xylo-oligosaccharides manufacturing waste residue for L-lactic acid production by *Rhizopus oryzae*, Biochem. Eng. J. **94** (2015) 92–99.

[28] F.A.C. Martinez, E.M. Balciunas, J.M. Salgado, J.M.D. González, A. Converti, R.P.S. Oliveira, Lactic acid properties, applications and production: A review, Trends Food Sci. Technol. **30** (2013) 70-83.

[29] Y. Wang, Y. Tashiro, K. Sonomoto, Fermentative production of lactic acid from renewable materials: Recent achievements, prospects, and limits, J. Biosci. Bioeng. **119** (2015) 10–18.

[30] K.C. Fugelsang, C.G. Edwards, Wine Microbiology: Practical Applications and Procedures, Springer Science & Business Media, Berlin, 2007, pp. 29–39.

[31] B. Upadhyaya, L. DeVeaux, L. Christopher, Metabolic engineering as a tool for enhanced lactic acid production, Trends Biotechnol. **32** (2014) 637–644.

[32] A. Prazeres, F. Carvalho, J. Rivas, Cheese whey management: A review, J. Environ. Manage. **110** (2012) 48–68.

[33] M. Bulatović, M. Rakin, L. Mojović, S. Nikolić, M. Vukašinović Sekulić, A. Đukić Vuković, Surutka kao sirovina za

proizvodnju funkcionalnih napitaka, Hem. Ind. **66** (2012) 567–579.

[34] A. Vasala, J. Panula, P. Neubauer, Efficient lactic acid production from high salt containing dairy by-products by *Lactobacillus salivarius* ssp. *salicinius* with pre-treatment by proteolytic microorganisms, J. Biotechnol. **117** (2005) 421–431.

[35] P.S. Panesar, J.F. Kennedy, D.N. Gandhi, K. Bunko, Bio-utilisation of whey for lactic acid production, Food Chem. **105** (2007) 1–14.

[36] M.I. González, S. Álvarez, F. Riera, R. Álvarez, Economic evaluation of an integrated process for lactic acid production from ultrafiltered whey, J. Food Eng. **80** (2007) 553–561.

[37] S. Šušić, S. Petrov, G. Kukić, V. Sinobad, P. Perunović, B. Koronsovac, Đ. Bašić, Osnovi tehnologije šećera, Beograd, 1995, pp. 193–212.

[38] H. Olbrich, The Molasses, Fermentation Technologist, Institut für Zuckerindustrie, Berlin, 1963.

[39] E. Stoppok, K. Buchholz, Sugar-Based Raw materials for fermentation-Applications, in Biotechnology Set, 2nd ed., H.-J. Rehm, G. Reed (Eds.), Wiley-VCH Verlag GmbH, Weinheim, 2001, pp. 4–29.

[40] T. Roukas, Pretreatment of beet molasses to increase pullulan production, Process Biochem. **33** (1998) 805––810.

[41] F. Küçükaşik, H. Kazak, D. Güney, I. Finore, A. Poli, O. Yenigün, B. Nicolaus, E.T. Öner, Molasses as fermentation substrate for levan production by *Halomonas* sp. Appl. Microbiol. Biotechnol. **89** (2011) 1729–1740.

[42] Ch. Kotzamanidis, T. Roukas, G. Skaracis, Optimization of lactic acid production from beet molasses by *Lactobacillus delbrueckii* NCIMB 8130, World J. Microbiol. Biotechnol. **18** (2002) 441–448.

[43] L.T. Fuess, M.L. Garcia, Implications of stillage land disposal: A critical review on the impacts of fertigation, J. Environ. Manage. **145** (2014) 210–229.

[44] A. Wilkie, K. Riedesel, J. Owens, Stillage characterization and anaerobic treatment of ethanol stillage from conventional and cellulosic feedstock, Biomass Bioenerg. **19** (2000) 63–102.

[45] M.M. Shan, F. Akanbi, M. Cheryan, Potassium Acetate by Fermentation with *Clostridium thermoaceticum,* Appl. Biochem. Biotechnol. **63–65** (1997) 423–433.

[46] A. Djukić-Vuković, L. Mojović, M. Vukašinović-Sekulić, M. Rakin, S. Nikolić, J. Pejin, M. Bulatović, Effect of different fermentation parameters on L-lactic acid production from liquid distillery stillage, Food Chem. **134** (2012) 1038–1043.

[47] L. Mojović, M. Vukašinović-Sekulić, A. Djukić, D. Pejin, M. Rakin, J. Pejin, S. Nikolić, Proizvodnja mlečne kiseline na tečnoj destilerijskoj džibri, PTEP **15** (2011) 1–5.

[48] M. Marković, S. Markov, O. Grujić, L. Mojović, S. Kocić-Tanackov, M. Vukašinović Sekulić, J. Pejin, Microwave as a pre-treatment of triticale for bioethanol fermentation and utilization of the stillage for lactic acid fermentation, Biochem. Eng. J. **85** (2014) 132–138.

[49] S. Karp, A. Igashiyama, P. Siqueira, J. Carvalho, L. van den Berghe, V. Thomaz-Soccol, J. Coral, J.L. Tholozan, A. Pandey, C. Soccol, Application of the biorefinery concept to produce L-lactic acid from the soybean vinasse at laboratory and pilot scale, Bioresour. Technol. **102** (2011) 1765–1772.

[50] A. Djukić-Vuković, L. Mojović, V. Semenčenko, M. Radosavljević, J. Pejin, S. Kocić-Tanackov, Effective valorisation of distillery stillage by integrated production of lactic acid and high quality feed, Food Res. Int. **73** (2015) 75–80.

[51] B. Jin, L.P. Huang, P. Lant, *Rhizopus arrhizus* - a producer for simultaneous saccharification and fermentation of starch waste materials to L(+)-lactic acid, Biotechnol. Lett. **25** (2003) 1983–1987.

[52] R. John, R. Sukumaran, K. Nampoothiri, A. Pandey, Statistical optimization of simultaneous saccharification and L(+)-lactic acid fermentation from cassava bagasse using mixed culture of lactobacilli by response surface methodology, Biochem. Eng. J. **36** (2007) 262–267.

[53] S. Nakano, C. Ugwu, Y. Tokiwa, Efficient production of D-(–)-lactic acid from broken rice by *Lactobacillus delbrueckii* using $Ca(OH)_2$ as a neutralizing agent, Bioresour. Technol. **104** (2012) 791–794.

[54] R. John, K.M. Nampoothiri, A. Pandey, Simultaneous saccharification and L-(+)-lactic acid fermentation of protease-treated wheat bran using mixed culture of lactobacilli, Biotechnol. Lett. **28** (2006) 1823–1826.

[55] Z. Li, L. Han, Y. Ji, X. Wang, T. Tan, Fermentative production of l-lactic acid from hydrolysate of wheat bran by *Lactobacillus rhamnosus,* Biochem. Eng. J. **49** (2010) 138–142.

[56] L. Mojović, D. Pejin, M. Lazić, Bioetanol kao gorivo stanje i perspektive, Tehnološki fakultet, Leskovac, 2007, pp. 65–69.

[57] R.P. John, G.S. Anisha, K.M. Nampoothiri, A. Pandey, Direct lactic acid fermentation: Focus on simultaneous saccharification and lactic acid production, Biotechnol. Adv. **27** (2009) 145–152.

[58] L. Wang, B. Zhao, B. Liu, Ch. Yang, B. Yu, Q. Li, C. M, P. Xu, Y. Ma, Efficient production of L-lactic acid from cassava powder by *Lactobacillus rhamnosus*, Bioresour. Technol. **101** (2010) 7895–7901.

[59] C. Vishnu, G. Seenayya, G. Reddy, Direct fermentation of various pure and crude starchy substrates to L-(+)-lactic acid using *Lactobacillus amylophilus* GV6, World J. Microbiol. Biotechnol. **18** (2002) 429–433.

[60] M.A. Abdel-Rahman, Y. Tashiro, K. Sonomoto, Lactic acid production from lignocellulose-derived sugars using lactic acid bacteria: overview and limits, J. Biotechnol. **156** (2011) 286–301.

[61] A.T.W.M. Hendriks, G. Zeeman, Pretreatments to enhance the digestibility of lignocellulosic biomass, Bioresour. Technol. **100** (2009) 10–18.

[62] J. Pejin, M. Radosavljević, O. Grujić, L. Mojović, S. Kocić-Tanackov, S. Nikolić, A. Djukić-Vuković, Mogućnosti primene pivskog tropa u biotehnologiji, Hem. Ind. **67** (2013) 277–291.

[63] S. Mussatto, M. Fernandes, I. Mancilha, I. Roberto, Effect of medium supplementation and pH control on

lactic acid production from brewer's spent grain, Biochem. Eng. J. **40** (2008) 437–444.

[64] J. Pejin, M. Radosavljević, L. Mojović, S. Kocić-Tanackov, A. Djukić-Vuković, The influence of calcium-carbonate and yeast extract addition on lactic acid fermentation of brewer's spent grain hydrolysate, Food Res. Int. **73** (2015) 31–37.

[65] A. Nancib, N. Nancib, J. Boudrant, Production of lactic acid from date juice extract with free cells of single and mixed cultures of *Lactobacillus casei* and *Lactococcus lactis*, World J. Microbiol. Biotechnol. **25** (2009) 1423––1429.

[66] K.B. Lee, Comparison of fermentative capacities of lactobacilli in single and mixed culture in industrial media, Process Biochem. **40** (2005) 1559–1564.

[67] F. Cui, Y. Li, C. Wan, Lactic acid production from corn stover using mixed cultures of *Lactobacillus rhamnosus* and *Lactobacillus brevis*, Bioresour. Technol. **102** (2011) 1831–1836.

[68] X.-Y. Ge, H. Qian, W.-G. Zhang, Improvement of L-lactic acid production from Jerusalem artichoke tubers by mixed culture of *Aspergillus niger* and *Lactobacillus* sp. Bioresour. Technol. **100** (2009) 1872–1874.

[69] J. Ouyang, R. Ma, Z. Zheng, C. Cai, M. Zhang, T. Jiang, Open fermentative production of L-lactic acid by *Bacillus* sp. strain NL01 using lignocellulosic hydrolyzates as low-cost raw material, Bioresour. Technol. **135** (2013) 475––480.

[70] K. Ma, T. Maeda, H. You, Y. Shirai, Open fermentative production of L-lactic acid with high optical purity by thermophilic *Bacillus coagulans* using excess sludge as nutrient, Bioresour. Technol. **151** (2014) 28–35.

[71] M.A. Abdel-Rahman, Y. Tashiro, T. Zendo, K. Sonomoto, Improved lactic acid productivity by an open repeated batch fermentation system using *Enterococcus mundtii* QU 25, RSC Adv. **3** (2013) 8437–8445.

[72] M.A. Abdel-Rahman, Y. Tashiro, K. Sonomoto, Recent advances in lactic acid production by microbial fermentation processes, Biotechnol. Adv. **31** (2013) 877–902.

[73] L. Yu, T. Lei, X. Ren, X. Pei, Y. Feng, Response surface optimization of l-(+)-lactic acid production using corn steep liquor as an alternative nitrogen source by *Lactobacillus rhamnosus* CGMCC 1466, Biochem. Eng. J. **39** (2008) 496–502.

[74] M. Taskin, N. Esim, S. Ortucu, Efficient production of l-lactic acid from chicken feather protein hydrolysate and sugar beet molasses by the newly isolated *Rhizopus oryzae* TS-61, Food Bioprod. Process. **90** (2012) 773–779.

[75] Z. Lu, F. He, Y. Shi, M. Lu, L. Yu, Fermentative production of L(+)-lactic acid using hydrolyzed acorn starch, persimmon juice and wheat bran hydrolysate as nutrients, Bioresour. Technol. **101** (2010) 3642–3648.

[76] S. Kwon, P.C. Lee, E.G. Lee, Y.K. Chang, N. Chang, Production of lactic acid by *Lactobacillus rhamnosus* with vitamin-supplemented soybean hydrolysate, Enzyme Microb. Technol. **26** (2000) 209–215.

[77] K. Hetényi, Á. Németh, B. Sevella, Role of pH-regulation in lactic acid fermentation: Second steps in a process improvement, Chem. Eng. Process. **50** (2011) 293–299.

[78] R.P. John, K.M. Nampoothiri, Strain improvement of *Lactobacillus delbrueckii* using nitrous acid mutation for L-lactic acid production, World J. Microbiol. Biotechnol. **24** (2008) 3105–3109.

[79] L. Ye, H. Zhao, Zh. Li, J.Ch. Wu, Improved acid tolerance of *Lactobacillus pentosus* by error-prone whole genome amplification, Bioresour. Technol. **135** (2013) 459–463.

[80] S. Ding, T. Tan, L-lactic acid production by *Lactobacillus casei* fermentation using different fed-batch feeding strategies, Process Biochem. **41** (2006) 1451–1454.

[81] Y. Zhang, W. Cong, S.Y. Shi, Application of a pH Feedback-Controlled Substrate Feeding Method in Lactic Acid Production, Appl. Biochem. Biotechnol. **162** (2010) 2149–2156.

[82] D.M. Bai, Q. Wei, Z.H. Yan, X.M. Zhao, X.G. Li, S.M. Xu, Fed-batch fermentation of *Lactobacillus lactis* for hyper--production of L-lactic acid, Biotechnol. Lett. **25** (2003) 1833–1835.

[83] A. Djukić-Vuković, L. Mojović, M. Vukašinović-Sekulić, S. Nikolić, J. Pejin, Integrated production of lactic acid and biomass on distillery stillage, Bioprocess Biosyst. Eng. **36** (2013) 1157–1164.

[84] Y. Göksungur, U. Güvenç, Production of lactic acid from beet molasses by calcium alginate immobilized *Lactobacillus delbrueckii* IFO 3202, J. Chem. Technol. Biotechnol. **74** (1999) 131–136.

[85] A. Idris, W. Suzana, Effect of sodium alginate concentration, bead diameter, initial pH and temperature on lactic acid production from pineapple waste using immobilized *Lactobacillus delbrueckii*, Process Biochem. **41** (2006) 1117–1123.

[86] N.A. Mostafa, Production of lactic acid from whey with agar immobilized cells in a continuous packed tubular reactor, Energ. Convers. Manage. **37** (1996) 253–260.

[87] T. Roukas, P. Kotzekidou, Production of lactic acid from deproteinized whey by coimmobilized *Lactobacillus casei* and *Lactococcus lactis* cells, Enzyme Microb. Technol. **13** (1991) 33–38.

[88] K. Petrov, D. Yankov, V. Beschkov, Lactic acid fermentation by cells of *Lactobacillus rhamnosus* immobilized in polyacrylamide gel, World J. Microbiol. Biotechnol. **22** (2006) 337–345.

[89] P. Wang, Z. Chen, J. Li, L. Wang, G. Gong, G. Zhao, H. Liu, Z. Zheng, Immobilization of *Rhizopus oryzae* in a modified polyvinyl alcohol gel for L(+)-lactic acid production, Ann. Microbiol. **63** (2013) 957–964.

[90] Y. Göksungur, M. Gündüz, Ş. Harsa, Optimization of lactic acid production from whey by *L casei* NRRL B-441 immobilized in chitosan stabilized Ca-alginate beads, J. Chem. Technol. Biotechnol. **80** (2005) 1282–1290.

[91] A.C. Velázquez, A.L. Pometto III, K.L. Ho, A. Demirci, Evaluation of plastic-composite supports in repeated fed-batch biofilm lactic acid fermentation by *Lactobacillus casei*, Appl. Microbiol. Biotechnol. **55** (2001) 434–441.

[92] V. Rangaswamy, S.V. Ramakrishna, Lactic acid production by *Lactobacillus delbrueckii* in a dual reactor system using packed bed biofilm reactor, Lett. Appl. Microbiol. **46** (2008) 661–666.

[93] A. Djukić-Vuković, L. Mojović, B. Jokić, S. Nikolić, J. Pejin, Lactic acid production on liquid distillery stillage by *Lactobacillus rhamnosus* immobilized onto zeolite, Bioresour. Technol. **135** (2013) 454–458.

[94] M.N. Kumar, A.I. Gialleli, J.B. Masson, P. Kandylis, A. Bekatorou, A.A. Koutinas, M. Kanellaki, Lactic acid fermentation by cells immobilised on various porous cellulosic materials and their alginate/poly-lactic acid composites, Bioresour. Technol. **165** (2014) 332–335.

[95] G. Chronopoulos, A. Bekatorou, E. Bezirtzoglou, A. Kaliafas, A.A. Koutinas, R. Marchant, I.M. Banat, Lactic acid fermentation by *Lactobacillus casei* in free cell form and immobilised on gluten pellets, Biotechnol. Lett. **24** (2002) 1233–1236.

[96] L. Li, D. Cai, C. Wang, J. Han, W. Ren, J. Zheng, Z. Wang, T. Tan, Continuous L-lactic acid production from defatted rice bran hydrolysate using corn stover bagasse immobilized carrier, RSC Adv. **5** (2015) 18511–18517.

[97] Z. Shi, P. Wei, X. Zhu, J. Cai, L. Huang, Z. Xu, Efficient production of l-lactic acid from hydrolysate of Jerusalem artichoke with immobilized cells of *Lactococcus lactis* in fibrous bed bioreactors, Enzyme Microb. Technol. **51** (2012) 263–268.

[98] T. Zhao, D. Liu, H. Ren, X. Shi, N. Zhao, Y. Chen, H. Ying, *D*-Lactic Acid Production by *Sporolactobacillus inulinus* Y2-8 Immobilized in Fibrous Bed Bioreactor Using Corn Flour Hydrolyzate, J. Microbiol. Biotechnol. **24**(12) (2014) 1664–1672.

[99] H.O. Kim, Y.J. Wee, J.N. Kim, J.S. Yun, H.W. Ryu, Production of Lactic Acid From Cheese Whey by Batch and Repeated Batch Cultures of *Lactobacillus* sp. RKY2, Appl. Biochem. Biotechnol. **131** (2006) 694–704.

[100] V. Arasaratnam, A. Senthuran, K. Balasubramaniam, Supplementation of whey with glucose and different nitrogen sources for lactic acid production by *Lactobacillus delbrueckii,* Enzyme Microb. Technol. **19** (1996) 482––486.

[101] A.O. Büyükkileci, S. Harsa, Batch production of L(+)-lactic acid from whey by *Lactobacillus casei* (NRRL B-441), J. Chem. Technol. Biotechnol. **79** (2004) 1036–1040.

[102] N. Secchi, D. Giunta, L. Pretti, M. R. García, T. Roggio, I. Mannazzu, P. Catzeddu, Bioconversion of ovine *scotta* into lactic acid with pure and mixed cultures of lactic acid bacteria, J. Ind. Microbiol. Biotechnol. **39** (2012) 175–181.

[103] Y.J. Wee, J.N. Kim, J.S. Yun, H.W. Ryu, Utilisation of sugar molasses for economical L(+)-lactic acid production by batch fermentation of *Enterococcus faecalis*. Enzyme Microb. Technol. **35** (2004) 568–573.

[104] Y. Göksungur, U. Güvenç, Batch and continuous production of lactic acid from beet molasses by *Lactobacillus delbrueckii* IFO 3202. J. Chem. Technol. Biotechnol. **69** (1997) 399–404.

[105] J. Monteagudo, L. Rodríguez, J. Rincón, J. Fuertes, Optimization of the conditions of the fermentation of beet molasses to lactic acid by *Lactobacillus delbrueckii*. Acta Biotechnol. **14** (1994) 251–260.

[106] S. Bulut, M. Elibol, D. Ozer, Effect of different carbon sources on l(+) -lactic acid production by *Rhizopus oryzae,* Biochem. Eng. J. **21** (2004) 33–37.

[107] A. Srivastava, A. Poonia, A.D. Tripathi, R.P. Singh, S.K. Srivastava, Optimization of nutritional supplements for enhanced lactic acid production utilizing sugar refinery by-products, Ann. Microbiol. **64** (2014) 1211–1221.

[108] B.P. Calabia, Y. Tokiwa, Production of D-lactic acid from sugarcane molasses, sugarcane juice and sugar beet juice by *Lactobacillus delbrueckii*, Biotechnol. Lett. **29** (2007) 1329–1332.

[109] K. Xu, P. Xu, Efficient production of L-lactic acid using cofeeding strategy based on cane molasses/glucose carbon sources, Bioresour. Technol. **153** (2014) 23–29.

[110] L. Zhang, K.Q. Shia, G.Y. Shib, Production of L-lactic acid with very high gravity distillery wastewater from ethanol fermentation by a newly isolated *Enterococcus hawaiiensis,* J. Chem. Technol. Biotechnol. **86** (2011) 213––216.

[111] Z. Li, L. Han, Y. Ji, X. Wang, T. Tan, Fermentative production of l-lactic acid from hydrolysate of wheat bran by *Lactobacillus rhamnosus*, Biochem. Eng. J. **49** (2010) 138–142.

[112] B. Jin, L.P. Huang, P. Lant, *Rhizopus arrhizus*-a producer for simultaneous saccharification and fermentation of starch waste materials to L(+)-lactic acid, Biotechnol. Lett. **25** (2003) 1983–1987.

[113] S. Mussatto, M. Fernandes, G. Dragone, I. Mancilha, I. Roberto, Brewer's spent grain as raw material for lactic acid production by *Lactobacillus delbrueckii*, Biotechnol. Lett. **29** (2007) 1973–1976.

[114] L. Wang, B. Zhao, B. Liu, B. Yu, C. Ma, F. Su, D. Hu, Q. Li, Y. Ma, P. Xu, Efficient production of L-lactic acid from corncob molasses, a waste by-product in xylitol production, by a newly isolated xylose utilizing *Bacillus sp.* strain, Bioresour. Technol. **101** (2010) 7908–7915.

[115] D.M. Bai, Z.H. Yan, Q. Wei, X.M. Zhao, X.G. Li, S.M. Xu, Ammonium lactate production by *Lactobacillus lactis* BME5-18M in pH-controlled fed-batch fermentations, Biochem. Eng. J. **19** (2004) 47–51.

[116] M. Ou, L. Ingram, K. Shanmugam, L(+)-Lactic acid production from non-food carbohydrates by thermotolerant *Bacillus coagulans,* J. Ind. Microbiol. Biotechnol. **38** (2011) 599–605.

[117] T. Roukas, P. Kotzekidou, Lactic acid production from deproteinized whey by mixed cultures of free and coimmobilized *Lactobacillus casei* and *Lactococcus lactis* cells using fedbatch culture, Enzyme Microb. Technol. **22** (1998) 199–204.

[118] Y. Göksungur, U. Güvenç, Production of lactic acid from beet molasses by calcium alginate immobilized *Lactobacillus delbrueckii* IFO 3202, J. Chem. Technol. Biotechnol. **74** (1999) 131–136.

SUMMARY

OPPORTUNITIES, PERSPECTIVES AND LIMITS IN LACTIC ACID PRODUCTION FROM WASTE AND INDUSTRIAL BY-PRODUCTS

Dragana D. Mladenović[1], Aleksandra P. Djukić-Vuković[1], Jelena D. Pejin[2], Sunčica D. Kocić-Tanackov[2], Ljiljana V. Mojović[1]

[1]*Faculty of Technology and Metallurgy, University of Belgrade, Belgrade, Serbia*
[2]*Faculty of Technology, University of Novi Sad, Novi Sad, Serbia*

(Review paper)

In line with the goals of sustainable development and environmental protection today great attention is directed towards new technologies for waste and industrial by-products utilization. Waste products represent potentially good raw material for production other valuable products, such as bioethanol, biogas, biodiesel, organic acids, enzymes, microbial biomass, etc. Since the first industrial production to the present, lactic acid has found wide application in food, cosmetic, pharmaceutical and chemical industries. In recent years, the demand for lactic acid has been increasing considerably owing to its potential use as a monomer for the production of poly-lactic acid (PLA) polymers which are biodegradable and biocompatible with wide applications. Waste and industrial by-products such are whey, molasses, stillage, waste starch and lignocellulosic materials are a good source of fermentable sugars and many other substances of great importance for the growth of microorganisms, such as proteins, minerals and vitamins. Utilization of waste products for production of lactic acid could help to reduce the total cost of lactic acid production and except the economic viability of the process offers a solution of their disposal. Fermentation process depends on chemical and physical nature of feedstocks and the lactic acid producer. This review describes the characteristics, abilities and limits of microorganisms involved in lactic acid production, as well as the characteristics and types of waste products for lactic acid production. The fermentation methods that have been recently reported to improve lactic acid production are summarized and compared. In order to improve processes and productivity, fed-batch fermentation, fermentation with immobilized cell systems and mixed cultures and opportunities of open (non-sterilized) fermentation have been investigated.

Keywords: Lactic acid • Lactic acid bacteria • Waste products • Industrial by-products • Fermentation

Estimating precision and accuracy of GC-TCD method for carbon dioxide, propane and carbon monoxide determination at different flow rate of carrier gas

Oman Zuas, Harry Budiman

Gas Analysis Laboratory (GasAL), Electrochemistry & Gas Metrology Research Group, Research Centre for Chemistry-Indonesian Institute of Sciences (RCChem-LIPI), Kawasan PUSPIPTEK Serpong 15314, Tangerang, Indonesia

Abstract

Investigation on precision and accuracy of gas chromatography equipped with thermal conductivity detector (GC-TCD) method for the measurement of CO_2, C_3H_8, and CO as pollutant models at different flow rate of helium (He) carrier gas ranging from 17.50 to 36.25 ml/min were conducted. It was found that percentage of relative standard deviation (*%RSD*) values for both precision an accuracy show an overall gradual decrease as the carrier gas flow rates increased up to 25 ml/min. After that, the *%RSD* was found to increase with a further increase in the flow rate. These findings indicate that the flow rate of 25 ml/min was found to be the most precise and accurate level among all flow rates tested under experimental conditions of this study. While the *%RSD* values obtained at all flow rate are given in details. Consequently, our results suggest that the flow rate of carrier gas was a determining parameter for varying the precision and accuracy of the GC-TCD method. Owing to the fact that carrier gas acts as a transporter of components of the mixture in the form of vapor or gas through the column, setting of the flow rate of carrier gas should in proper level to achieve a precision and accuracy of the GC-TCD method.

Keywords: precision, accuracy, gas chromatography, vehicle emission, pollutant.

Available online at the Journal website: http://www.ache.org.rs/HI/

SCIENTIFIC PAPER

UDC 504.5:543.544.3:628.5

Hem. Ind. **70** (4) 451–459 (2016)

doi: 10.2298/HEMIND150315051Z

High concentrations of air pollutants emitted during vehicle and industrial operations are of great concern because they play an important role in atmospheric environment. Some common pollutants found in atmospheric environment include oxides of nitrogen, sulfur dioxide, carbon dioxide, carbon monoxide, volatile and persistent organic compounds [1–3]. The presences of those harmful substances have significantly decreased the air quality, which create serious human health concerns. For people who live under poor air quality, the pollution has the potential for serious adverse health effects such as human respiratory ailments like asthma and bronchitis [4], immaturity health effect like loss of children's IQ point and babies born with birth defects [5,6], and the risk of life-threatening conditions like cancer all leading to decrease in the human life expectancy [7].

Continuous increase of the air pollutant concentrations in the atmospheric environment has devised the more stringent of regulations with the purpose to keep the concentration at allowable levels. However, the more stringent of regulation alone might be not enough to ensure an adequate protection of atmospheric environment, but an efficient control of the regulation via regulatory monitoring programs and its enforcement are also crucial. In conjunction with enforcement of the regulatory monitoring programs, the usage of analytical chemistry instrument for gaseous pollutant measurement remains of vital importance. In the area of concern, several analytical chemistry techniques having reliable and rapid procedure have been exploited such as those based on chromatography [8], infrared spectroscopy [9], fluorometry [10], and ring down spectroscopy techniques [11]. Among others, the chromatography-based technique is one of the most preferred techniques over the last century owing to its distinct advantages including separation of very complex mixtures, relatively simple equipment, procedures that are applicable to a broad spectrum of chemicals, and adaptable to micro- and macro-size samples [12]. Nowadays, the gas chromatography (GC) is easily available worldwide to both government and private sector including university, research institute and industry. In spite of the progress that has been made, there is still effort remaining that can be directed toward development of GC applications for gaseous pollution measurement. Practically, to achieve high quality results from a GC measurement, several conditions must be taken into account during its operational like detector temperature, oven temperature, and flow rate of carrier gas [13]. Among others, carrier gas is one of the most

Correspondence: O. Zuas, Gas Analysis Laboratory (GasAL), Electrochemistry & Gas Metrology Research Group, Research Centre for Chemistry-Indonesian Institute of Sciences (RCChem-LIPI), Kawasan PUSPIPTEK Serpong 15314, Tangerang, Indonesia.

E-mail: oman.zuas@lipi.go.id

Paper received: 15 March, 2015

Paper accepted: 2 September, 2015

important one. Results from our preliminary study (data not shown here) show that the GC's key parameters (such as peak area, peak height, retention time, detector response, and resolution) are highly affected by flow rate change of the carrier gas [14]. It is in very good agreement with some experimental results as can be found in literatures [13,15,16]. Despite the fact that experimental studies related to the effects of carrier gas flow rate on the GC's key parameters have been well-documented, exploring the effect of flow rate of carrier gas on precision and accuracy in the GC method is still facing challenges. It might be an acceptable idea that modification of the flow rate of carrier gas may lead to significant change the separation efficiency and effective speeds of transport. In addition, understanding how rate modifications of carrier gas flow is generally designated to achieve a high-quality measurement results that is otherwise unreliable.

In previous investigations, the use of He as carrier gas in the application of gas chromatography equipped with thermal conductivity detector (GC-TCD) method has been mainly addressed at constant flow rate including 11.3 [17], 20 [18], 23 [19], 25 [20], 30 [21] and 35 ml/min [22]. Nevertheless, to our knowledge, there is no reported study focusing on the effect of flow rate of He carrier gas on the precision and accuracy of GC-TCD method. Hence, the effects of flow rate of He carrier gas on precision and accuracy of GC-TCD method is experimentally investigated in this study. The flow rate range of He carrier gas investigated herein was 17.5––36.25 ml/min with 3.75 ml/min intervals. To achieve the study purposes, three component of gaseous vehicle emission including carbon dioxide (CO_2), propane (C_3H_8) and carbon monoxide (CO) were used as practical example and investigated using GC-TCD. These three gaseous pollutants were used because they are listed by the United Nation as the technical requirements for the type approval of motor vehicles, which is further adopted by Indonesian Government for vehicle emission standard requiring reporting and testing of both new [23] and used car [24].

EXPERIMENTAL

Materials

Two different cylinders of gravimetric certified standard gas mixtures (SGM) in N_2 matrix were purchased from a commercial available source (MESA specialty gas company, USA). One SGM (denoted as SGM-A) containing mixture of 2.18 mol% carbon dioxide (CO_2), 1.81 mol% propane (C_3H_8) and 3.44 mol% carbon monoxide (CO) was used as test standard in all experiment runs. Another SGM (denoted as SGM-B) containing mixture of 4.14 mol% carbon dioxide (CO_2), 0.65 mol% propane (C_3H_8) and 0.94 mol% carbon monoxide (CO) was only used as test sample during method accuracy assessment.

GC instrumentation system and operating conditions

The GC instrumentation used was Agilent model 6890 series (Agilent, CA, USA) equipped with a single stage dual-packed column (Figure 1) for separating the target gas component (CO_2, C_3H_8, and CO) from their mixture. In such dual-packed column, a packed J&W porapack Q column (6 ft×1/8 in o.d.×2 mm, 80–100 mesh particle size) was connected in series to a packed J&W molsieve 5A column (9 ft×1/8 in o.d.×2 mm, 80––100 mesh particle size). The detection was performed by using a thermal conductivity detector (TCD) and the output signal was monitored using OpenLAB CDS Chemstation version A.2.3.57, which is installed on a HP personal computer (HP Pavilion Slimline 400 PC series). For introducing the gas sample into the GC system, a Brooks 5890E mass flow controller (Brooks Instrument, Hatfield, PA, USA) was used to ensure a consistent sample flow. The mass flow controller (MFC) was installed just before the injection system consisted of a stainless steel tubing having 1/16 in in diameters up to the loop inlet, a 2 ml stainless steel loop (Agilent, CA, USA).

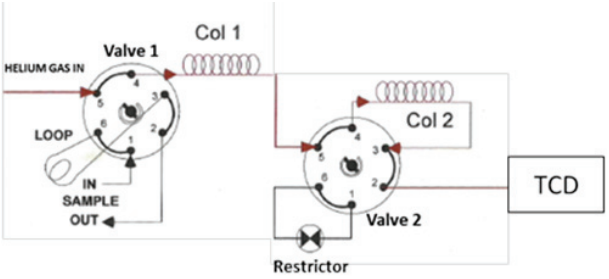

Figure 1. A schematic diagram of a single stage dual-packed column of GC-TCD used in this study (for interpretation of the references to colour in the figure the reader is referred to the web version of the article).

Gaseous sample analyses

Analyses of the gas components in the sample were conducted based on our previous experimental procedure [14], where all analyses were carried out under the same condition except for the carrier gas flow rate . The details of the analyses procedure [14] is as follows: a certain amount of gas sample from aluminum sample cylinder was introduced to the column in the GC system through an MFC at flow rate of 100 ml/min. The injector and detector temperatures are 200 and 250 °C, respectively. The elution of the studied gas mixture was achieved with following temperature program: 40 °C for 10 min, 40 to 160 °C at 60 °C/min, and 160 °C was held for 2 min. The data was estimated by automated integration of the area under the resolved chromatographic profile, using the HP computer (Hewlett Pack-

ard Pavilion Slimline 400 PC series) of OpenLAB CDS Chemstation version A.2.3.57. In addition, the concentrations of all components in the gas sample were determined by inserting the peak area of corresponding gas component into their calibration curve. The calibrations curves were made using procedure as described in the next section.

The following flow rates of He carrier gas were investigated: 17.5; 21.25; 25.0; 28.75, 32.5 and 36.25 ml/min and their effect on the precision and accuracy of the GC-TCD method were assessed. This flow rate range was employed because it is recommended as the instrument technical specification that would otherwise diminish its performance.

GC instrument calibration

The GC-TCD instrument was calibrated before each analysis run using a series of SGM containing all gas components (CO_2, C_3H_6 and CO) at different concentration level. The calibration curve was made by plotting the peak area of gas components in the SGM *versus* their concentration.

Calculation procedure

The precision of the GC-TCD was assessed in term of repeatability and reproducibility. The repeatability precision study was established by measuring the response of the target gas component in the certified SGM-A and expressed as percentage relative standard deviation (*%RSD*) of seven replicate injections (n = 7). The *RSD* is calculated by means of the following expression:

$$RSD = \frac{100}{\bar{y}} \sqrt{\sum \frac{(y_i - \bar{y})^2}{n-1}} \quad (1)$$

in which y_i is individual value expressed as peak area, $\bar{y}$ is mean of peak area value of n injection replication, and n is number of injection replication. The repeatability of the method is categorized acceptable when *RSD* value is less than 0.67 of coefficient of variability Hortwitz (CV-Hortwitz) [25]. The CV-Hortwitz is a predicted *RSD* and its value was obtained by using the Hortwitz function (Eq. (2)) [25,26]. The lower *RSD* value is ascribable to the better repeatability of the flow rate level. In addition, the differences between *RSD* of the two consecutive flow rates were statistically analyzed using the least significant difference test in one-way analysis of variance (ANOVA). A 95% confidence limit (p < 0.05) was applied for the indication of significant difference between the two consecutive flow rate levels:

$$\text{CV-Hortwitz}(\%) = 2^{(1-0.5\log c)} \quad (2)$$

in which c is the concentration of gas components in decimal fraction.

Moreover, the precision in terms of reproducibility was carried out by injecting the certified SGM-A with similar procedure to that of repeatability precision except different day of time interval was used instead of the same day. The determinations of reproducibility precision were completed for 22 days with 7-day interval between courses of measurement. The acceptance criteria were set up where the *RSD* value is below the CV-Hortwitz value (*RSD* ≤ CV Hortwitz). At a certain flow rate level, the more reproducible of the GC-TCD measurement will be obtained when the lower the *RSD* value of response was achieved. Similar to the repeatability, statistical analysis for the reproducibility were also conducted under similar criteria to indicate the significance different between *RSD* of the two consecutive flow rate levels. In addition, the assessment of reproducibility was also conducted by setting up a control limit chart. The control limit chart normally has five lines which is consisting of one average line (AL), two warning limit (WL) lines, and two control limit (CL) lines. The AL represents the mean of the control values. Two WL lines are located at a distance of ± two times the standard deviation (*SD*) from the AL line (*AL*±2*SD*), while two CL lines are located at a distance of ± three times the SD from the AL (*AL*±3*SD*) [27].

The accuracy value is dependent on two factors, *i.e.*, the bias and precision [25,28]. The bias of method is the difference between the measured value and the value from certificate of SGM-B, which is calculated using the expression:

$$\Delta = \bar{X} - \text{Y} \quad (3)$$

in which $\bar{X}$ is the average of measured value of SGM-B, and Y is value from certificate of SGM-B. In the method accuracy assessment, the precision of analytical method (σ, Eq. (4)) from repeatability and reproducibility are included. In addition, the uncertainty value from certificate of SGM-B also contributes to the estimation of σ value. Thus, the value of σ is obtained by combining those three components by using the following expression [26]:

$$\sigma = \sqrt{SD_b^2 + \frac{SD_w^2}{n} + \mu_{RM}^2} \quad (4)$$

in which SD_b is the *SD* from reproducibility precision. SD_w is the *SD* from repeatability precision, and μ_{RM} is the uncertainty of standard SGM-B stated in the certificate. The acceptance criteria is set according to the ISO Guide 33:2000 "Uses of certified reference materials" [29], where no bias of the method is found if the observed bias of method falls within ±2σ at confidence level 95%:

$$-2Df < \text{bias} < 2Df \quad (5)$$

RESULTS AND DISCUSSION

Method Linearity

Results of GC-TCD calibration for all gas components are summarized in Figure 1. It can be seen in Figure 1 that calibration curve for all gas components show an excellent in term of their linearity properties.

Gas component	Slope	intercept	Linearity range (% mol/mol)	*n* (number of injection)	R^2
CO_2	489.65	-47.15	0 - 13.50	8	0.9993
C_3H_8	888.32	-13.73	0 - 2.18	8	0.9991
CO	437.10	-1.92	0 - 4.18	8	0.9998

Figure 2. Data indicating linearity of the GC-TCD method.

Response identity of target analyte

In a GC measurement, the response identity of target analytes is a very common criterion in the design of a GC method and it has to be identified clearly, before a quantitative analysis is carried out. In such identification process, it is necessary to establish that the analyte response in the form of signal produced is only due to the analyte and not from the presence of other components as interferences [28,30]. In a word, an adequate peak separation of different analytes should be obtained.

In this study, separation of the target analytes in the gas mixture including CO_2, C_3H_8 and CO were conducted on a GC system equipped with dual column. Based on this basic configuration, the separation process of the target analytes may have a consecutive step as follows: CO_2 was separated from the gas mixture in Column 1. After the CO_2 was detected (R_t = 2.99 min), the valve is switched to Column 2 and C_3H_8 is eluted from Column 2 to detector. After the C_3H_8 (R_t = 13.32 min) is detected, the valve is switched back to Column 1 and CO is eluted from column 1 to the detector and CO is then detected (R_t = 16.57 min). One can be noticed under this column configuration, neither column alone is able to separate those three target analytes using the GC-TCD system, but a combination of the two (column 1 and 2) results in complete resolution where the chromatogram of the separation result is shown in Figure 3. No other interfering peaks at or nearby the retention times of CO_2, C_3H_8 and CO were observed, demonstrating that a good separation of the target analytes has been well-achieved [31].

The flow rate of carrier gas is undoubtedly one of the factors affecting some key parameters of the GC measurement process and it will therefore lead to a corresponding variation in the quantification results. In a GC system, the carrier gas is an inert gas that does not react with the sample component. The GC carrier gas has a function to transport the components of the mixture in the form of vapor or gas through the column where they are retained by the stationary phase in the column to a different extent [32]. The flow rate of carrier gas may have a significant contribution to the operational efficiency of a GC system [33]; thus probably affect to the precision and accuracy of the GC-TCD method.

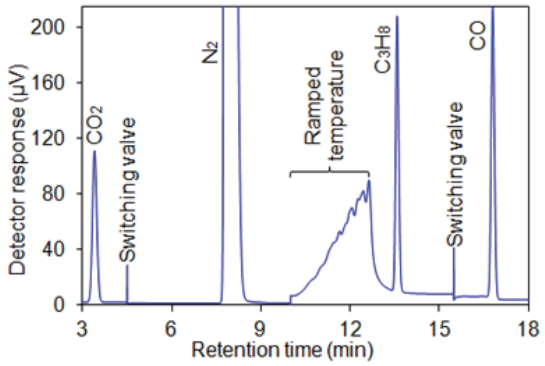

Figure 3. A typical chromatogram of gas component in SGM obtained using GC-TCD at carrier gas flow rate of 25.00 ml/min, showing the separation of CO_2, C_3H_8 and CO (for interpretation of the references to colour in the figure the reader is referred to the web version of the article).

Precision

Precision has become a critical factor in a GC measurement process [34]. In this study, the measurement precision was determined in terms of repeatability (intra-day precision) and reproducibility (inter-day precision).

The repeatability precision is the nature of variation observed arising when a successive GC measurement is carried out under the same method on identical test items in the same laboratory by the same operator using the same equipment within short intervals of time [35,36]. In the present study, the repeatability precision was carried out in the same day as time interval. The results showed that the repeatability precision (*RSD*) of the CO_2, C_3H_8 and CO at different flow rate of carrier gas was found in the range of 0.10–0.40%, 0.10––0.27%, and 0.12–0.23%, respectively. All the values (Figure 4) were in the acceptable range of repeatability precision for target gas components, because all the values lie below the 0.67 of CV-Hortwitz [25].

As it can be seen from Figure 4, the *RSD* of the repeatability precision shows an overall gradual decrease as the flow rates increased up to 25 ml/min, giving the lowest *RSD* values among all gas components. The lowest *RSD* values means that the most repeatable of flow rate. In addition, the *RSD* was found to increase with a further increase in the flow rate. Over all, it was found that the worst repeatability precision was obtained at the flow rate of 17.5 ml/min having the highest *RSD* values. It can be concluded that

Flow Rate (ml/min)	CO_2 0.67 CVH	CO_2 %RSD	CO_2 LSD test	C_3H_8 0.67 CVH	C_3H_8 %RSD	C_3H_8 LSD test	CO 0.67 CVH	CO %RSD	CO LSD test
17.50	2.38	0.40	s	2.45	0.27	s	2.22	0.23	s
21.25	2.38	0.17	s	2.45	0.15	s	2.22	0.19	s
25.00	2.38	0.10	s	2.45	0.10	s	2.22	0.12	s
28.75	2.38	0.19	s	2.45	0.18	s	2.22	0.20	s
32.50	2.38	0.23	ns	2.45	0.20	ns	2.22	0.21	s
36.25	2.38	0.23		2.45	0.20		2.22	0.22	

Notes: 0.67CVH = 0.67 x CV Hortwitz (%); LSD test = least significant difference test; *s* = statistically significant difference in %RSD between the two consecutive flow rate levels ($p < 0.05$); *ns* = not significant ($p > 0.05$).

Figure 4. The %RSD for repeatability precision at difference flow rate of carrier gas and their corresponding 0.67 of CV-Hortwitz values.

the repeatability precision for all gas components increases with increasing the flow rate of the He carrier gas up to 25 ml/min; however, further increase the flow rate above 25 ml/min lead to decrease in the repeatability precision. According to the results of statistical analysis, as shown in Figure 4, the changes of flow rate of carrier gas for the two consecutive flow rate levels has affected the repeatability precision of the GC-TCD method. Generally, it was found that the *RSD* values between the two flow rate levels are differ significantly ($p < 0.05$), except for the *RSD* of CO_2 and C_3H_8 at flow rate of 32.50 and 36.25 ml/min ($p > 0.05$).

The reproducibility precision, also called as intermediate precision, is the variation arising from repeated measurement results that are obtained with the same test method at different or longer time periods by different operator [37]. In this reproducibility precision estimation, the value in term of *RSD* of seven repeated measurements was compared and the results were listed in Figure 5. From the Figure 5, it can be seen that the *RSD* values of CO_2, C_3H_8 and CO component are less than their corresponding CV-Hortwitz. In a word, all the *RSD* values of the reproducibility precision met the required criterion as the values of *RSD* are lower than their corresponding CV-Hortwitz [25].

Although the reproducibility precision values across the carrier gas flow rate level are acceptable (Figure 5), it was observed that flow rate of 25.00 ml/min showed its exceptional repeatability precision having the lowest %RSD values. From the Figure 5, the *RSD* values of CO_2, C_3H_8 and CO obtained at 25 ml/min are 0.90; 0.89 and 0.96, respectively. This finding has obviously suggested that the flow rate of 25 ml/min was found to be the most reproducible measurement, while flow rate of 17.50 and 36.25 ml/min were found to be of the poorest reproducibility. Moreover, the statistical analysis (Figure 5) indicates that there was significance correlation between the flow rate changes and reproducibility level of the GC-TCD method. The *RSD* values of the two consecutive flow rate levels were significantly different, which illustrates that the reproducibility performance (*RSD*) of the GC-TCD method may be related to the change of the carrier gas flow rate.

Flow Rate (ml/min)	CO_2 0.67 CVH	CO_2 %RSD	CO_2 LSD test	C_3H_8 0.67 CVH	C_3H_8 %RSD	C_3H_8 LSD test	CO 0.67 CVH	CO %RSD	CO LSD test
17.50	3.56	2.10	s	3.66	3.61	s	3.32	1.68	s
21.25	3.56	2.05	s	3.66	3.19	s	3.32	1.24	s
25.00	3.56	0.90	s	3.66	0.89	s	3.32	0.96	s
28.75	3.56	1.47	s	3.66	1.46	s	3.32	1.31	s
32.50	3.56	1.76	s	3.66	1.61	s	3.32	1.84	s
36.25	3.56	1.83		3.66	1.98		3.32	2.43	

Notes: CVH = CV Hortwitz (%); LSD test = least significant difference test; *s* = statistically significant difference in %RSD between the two consecutive flow rate levels ($p < 0.05$).

Figure 5. The %RSD for reproducibility precision at difference of carrier gas flow rate and their corresponding CV-Hortwitz.

In general, the *RSD* of reproducibility precision for all measurement at different of carrier gas flow rate (Figure 5) has the higher values in comparison to that of *RSD* of repeatability precision (Figure 4), indicating that reproducibility of the GC-TCD method was worse than repeatability. From the whole finding, one may expect that there were some user-related effects [38]. In addition, it is also essential to have in mind a concept of fit for purpose for establishing the reproducibility of GC measurements. Within this concept, the quality control of the measurement results is required and for what the purposes of the measurement results [39]. Therefore, setting up a control program is extremely important. The control limit (warning and action limit) remains the most common control program in the area of GC measurement [27]. The evaluation of control program was emphasized on the flow rate level of 25 ml/min because of its excellent in term of reproducibility over all flow rate levels. Figure 6a–c present the chart of control limit for the measurement obtained at different days using carrier gas flow rate of 25.00 ml/min. It can be seen from Figure 6 that all control data values obtained from measurement in all time period lie within or inside the warning limit, implying that no error of reproducibility measurement are found. On the other hand, if the control data values fall outside the limit, no reproducible measurement are obtained and remedial action have to be taken to identify the source of error and remove such errors [39].

Accuracy

In analytical chemistry method, the accuracy reflects the closeness or the agreement between the measured result of a measurement and an accepted/true value [25]. Accuracy is a combination of the bias and precision of an analytical procedure [25,26,28,35]. In this study, the accuracy means the closeness of measured values of target gas components (CO_2, C_3H_8 and CO) in SGM-A sample cylinder to the known values of gas components (CO_2, C_3H_8 and CO) in SGM-B reference standard cylinder. Taking into account the repeatability results of precision studies as previously discussed, the accuracy was only evaluated at three level of flow rate having the lowest *RSD* among the tested flow rate. Hence, the evaluation of the method accuracy was focused for the following flow rate levels: 21.25, 25.00 and 28.75 ml/min. Assessing accuracy of the measurement was established by measuring seven replication of the certified gas mixture containing target gas components (CO_2, C_3H_8 and CO), then the bias and precision were calculated and the results are listed in Figure 7. From the Figure 7, it was clearly observed that all bias value of CO_2, C_3H_8 and CO measured at those three different flow rates are lower than their corresponding

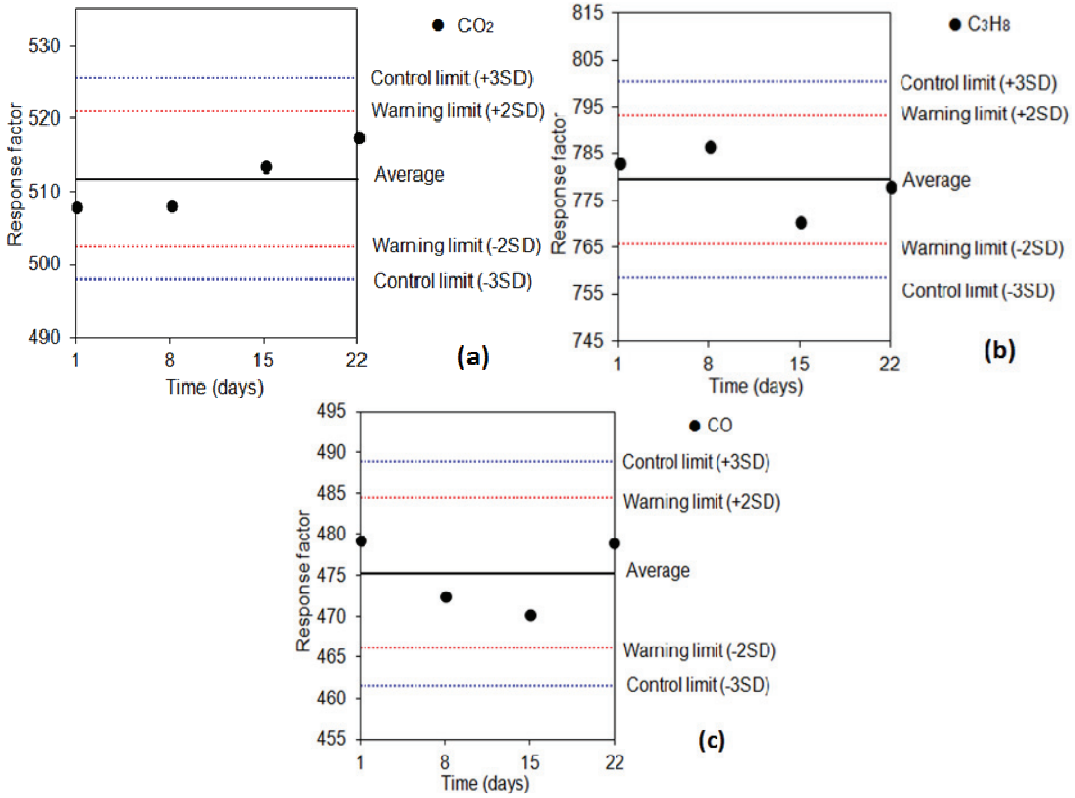

Figure 6. The chart of control limit for the measurement obtained at different days using carrier gas flow rate of 25.00 ml/min for: a) CO_2, b) C_3H_8 and c) CO_2 gas component (for interpretation of the references to colour in the figure the reader is referred to the web version of the article).

Parameter	Carrier gas flow rate								
	21.25 (ml/min)			25.00 (ml/min)			28.75 (ml/min)		
	CO_2	C_3H_8	CO	CO_2	C_3H_8	CO	CO_2	C_3H_8	CO
Bias (% mol/mol)	-0.011	-0.016	-0.036	0.044	-0.039	-0.039	-0.180	-0.039	-0.075
Precision method (σ) (% mol/mol)	0.132	0.061	0.048	0.126	0.025	0.044	0.129	0.040	0.084
$\pm 2\sigma$ (% mol/mol)	0.264	0.122	0.097	0.251	0.050	0.087	0.258	0.079	0.169

Note: All the bias values fall within the acceptance criteria $-2\sigma < \text{bias} < 2\sigma$

Figure 7. Accuracy of the GC-TCD for the measurement of CO_2, C_3H_8 and CO in the SGM obtained using GC-TCD at different flow rate of carrier gas and their corresponding theta values.

$\pm 2\sigma$ value. This finding indicated that the GC-TCD method applying those three different flow rate are accurate, on the basis of criteria given [29].

It may simply be that, although the flow rate of carrier gas discussed above affords an obvious effect on the precision and accuracy of the GC-TCD method, contribution of different characteristic of individual gas component, like their chemical structure, on such precision and accuracy is indistinguishable. Generally speaking, changes in the precision and accuracy of the GC-TCD method was found only due to modification of the flow rate of carrier gas. However, in a GC-TCD technique, the difference in thermal conductivity between the carrier gas and the individual gas component may affect to the precision and accuracy of a measurement. Therefore, there is a need for further study on the relationship between He carrier gas flow rate and individual chemical structure of gas component for a measurement in term of precision and accuracy of GC-TCD method.

CONCLUSION

A complete and good separation of individual peak of the target analytes CO_2, C_3H_8 and CO was achieved and no other interference peaks appeared in company with peaks of CO_2, C_3H_8 and CO were identified. It was found that the precision and accuracy of the GC-TCD method varies directly with the flow rate of carrier gas. The flow rate of carrier gas at level of 25.00 ml/min was found to be the most precise and accurate in comparison to other flow rate levels based on the given criteria, so the flow rate of carrier gas at 25.00 ml/min is considered as the most valid GC-TCD method under experimental condition of the present study. A further study focusing on the effect of individual chemical characteristics of the gas component on the precision and accuracy of the GC-TCD method should be carried out.

Acknowledgement

The authors gratefully acknowledged the Indonesian Government for financially supporting this study within the scope of RCChem-LIPI's project "Competency Development Program" under Project No. SP.DIPA-079.01.2.524341/2015. Special thanks to Zulvana Anggraeni and Inas Cintya Pramurtya for helping in GC-TCD analysis at the Gas Analysis Laboratory (GasAL), RCChem-LIPI, PUPIPTEK, Serpong. The authors are also very much thankful to anonymous reviewers for their valuable comments, which helped the authors to improve the manuscript.

REFERENCES

[1] S.M. Šerbula, D.T. Živković, A.A. Radojević, T S. Kalinović, J.V. Kalinović, Emission of SO_2 and SO_4^{2-} from copper smelter and its influence on the level of total S in soil and moss in Bor, Serbia, and the surroundings, Hem. Ind. **69** (2015) 51–58.

[2] K.S. John, K. Feyisayo, Air pollution by carbon monoxide (CO) poisonous gas in Lagos area Southwestern Nigeria, ACS **3** (2013) 510–514.

[3] A. Dubey, Studies on the Air Pollution Around Cement and Lime Factories, J. Environ. Earth Sci. **3** (2013) 191––194.

[4] A.J. Chauhan, S.L. Johnston, Air pollution and infection in respiratory illness, Br. Med. Bull. **68** (2003) 95–112.

[5] F. Pereraa, K. Weiland, M. Neidelld, S. Wang, Prenatal exposure to airborne polycyclic aromatic hydrocarbons and IQ: Estimated benefit of pollution reduction, J. Public Health Policy **35** (2014) 327–336.

[6] B. Ritz, F. Yu, S. Fruin, G. Chapa, G.M. Shaw, J.A. Harris, Ambient air pollution and risk of birth defects in Southern California, Am. J. Epidemiol. **155** (2002) 17–25.

[7] P. Vineis, K. Husgafvel-Pursiainen, Air pollution and cancer: biomarker studies in human populations, Carcinogenesis **26** (2005) 1846–1855.

[8] V.G. Berezkin, Y.S. Drugov, Gas Chromatography in Air Pollution Analysis, Elsevier Science, Amsterdam, 1991.

[9] J. Orphal, G. Bergametti, B. Beghin, P.-J. Hébert, T. Steck, J.-M. Flaud, Monitoring tropospheric pollution using infrared spectroscopy from geostationary orbit, C.R. Phys. **6** (2005) 888–889.

[10] W. Chang, M. Okamoto, T. Korenaga, A simple fluorometric method for the determination of sulfur dioxide in

ambient air with a passive sampler, Environ Sci. **13** (2006) 257–262.

[11] S.S. Brown, H. Stark, S.J. Ciciora, A.R. Ravishankara, In situ measurement of atmospheric NO_3 and N_2O_5 *via* cavity ring-down spectroscopy, Geophys. Res. Lett. **28** (2001) 3227–3230.

[12] G.G. Esposito, in: H.A. Gardner, G.G. Sward (Eds.), Chromatography in Paint Testing Manual, American Society for Testing and Materials, USA, 1972.

[13] V.J. Barwick, Sources of uncertainty in gas chromatography and high-performance liquid chromatography, J. Chromatogr., A **849** (1999) 13–33.

[14] O. Zuas, H. Budiman, Optimization of GC-TCD method for the measurement of CO_2, C_3H_8, and CO: Effec of flow rate carrier gas on GC's key parameters: A technical report RCChem-LIPI Serpong, 2014. (Unpublished)

[15] F.J. Bebbrecht, in: R.L. Grob (Eds.), Modern Practice of Gas Chromatography, 3rd ed., John Wiley & Sons, Canada, 1995.

[16] A.Y. El-Naggar, Factors affecting selection of mobile phase in gas chromatography, Am. J. Res. Commun. **1** (2013) 219–228.

[17] B.F. Tapah, R.C.D. Santos, G.A. Leeke, Processing of glycerol under sub and supercritical water conditions, Renew. Energ. **62** (2014) 353–361.

[18] S.S. Yaru, I.K. Adegun, M.A. Akintunde, Determination of thermo-physical properties of forty day incubation cattle dung biogas, Appl. Sci. Rep. **8** (2014) 168–174.

[19] Ó.L. Ramos, I. Reinas, S.I. Silva, J.C. Fernandes, M.A. Cerqueira, R.N. Pereira, A.A. Vicente, M.F. Poças, M.E. Pintado, F.X. Malcata, Effect of whey protein purity and glycerol content upon physical properties of edible films manufactured therefrom, Food Hydrocolloid **30** (2013) 110–122.

[20] Y. Liske, S. Kapila, V. Flanigan, P. Nam, S. Lorbert, Evaluation of Combustion Processes for Production of feedstock chemicals from ammonium sulfate and ammonium bisulfate, J. Hazard. Subst. Res. **2** (2000) 1–14.

[21] Z.S. Wu, M. Zhang, S. Wang, Effects of high pressure argon treatments on the quality of fresh-cut apples at cold storage, Food Control **23** (2012) 120–127.

[22] S. O-Thong, C. Mamimin, P. Prasertsan, Effect of temperature and initial pH on biohydrogen production from palm oil mill effluent: long-term evaluation and microbial community analysis, Elect. J. Biotechnol. **14** (2011) 1–12.

[23] Indonesian Ministry of Environmental, Regualtaion for Maxium emission level for motor vehicle: type new and current production. Reg. No. 04, 2009.

[24] Indonesian Ministry of Environmental, Regualtion for maximum emission level for motor vehicles: Type used, Reg. No. 05, 2006.

[25] I. Taverniers, M.D. Loose, E.V. Bockstaele, Trends in quality in the analytical laboratory, II: Analytical method validation and quality assurance, Trac-Trend Anal. Chem. **23** (2004) 535–552.

[26] R. Walker, I. Lumley, Pitfalls in terminology and use of reference materials, Trac-Trends Anal. Chem. **18** (1999) 594–616.

[27] P. Masson, Quality control techniques for routine analysis with liquid chromatography in laboratories, J. Chromatogr., A **1158** (2007) 168–173.

[28] EURACHEM, The Fitness for Purpose of Analytical Methods A Laboratory Guide to Method Validation and Related Topics, 1998, https://www.eurachem.org/.

[29] International Organization for Standardization, Guide 33: Uses of certified reference materials, 2000, http://www.iso.org/iso/

[30] V.P. Shah, K.K. Midha, J.W.A. Findlay, H.M. Hill, J.D. Hulse, I.J. McGilveray, G. McKay, K.J. Miller, R.N. Patnaik, M.L. Powell, A. Tonelli, C.T. Viswanathan, Bioanalytical method validation: A revisit with a decade of progress, Pharm. Res. **17** (2000) 1551–1557.

[31] G. Di Marco, M. de Andrade, C. Felipe, F. Alfieri, A. Gooding, H.T.J. Silva, J.O. Pestana, D. Casarini, Determination of sirolimus blood concentration using high-performance liquid chromatography with ultraviolet detection, Ther. Drug Monit. **25** (2003) 558–264.

[32] R.P.W. Scvott, Introduction to Analytical Gas Chromatography, 2nd ed., CRC Press, United Kingdom, 1997.

[33] E. Heftmann, Chromatography: Fundamentals and applications of chromatography and related differential migration methods - Part A: Fundamentals and techniques, Vol. 69, Elsevier Science, Amsterdam, 2004.

[34] D. Styarini, O. Zuas, H. Hamim, Validation and uncertainty estimation of analytical method for determination of benzene in beverages, Eurasian .J. Anal. Chem. **6** (2011) 159–172.

[35] Association of Official Analytical Chemists, Guide 3: How to Meet ISO 17025 Requirements for Method Verfication in The Analytical Laboratory Accreditation Criteria Committee, 2007, http://www.aoac.org

[36] National Association of Testing Authorities, Guidelines for the validation and verification of quantitative and qualitative test methods, 2013, http://www.nata.com.au

[37] International Organization for Standardization, IS0 5725-1986(E): Precision of Test Methods-Repeatability and reproducibility, 1986, http://www.iso.org/

[38] C. McAlinden, J. Khadka, K. Pesudovs, A Comprehensive Evaluation of the Precision (Repeatability and Reproducibility) of the Oculus Pentacam HR, Invest. Ophthalmol. Vis. Sci. **52** (2011) 7731–7737.

[39] H. Hovind, B. Magnusson, M. Krysell, U. Lund, I. Mäkine, Internal Quality Controll–Handbook for chemical laboratories, NORDTEST Report TR 569, Nordic Innovation Stensberggata, Oslo, 2011.

IZVOD

PROCENJIVANJE PERCIZNOSTI I TAČNOSTI GC-TCD METODE ZA ODREDJIVANJE UGLJEN-DIOKSIDA, PROPANA I UGLJEN-MONOKSIDA PRI RAZLIČITIM PROTOCIMA GASNOG NOSAČA

Oman Zuas, Harry Budiman

Gas Analysis Laboratory (GasAL), Electrochemistry & Gas Metrology Research Group, Research Centre for Chemistry--Indonesian Institute of Sciences (RCChem-LIPI), Kawasan PUSPIPTEK Serpong 15314, Tangerang, Indonesia

(Naučni rad)

U radu je sprovedeno istraživanje preciznosti i tačnosti metode gasne hromatografije opremljene toplotnim konduktivnim detektorom (GC-TCD) za merenje CO_2, C_3H_8 i CO postavljenih za modele zagadjivača pri različitim iznosima helijuma (He) kao gasnog nosača u rasponu od 17,50 do 36,25 ml/min. Pronadjeno je da je vrednost standardne devijacije (*RSD*) i za preciznost i za tačnost pokazala sveukupni postepeni pad sa povećanjem protoka gasnog nosača sve do 25ml/min. *RSD* se i dalje povećavala rastao sa povećanjem protoka i preko ove vrednosti. Ovi nalazi su ukazali na to da je protok od 25 ml/min je najpouzdaniji od svih protoka testiranih pod eksperimentalnim uslovima u toku ovog istraživanja. Detaljno su prikazane sve vrednosti *RSD* koje su dobijene. Rezultati ukazuju na to da je protok gasnog nosača ključni parametar za preciznost GC-TCD metode. Imajući u vidu da je gasni nosač transporter komponenti kroz kolonu, uspostavljanje optimalnog protoka gasnog nosača je važno kako bi se dostigla preciznost i tačnost GC-TCD metode.

Ključne reči: Preciznost • Tačnost • Gasna hromatografija • Izduvni gasovi vozila • Zagadjivač

N-alkylphenothiazines – synthesis, structure and application as ligands in metal complexes

Milena Krstić[1], Sofija Sovilj[2], Sunčica Borozan[1], Milica Rančić[3], Jelena Poljarević[2], Sanja R. Grgurić-Šipka[2]

[1]*Faculty of Veterinary Medicine, University of Belgrade, Serbia*
[2]*Faculty of Chemistry, University of Belgrade, Serbia*
[3]*Faculty of Forestry, University of Belgrade, Serbia*

Abstract

Phenothiazines are a large group of heterocyclic, aromatic molecules with nitrogen and sulphur between two benzene rings. Their derivatives, *N*-alkylphenothiazines have substituent on heterocyclic nitrogen atom which gives them different properties. Also, a series of these molecules have substitution on carbon atom at place 2 of phenothiazine benzene ring. Alkylphenothiazines contain aminoalkyl substituent and their alkyl, acyl and sulphonil derivatives, as well as monocyclic and bicyclic heterocycles attached at thiazine nitrogen atom or directly linked to benzene ring. The *N*-alkylphenothiazines have been known as antipsychotic drugs, but they also possess antibacterial, antifungal, anticancer activity, and ability to react with macromolecules and to coordinate to the metals. Metal complexes with *N*-alkylphenothiazines are biological active compounds with different antimicrobial activities and cytotoxic effect against tumor cell lines. The large field of application of *N*-alkylphenothiazines is very attractive in terms of synthesis of new related derivatives, metal complexes, studying their properties and applications. This article presents a review of the literature and a contemporary view at *N*-alkylphenothiazines – their synthesis and application, as well as their metal complexes which have promising biological effects.

Keywords: *N*-alkylphenothiazines, antipsychotic drugs, anticancer, antibacterial.

Available online at the Journal website: http://www.ache.org.rs/HI/

REVIEW PAPER

UDC 547.869:61:615

Hem. Ind. **70** (4) 461–471 (2016)

doi: 10.2298/HEMIND150331052K

The *N*-alkylphenothiazines are heterocyclic aromatic compounds with nitrogen and sulphur atoms and substituents on aromatic ring and nitrogen. The central place of these molecules is a molecule of 10*H*-dibenzo-1,4-thiazine, phenothiazine (Fig. 1) known more than a hundred years [1].

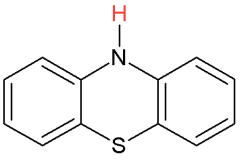

Figure 1. Structure of the 10-H-dibenzo-1,4-thiazine, phenothiazine.

The first phenothiazines, thionine and methylene blue (Fig. 2) were synthesized in reaction of *p*-phenylendiamine/*p*-aminodimethylaniline with sulphur in hydrochloric acid solution, in the middle of the 19th century [2]. In that time, these compounds with phenothiazine ring had an application in aniline dye industry.

After 20 years, the parent compound, 10*H*-dibenzo-1,4-thiazine was obtained in reaction of diphenylamine with sulphur by Bernthsen (Scheme 1). Until today, more than 5000 phenothiazine derivatives were synthesized with wide range of application [1].

Phenothiazines have many different applications, from industry to medicine. As biological active compounds, these molecules have antipsychotic, antiemetic, anthelmintic, antibacterial, antifungal and insecticidal properties, and they also represent promising anticancer drugs [1–8]. These activities represent the result of the interaction of phenothiazines with biological systems through their pharmacophoric substituent, the multicyclic ring system (π-π interaction, intercalation in DNA) or the lipophilic character allowing the penetration through the biological membranes. The activities were examined by using various biological systems such as cell lines, bacteria, viruses, parasites, laboratory mice, rats and rabbits, and monolayer and bilayer membranes [2]. The *N*-alkylphenothiazines as ligands are used in metal complexes, but biological properties of these complexes are investigated in recent years. This review shows current importance of the *N*-alkylphenothiazines and reveals their metal complexes as potent pharmacological group which can be a rich source of new compounds having desirable biological activities.

Structure of *N*-alkylphenothiazines

Most often, phenothiazines have substituted hydrogen atoms at position 2 (with some small molecule)

Correspondence: M. Krstić, Faculty of Veterinary Medicine, University of Belgrade, Bulevar oslobodjenja 18, 11000 Belgrade, Serbia.
E-mail: milena@vet.bg.ac.rs
Paper received: 31 March, 2015
Paper accepted: 25 August, 2015

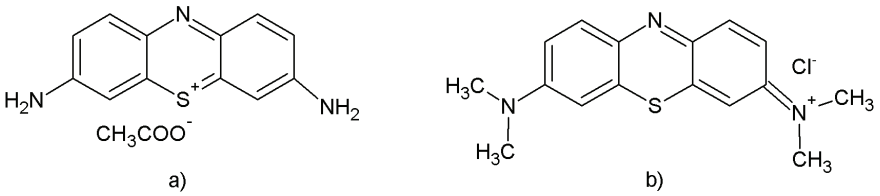

Figure 2. Structure of the 3,7-diamino-5-phenothiazinium acetate (thionine) and 3,7-bis(dimethylamino)phenazathionium chloride (methylene blue).

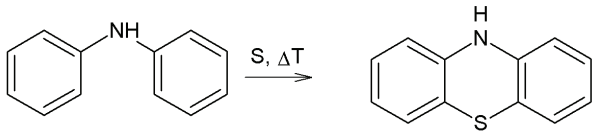

Scheme 1. Synthesis of 10-H-dibenzo-1,4-thiazine (phenothiazine).

and position 10 (with aminoalkyl groups). At this point, *N*-alkylphenothiazines (Figure 3) are classified into three groups depending on the type of the substitution on the nitrogen atom of phenothiazine ring [9,10]. First group contains phenothiazines with an aliphatic side chain, then the second group with the piperidine, and the third group contains piperazine derivatives (Table 1).

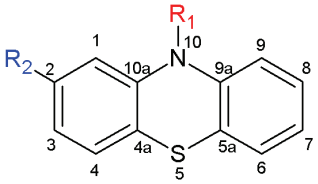

Figure 3. General structure of N-alkylphenothiazine.

Table 1. N-alkylphenothiazines classification depends on the type of substituent on N-10 and C-2 atoms

Compound	R_1	R_2
Phenothiazines with an aliphatic side chain		
Promazine (Pr)	$(CH_2)_3$–$N(CH_3)_2$	H
Chlorpromazine (Cpz)	$(CH_2)_3$–$N(CH_3)_2$	Cl
Triflupromazine (Tm)	$(CH_2)_3$–$N(CH_3)_2$	CF_3
Methotrimeprazine (Mtm)	CH_2–$CH(CH_3)$–$N(CH_3)_2$	OCH_3
Phenothiazines with a piperidine side chain		
Thioridazine (Tr)	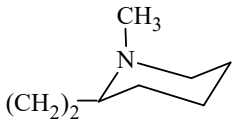	$S(CH_3)$
Mesoridazine (Mr)	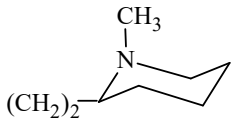	$SO(CH_3)$
Sulphoridazine (Sr)	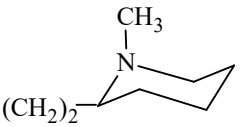	$OSO(CH_3)$
Phenothiazines with a piperazine side chain		
Prochlorperazine (Pc)	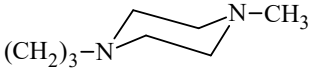	Cl
Trifluoperazine (Tf)	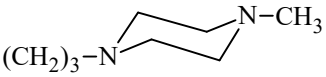	CF_3
Perphenazine (Pz)	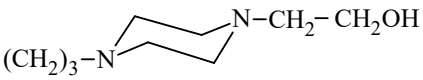	Cl

Table 1. Continued

Compound	R_1	R_2
	Phenothiazines with a piperazine side chain	
Fluphenazine (Fz)	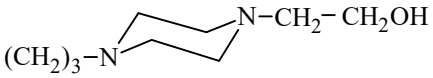	CF_3
Thioprozapate (Tp)	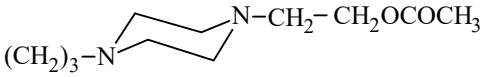	Cl

The new derivatives of phenothiazines are synthesized from the parent phenothiazines in several directions: substitution of new groups with the thiazine nitrogen atom [11], an introduction of a new substituent at positions 1–4 and 6–9 aromatic rings, oxidation of the sulfide sulfur atom to a sulfoxide or sulfone group, as well as a substitution one or both benzene ring with homoaromatic or heteroaromatic rings [1].

Synthesis of *N*-alkylphenothiazines

Promazine, *N*,*N*-dimethyl-3-(10*H*-phenothiazin-10--yl)-propan-1-amine, is synthesized by the alkylation of phenothiazines with 3-dimethylaminopropylchloride in the presence of sodium amide (Scheme 2) [12].

Chlorpromazine, 3-(2-chloro-10*H*-phenothiazin-10--yl)-*N*,*N*-dimethyl-propan-1-amine is prepared following two steps: in the first step, 3-chlorodiphenylamine with sulphur gives as product 2-chloro-10*H*-phenothiazine, while in the second step, this compound reacts with 3-dimethylaminopropylchloride, similar to the synthesis of promazine (Scheme 3) [12].

Trifluopromazine, *N*,*N*-dimethyl-3-[2-(trifluoromethyl)-10*H*-phenothiazin-10-yl]propan-1-amine (Fig. 4) is also prepared by alkylation of 2-trifluoromethyl--10*H*-phenothiazine in the presence of sodium amide [12].

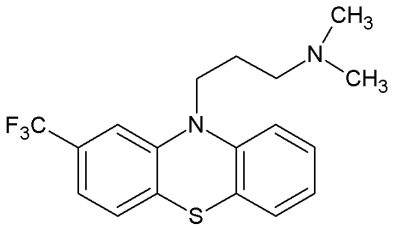

Figure 4. Structure of the N,N-dimethyl-3-[2-(trifluoromethyl)--10H-phenothiazin-10-yl]propan-1-amine, (trifluopromazine).

A series of molecules has substitution on carbon atom at position 2 of phenothiazine benzene ring of promazine as methopromazine (possess methoxy group) and acetopromazine (with aceto group on C-2 atom) which are synthesized in similar way.

Phenothiazines with a piperidine side chain, thioridazine 10-[2-(1-methyl-2-piperidyl)ethyl]-2-(methylthio)-10*H*-phenothiazine and mesoridazine 10-[2-(1--methyl-2-piperidyl)ethyl]-2-(methylsulfinyl)-10*H*-phenothiazine are also synthesized by alkylation of methylsulphonil-10*H*-phenothiazine/2-methylthio-10*H*-pheno-

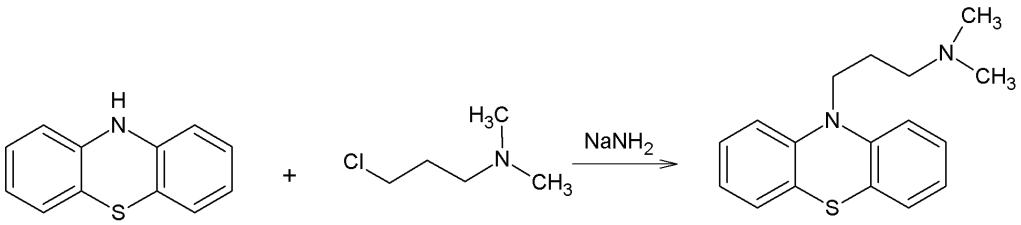

Scheme 2. Synthesis of N,N-dimethyl-3-(10H-phenothiazin-10-yl)-propan-1-amine(promazine).

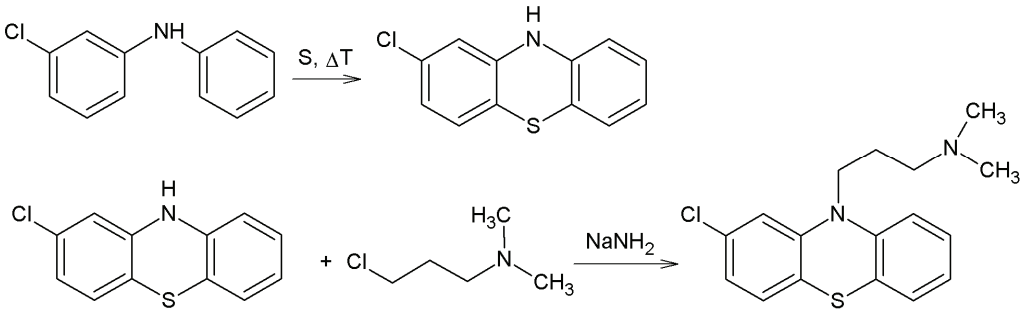

Scheme 3. Synthesis of 3-(2-chloro-10H-phenothiazin-10-yl)-N,N-dimethyl-propan-1-amine (chlorpromazine).

thiazine using 2-(2-chloroethyl)-1-methylpiperidine in the presence of sodium amide (Scheme 4) [12].

At last, phenothiazines with piperazines chain, prochlorperazine, 2-chloro-10-[3-(4-methyl-1-piperazinyl)-propyl]-10*H*-phenothiazine and trifluoperazine, 10-[3--(4-methylpiperazin-1-yl)propyl]-2-(trifluoromethyl)--10*H*-phenothiazine are prepared by alkylation of 2-chloro-10*H*-phenothiazine/2-trifluoromethyl-10*H*-phenothiazine using 4-methyl-1-piperazinylpropylchloride in presence of sodium amide (Scheme 5) [12].

Perphenazine, 2-[4-[3-(2-chloro-10*H*-phenothiazin--10-yl)propyl]piperazin-1-yl]ethanol, and fluphenazine, 2-[4-[3-(2-(trifluoromethyl)-10*H*-phenothiazin-10-yl)propyl]piperazin-1-yl]ethanol, are synthesized in a similar way as previously described. In the first step, 2-chloro--10*H*-phenothiazine/2-trifluoromethyl-10*H*-phenothiazine is alkylated using 4-formyl-1-piperazinylpropylchloride in the presence of sodium amide and then *N*-formyl group was removed by alkaline hydrolysis giving the intermediate product (Scheme 6). The final step is alkylation of intermediate compound by 2-bro-

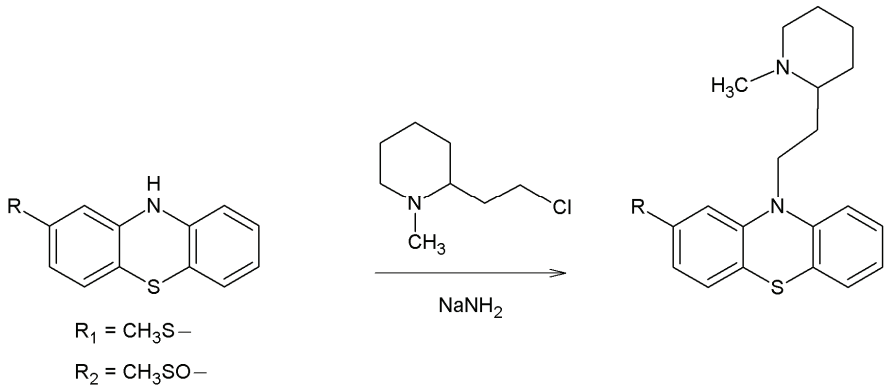

Scheme 4. Synthesis of 10-[2-(1-methyl-2-piperidyl)ethyl]-2-(methylthio)-10H-phenothiazine (thioridazine, R_1) and 10-[2-(1-methyl-2--piperidyl)ethyl]-2-(methylsulfinyl)-10H-phenothiazine (mesoridazine, R_2).

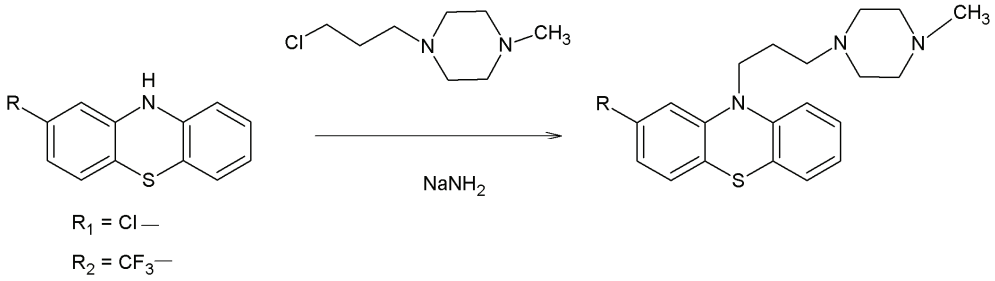

Scheme 5. Synthesis of 2-chloro-10-[3-(4-methyl-1-piperazinyl)propyl]-10H-phenothiazine (prochlorperazine, R_1) and 10-[3-(4-methyl-piperazin-1-yl)propyl]-2-(trifluoromethyl)-10H-phenothiazine (trifluoperazine, R_2).

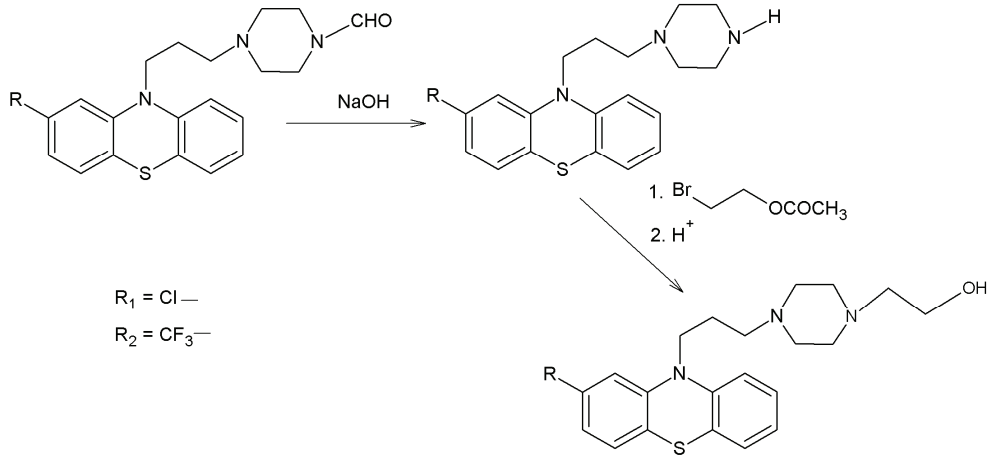

Scheme 6. Synthesis of 2-[4-[3-(2-chloro-10H-phenothiazin-10-yl)propyl]piperazin-1-yl]ethanol (perphenazine, R_1) and 2-[4-[3-[2-(trifluoromethyl)-10H-phenothiazin-10-yl]propyl]piperazin-1-yl]ethanol (fluphenazine, R_2).

methanol-1-acetate by acid hydrolysis which removes acetyl group [12]. Also, these molecules contain an alcohol group which provides an opportunity for derivatization in order to obtain new compounds with pharmacological using.

Use and application

The phenothiazine group of compounds has the great spectrum of application from industry to medicine for more than a century due to their diverse syntheses. Substituted phenothiazines have been used for the preparation of the polymers [13], the solar cells [14,15], biological stains [16], as well as medicaments [12]. They possess antimicrobial [6,21–24], anthelmintic [7], antiemetic [8], antihistaminic [8] anticancer properties [2], and they are used in clinical practice more than 50 years as antipsychotics [12,17].

In many researches, it was shown that *N*-alkylphenothiazines possess antimicrobial activity [18–20]. Kristiansen *et al*. [18] demonstrated that chlorpromazine and thioridazine reduce the susceptibility of methicillin-resistant *Staphylococcus aureus* (MRSA) while Martins *et al*. [19] in their research classified a few *N*-alkylphenothiazines as non-antibiotics (helper compounds) in the treatment of multidrug resistant Gram-negative infections. As anthelmintics, phenothiazines reduced faecal eggs of resistant strains of three nematodes*, Haemonchus contortus, Trichostrongylus colubriformis* and *Ostertagia spp.*, but without significant effect on worm number [7].

Phenothiazines have been shown to inhibit *in vitro* growth of multi drug resistance strain (resistant to rifampin and isoniazid) *Mycobacterium tuberculosis*. The killing of intracellular bacteria promoted by phenothiazine can inhibit many transport processes of potassium and calcium pump activation. The increased permeability ensures phenothiazine molecules to reach the DNA, intercalate between the bases, inhibit the entire DNA and hence inhibit transcription and translation processes [21]. The ability of chlorpromazine to cure tuberculosis resulted in a series of *in vitro* studies that showed that chlorpromazine was more effective antimycobacterial compound than other *N*-alkylphenothiazines [21–24]. Because chronic administration of chlorpromazine is known to produce a wide range of mild-to-severe side effects, the use of this compound in tuberculosis therapy was not seriously considered. Thioridazine can more effectively accelerate the recovery of infected mice from *Mycobacterium tuberculosis,* as shown in preliminary study [24], providing strong direct evidence that thioridazine, a neuroleptic that is milder and less toxic than chlorpromazine, kills intracellular *Mycobacterium tuberculosis* isolates that are resistant to two or more antibiotics [22]. These investigations indicate that phenothiazines have been considered as an adjuvant for the treatment of *Mycobacterium tuberculosis.*

The blockade of histamine receptors in brain gives sedative effect to the most of *N*-alkylphenothiazines. Prochlorperazine, promethazine and perphenazine are known as antipsychotic drugs which block postsynaptic dopaminergic receptors in the brain and have antiemetic effects by their antagonic actions in the dopamine receptors (D2) predominantly, but also may possess antagonist actions at histamine 1, cholinergic M1 and α_1-adrenergic receptors in the vomiting center to reduce nausea and vomiting [8]. Promethazine hydrochloride is in pharmacological use as Phenergan cream, topical antihistaminic preparation for systemic eczematous dermatitis.

Phenothiazines as lipophylic molecules are interacting with various macromolecules and possess anticancer activity. Chlorpromazine, promethazine, thioridazine and trifluoperazine, in clinically relevant plasma concentrations 2–36 μM, markedly decreased the viability of leukemic cells without any toxic effects on normal lymphocytes [25]. Phenothiazines show antiproliferative activity against breast, ovarian, lung, CNS, prostate and melanoma cell lines. Trifluoperazine, chlorpromazine and thioridazine in concentration up to 20 μM expressed a selective cytotoxicity, as well as antiproliferative activity and induced apoptosis [4]. Also, *N*-alkylphenothiazines have the capacity to increase the lethal effect at low doses of the therapeutic drugs [26]. Cytotoxicity of these compounds could be attributed to oxidative stress, *via* glutathione oxidation and lipid peroxidation.

The most common application of phenothiazines is in psychiatry [10,17]. Modern psychopharmacology cannot be imagined without chlorpromazine. Chlorpromazine was synthesized in 1951 by Paul Charpentier, and became available on prescription in France in 1952, under the proprietary name of Largactil as pharmaceutical drug [17]. In medical practice, chlorpromazine is used in the treatment of patients with schizophrenia, neurosis, manic-depressive condition and chronic paranoids, alcoholic psychoses as well as for stress-sampled neuroses, insomnia and fears. Promazine and triflupromazine have similar application. Trifluoperazine is one of the most active antipsychotic drugs with common synonyms in pharmacy as stelazine, triftazin and others. This drug has strong anticonvulsant activity and it is used in treatment for schizophrenia and other mental diseases. Mesoridazine has application for behavior problems, schizophrenia, chronic alcoholism and other. Phenothiazines with aliphatic side chain and piperidine substituent have more pronounced sedative effect than piperazine derivatives. These molecules are non-selective and competitive D_1 and D_2 antagonists that block dopamine activity at corresponding receptor

site. Also, their activity could be expressed by blocking α-adenoreceptors, serotonine, cholinergic, nicotine and muscarinic receptors [12].

In the aim of finding new applications of these compounds, they are used as ligands in coordination chemistry. Until today many complexes containing *N*-alkylphenotiazines are synthesized and characterized. Gowda and his group [27,28] prepared Ir(III) and Pd(II) complexes with *N*-alkylphenothazines and proposed heterocyclic S atom coordination. Keshavan *et al*. synthesized many complexes of lanthanide with *N*-alkylphenothiazines indicating that the tertiary nitrogen, as well as phenothiazine's nitrogen, represents the coordination site of ligand [29,30]. Also, complexes of lanthanide showed moderately antibacterial activity against some Gram-positive and Gram-negative bacteria. The structure of lanthanide complexes with phenothiazine was determined by X-ray single crystal diffraction analysis (Fig. 5) displaying lantanide- nitrogen bond [31].

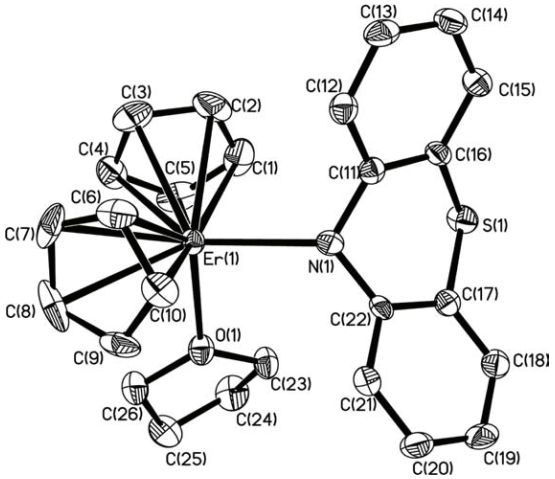

Figure 5. ORTEP diagram of complex (C_5H_5)2ErPtz(THF) [22].

The complex $HgCl_2(ptz)]_2{\cdot}HgCl_2$ was synthesized by reaction of $HgCl_2$ and phenothiazine in benzene as dark-blue powder [32]. The final products were characterized by X-ray diffraction which confirmed S-coordination of phenothiazine (Fig. 6).

A series of conjugated polymers with bipyridine groups were synthesized successfully *via* Suzuki coupling polycondensation using carbazole and phenothiazine as the main chain moieties. Through a one-pot post-functionalization reaction, ruthenium complexes were introduced into the polymer through a flexible spacer in high yields, which lead to a new simplified strategy to synthesize this special type of conjugated polymer with metal complex linked to pendant groups through a flexible chain. Furthermore, the obtained Ru-containing polymers PM1PT-x-Ru exhibited broad absorption in the visible region, and possessed a narrow electrochemical band gap (approximately 1.36–1.42 eV) and low HOMO energy level (about 5.47–5.34 eV), indicating that they are suitable candidates as photosensitive materials for solar cells [33].

Platinum complexes with chlorpromazine and trifluoperazine were prepared from $K_2[PtCl_6]$ in water (Scheme 7). Complexes were characterized by spectral (IR, ^1H, ^{13}C, 2D ^1H–^{13}C heteronuclear correlation spectra, ^{195}Pt NMR and MS) analysis. Outer-coordination sphere was proposed for ((TFH·HCl)$[PtCl_5H_2O]$), while in ((CP·H)$[Pt(CP{\cdot}HCl)Cl_5]{\cdot}H_2O$), the ligand was coordinated to the metal *via* heterocyclic sulphur. The complexes exhibit antibacterial effect on strains of *Bacillus subtilis, Bacillus cereus, Bacillus pumilus* and methicillin-resistant *Staphylococci* as Gram-positive bacteria, and an *Escherichia coli* as Gram-negative bacteria, as well as the reference strains [34].

Ru(II) complexes with *N*-alkylphenothiazines

Three new complexes of the general formula $L[RuCl_3(DMSO)_3]$ (**1**–**3**), where L is chlorpromazine hydrochloride, trifluoperazine dihydrochloride or thioridazine hydrochloride, were prepared by the reaction of the starting complex $[RuCl_2(DMSO)_4]$ and the corresponding ligands in a mole ratio of 1:1.6 in absolute ethanol [35]. The complexes were characterized by elemental analysis and spectroscopic methods. The crystal structure of the complex (TF.H2)$[RuCl_3(DMSO)_3]Cl{\cdot}C_2H_5OH$ contains trifluoperazine dihydrochloride in outsphere position, but its chloride atom had substituted one of DMSO molecules in starting complex and coordinated to the Ru(II) atom (Fig. 7).

The investigation of antitumor properties of complexes **1**–**3** in four human cell lines (MCF-7, MDA-MB-453, SW-480 and IM9) showed dose-dependence and

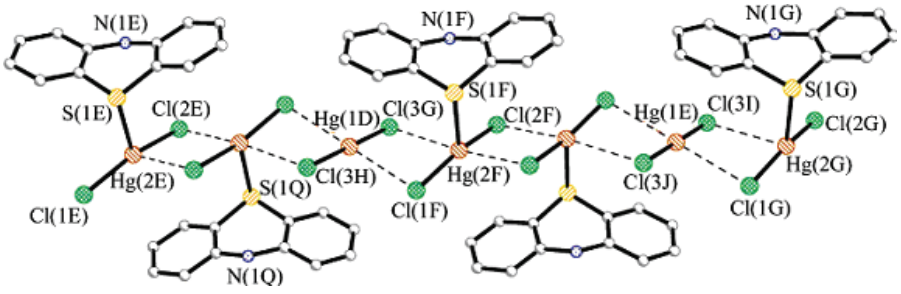

Figure 6. ORTEP diagram of complex $[HgCl_2(ptz)]_2{\cdot}HgCl_2$ [23].

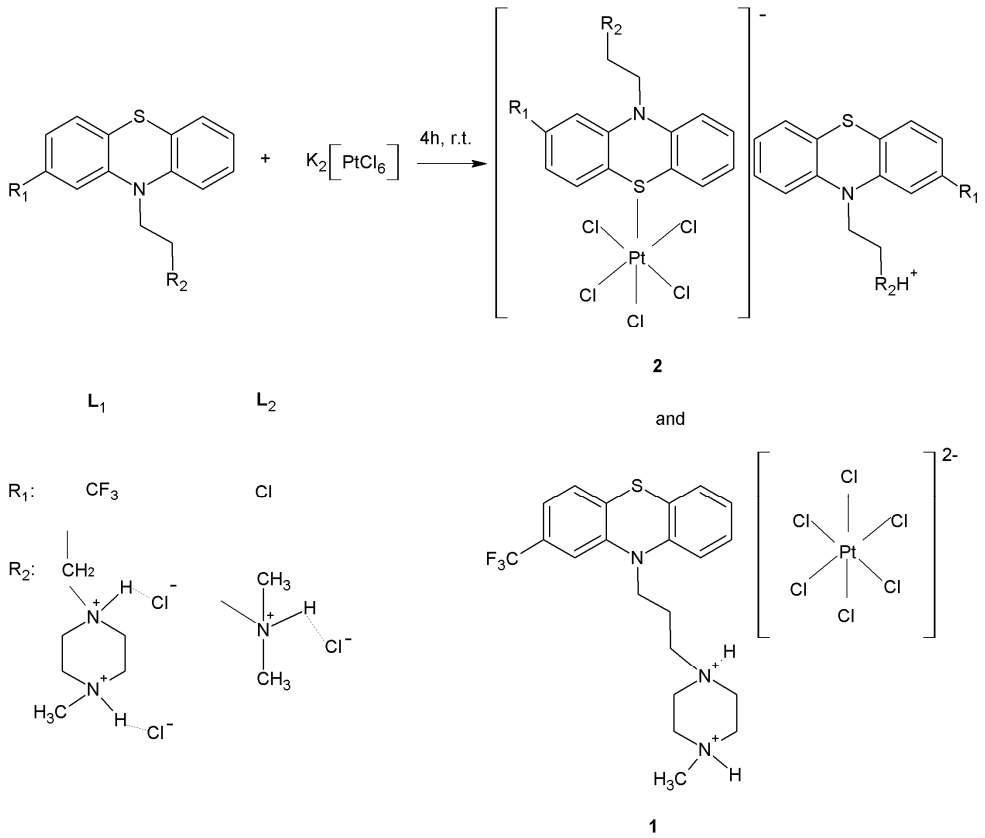

Scheme 7. Reaction scheme for synthesis Pt(II) complexes with chlorpromazine hydrochloride and trifluoperazine dihydrochloride.

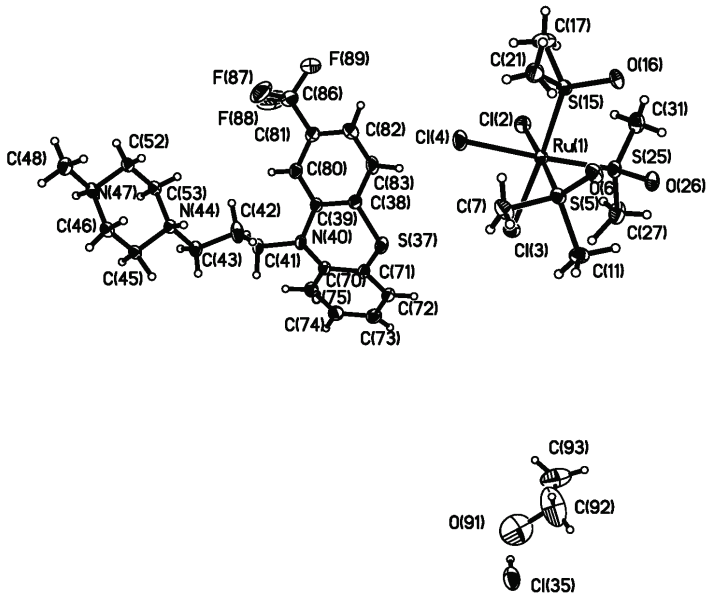

Figure 7. Asymmetric unit of (TF.H2)[$RuCl_3(DMSO)_3$]Cl·C_2H_5OH.

variation by cell types. The most active compound is complex (CP.H)[$RuCl_3(DMSO)_3$]·C_2H_5OH, which demonstrates a higher activity against MCF-7 and IM9, but it is less effective against other cell lines and did not cause complete cell death. Complex:
(TF.H2)[$RuCl_3(DMSO)_3$]Cl·C_2H_5OH is the most sensitive against human breast cancer cell line (MDA-MB-453) and human colon adenocarcinoma cell line (SW-480), while other two complexes were active even in low concentrations, and induced almost total cell death at 25 μM during 48 h of treatment. Moreover, complex (TF.H2)[$RuCl_3(DMSO)_3$]Cl·C_2H_5OH is

the only compound in our investigations displaying cytotoxic activities against all tumour cell lines. The selective cytotoxicity of these complexes, especially complex (TF.H2)[$RuCl_3(DMSO)_3$]Cl·C_2H_5OH, against the cancer cells suggests their great potential for development as anticancer drugs. It is also investigated the effect of this complex on antioxidative enzymes in rat blood. Biological assays provide the clear evidence that complex (TF.H2)[$RuCl_3(DMSO)_3$]Cl·C_2H_5OH under physiological conditions can act as a scavenger of $NO^{\cdot}$ radicals in lower doses of 0.4 and 4.5 μM/kg bw, and as a scavenger of free radicals, such as superoxide anion and hydroxyl radicals (Fig. 8). This compound also influences the SOD and CAT activities, even in dose of 90.4 μM/kg bw. As non-toxic compound under physiological conditions, this complex could provide potential therapeutic benefits in lower doses (0.4 and 4.5 μM/kg bw) for disorders where these reactive species are involved.

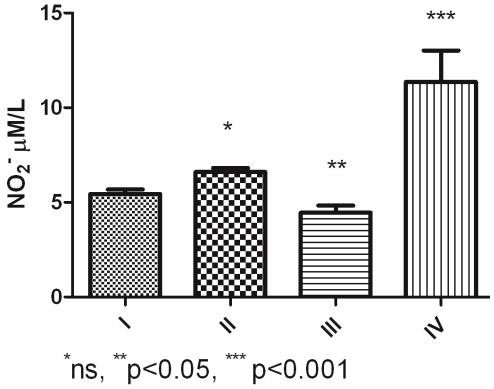

Figure 8. Content of $NO_2^{\cdot}$: I – control group; I – rats treated i.p. with complex (TF.H2)[$RuCl_3(DMSO)_3$]Cl·C_2H_5OH at dose of 0.4 μM/kg bw; III-rats treated i.p. with complex (TF.H2)[$RuCl_3(DMSO)_3$]Cl·C_2H_5OH at dose of 4.5 μM/kg bw; IV – rats treated i.p. with complex (TF.H2)[$RuCl_3(DMSO)_3$]Cl·C_2H_5OH at dose of 90.4 μM/kg bw.

The thermal decomposition pattern of the starting complex [$RuCl_2(DMSO)_4$] and complexes L[$RuCl_3(DMSO)_3$], where L is protonated chlorpromazine hydrochloride, trifluoperazine dihydrochloride or thioridazine hydrochloride, does not depend on the atmosphere: the thermal curves are almost identical in nitrogen and air atmospheres [36]. Also, decomposition of these complexes is not completed at 700, but near 1000 °C as residue is elemental ruthenium. This property of complexes is in agreement to biological potential and provides an opportunity for these compounds to adapt to different ambient conditions.

In reaction of *N*-alkylphenothiazines with [$RuCl_2(\eta^6$-*p*-cymene)]$_2$ in 2-propanol, after about 3 h, orange precipitate was formed. As in previously research, complex with trifluoperazine gave single crystal for X-ray analysis (Fig. 9). The crystal structure of complex 2 contains the Ru center in a pseudo-octahedral "piano-stool" geometry, with *p*-cymene and three chloride ions in the coordination sphere, and *N*-alkylphenothiazine in the outer-sphere. *In vitro* cytotoxic activities of complexes were assayed in four human carcinoma cell lines MCF-7, MDA-MB-453, SW-480 and IM9. The highest cytotoxicity (12.1 ≤ *IC50* ≤ 17.3 μM) and induced a total (SW-480) or almost total cell death (MCF-7, MDA-MB-453) at 25 μM in 48 h of treatment were observed for complex (TF.H2)[$RuCl_3(\eta^6$-*p*-cymene)] Cl·C_3H_7OH [37].

Biological assays provide clear evidence that this compound demonstrates a positive effect on the heart muscle, as suggested by unchanged LDH1 levels and a lower level of LDH2. Complex (TF.H2)[$RuCl_3(\eta^6$-*p*-cymene)] Cl·C_3H_7OH inhibited SOD activity in all doses, although influence on CAT activity was not observed. Results of this study suggest the cardio protective potential of complex (TF.H2)[$RuCl_3(\eta^6$-*p*-cymene)] Cl·C_3H_7OH, since the decreased activity of LDH2 was revealed after its oral administration. This investigation illustrates the potential of Ru(II)-cymene complexes with pharmacologically active substances as novel and promising bioinorganic drugs.

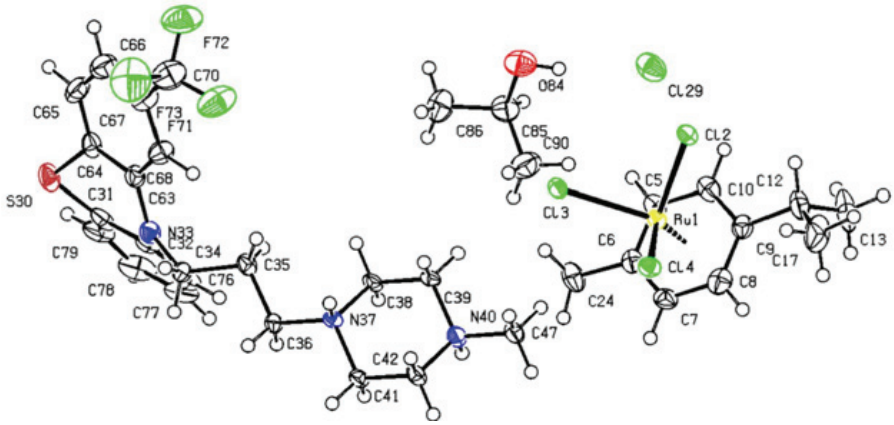

Figure 9. Asymmetric unit of (TF.H2)[$RuCl_3(\eta^6$-p-cymene)] Cl·C_3H_7OH.

Thermal analysis of these complexes were shown a great thermal stability of starting complex $[RuCl_2(\eta^6\text{-}p\text{-cymene})]_2$, while thermal decomposition of chlorpromazine's and trifluoperazine's Ru-complex began at low temperature [38].

CONCLUSIONS

The phenothiazine belongs to the group of heterocyclic aromatic compounds with nitrogen and sulphur atoms. The *N*-alkylphenothiazines are formed in the reaction of substitution on the nitrogen atom of phenothiazines ring with aliphatic side chain, piperidine, piperazine or with some new group of molecule. The other substituent is at carbon atoms in position 2 of benzene ring, but new generation of *N*-alkylphenothiazines introduces substituent at position 1-4 and 6-9 at the benzene ring. These molecules possess many applications, but the most important implementation is in medicine. They are medicinal drugs with the major effect on central nervous system almost irreplaceable in treatment of mental diseases. Many of them have shown cytotoxic effect against different cancer cell lines or in small doses supported the therapeutic drugs to lead apoptosis of cancer cells.

N-alkyphenothiazines are also used in synthesis of metal complexes which showed antibacterial activity. Complexes of Ru(II) with *N*-alkylphenothoazines showed significant anticancer activity against four cancer lines. These complexes possess positive effect in small doses on antioxidant enzymes, as well as the complex (TF.H2)[$RuCl_3(\eta^6\text{-}p\text{-cymene})$] $Cl{\cdot}C_3H_7OH$ demonstrated cardio protective potential by decreased activity of LDH2 isoenzymes. Having into consideration all of the above, *N*-akylphenothiazines have promising potential in both bioinorganic chemistry and medicine in the future.

Acknowledgements

The study was financed by the Ministry of Education, Science and Technological Development of the Republic of Serbia (Grant No. 172014).

REFERENCES

[1] K. Pluta, B. Morak-M1odawska, M. Jeleń, Recent progress in biological activities of synthesized phenothiazines, Eur. J. Med. Chem. **46** (2011) 3179–3189.

[2] S.C. Mitchell, Phenothiazines: The Parent Molecule, Curr. Drug Targets **7** (2006) 1181–1189.

[3] J.J. Aaron, M.D.G. Seye, S. Trajkovska, N. Motohashi, Bioactive Phenothiazines and Benzo[*a*]phenothiazines: Spectroscopic Studies, and Biological and Biomedical Properties and Applications, Top. Heterocycl. Chem. **16** (2009) 153–231.

[4] N. Motohashi, M. Kawase, K. Satoh, H. Sakagami, Cytotoxic Potential of Phenothiazines, Curr. Drug Targets **7** (2006) 1055–1066.

[5] Z. Zhelev, H. Ohba, R. Bakalova, V. Hadjimitova, M. Ishikawa, Y. Shinohara, Y. Baba, Phenothiazines suppress proliferation and induce apoptosis in cultured leukemic cells without any influence on the viability of normal lymphocytes, Cancer Chemother. Pharmacol. **53** (2004) 267–275.

[6] M. Martins, S.G. Dastidar, S. Fanning, J.E. Kristiansen, J. Molnar, J.-M. Pages, Z. Schelz, G. Spengler, M. Viveiros, L. Amaral, Potential role of non-antibiotics (helper compounds) in the treatment of multidrug-resistant Gram-negative infections: mechanisms for their direct and indirect activities, Int. J. Antimicrob. Agents **31** (2008) 198–208.

[7] J.D. Kelly, H.V. Whitlock, M. Gunawan, D. Griffin, C.J. Porter, I.C. Martin, Anthelmintic efficacy of low-dose phenothiazine against strains of sheep nematodes susceptible or resistant to thiabendazole, levamisole and morantel tartrate: effect on patent infections, Res. Vet. Sci. **30** (1981) 161–169.

[8] H.S. Smith, L.R. Cox, B.R. Smith, Dopamine receptor antagonists, Ann. Palliat. Med. **1** (2012) 137–142.

[9] K.H. Chen, C.E. Lin, W.S. Liao, W. Y. Lin, Y.Y. Hsiao, Separation and migration behavior of structurally related phenothiazines in cyclodextrin-modified capillary zone electrophoresis, J. Chromatogr., A **979** (2002) 399–408.

[10] A. Jaszczyszyn, K. Gsiorowski, P. Switaek, W. Malinka, K. Cieoelik-Boczula, J. Petrus, B. Czarnik-Matusewicz, Chemical structure of phenothiazines and their biological activity, Pharmacol. Rep. **64** (2012) 16–23.

[11] G.C. González-Muñoz, M.P. Arce, B. López, C. Pérez, A. Romero, L. Barrio, M.D.M. Saavedra, J. Egea, R. León, M. Villarroya, M.G. López, A.G. García, S Conde, M.I.R. Franco, *N*-acylaminophenothiazines: Neuroprotective agents displaying multifunctional activities for a potential treatment of Alzheimer's disease, Eur. J. Med. Chem. **46** (2011) 2224–2235.

[12] R.S. Vardanyan, V.J. Hruby, Synthesis of Essential Drugs, Elsevier, Amsterdam, 2006.

[13] S.S. Nikulin, V.M. Misin, V.M. Komarov, M.V. Misin, Synthesis and Properties of 2-Vinylphenothiazine Polymers, Russ. J. App. Chem. **76** (2003) 1327–1330.

[14] M.A. Reddy, B. Vinayak, T. Suresh, S. Niveditha, K. Bhanuprakas, S.P. Singh, A. Islam, L. Han, M. Chandrasekharam, Highly conjugated electron rich thiophene antennas on phenothiazineand phenoxazine-based sensitizers for dye sensitized solar cells, Synthetic Met. **195** (2014) 208–216.

[15] R.Y.Y. Lin, T.M. Chuang, F.L. Wu, P.Y. Chen, T.C. Chu, J.S. Ni, M.S. Fan, Y.H. Lo, K.C. Ho, J.T. Lin, Anthracene/Phenothiazine p-Conjugated Sensitizers for Dye-Sensitized Solar Cells using Redox Mediator in Organic and Water-based Solvents, Chem. Sus. Chem. **8** (2015) 105–113.

[16] M. Wainwright, The use of dyes in modern biomedicine, Biotech. Histochem. **78** (2003) 147–155.

[17] T.A. Ban, Fifty years chlorpromazine: a historical perspective, Neuropsych. Dis.Treat. **3** (2007) 495–500.

[18] M.M. Kristiansen, C. Leandro, D. Ordway, M. Martins, M. Viveiros, T. Pacheco, J.E. Kristiansen, L. Amaral, Phe-

nothiazines alter resistance of methicillin-resistant strains of *Staphylococcus aureus* (MRSA) to oxacillin in vitro, Int. J. Antimicrob. Agents **22** (2003) 250–253.

[19] M. Martins, S.G. Dastidar, S. Fanning, J.E. Kristiansen, J. Molnar, J.M. Pages, Z. Schelz, G. Spengler, M. Viveiros, L. Amaral, Potential role of non-antibiotics (helper compounds) in the treatment of multidrug-resistant Gram-negative infections: mechanisms for their direct and indirect activities, Int. J. Antimicrob. Agents **31** (2008) 198–208.

[20] M. Kolaczkowski, K. Michalak, N. Motohashi, Phenothiazines as potent modulators of yeast multidrug resistance, Int. J. Antimicrob. Agents **22** (2003) 279–283.

[21] K. Akilandeswari, K. Ruckmani, Studies on Anti microbial Potential of Non-antibiotics on Resistant Bacteria – A Review, J. Young Pharm. **7** (2015) 63–68.

[22] D. Ordway, M. Viveiros, C. Leandro, R. Bettencourt, J. Almeida, M. Martins, J.E. Kristiansen, J. Molnar, L. Amaral, Clinical Concentrations of Thioridazine Kill Intracellular Multidrug-Resistant *Mycobacterium tuberculosis*, Antimicrob. Agents Ch. **47** (2003) 917–922.

[23] L. Amaral, M. Martins, M. Viveiros, Enhanced killing of intracellular multidrug-resistant Mycobacterium tuberculosis by compounds that affect the activity of efflux pumps, J. Antimicrob. Chemoth. **59** (2007), 1237–1246.

[24] L. Amaral, Z. Udwadia, E. Abbate, D. Soolingen, The added effect of thioridazine in the treatment of drug-resistant tuberculosis, Int. J. Tuberc. Lung D. **16** (2012) 1706–1712.

[25] Z. Zhelev, H. Ohba, R. Bakalova, V. Hadjimitova, M. Ishikawa, Y. Shinohara, Y. Baba, Phenothiazines suppress proliferation and induce apoptosis in cultured leukemic cells without any influence on the viability of normal lymphocytes, Cancer Chemother. Pharmacol. **53** (2004) 267–275.

[26] G. Sudeshna, K. Parimal, Multiple non-psychiatric effects of phenothiazines: A review, Eur. J. Pharmacol. **648** (2010) 6–14.

[27] N.M.M. Gowda, M.M. Kyi, L. Zhang, Synthesis and characterization of iridium chloride complex I Use of *N*-alkylphenothiazine drugs as ligands. Transition Met. Chem. **18** (1993) 518–522.

[28] N.M.M. Gowda, R.K. Vallabhaneni, I. Gajula, S. Ananda, Palladium(II)-phenothiazine complexes: synthesis and characterization, J. Mol. Struct. **407** (1997) 125–130.

[29] B. Keshavan, P.G. Chandrashekara, N.M.M. Gowda, Synthesis, characterization, and spectral studies of lanthanide(III) nitrate complexes of promethazine, J. Mol. Struct. **553** (2000) 193–197.

[30] B. Keshavan, K. Gowda, Dioxobridged complexes of molybdenum (IV) and tungsten (IV) with *N*-alkylphenothiazines and their interactions with L-cysteine and L-histidine Proc. Indian Acad. Sci. (Chem. Sci.) **113** (2001) 165–172.

[31] L. Ma, Z. Jie, C. Ruifang, C. Zhenxia, W. Linhong , Z. Xigeng, Synthesis and reactivity of organolanthanide complexes containing phenothiazine ligand toward carbodiimide and isothiocyanate, J. Organomet. Chem. **690** (2005) 4926–4932.

[32] X. Zhang, Y. Xie, W. Yu, Q. Zhao, M. Jiang, Y. Tian, Formation of A Novel 1D Supramolecule $[HgCl_2(ptz)]_2$ $HgCl_2$ (pt z= Phenothiazine): A New Precursor to Submicrometer Hg_2Cl_2 Rods, Inorg. Chem. **42** (2003) 3732–3737.

[33] Y. Jin, Y. Liu , W. Wu, Q. Wu , H. Gao , C. Wang , S. Xu, S. Cao, Synthesis of conjugated polymers bearing pendant bipyridine ruthenium complexes, React. Funct. Polym. **90** (2015) 7–14.

[34] J.M. Poljarević, M.P. Krstić, S. Grgurić-Šipka, S.P. Sovilj, D.R. Mišić, T.J. Sabo, Platinum(IV) complexes with *N*-alkylphenothiazines: synthesis, characterization, and antibacterial activity, J. Coord. Chem. **66** (2013) 3760––3769.

[35] M. Krstić, S.P. Sovilj, S. Grgurić-Šipka, I. Radosavljević Evans, S. Borozan, J.F. Santibanez, J. Kocić, New ruthenium(II) complexes with *N*-alkylphenothiazines: Synthesis, structure, *in vivo* activity as free radical scavengers and in vitro cytotoxicity, Eur. J. Med. Chem. **45** (2010) 3669–3676.

[36] B. Hóllo, M. Krstić, S.P. Sovilj, G. Pokol, K.M. Szécsényi, Thermal decomposition of new ruthenium(II) complexes containing *N*-alkylphenothiazines. J. Therm. Anal. Calorim. **105** (2011) 27–32.

[37] M. Krstić, S.P. Sovilj, S. Grgurić-Šipka, I. Radosavljević Evans, S. Borozan, J.F. Santibanez, Synthesis, structural and spectroscopic characterization, in vitro cytotoxicity and in vivo activity as free radical scavengers of chlorido(*p*-cymene) complexes of ruthenium(II) containing *N*-alkylphenothiazines, Eur. J. Med. Chem. **46** (2010) 4168–4177.

[38] B. Hóllo, M. Krstić, S.P. Sovilj, K.M. Szécsényi, Thermal decomposition of new chlorido(p-cymene) ruthenium(II) complexes containing *N*-alkylphenothiazines, J. Therm. Anal. Calorim. **111** (2013) 1927–1932.

IZVOD

N-ALKILFENOTIAZINI – SINTEZA, STRUKTURA I PRIMENA KAO LIGANADA U KOMPLEKSIMA METALA

Milena Krstić[1], Sofija Sovilj[2], Sunčica Borozan[1], Milica Rančić[3], Jelena Poljarević[2], Sanja R. Grgurić-Šipka[2]

[1]*Fakultet veterinarske medicine, Univerzitet u Beogradu, Beograd, Srbija*
[2]*Hemijski fakultet, Univerzitet u Beogradu, Beograd, Srbija*
[3]*Šumarski fakultet, Univerzitet u Beogradu, Beograd, Srbija*

(Pregledni rad)

Fenotiazini pripadaju velikoj grupi heterocikličnih, aromatičnih molekula koji između dva benzenova prstena sadrže azot i sumpor. Njihovi derivati, *N*-alkilfenotiazini poseduju supstituent na heterocikličnom azotovom atomu koji molekulima daje različita svojstva. Takođe, serija ovih jedinjenja ima supstituent i na ugljenikovom atomu u položaju 2 benzenovog prstena fenotiazina. Alkilfenotiazini sadrže aminoalkil grupu kao supstituent i njegovi alkil, acil i sulfonil derivati, kao i mono- i biciklični heterocikli vezani su za tiazinski azotov atom ili direktno za benzenov prsten. *N*-alkilfenotiazini su poznati kao antipsihotici, ali poseduju i antibakterijsku, antifungalnu, antitumorsku aktivnost, kao i sposobnost da reaguju sa makromolekulima i da se koordinuju za jone metala. Kompleksi metala sa *N*-alkilfenotiazinima pokazala su se kao biološki aktivna jedinjenja sa različitom antimikrobnom aktivnošću i citotoksičnim efektom na različite tumorske ćelijske linije. Upravo zbog njihovog širokog polja primene *N*-alkilfenotiazini su veoma atraktivni u smislu sinteza novih srodnih derivata, komleksa metala, proučavanja njihovih svojstava i istraživanjima na polju njihove dalje primene. Ovaj rad predstavlja pregled literature i savremeni pogled na *N*-alkilfenotiazine – njihovu sintezu i primenu, kao i njihovih metalnih kompleksa koji poseduju značajna biološka svojstva.

Ključne reči: *N*-Alkilfenotiazini • Antipsihotici • Antitumorski efekat • Antibakterijski efekat

Optimization of extraction conditions for secondary biomolecules from various plant species

Filip S. Šibul, Dejan Z. Orčić, Emilija Svirčev, Neda M. Mimica-Dukić

Department for Chemistry, Biochemistry and Environmental Protection, University of Novi Sad Faculty of Sciences, Novi Sad, Serbia

Abstract

Extraction of plant secondary metabolites is an essential step in isolation of natural products. Non-optimized extraction conditions can lead to losses, degradation and modification of the biomolecules. In this paper, the influence of different solvent mixtures, solvent amounts, temperature, extraction time, and procedures for defatting on yield and profile of various classes of secondary metabolites was investigated. *Rumex alpinus* was used for the extraction of anthraquinones, *Glycine max* for isoflavonoids, *Chaerophyllum bulbosum* for flavonoids and phenolic acids, *Anthriscus sylvestris* for lignans and coumarins, alkaloids were extracted from *Lupinus albus* and sesquiterpene lactones from *Artemisia absinthium*. Extraction efficiency was evaluated by use of LC-DAD-ESI-MS/MS. The compromise extraction solvent for all of the examined compounds is 80% methanol, mixed in ratio 13:1 with plant material. Maceration should last for six hours, repeated four times with fresh solvent. Defatting of the extracts does not lead to significant losses of the compounds of interest. It is acceptable to use extraction and evaporation temperature of 60 °C, while the extracts should be stored in the dark, on –20 °C.

Keywords: extraction, secondary biomolecules, plant phenolics, flavonoids, phenolic acids.

Available online at the Journal website: http://www.ache.org.rs/HI/

SCIENTIFIC PAPER

UDC 66.061:58:54

Hem. Ind. **70** (4) 473–483 (2016)

doi: 10.2298/HEMIND150531053S

For centuries, Chinese traditional medicine has been using nature as a source of compounds which can be used in treatment of various diseases. Today, major attention of pharmaceutical industry is focused on natural products as possible sources of natural remedies. Therefore, there is a growing interest for chemical characterization of medicinal plants [1].

Plants synthesize a wide range of secondary metabolites, as a specific mechanism of their defense from herbivores, bacteria, viruses, fungi and other organisms. By targeting different receptors and enzymes in predators and parasites, they have developed different mechanisms of action. Alkaloids can have agonistic or antagonistic activity towards neurotransmitters, while isoflavonoids have phytoestrogen abilities, due to their structural similarity with estrogen hormones in animals [2,3].

Plant secondary metabolites possess various biological activities. Anthraquinones, major components extracted from *Rumex alpinus* (Polygonaceae), are reported to have anti-inflammatory, antifungal and antibacterial activity. Isoflavonoids extracted from *Glycine max* (Fabaceae) are phytoestrogens, while flavonoids and phenolic acids from *Chaerophyllum bulbosum* (Apiaceae) exhibit immunomodulating, anticancer and hepatoprotective effects. *Anthriscus sylvestris* (Apiaceae) is rich in lignans and coumarins, known for their anticancer, antifungal and anti-inflammatory activities. Alkaloids extracted from *Lupinus albus* (Fabaceae) and sesquiterpene lactones from *Artemisia absinthium* (Asteraceae) are responsible for their bitter taste, as well as their antimicrobial activity [2,4].

Extraction of the active principles is an essential step in evaluation of their bioactivity and chemical characterization. Maceration is widely used technique suitable for extractions of small amounts of plant material in laboratory. However, non-optimized extraction conditions can lead to losses, degradation and modification of the biomolecules. Inaccurate analysis can result in invalid conclusions about the chemical composition and the amount of secondary metabolites present in plant. Therefore, optimization of extraction conditions is important for maximizing yields of the compounds of interest, while minimizing the extraction of unwanted compounds. In this paper, we investigated the influence of different solvent mixtures, solvent amounts, temperature, extraction time, techniques and procedures for fatty acid and chlorophyll removal on yield and profile of various classes of secondary metabolites from the selected plant species, during maceration. Extraction efficiency was evaluated by using several LC-DAD-ESI–MS/MS methods developed to monitor the selected compounds and compound classes.

Correspondence: F.S. Šibul, Department for Chemistry, Biochemistry and Environmental Protection, University of Novi Sad Faculty of Sciences, Trg Dositeja Obradovića 3, 21000 Novi Sad, Serbia.

E-mail: filip.sibul@dh.uns.ac.rs

Paper received: 31 May, 2015

Paper accepted: 10 September, 2015

EXPERIMENTAL

Chemicals and reagents. HPLC gradient grade methanol, p.a. ethanol and methanol were purchased from J. T. Baker (Deventer, The Netherlands), and p.a. DMSO from Merck (Darmstadt, Germany).

Plant materials. The plant material used for extraction and analysis was collected from different locations in Serbia – *Chaerophyllum bulbosum* (CB) from Vlasinsko Jezero lake and *Anthriscus sylvestris* (AS) from Fruska Gora mountain in 2009, *Artemisia absinthium* (AA) from Stara Planina mountain in 2011, *Rumex alpinus* (RA) from Kopaonik mountain in 2012, while *Glycine max* (GM) and *Lupinus albus* (LA) were collected from Rimski Sancevi, agrarian area in the Pannonian basin, in 2013. Voucher specimens were prepared, identified and deposited at the Herbarium of the Department of Biology and Ecology (BUNS Herbarium), University of Novi Sad, Faculty of Sciences.

The selected plant species were used for extraction of different secondary metabolites present in their aerial parts, as determined by our preliminary studies. Herb of *Rumex alpinus* (monk's rhubarb, Alpine dock) was used for extraction of anthraquinones, *Glycine max* (soy) for isoflavonoids, and *Chaerophyllum bulbosum* (turnip-rooted chervil) for flavonoids and phenolic acids. Aerial parts of *Anthriscus sylvestris* (wild chervil) were used as a source of lignans, *Lupinus albus* (white lupin) contains alkaloids, while the herb of *Artemisia absinthium* (absinthium, wormwood) is rich in sesquiterpene lactones.

Extracts preparation

Plant material was air-dried at room temperature, and aerial parts were separated from roots and powdered afterwards. All extracts were prepared by maceration. During the extraction process, aerial parts were constantly shaken at three different temperatures, during various periods of time, and using several solvent mixtures (as described in the following subsections). The composition of the extraction medium, as well as the volume of the solvent, extraction time and temperature were optimized during the experiment to obtain the highest content of extractables (monitored by LC-ESI–MS/MS in MS2Scan mode or by LC-DAD, depending on the compound class). Plant material was removed by filtration, raw extracts were evaporated under the reduced pressure and reconstituted in DMSO to the final concentration of 50 mg/mL.

Solvent mixture selection. For the purpose of testing the influence of different solvent mixtures on secondary metabolites extraction, 100 mg portions of each dried plant material were mixed in 1.8 mL HPLC vial with 1 mL of the following solvents: water, 60% methanol, 80% methanol, methanol, 60% ethanol, 80% ethanol and ethanol. The mixtures were shaken for 60 min at room temperature on vortex mixer, and filtered through millipore filters (0.45 μm) before analysis by LC-DAD-ESI–MS/MS in MS2Scan mode. Peaks of the targeted compounds were identified by comparing their molecular weights, mass spectra and UV/Vis spectra with the literature (refer to the Section "Identification of compounds present in plant extracts"). Further on, their abundance profiles obtained from extraction by different solvents were compared. The goal was to achieve the maximum possible yield of a wide range of biomolecules identified in the selected plants. Afterwards, for each of the extracts, LC-MS/MS or LC-DAD method was created to monitor the yield of the compounds of interest.

Optimal extraction volume selection. To find the optimal extraction medium volume, 1 mL of the optimal solvent was mixed with 50 mg (solvent mixture to plant material ratio of 1:20), 75 mg (1:13.3), 100 mg (1:10), and 125 mg (1:8) of the dry plant material. After shaking for 60 min on vortex mixer and filtering through millipore filters, all mixtures were diluted to the concentration of 50 mg/mL, for analysis with LC--ESI–MS/MS. Plots showing peak areas versus extraction solvent volume were constructed (Fig. 1).

*Extraction kinetics***.** For the purpose of extraction kinetics evaluation, 5 g of the drug was mixed with the optimal volume of extraction solvent in 250 mL Erlenmeyer flask, closed to avoid evaporation of solvents, and shaken at room temperature for 73 h. Sample aliquots of 500 μL were taken out at 0, 15 and 30 min, and at 1, 2, 6, 10, 24, 49 and 73 h after adding the extraction medium, filtered and analyzed by LC-DAD--ESI–MS technique. The yield was plotted against the extraction time (Fig. 2).

Multiple extractions. 500 mg of the plant material was repeatedly extracted for 5 times with an optimal solvent volume. Each of the five extractions was performed by shaking the mixture for 1 h at room temperature, filtering out the extract using vacuum, and re-extracting the remaining plant material with the same amount of fresh extraction medium. 500 μL of each portion is analyzed separately by LC-DAD-ESI–MS/MS. Cumulative yield of each extraction cycle was calculated, assuming approximately 100 % recovery after the fifth extraction, and was plotted against the number of extraction cycles (Fig. 3).

Optimal temperature selection. Optimization of extraction temperature was performed by shaking 100 mg of the plant material with the optimal extraction medium for 60 min at room temperature (25 °C), and at 60 and 100 °C in water bath. After filtering, the extracts were analyzed by LC-DAD-ESI–MS/MS and compound profiles were compared (Fig. 4). In addition, MS2Scan chromatograms were recorded to monitor possible degradation products.

Evaporation under reduced pressure. To increase the throughput, the maximum acceptable evaporation temperature was assayed. Extracts prepared in the experiment evaluating the extraction kinetics (after 73 h) were evaporated under the reduced pressure, using rotary evaporator with bath temperature set on 30, 45 and 60 °C. Dry residues were reconstituted to the concentration of 50 mg/mL and analyzed by LC-DAD-ESI––MS/MS after filtration. Additionally, MS2Scan chromatograms were acquired and evaluated for identification of possible degradation products.

Unwanted compounds removal. Examination of losses during removal of fats and pigments (chlorophylls and carotenoids) was performed by liquid-liquid extraction with hexane. 1 mL of extracts, prepared in the experiment evaluating extraction kinetics, was evaporated *in vacuo*. Dry residue was suspended in 1 mL of warm water (~60 °C), additional 1 mL of water was then added to wash the evaporation flask, and the water solutions were mixed. To 2 mL of this solution, 2 mL of hexane was added, the content was shaken on vortex mixer and then frozen using dry ice. Hexane layer was decanted from the frozen aqueous layer, and then new portion of hexane (2 mL) was added to the thawed aqueous layer. This procedure was repeated for five times, resulting in 2 mL of aqueous phase and 10 mL of pooled hexane extracts. Both phases were evaporated separately *in vacuo*, dry residues were reconstituted to the concentration of 50 mg/mL, and analyzed by LC-DAD-ESI–MS/MS in MS2Scan mode. The obtained chromatograms were compared to evaluate the compound distribution between the two phases.

Effects of storage conditions. Extracts prepared using previously optimized extraction conditions were stored for 6 months under different conditions: at room temperature exposed to sunlight, at room temperature in the darkness, at 4 °C in the darkness, and at –20 °C in the darkness. In addition, one portion was diluted in typical HPLC mobile phase (0.05% aqueous formic acid:methanol = 1:1) and kept at 4 °C in the darkness. After six months, LC-DAD-ESI–MS/MS analysis of all samples was performed, and profiles of the compounds of interest were compared for the purpose of evaluating possible losses and degradation.

LC-ESI–MS analysis

Extracts were diluted with mobile phase solvents A (0.05% aqueous formic acid) and B (methanol), premixed in 1:1 ratio, to obtain a final concentration of 50 mg/mL. Extracts were analysed using Agilent Technologies series 1200 HPLC instrument coupled with Agilent Technologies 6410A Triple Quad tandem mass spectrometer with electrospray ion source, and controlled by Agilent Technologies MassHunter Workstation software – Data Acquisition (ver. B.03.01). Five μL were injected into the system, and compounds were separated on Zorbax Eclipse XDB-C18 (50 mm×4.6 mm, 1.8 μm) rapid resolution column held at 50 °C. Mobile phase was delivered at flow rate of 1 mL/min in gradient mode (0 min, 30% B, 6 min, 70% B, 9 min, 100% B, 12 min, 100% B, re-equilibration time 3 min). Eluted components were detected by DAD detector and sent to the MS detector.

MS(–) experiments. For detection of flavonoids and phenolic acids from *Chaerophyllum bulbosum* and isoflavonoids from *Glycine max*, MS–ESI ion source parameters were as follows: nebulization gas (N_2) pressure 50 psi, drying gas (N_2) flow 9 L/min and temperature 350 °C, capillary voltage 4 kV, negative polarity (NI). For general screening, data were acquired in MS2Scan mode, using *m/z* range from 120 to 1000 and fragmentor voltage of 100 V. For targeting compounds of interest, MS2SIM mode was used, with specific *m/z* values: 643, 601, 515 and 353 for acetylmalonyl-dicaffeoylquinic acid ($AcMalC_2QA$), malonyl-dicaffeoylquinic acid ($MalC_2QA$), dicaffeoylquinic acid (C_2QA) and caffeoylquinic acid (CQA); 489, 463, 447, 431, and 285 for luteolin/kaempferol acetylhexosides (Lut/Kaempf--AcHex), quercetin-3-O-glucoside (Quer-3-Glc), luteolin/kaempferol-7-O-glucoside (Lut/Kaempf-7-Glc), apigenin-7-O-glucoside and luteolin/kaempferol deoxyhexoside (Api-7-Glc, Lut/Kaempf-dHex) and luteolin/ /kaempferol (Lut/Kaempf), respectively, all detected in *Chaerophyllum bulbosum*. In *Glycine max*, *m/z* 269 and 253 were targeted for genistein and daidzein, respectively.

MS(+) experiments. Ion source parameters for screening of alkaloids from *Lupinus albus* were identical to those described in previous section, except for the use of positive polarity (PI). For targeting the compounds of interest, MS2SIM in positive mode was used, with specific *m/z* values: 347, 265 and 249 for angeloyloxy/tigloyloxy-lupanin, hydroxylupanin and lupanin, respectively.

The above said parameters were not suitable for analysis of sesquiterpene lactones from *Artemisia absinthium*, due to inefficient ionization by ESI source. Therefore, the analysis of this plant's extracts was performed using an instrument with multimode ion source. Instrument configuration was identical to the one above, with a difference in MMI source parameters: nebulization gas (N_2) pressure 50 psi, vaporizer temperature (APCI heater) 200 °C, drying gas (N_2) flow 5 L/min and temperature 325 °C, capillary voltage 2.5 kV, positive polarity (PI). In MS2SIM mode, compounds of interest were targeted on *m/z* values: 513, 497 and 249 for anabsin, absinthin and artabsin, respectively.

UV/Vis Detection. For analysis of lignans present in *Anthriscus sylvestris* herb extract, UV signals at 280 nm and 330 nm were monitored, with bandwidth of 16 nm. Anthraquinones from extract of *Rumex alpinus* were

monitored in visible area at 430 nm, with bandwidth of 16 nm. For both classes, UV/Vis was found to be more practical than MS in detecting all compounds of the same class.

Additionally, to confirm the identity of peaks, continuous spectra were obtained in range from 190 to 700 nm.

RESULTS AND DISSCUSION

Identification of compounds present in plant extracts

Phenolic acids and flavonoids from Chaerophyllum bulbosum. Phenolic acids in *Chaerophyllum bulbosum* extracts were identified by MS^1 and MS^2 analysis in negative ionization (NI) mode, according to the rules set by Clifford *et al*., 2003 [5]. Examination of the total ion chromatograms (TIC) resulted in four signals: *m/z* 353 for caffeolyquinic acids (CQA), *m/z* 515 for dicaffeoylquinic acids (C_2QA), *m/z* 601 for malonyl-dicaffeoylquinic acids ($MalC_2$QA), and *m/z* 643 for acetyl-malonyl-dicaffeoylquinic acids ($AcMalC_2$QA). CQAs were identified at retention times (t_R) of 0.7, 0.8 and 1.4 min. C_2QAs eluted at t_R 1.7, 1.8, 1.9 and 2.35 min, $MalC_2$QAs at 1.6 and 1.85 min, and $AcMalC_2$QAs at 2.65 and 2.8 min.

Flavonoids were also identified in *Chaerophyllum bulbosum* extracts after MS^1 and MS^2 analysis in negative ionization (NI) mode, according to the rules set by Cuyckens *et al*. (2000) [6]. Examination of the total ion chromatogram (TIC) resulted in five signals: *m/z* 285 for luteolin and kaempferol (Lut/Kaempf), *m/z* 431 for apigenin hexosides and luteolin/kaempferol deoxyhexosides (Api-Hex, Lut/Kaempf-dHex), *m/z* 447 for luteolin and kaempferol hexosides (Lut/Kaempf-Hex), 463 for quercetine hexosides (Quer-Hex), and *m/z* 489 for luteolin and kaempferol acetyl hexoside (Lut/Kaempf--AcHex). The only peak in the EIC signal at *m/z* 285 was identified as luteolin (Lut) by comparison of the retention time (t_R = 3.8 min) with the reference standard. The EIC signal at *m/z* 431 contained two major peaks. The first peak, at t_R 2.6 min, was confirmed to be apigenin-7-*O*-glucoside (Api-7-Glc) by comparison with the reference standard. The second peak, with the retention time of 3.32 min, was identified as kaempferol-3-*O*--deoxyhexoside (Kaempf-3-dHex), according to molecular weight and characteristic UV spectra. Two compounds were detected in EIC chromatogram at *m/z* 447. By comparing the retention times with the reference standards, luteolin-7-*O*-glucoside (Lut-7-Glc, t_R = = 2.09 min) and kaempferol-7-*O*-glucoside (Kaempf-7--Glc, t_R = 2.7 min) were identified. The signal at *m/z* 463 exhibited one major and one minor peak, both corresponding to quercetin hexosides. By comparing the retention times with the reference standards, it was confirmed that the first peak at t_R 2.04 min was quercetin-3-*O*-galactoside (hiperoside), while the dominant peak at 2.15 min was quercetin-3-*O*-glucoside (isoquercitrin). Finally, Lut/Kaempf-AcHexs were identified at t_R 2.4, 2.74 and 2.9 min.

Isoflavonoids from Glycine max. Isoflavonoids in *Glycine max* extracts were identified after MS2Scan analysis in negative ionization (NI) mode. Examination of the total ion chromatogram (TIC) and the extracted ion chromatograms (EIC) resulted in two signals: *m/z* 253 for daidzein (Da) and *m/z* 269 for genistein (Gen). These compounds represent the two major isoflavonoids present in soy, and were identified by their molecular masses, as well as by comparing their MS^2 and UV spectra with the reference data [7].

*Alkaloids from Lupinus albus***.** Alkaloids in *Lupinus albus* extracts were detected by MS^1 and MS^2 analysis in positive ionization (PI) mode. Spectral data from the literature helped in identification of the major compounds present in this plant [8,9]. Peak at 0.57 min belongs to lupanin (*m/z* 249). Overlapping peaks with t_R 0.54 and 0.69 min are identified as two isomeric hydroxylupanins (*m/z* 265). Peak at 1.17 min corresponds to one of the two isomeric hydroxylupanin esters: tigloyloxy- or angeloyloxy-lupanin (*m/z* 347).

*Sesquiterpene lactones from Artemisia absinthium***.** Analysis of sesquiterpene lactones present in *Artemisia absinthium* was performed using APCI MS in MS2SIM mode. The compounds of interest were identified by comparison with the literature spectral data [8,10]. According to the data, peak at 4.9 min represents artabsin (*m/z* 249), anabsin eluted at t_R 5.25 min (*m/z* 513), and peak at 6.93 min is absinthin (*m/z* 497).

*Lignans from Anthriscus sylvestris***.** The lignans dominant in *Anthriscus sylvestris* extracts were identified by using the literature data about this plant's chemical composition, including UV spectra and retention information [11,12], as well as the fragmentation rules set by Wong *et al*., 2000 [13]. Peaks at 4.47, 5.47 and 5.65 min have UV spectra characteristic for aryltetralin and saturated dibenzobutyrolactone lignans: absorbance maximum below 290 nm and lack of maxima above 300 nm. Based on MS^2 data, these compounds were identified as podophyllotoxin, deoxypodophyllotoxin, and yatein, respectively. Peaks at 5.79, 5.87 and 6.49 min have absorbance maximum between 320 and 330 nm, and have been identified as chaerophyllin, nemerosin and sylvestrin/isochaerophyllin. Additional minor peaks were detected, with retention and UV spectra similar to those of the compounds identified.

*Anthraquinones from Rumex alpinus***.** Peaks of anthraquinone aglycones and glycosides were identified by their characteristic UV/Vis spectra, with a prominent absorbtion maximum at 430 nm and a series of maxima under 300 nm. Compounds eluting between

4.5 and 5.5 min were identified according to their molecular masses and retention times as anthraquinone glycosides, while the compounds eluting later (from 7.9 to 9 min) were identified as anthraquinone aglycones.

Extraction conditions optimization

*Extraction medium optimization***.** Various extraction mediums, differing in polarity, proton-donating and proton-accepting abilities, extract different classes of compounds from plant material with a varying yield. With a goal of maximizing the yield of a wide range of molecules of interest, the optimal extraction medium was selected by comparison of abundance profiles of the selected compounds, obtained by analysis after the extraction by different solvent mixtures. According to literature data, optimal extraction mediums for most of the plant compounds are methanol and ethanol, mixed with water in different ratio [14,15]. For all of the identified chlorogenic acids, 60 and 80% methanol were found to be the most efficient in their extraction from *Chaerophyllum bulbosum*. 60% ethanol provided a high yield for dicaffeoylquinic acids and their malonyl derivatives, but lower for caffeoylquinic and acetyl-malonyl-dicaffeoylquinic acids. Furthermore, it was noticed that water and neat ethanol are not suitable for chlorogenic acids extraction, due to very low yields.

Extraction profiles for flavonoids from *Chaerophyllum bulbosum* depend on the structure. Efficiency of glycosides extraction increased with methanol content, while for the ethanol-based solvents it peaked at 80% ethanol. Generally, the pure methanol was found to be the most efficient, followed by 80% methanol. As for lutheolin and its acetylhexosides, the pattern was reversed, showing that 60 and 80% methanol provide higher yields than pure methanol. Yields of flavonoids, obtained using water extraction, were very low. Surprisingly, isoflavonoid aglycones daidzein and genistein were the most efficiently extracted with solvents of intermediate polarity, while neat water and alcohols provided lower yields. The effect of the solvent on the investigated sesquiterpene lactones extraction from *Artemisia absinthium* was less pronounced. While the extraction efficiency of water was low, 60–100% alcoholic solvents provided high yields. Similarly, the most suitable extraction solvents for hydrophobic, permethylated lignans from *Anthriscus sylvestris* were 60 and 80% ethanol. Methanolic extraction provided a somewhat lower yield of these compounds, while water and ethanol were found to be inefficient. Polar solvents – water, 60–80% methanol and 60% ethanol – were found to be the most efficient for extraction of the selected alkaloids (lupanin, hydroxylupanin and angeloyl/tigloyloxylupanin) from *Lupinus albus*, while pure ethanol gave very low yields. It should be noted that a pH adjustment of the sample may be needed for obtaining the maximum yield of alkaloids. Finally, for anthraquinones, as hydrophobic compounds, water was found to be the unsatisfactory solvent. To obtain the maximum yield of both glycosides and aglycones, 80% methanol or 80% ethanol should be used.

This experiment resulted in conclusion that 80% methanol is an adequate medium for extraction of the majority of compounds present in plants used in this experiment, with 60% ethanol as a viable alternative. This is in accordance with the literature data [14,15].

Extraction efficiency of different solvent mixtures towards various plant pigments, such as chlorophylls and carotenes, was also evaluated. The pigments were identified by their UV/Vis spectra, and their content was estimated from the total signal on λ 400–700 nm in late-eluting region of a chromatogram. Pigments can interfere with the analysis of extracts, especially when using spectrophotometric methods for evaluation of chemical composition and biological activity. Therefore, the optimal sample preparation procedure should minimize co-extraction of pigments with the compounds of interest. It was found that the selected optimal extraction solvent, 80% methanol, also extracts high amounts of pigments (although less than 60% methanol, pure methanol and 80% ethanol), therefore the extract purification may be necessary. It was also observed that 80% methanol extracts the highest amount of fatty acids that can interfere with anthraquinones determination due to similar elution and isobaric molecular weights, although these problems can be alleviated by using MS/MS or UV/Vis detection.

*Optimal extraction medium volume***.** Optimal extraction medium volume represents the ratio of dry plant material weight to volume of the extraction solvent. Volume optimization leads to use of the minimum amount of the extraction medium needed for a high yield of the extracted compounds, thus saving large amounts of toxic and expensive solvents. Furthermore, evaporating smaller amounts of solvent increases the extraction throughput and reduces energy expenditure. As expected, the results show that the extraction yield dramatically increases with the increase of solvent-to-drug ratio, due to increase of the concentration gradient needed for efficient extraction. To obtain a high yield in one-step extraction, the ratio of at least 20:1 should be used (Fig. 1). Since this results in a very high solvent usage, a lower ratio of approx. 13:1, which provides approximately twice the yield of commonly used 8:1 extraction for majority of the compounds investigated, was selected for the following experiments. This result is in correlation with the recommended ratio of between 1:10 and 1:15 [14].

*Optimal extraction time***.** Extraction yield increases with time until the equilibrium is reached. Prolonging the extraction after this point has little sense, since it

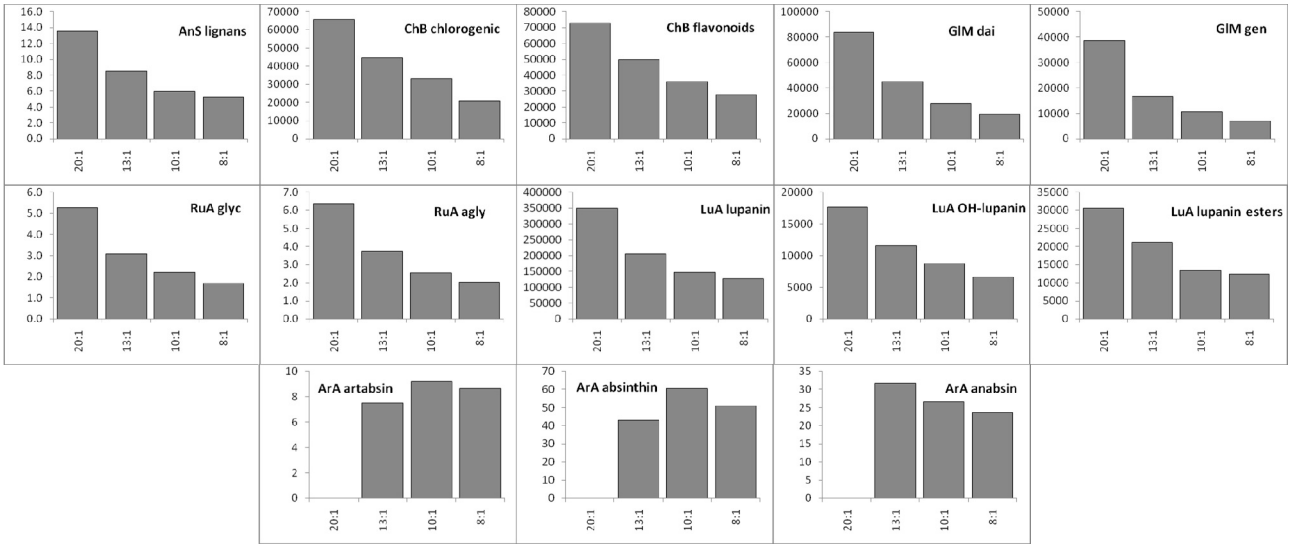

Figure 1. Peak areas of compounds extracted with different solvent volumes.

leads to longer experiment time, and also increases the chance of artefact formation through hydrolysis, oxidation, isomerisation etc. Extraction time is optimized by evaluation of extraction kinetics, *i.e*., by monitoring the change of the investigated substances concentrations in time.

The obtained results show that concentrations of all compounds grow rapidly during the first two hours of extraction, reaching the estimated yields of 70–90%. Afterwards, the yield rises slowly due to solvent saturation by the compounds present in plant material, to reach equilibrium after over 70 h (Fig. 2). By analysing of kinetic plots, we concluded that 6 h extraction provides a satisfactory yield (approx. 84–93%) within a reasonable amount of time, which is in correlation with other studies in this field [15].

Number of solvent portions for extraction. To increase efficiency, extraction should be repeated several times with a fresh portion of an extracting solvent. However, multistep extraction leads to increased solvent usage, prolonged procedure, and a larger volume of extract that needs to be evaporated. Thus, it is essential to optimize the number of solvent portions needed for efficient extraction.

Results show that the yield of one extraction step is between 42 and 68%, depending on the compound class. The average cumulative yield increases at an expected rate in subsequent steps, reaching 66–88%, 84–94 and 95–97% in the second, third and fourth step. Therefore, at least four consecutive extractions are required for obtaining acceptable yields (Fig. 3). Considering the previous results, which showed that most of the components are extracted after 6 h, we concluded that the optimal extraction should be performed 4 times for 90 min in order to get the maximum extraction yield within a reasonable time.

*Extraction temperature***.** With increasing the temperature, solvent viscosity decreases, which enhances a solvent penetration into plant material and increases the rate of extraction process. In addition, solubility of many compounds increases at higher temperatures due to either thermodynamic factors (if dissolution is endothermic process) or to decreased water polarity at higher temperatures. However, high temperature may lead to degradation of the thermolabile compounds and evaporation of the volatile ones. Extraction temperature is thus optimized to provide a maximum yield of the compounds of interest, without their further degradation.

For extraction of lignans from *Anthriscus sylvestris*, that are non-polar due to permethylation, higher temperatures (100 °C) were found to be beneficial, with yield at 100 °C about 33% higher than the one at 25 °C. This can be explained by increased solubility due to a decrease of polarity of water in the extraction solvent [16]. The profile of the dominant lignans was mostly unaffected by temperature. However, it should be noted that abundances of some minor components either decreased or increased at 100 °C, thus indicating interconversion.

A very similar yield increase was observed for flavonoid aglycones and non-conjugated glycosides from *Chaerophyllum bulbosum*. However, upon a detailed chromatogram analysis, changes in acylated glycosides profile were observed at 100 °C as compared to 25 and 60 °C. Notably, peaks of quercetin-, luteolin- and kaempferol-malonylglycosides decreased, while an equal number of peaks of the corresponding acetylhexosides increased. This was expected, since it is well-known that malonyl esters undergo decarboxylation into acetates at elevated temperatures [17].

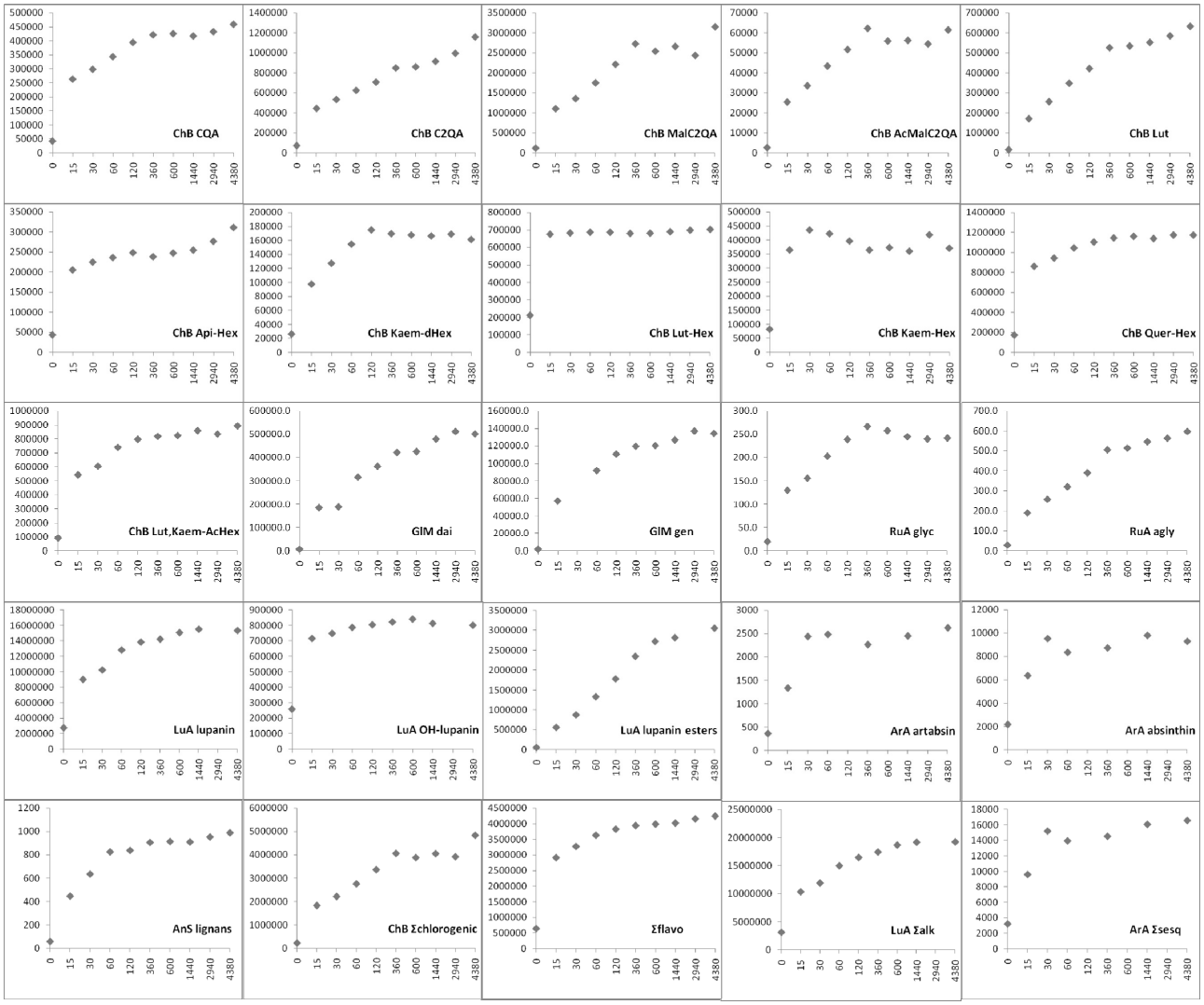

Figure 2. Peak areas of compounds extracted during different periods of time, cumulatively.

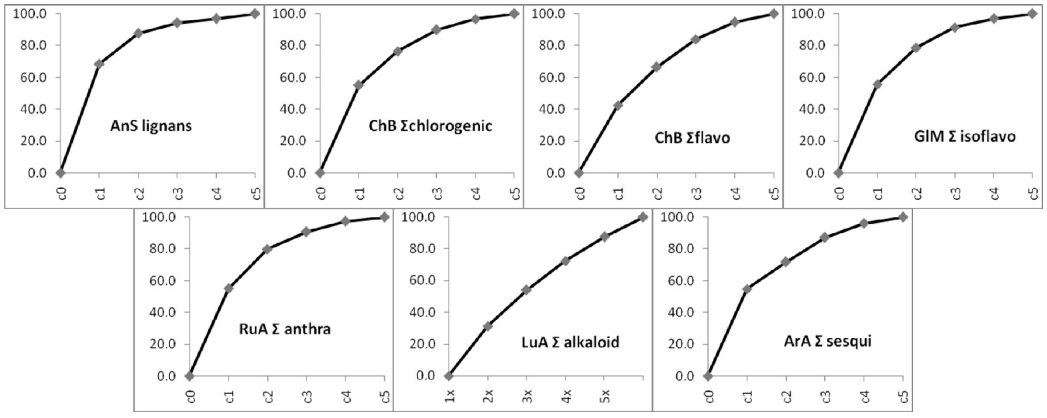

Figure 3. Peak areas of compounds extracted with different number of solvent portions.

Similar effects were observed for chlorogenic acids from *Chaerophyllum bulbosum*. The increase of temperature from 25 to 60 °C provides only a slight increase in yield of these compounds. Further heating to 100 °C resulted in approximately a twofold drop of $MalC_2QA$ levels, and an increase in content of C_2QA, AcC_2QA and $AcMalC_2QA$ (and CQA, to a lesser extent). This indicates that, at elevated temperatures, $MalC_2QA$ undergoes hydrolysis (into C_2QA and CQA) and malonyl moiety decomposition (into AcC_2QA). The conversion

into $AcMalC_2QA$ has not been previously observed, to the best of our knowledge.

Isoflavonoids from *Glycine max*, despite their structural similarity to other flavonoid aglycones, behaved differently. While genistein yield changed only slightly, losses of daidzein were observed at 60 °C and, especially, at 100 °C. The results are in agreement with the previous findings demonstrating thermal lability of isoflavonoids. Studies conducted by Ungar et al. indicated that daidzein is fairly stable while genistein undergoes decomposition, as opposed to our findings. This discrepancy may be attributed to a difference in test systems, *i.e.*, neat compounds in buffer *vs*. plant material in aqueous-methanolic solvent.

In case of *Rumex alpinus*, a temperature increase from 25 to 60 °C was found to be beneficial, increasing the yield of anthraquinone aglycones and glycosides by approximately 30%. Higher temperatures (100 °C) have no further effect on glycosides levels, while aglycones yield drops. It should be noted that glycosides profile changes at 100 °C, indicating possible interconversion.

Yield of alkaloids from *Lupinus albus* exhibited only a small change with a temperature increase from 25 to 60 °C, while heating to 100 °C resulted in a more pronounced yield drop. In the case of esterified hydroxylupanin, the highest yield was observed at 60 °C (Fig. 4).

Based on the results obtained, elevated temperature of 60 °C appears to be relatively safe, not resulting in degradation of majority of the investigated compounds (even malonyl esters, that are commonly claimed to degrade at above 35 °C), while increasing the yield of some compounds. It can also be expected

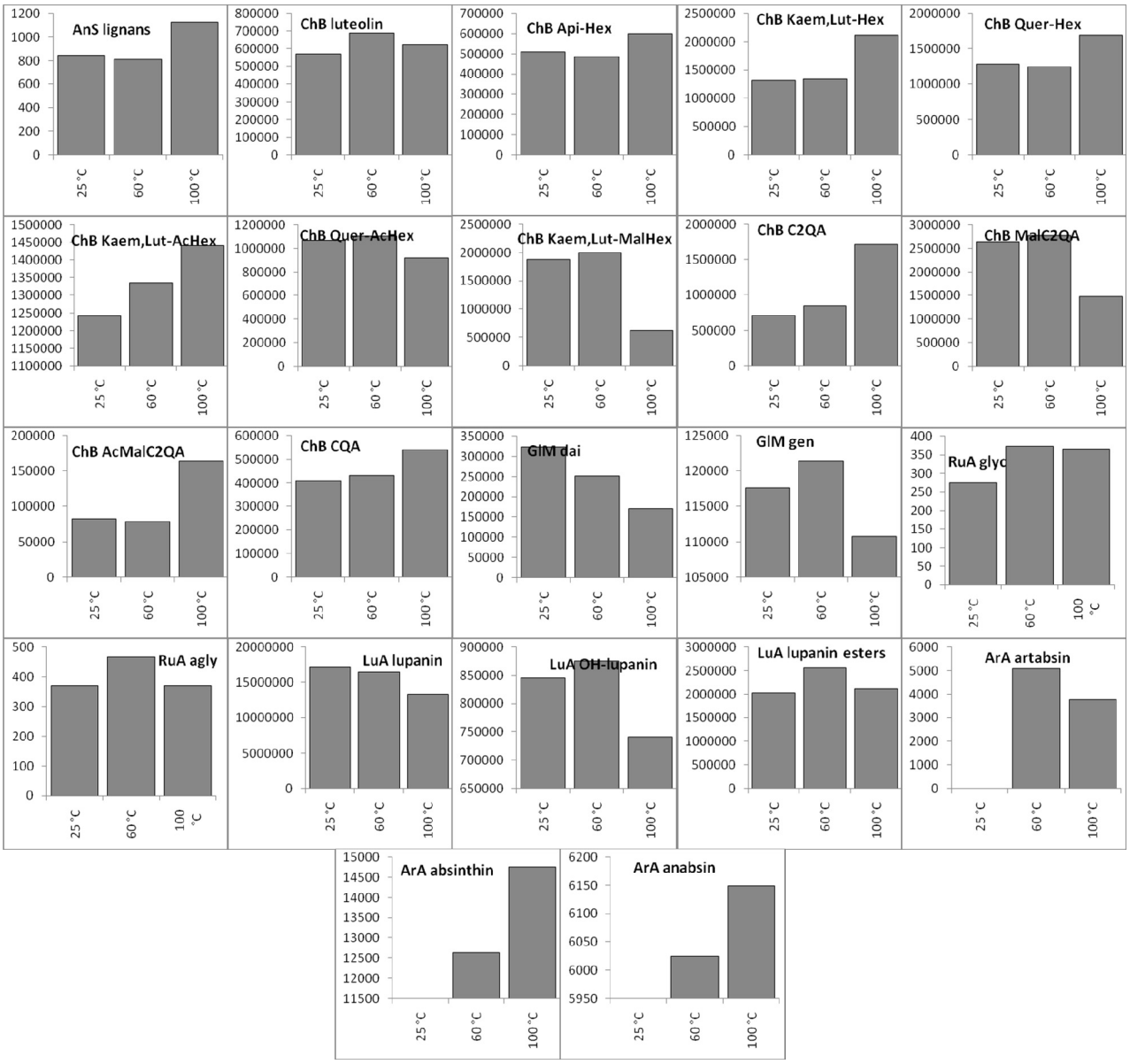

Figure 4. Peak areas of compounds extracted on different temperatures.

that the extraction equilibrium is reached faster due to a decreased solvent viscosity, leading to better penetration. Temperature of 100 °C should be avoided (except when specifically studying decoctions) since it leads to losses in several compounds classes.

Evaporation temperature. After extraction, evaporation is needed to concentrate the extract, usually by using rotary evaporator under reduced pressure and below the solvent boiling point. While elevated temperature enhances the process, it may lead to chemical modification, degradation, or evaporation of the compounds of interest. Thus, it is necessary to find the optimal temperature for evaporation of extracts.

Results show that for the majority of the investigated compound classes there are no differences in abundances of the extracted compounds after evaporation at different temperatures. Thus, the temperatures of up to 60 °C can be used if a high-throughput sample preparation is needed. The notable exceptions are isoflavonoids daidzein and genistein, which exhibit a sharp drop in concentration when evaporated at 60 °C. These compounds have previously been reported to react with proteins at elevated temperatures, which decreases their abundance in solvent [18, 19].

*Losses during the defatting process***.** Extraction of the compounds of interest is usually accompanied by co-extraction of the unwanted matrix compounds, both hydrophilic (sugars, amino acids, metabolic intermediates) and lipophilic (chlorophylls, carotenoids, triacylglycerols and phospholipids). Since these compounds can interfere with compounds of interest in further analyses, they should be removed. Removal of the lipophilic components is performed by liquid-liquid extraction using non-polar solvents like hexane or petroleum ether. However, some compounds of interest can also transfer to organic phase, resulting in a decreased yield or negative systematic error in quantification. Thus, it is of essence to get an insight into the amount of compounds lost during this process.

Results show that defatting does not influence the yield of phenolic acids, flavonoids, isoflavonoids and anthraquinone glycosides, due to their polar nature. Average losses were about 0.8%, and did not exceed 2.2%. Transfer to hexane phase was more pronounced with lupin alkaloids, reaching up to 8.5% for hydroxylupanin. On the other hand, non-polar compounds like sesquiterpene lactones from *Artemisia absinthium* and especially lignans from *Anthriscus sylvestris* are lost to a significant extent during the defatting process (76% for lignanes and 29–57% for sesquiterpenes). The situation is more complex with anthraquinone aglycones. While apparent total loss is about 22%, individual compounds differ in their partitioning behavior, some remaining in water while others predominantly extracting into organic phase.

Consequently, while there are no major losses of polar compounds of interest during the removal of non-polar matrix compounds, there is a need for re-extraction of lipophilic compounds from hexane phase (e.g. with methanol).

Storage conditions. Often, it is not possible to analyze the extracts immediately after extraction, which leads to the need for their storage for a prolonged period. During the storage, partial or complete decomposition of compounds can take place, depending on the storage conditions, such as temperature and illumination.

Results show that after a period of six months, CQA, C_2QA, MalC_2QA and AcMalC_2QA are almost completely degraded at room temperature in the presence of light, with their content dropping to 0.1–13% of the one observed in samples stored at –20 °C. While the abundance of free quinic acid was slightly elevated, it was not possible to identify any other degradation products, implying that chlorogenic acids decomposed mainly to low molecular weight compounds (below used *m*/*z* threshold of 120). Caffeoyilquinic acid was stable at room temperature in the dark. Under the same conditions, malonylated chlorogenic acids – MalC_2QA and AcMalC_2QA – decomposed almost completely, but this time clearly giving rise to mono- and dicaffeoylquinic acids as the main products. At 4 °C, only MalC_2QA degradation was observed, although to a lesser extent – about 30% drop, accompanied by a proportional rise in C_2QA content. It can be concluded that, due to instability of chlorogenic acids, samples should be kept in dark at –20 °C. The solvent also influences the stability of chlorogenic acids – the sample kept at 4 °C in solvent containing 0.01% formic acid and methanol (1:1) exhibited a 25–45% drop in concentration of all chlorogenic acids, accompanied by a rise of quinic acid content, indicating hydrolysis.

Flavonoid aglycones were significantly (about 80%) degraded during storage at room temperature while being exposed to sunlight. The behaviour of flavonoid glycosides in the absence of light depended on the structure. Levels of malonylhexosides decreased 1.6–2.6 times during storage at 4 °C, while decomposition at room temperature was practically complete, independent of insolation. Levels of acetylhexosides also dropped when exposed to light and room temperature. Kaempferol acetylhexosides appeared to be the most stable, while quercetin acetylhexosides decomposed almost completely upon storage at room temperature. Finally, levels of hexosides increased with the temperature in the absence of illumination, indicating a possible conversion of malonylhexosyl and acetylhexosyl moiety into hexosyl, while exposure to sunlight resulted in degradation, especially of quercetin derivative. Thus, it can be concluded that, if flavonoid glycosides spe-

ciation is to be done, samples must be stored at –20 °C, protected from light. Due to lower solubility of flavonoid aglycones in water, a less polar solvent (*e.g.*, methanol) should be present in sufficient amount (*e.g.*, 80%), otherwise precipitation will occur, resulting in losses during filtration prior to HPLC analysis.

Genistein decomposed to a great extent in samples kept at room temperature (especially under insolation), while daidzein was stable under all examined conditions. In samples diluted in mobile phase and kept at 4 °C, both of the examined isoflavonoids partially precipitated were lost during filtration process.

The obtained results show that light causes only partial degradation of lignans, less pronounced than with chlorogenic acids and flavonoids. However, due to low polarity, aqueous-alcoholic mixtures with high alcohol content should be used for storage if losses due to precipitation are to be avoided.

Anthraquinones from *Rumex alpinus* are known to be photosensitizers. Their aglycones were significantly degraded (approx. 90%) upon storage at room temperature in the presence of light, while glycosides seem to be more resistant (only about 15% was lost, when compared to content in non-illuminated sample stored at room temperature).

Decrease of angeloyl/tigloyloxy lupanin amount with simultaneous increase of hydroxylupanin content, points out their gradual hydrolysis at room temperature in the presence of light. In the non-illuminated sample stored at room temperature, as well as in the sample stored in acidic solvent (premixed mobile phase), the content of esters dropped to a similar level, but without the accompanying rise in free alcohol, indicating different degradation mechanism.

Based on the results obtained, it can be concluded that, due to instability of the majority of the compounds investigated, samples should be stored in the freezer (–20 °C) and protected from light.

CONCLUSION

The proposed optimized method is simple, and can be used for extraction of a wide range of plant secondary biomolecules, namely anthraquinones, isoflavonoids, flavonoids, phenolic acids, lignans, coumarins, and sesquiterpene lactones. 80% methanol provides acceptable extraction yield for all examined compounds, mixed in ratio 13:1 with dry plant material. Six-hour maceration, repeated for four times with fresh extraction solvent, provides a satisfactory yield of about 90%, within a reasonable amount of time. Temperature of 60 °C provides highly efficient extraction. Since it does not lead to compound degradation, it can be also used for crude extract evaporation. Defatting of extracts with hexane does not lead to major losses of compounds of interest. Thus, it can be used for removal of fats and pigments. Finally, results show that prepared extracts should be stored away from sunlight, on –20 °C.

Acknowledgments

This article was financially supported by a research grant from the Ministry of Education, Science and Technological Development of the Republic of Serbia (Grant No. 172058).

REFERENCES

[1] S.D. Sarker, Z. Latif, A.I. Gray, in: S.D. Sarker, Z. Latif, A.I. Gray (Eds.), Natural Product Isolation: An Overview; In Methods in Biotechnology, Vol. 20, Humana Press, New York, 2005, pp. 1–25.

[2] M. Wink, Evolution of secondary metabolites from an ecological and molecular phylogenetic perspective, Phytochemistry **64** (2003) 3–19.

[3] D.C. Vitale, C. Plazza, B. Melilli, F. Drago, S. Salomone, Isoflavones: estrogenic activity, biological effect and bioavailability, Eur. J. Drug. Metab. Pharmacokinet. **38** (2013) 15–25.

[4] A. Crozier, B. Indu, I.B. Jaganath, M.N. Clifford, in A. Crozier, M.N. Clifford, H. Ashihara (Eds.), Polyphenols and Tannins: An Overview; Plant Secondary Metabolites: Occurrence, Structure and Role in the Human Diet, Blackwell Publishing, Oxford, 2006, pp. 1–24.

[5] M.N. Clifford, K.L. Johnston, S. Knight, N. Kuhnert, Hierarchical scheme for LC/MS^n identification of chlorogenic acids, J. Agric. Food. Chem. **51** (2003) 2900–2911.

[6] F. Cuyckens, Y.L. Ma, G. Pocsfalvi, M. Claeys Tandem mass spectral strategies for the structural characterization of flavonoid glycosides, Analysis **28** (2000) 888––895.

[7] T.J. Mabry, K.R. Markham, M.B. Thomas, The systematic identification of flavonoids, Springer-Verlag, New York, 1970.

[8] J. Buckingham, Dictionary of Natural Products, Ver. 15.1, Chapman & Hall/CRC Press, London/New York, 2007.

[9] A. El-Shazly, A.M. Ateya, M. Wink, Quinolizidine alkaloid profiles of *Lupinus varius orientalis, L. albus albus, L. hartwegii* and *L. densiflorus*, Z. Naturforsch C **56** (2001) 21–30.

[10] A. Aberham, S.S. Cicek, P. Schneider, H. Stuppner, Analysis of sesquiterpene lactones, lignans, and flavonoids in wormwood (*Artemisia absinthium* L.) using high-performance liquid chromatography (HPLC)–mass spectrometry, reversed phase HPLC, and HPLC-solid phase extraction-nuclear magnetic resonance, J. Agric. Food. Chem. **58** (2010) 10817–10823.

[11] G.S. Jeong, O.K. Kwon, B.Y. Park, S.R. Oh, K.S. Ahn, M.J. Chang, W.K. Oh, J.C. Kim, B.S. Min, Y.C. Kim, H.K. Lee, Lignans and Coumarins from the Roots of *Anthriscus sylvestris* and Their Increase of Caspase-3 Activity in HL-60 Cells, Biol. Pharm. Bull. **30** (2007) 1340–1343.

[12] A. Koulman, S. Batterman, F.M. van Putten, R. Bos, W.J. Quax, Lignan profiles of indoor-cultivated *Anthriscus sylvestris*, Planta Med. **69** (2003) 959–961.

[13] S.K. Wong, S.K. Tsui, S.Y. Kwan, X.L. Su, R.C. Lin, Identification and characterization of *Podophyllum emodi* by API-LC/MS/MS, J. Mass. Spectrom. **35** (2000) 1246–1251.

[14] N.I. Bazykina, A.N. Nikolaevskii, T.A. Filippenko, V.G. Kaloerova, Optimization of conditions for the extraction of natural antioxidants from raw plant materials, Pharm. Chem. J. **36** (2002) 46–49.

[15] R.D. Renuka, C. Arumughan, Phytochemical characterization of defatted rice bran and optimization of a process for their extraction and enrichment, Bioresource Technol. **98** (2007) 3037–3043.

[16] S. Rovio, K. Hartonen, Y. Holm, R. Hiltunen, M.L. Riekkola, Extraction of clove using pressurized hot water, Flavour. Fragr. J. **14** (1999) 399–404.

[17] V. Švehlikova, R.N. Bennett, F.A. Mellon, P.W. Needs, S. Piacente, P.A. Kroon, Y. Bao, Isolation, identification and stability of acylated derivatives of apigenin 7-*O*-glucoside from chamomile (*Chamomilla recutita* [L.] Rauschert), Phytochemistry **65** (2004) 2323–2332.

[18] Y. Ungar, O.F. Osundahunsi, E. Shimoni, Thermal stability of genistein and daidzein and its effect on their antioxidant activity, J. Agric. Food. Chem. **51** (2003) 4394–4399.

[19] C.G.A. Davies, F.M. Netto, N. Glassenap, C.M. Gallaher, T.P. Labuza, D.D. Gallaher, Indication of the Maillard reaction during storage of protein isolates, J. Agric. Food. Chem. **46** (1998) 1485–2489.

IZVOD

OPTIMIZACIJA USLOVA EKSTRAKCIJE SEKUNDARNIH METABOLITA IZ RAZLIČITIH BILJNIH VRSTA

Filip S. Šibul, Dejan Z. Orčić, Emilija Svirčev, Neda M. Mimica-Dukić

Departman za hemiju, biohemiju i zaštitu životne sredine, Prirodno–matematički fakultet, Univerzitet u Novom Sadu

(Naučni rad)

Izolacija sekundarnih metabolita iz biljaka je veoma važna za njihovu identifikaciju, karakterizaciju i ispitivanje biološke aktivnosti. Prvi korak u izolaciji biomolekula je njihova ekstrakcija iz biljnog materijala. Neoptimizovani uslovi ekstrakcije mogu dovesti do gubitaka, degradacije i modifikacije jedinjenja od interesa i rezultovati u pogrešnim zaključcima vezanim za hemijski sastav biljke. Usled toga, cilj ovog rada bio je ispitivanje uticaja raz ekstrakcionih smeša, količina ekstragensa, temperature ekstrakcije i uparavanja, vremena ekstrakcije, odmašćivanja i načina čuvanja na prinos i profil različitih klasa sekundarnih metabolita. *Rumex alpinus* je korišćen za ekstrakciju antrahinona, *Glycine max* za izoflavonoide, *Chaerophyllum bulbosum* za flavonoide i fenolne kiseline, *Anthriscus sylvestris* za lignane i kumarine, *Lupinus albus* za alkaloide i *Artemisia absinthium* za ekstrakciju seskviterpenskih laktona. Efikasnost ekstrakcije je ispitivana korišćenjem tečne hromatografije visokih performansi sa detektorom sa nizom dioda i trostrukim kvadrupolnim masenim detektorom sa elektrosprej jonizacijom (HPLC--DAD-ESI–MS/MS). Kao najpogodniji ekstragens za većinu ispitanih jedinjenja je 80% metanol, pomešan u odnosu 13:1 sa suvim, usitnjenim biljnim materijalom. Maceracija od šest sati je dovoljna za ekstrakciju oko 90% biljnih komponenti. Ekstrakciju je najbolje izvršiti u 4 ponavljanja (po 90 min), sa dodatkom svežeg ekstragensa. Odmašćivanje ekstrakata, vršeno u cilju uklanjanja hlorofila i prisutnih masnih kiselina, ne dovodi do velikih gubitaka jedinjenja od interesa. Ekstrakciju i uparavanje je prihvatljivo vršiti na temperaturi od 60 °C. Ekstrakte je najbolje čuvati zaštićene od svetlosti, na –20 °C.

Ključne reči: Ekstrakcija • Sekundarni metaboliti • Biljni polifenoli • Flavonoidi • Fenolne kiseline

Determination of critical micelle concentration of cetyltrimethylammonium bromide: Different procedures for analysis of experimental data

Jelena M. Goronja[1], Aleksandra M. Janošević Ležaić[2], Biljana M. Dimitrijević[2], Anđelija M. Malenović[1], Dragomir R. Stanisavljev[3], Nataša D. Pejić[2]

[1]*Faculty of Pharmacy, University of Belgrade, Department of Drug Analysis, Belgrade, Serbia*
[2]*University of Belgrade, Faculty of Pharmacy, Department of Physical Chemistry and Instrumental Methods, Belgrade, Serbia*
[3]*Faculty of Physical Chemistry, University of Belgrade, Belgrade, Serbia*

Abstract

Conductivity of two micellar systems was measured in order to determine critical micelle concentration (CMC) of cetyltrimethylammonium bromide (CTAB). Those systems were: CTAB in water and CTAB in binary mixture acetonitrile (ACN)–water. Conductivity (κ)–– concentration (c) data were treated by four different methods: conventional method, differential methods (first and second derivative) and method of integration (methods A–D, respectively). As CTAB in water micellar system shows a sharp transition between premicellar and postmicellar part of the κ/c curve, any of the applied methods gives reliable CMC values and there is no statistically significant difference between them. However, for CTAB in ACN–water mixture micellar system the integration method for CMC determination is recommended due to a weak curvature of κ/c plot.

Keywords: acetonitrile–water mixture, cetyltrimethylammonium bromide, conductometry, critical micellar concentration.

Available online at the Journal website: http://www.ache.org.rs/HI/

SCIENTIFIC PAPER

UDC 544.4:544:51:615

Hem. Ind. **70** (4) 485–492 (2016)

doi: 10.2298/HEMIND150622055G

Surfactants, surface active agents or tenzides, are among the most important chemicals and most prominent components of many consumer products such as pharmaceuticals, foods, soaps, *etc*. Those amphiphilic molecules possess two parts: a polar or an apolar ″head″ (liophylic part), and a long chain hydrocarbon, *i.e*., nonpolar ″tail″ (liophobic part), so that one of these two parts of the molecule always has a particular affinity for the molecules of the solvent (polar or nonpolar) [1,2].

Apart to the strong tendency to spontaneously accumulate at the boundary surfaces phase, surfactants molecules (monomers) in aqueous solution at relatively high concentration show a distinct tendency towards arranging themselves into organized thermodynamically stable molegular aggregates known as micelles. Those agregate structures in surfactant solutions are first to form over a narrow range of surfactant concentration called the critical micelle concentration (*CMC*). This property appears to be a fundamental micellar quantity to study the self-aggregation of amphiphilic molecules in solution. In order to obtain thermodynamic parameters of micellization process [3,4], the theoretically proposed models (the mass action model or the phase separation model) [5–7] use expressions in which, directly or indirectly, the knowledge of the *CMC* is absolutely necessary. Thus, obtaining precise value of the *CMC* has extraordinary scientific, as well as practical significance [1,8–12].

In the narrow concentration range over which micelles are formed, the surfactant solutions show an abrupt change of different physicochemical properties (specific conductivity, surface tension, light scattering, *etc.*). Significant methodological difference in the determination of the *CMC* can be found, depending on the used experimental technique, the way data are processed, as well as how they are plotted and then analysed [13,14]. The focus of this paper is on the conductometric method, commonly used electrochemical technique for CMC determination [15], because of its experimental simplicity and inexpensive instrumentation. Thus, for ionic surfactant, the *CMC* can be determined by measuring the specific conductivity (κ) of surfactant of certain concentration (c), and by constructing a graph $\kappa = f(c)$. The change of slope or discontinuity of κ/c dependence gives the *CMC**. Accord-

Correspondence: J. Goronja, University of Belgrade, Faculty of Pharmacy, Department of Drug Analysis, Vojvode Stepe 450, 11000 Belgrade, Serbia.
E-mail: jelena_goronja@yahoo.com
Paper received: 22 June, 2015
Paper accepted: 10 September, 2015

*Related to the experimental determination of the *CMC*, several definitions of this surfactant property have been proposed. For example, according to Williams and co-works [16], *CMC* is surfactant concentration at which the micelle

ing to the simplest approach (Williams method) [16], the intersection of two straight lines obtained for surfactant concentration, which are smaller (premicellar range) and higher (postmicellar range) related to *CMC* gives value of *CMC*. This ″conventional procedure″ can be used for accurate determination of *CMC*, if κ changes abruptly at the transition between premicellar and postmicellar regions, as it is often the case with aqueous surfactant solutions [18,19,11]. However, the addition of co-solvents in aqueous surfactant solution, often leads to an increase in the degree of ionization micelles (α), and consequently to a weak curvature in vicinity of *CMC*, making the precise determination of *CMC* difficult [4,20,21]. To solve this problem, analysis of the plots of differential conductivity (first or second order) *versus* surfactant concentration [5,22], or more sophisticated approaches such as the fitting of the experimental raw data to a simple nonlinear function obtained by the direct integration of a Boltzmann type sigmoidal function [23] were frequently used. Among those, some other fitting procedures to the experimental data were used to obtain precise value of *CMC* in systems with low aggregation numbers (*i.e.*, with high α), and slow variations of physical property/concentration curves (for example, the method based on deconvolution into Gaussians of the second derivative of κ–c data, followed by two consecutive numerical integrations [24], then the method which consists of the application of a combination of the Runge–Kutta numerical integrations method and the Levenberg––Marquardt least-squares fitting algorithm [17], or statistical method (the local polynomial regression method, based on a nonparametric estimation of the regression function [25]).

In this paper, for the application and comparison of well known methods (conventional, differentiation and integration), we analyzed the two micellar systems: an aqueous solution of a cationic surfactant, hexadecyltrimethylammonium bromide (hereinafter, cetyltrimethylammonium bromide, CTAB) and CTAB in a binary mixture of acetonitrile (ACN) and water. The *CMC* of CTAB in water at t = 25.0 °C, as well as the binary mixture ACN-water (20 vol.% at t = 20.0 °C, were determined by measuring specific conductivity. These micellar systems were chosen because in the case of an aqueous solution of CTAB, specific conductivity/concentration curve shows a clear break, while in the case of CTAB in the mixture ACN–water we found the appearance of curvature around *CMC*, so that the singular point can not be easily determined. Therefore, to determine accurately the *CMC* value in the latter case, we used the procedure that is commonly used to obtain *CMC* of surfactants with small aggregation number [4,20,22,26] and which has recently been proposed by Carpena and co-workes [23]. The aim of this paper is to show how/whether values of *CMC* change/depend on the applied mathematical analysis of κ–c data, as well as to find the best procedure that has appeared recently in literature [23], for *CMC* determination in the particular case.

EXPERIMENTAL

Material

The cationic surfactant, cetyltrimethylammonium bromide (CTAB) was obtained from Merck (Germany) having purity ≥ 97% used without any pretreatment. Acetonitrile ACN (HPLC grade purity ≥ 99.9%) was obtained from Sigma–Aldrich (USA). Deionized water (ρ = 18 MΩ cm, Milli-Q, Millipore, Bedford, MA, USA) was used for preparation of all solutions.

Fresh solutions of CTAB in CAN–water (20 vol.%) binary mixtures were prepared in the following way. The accurately weighed (Mettler electronic balance with a precession of 0.0001 g) mass of CTAB was quantitatively transferred into a 100 mL volumetric beaker, and dissolved in 90 mL of 20 vol.% ACN; that mixture was gently stirred with a glass rod in order to avoid the foam formation. Then, the solution was transferred in 100 mL volumetric flask and filled up to volume with 20 vol.% ACN.

Methods

The conductivity measurements were carried out using a digital conductivity meter HI8820N (Hanna instruments, Portugal) with the uncertainties ±0.5 μS cm^{-1}, and with the matching HI7684W probe that uses the 4-ring method. The conductivity meter was calibrated with different concentration of solutions of potassium chloride (Merck, purity > 99 %) prior to the experiment. The conductivity–concentration data were obtained from two micellar system (water solution of CTAB as well as CTAB in binary mixture of water and co-solvent (ACN)) at constant temperature (25.0 °C in the case of CTAB in water, and 20.0 °C in the case of CTAB in mixture ACN–water). A circulating water bath (Series U, MLW, Frietal, Germany) was used for maintaining the constant temperature within uncertainties of ±0.2 °C. The specific conductivity values of each set containing 18–21 different CTAB concentrations, at a fixed solvent composition (expressed as ACN vol.%), were measured while stirring after achieving temperature equilibrium at each dilution.

concentration would become zero if the micellar concentration continues to change at the same rate as it does at a slightly higher concentration [17]. On the other hand, Phillips [5] defined CMC as the surfactant concentration that corresponds to the maximum change in the gradient of a plot of the magnitude of the solution property (Φ) against concentration (c): $(d^3\Phi / dc^3)_{c=CMC} = 0$.

All measurements were conducted in glass vessel, $V \approx 100$ mL (Metrohm, model 876–20) wrapped in the water recirculation jacked connected to thermostat and equipped with the magnetic stirrer ((IKA–COMBIMAG RET, Staufen, Germany).

Data analysis

For processing (fitting) all experimental data, *i.e*., obtaining precise values of critical micelle concentration of the examined micellar systems, software package OriginPro 9.0 (OriginLab Corporation, US) was used.

Procedure

The 90 mL solution of CTAB of different concentrations was introduced into the glass vessel that was capped with openings through which thermometer and conductometric cell are always put in the same place. Then, CTAB solution was thermostated (~20 min) at the examined temperature (20.0 or 25.0 °C) along with stirring (300 rpm), and equilibrated until the conductivity value became constant. For each of the examined CTAB solution, the specific conductivity measurements were repeated three times.

RESULTS AND DISSCUSION

For the analysis of experimental data obtained by measuring specific conductivity of certain surfactant concentrations, *i.e*., the determination of *CMC* of the examined micellar systems, we used different methods (A, B, C and D, respectively) that are ″conventional procedure″ (Williams *et al*. method [16] methods of differentiation (either the first [22] or the second order [5]) as well as the method of integration (Carpena method) [22].

Conventional method – method A [16]. As the *CMC* is a "phase transition" between two different regimes of a surfactant solution, the plot of κ versus surfactant concentration is a curve which consists of two linear segments (premicellar and postmicellar) with different slopes; the intersection (singular point) of those straight lines below and the above *CMC* gives the value of *CMC*, while ratio of the slope of the postmicellar region (S_2) to that of the premicellar region (S_1) gives micelle ionization degree (α) [3,27–29].

The first derivative method – method B [22]. According to this method, one can analyze the dependence of the specific conductivity first derivative ($d\kappa/dc$) *versus* surfactant concentration, *c*. This derivative is of the sigmoidal type, and can be adequately described by using a Boltzmann type sigmoidal:

$$\frac{d\kappa}{dc} = A_2 + \frac{A_1 - A_2}{1 + e^{(c-c_0)/\Delta c}} \quad (1)$$

where A_1 (A_2) is the asymptotic value for small (large) values of surfactant concentration (horizontal asymptote), c_0 , *i.e*., *CMC* is center of sigmoidal curve (central point of the transition), and Δc is the width of the transition (fitting parameter, *i.e*., the time constant, which is directly related to the independent variable range, where the sudden change of κ occurs).

The second derivative method – method C (Phillips method [5]). According to this method, one can analyze the dependence of the second derivative of specific conductivity ($d^2\kappa/dc^2$) *versus* surfactant concentration, *c*. This method consists of directly fitting the second derivative of the conductivity/concentration data to a Gaussian without additional treatment of the data. The equation to use in Origin program for fitting the curve is:

$$\left(\frac{d^2\kappa}{dc^2}\right) = \left(\frac{d^2\kappa}{dc^2}\right)_{c=0} + \frac{A}{w\sqrt{\pi/2}}\exp\left(\frac{-2(c-CMC)^2}{w^2}\right) \quad (2)$$

where $(d^2\kappa/dc^2)_{c=0}$, *A* and *w* are baseline offset, total area under the curve from the baseline and the width of the peak at half height, respectively. The minimum of the inverted Gaussian corresponds to points of maximum variation, and coincides with the *CMC*.

Method of integration – method D (Carpena's method) [23]. This method is based on direct fitting of specific conductivity *versus* surfactant concentration data. If it is assumed that the dependence of the first derivative of specific conductivity *versus* surfactant concentration behaves as a sigmoid (Eq. (1)), then the original data should behave as the integral of the sigmoid. A direct integration of Eq. (1) yields:

$$\kappa = \kappa(0) + A_1 c + (A_2 - A_1)\Delta c \ln\left(\frac{1 + e^{(c-c_0)/\Delta c}}{1 + e^{-c_0/\Delta c}}\right) \quad (3)$$

where $\kappa(0)$ is the value of specific conductivity when surfactant concentration (*c*) is 0, A_1 and A_2 are the slopes obtained in the premicellar and postmicellar segments, c_0 (*CMC*) is the breakpoint of curve κ/c and Δc is a width of transition with c_0, *i.e*., concentration range in which there is a change of κ (fast or slow) around *CMC*.

The above described mathematical procedures have both some advantages and drawbacks. Generally, if there is an appropriate curvature and the break point is clear, any method is suitable for determination of the *CMC*. On the other hand, a frequent problem arises from the conductivity method that it is usually difficult to determine the *CMC* for micellar systems in which the κ/c plot does not show a sharp transition from the premicellar to the postmicellar region. As the result, the obtained *CMC* will be affected to a greater uncertainty.

Table 1 shows the *CMC* and the degree of micelle ionization, α of CTAB in water obtained at 25.0 °C, from conductivity/concentration plots by using the above described different treatments of the experimental data (conventional, differentiation and integration).

The dependence of the specific conductivity, κ on the concentration of CTAB, c_{CTAB} at t = 25.0 °C is presented in Fig. 1a. With c_{CTAB} increasing, κ also increases linearly. After a certain concentration of CTAB, κ further increases linearly, but the slope of the straight line decreases; concentration at which an abrupt change of κ occurs, represents *CMC*. As a point that corresponds to the *CMC* on κ/c plot divides graph on the two linear parts (premicellar and postmicellar) the value of *CMC* is determined as the intersection point [16,17,20] of two lines that correspond to the κ values in those segments. The data points were fitted by the least square method and the equations of lines in premicellar and postmicellar segment are obtained: κ = 3.0 (±0.81) + 123.8 (±1.45)c_{CTAB} (r^2 = 0.9995, p < 0.001) and κ = 72.4 (±0.66) +47.3 (±0.49)c_{CTAB} (r^2 = 0.9996, p < < 0.001). By solving these equations for c, we obtained the value of the intersection points (*CMC*, method A), which was 0.907±0.04 mM. Likewise, the degree of counterion dissociation was determined from the ratio of the slopes of lines in both premicellar (S_1) and postmicellar (S_2) region, $\alpha = S_2/S_1$, and the obtained value is 0.38±0.01.

Table 1. Critical micelle concentration (CMC) and degree of counterion dissociation (α) for examined micellar systems obtained by different treatments of the experimental data

Micellar system	Conventional (method A)		Differentiation			Integration (method D)	
			First order (method B)		Second order (method C)		
	CMC / mM	$\alpha(S_2/S_1)$[a]	*CMC* / mM	$\alpha(A_2/A_1)$[b]	*CMC* / mM	*CMC* / mM	$\alpha(A_2/A_1)$[b]
CTAB in water	0.907	0.38	0.900	0.37	0.907	0.911	0.39
CTAB in ACN–water	3.706	0.74	3.556	0.76	–	3.699	0.75

[a]Data obtained from the ratio between the slopes of line in the postmicellar region (S_2) to that in the premicellar region (S_1); [b]data obtained from the ratio between the slopes of line in the postmicellar region (A_2) to that in the premicellar region (A_1) (see Eqs. (1) and (3))

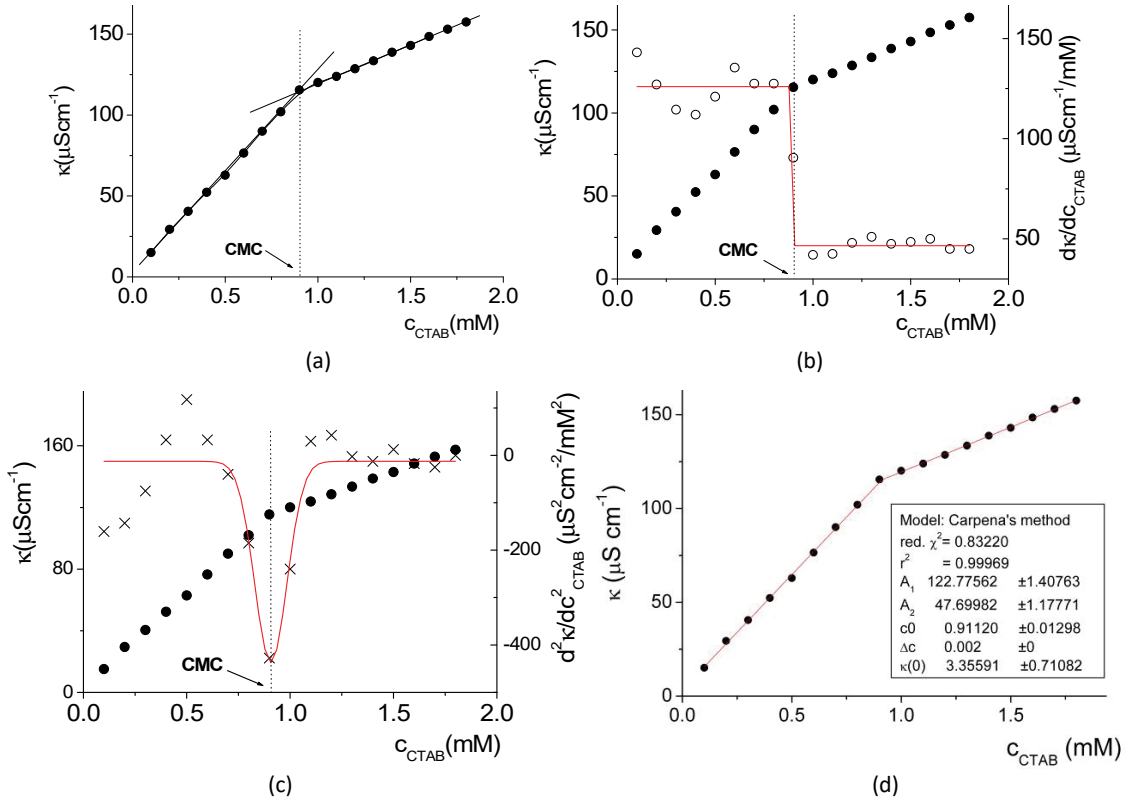

Figure 1. Graphical presentation of different methods of CMC determination for CTAB in water micellar system at 25.0 °C by: a) Williams method, b) first derivative method (solid line corresponds to a Boltzmann-type sigmoid), c) Phillips method (solid line corresponds to Gaussian) and d) Carpena method (solid line corresponds to integrated form of sigmoid of Boltzmann type); result of the fitting shown in the box. Experimental points, the first and the second derivative are denoted as ●, ○ and ×, respectively. The arrows denote CMC values.

In addition, the *CMC* was determined using the first derivative method (method B). Figure 1b shows plot of $d\kappa/dc$, as a function of the surfactant concentration. The data were fitted to a sigmoidal curve of Boltzmann type (Eq. (1)), and the obtained value of both *CMC* and α was 0.900 mM and 0.37, respectively. Figure 1c shows the application of the Phillips' method (method C) for the determination of *CMC*. Crosses denote the values of $d^2\kappa/dc^2$, and a solid line corresponds to the Gaussian function (Eq. (2)). Value of *CMC* determined by this method was 0.907 mM.

Apart from the above-described procedures for determination of C*MC*, the recently proposed method (the method D [23]) was used. The solid lines (Figure 1d) correspond to the Carpena fitting, where the obtained value of *CMC* is 0.911±0.013 mM. The values of both the *CMC* and α obtained by this approach (method D) as well as by previously described methods A–C are all listed in Table 1. Fitting parameters of κ–c data to Eq. (3) are shown in Figure 1d. Besides the most significant fit parameters, the Figure 1d includes the regression-square (r^2) and reduced shi-square (red. χ^2) coefficients.

Obviously, between the values of *CMC* obtained by methods A–D there is no significant difference (*RSD* = = 0.5%), so that in the case of CTAB in water, for determination of *CMC* one can use any of the given procedures. Moreover, since conductivity shows the abrupt change in going from the premicellar surfactant concentration range to the postmicellar surfactant concentration range, then Williams method allows one to calculate a reliable value for the *CMC* (for α also). This value has been confirmed by derivative method as well as the method of integration. Also, *CMC*s obtained from conductivity measurements are consistent with previously published results which show that the values of *CMC* at t = 25.0 °C lie in the range 0.88–1.02 mM [20,23,24,30–33,10,34,11,13].

In our previous papers [26], we reported the effect of co-solvent, propylene-glycol on the micellization of CTAB at different temperatures. In the present paper our study is extended to the micellar system CTAB in mixture acetonitrile–water at t = 20.0 °C. Although the *CMC* values for CTAB in this mixture at different temperatures were already obtained [35,36], to our knowledge there were no previous studies on the influence of ACN on CTAB micellization at t = 20.0 °C.

In Figure 2a the results of *CMC* determination for CTAB in mixture ACN–water (20 vol.%) at t = 20.0 °C obtained by the conventional method (method A) and the first derivative method (method B) are shown. The solid line corresponds to the first derivative of the conductivity/concentration curve, and the arrows denote the values of *CMC* obtained by the method A (CMC_1) as well as the method B (CMC_2). Again, according to method A, the data points were fitted by the least square method and the equations of lines in premicellar and postmicellar segment are obtained: κ = = –8.5 (±1.10) + 80.5 (±.53) c_{CTAB} (r^2 = 0.9997, p < 0.001) and κ = 67.8 (±7.41) + 59.9 (±1.61)c_{CTAB} (r^2 = 0.9978, p < < 0.001). Obtained value of critical micellar concentration was 3.706 ± 0.789 mM (CMC_1). On the other hand, this value obtained by method B was 3.556 mM (CMC_2). Moreover, due to a small curvature of the curve, in this micellar system it was not possible to get the second derivative (the method C).

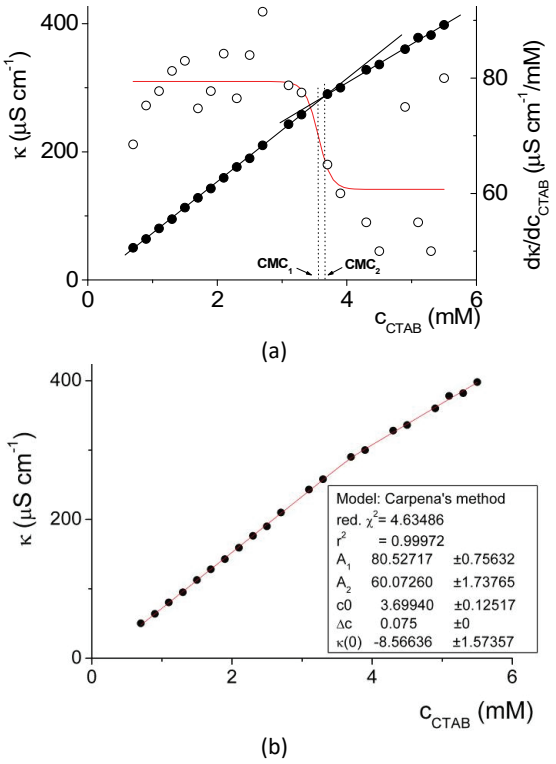

Figure 2. Graphical presentation of different methods of CMC determination for CTAB in CAN–water (20 vol.%) micellar system at 20.0 °C: a) Williams method as well as the first derivative method (solid line corresponds to a Boltzmann type sigmoid) and b) Carpena method (solid line corresponds to integrated form of sigmoid of Boltzmann type); result of the fitting shown in the box. Experimental points and the first derivative are denoted as ● and ○, respectively. The arrows denote CMC values.

In comparison to the previous examined micellar system (an aqueous solution of CTAB), in this case, the change κ with the CTAB concentration in the transition region (*i.e.*, the region between the two linear segments, premicellar and postmicellar) is gradual, thus, for the precise determination of *CMC*, the integration method (the method D) was used. The solid line (Figure 2b) represents fit according to the Eq. (3).

Data fitting was carried out by making use of initial values of $\kappa(0)$, A_1, A_2, c_0 and Δc to calculate an approximate value of conductivity (Eq. (3)). The values of $\kappa(0)$,

A_1, A_2 and c_0 were estimated graphically from the experimental plot by the method A. Once chosen, values of these parameters were not changed during fitting sessions as they didn't have a significant influence on the *CMC*, while this was not the case with Δc [20]. Initial values of Δc were chosen from a certain range shown in Figure 3a and changed for an each fitting session. It was noticed that low Δc starting values give lower reduced chi-square coefficient values (red. χ^2). Figure 3a shows that for the discussed micellar system there is a certain region of Δc initial values for which red. χ^2 obtained from these fitting sessions are constant. The final set of fitted parameters values was chosen according to this region. Namely, we took final set of fitted parameters values when red. χ^2 stopped decreasing and became constant as best-fit parameters. The dependence of C*MC* values obtained by a four-parameter fit procedure for different Δc is shown in Figure 3b. The most significant fitting parameters ($\kappa(0)$, A_1, A_2, c_0 and Δc), including the regression-square (r^2) and reduced chi-square (red. χ^2) coefficients are all summarized in Figure 2b. Obtained value of *CMC* was 3.699±0.125 mM. As we expected, uncertainty (expressed as *RSD*) in the *CMC* value obtained by method D, related to methods A, is much lower, and it is ±3.0%. The values of both the *CMC* and α for CTAB in the mixture CAN–water obtained by methods A, B and D are all listed in Table 1.

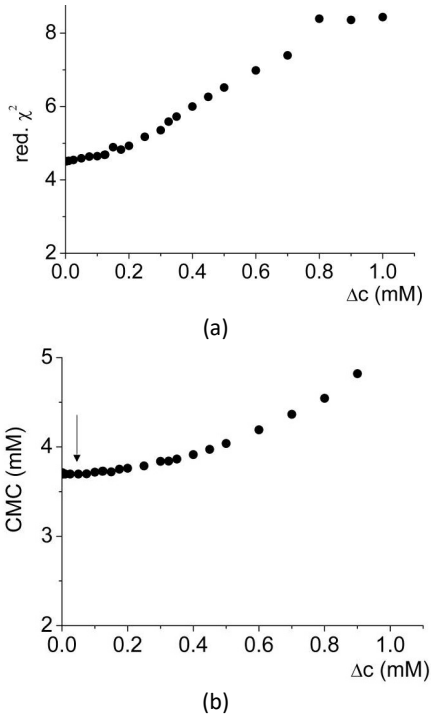

Figure 3. Initial values of the width of transition (Δc) influence on: a) reduced chi-square (red. χ^2) coefficient and b) the critical micelar concentration (CMC). These are obtained by fitting the raw experimental data for CTAB solution in mixture CAN–water (20 vol.%) at 20.0 °C to Eq. (3). The arrow denotes chosen (optimal) Δc.

CONCLUSION

In this paper, the *CMC* values of different micellar systems (CTAB in water, and CTAB in binary mixture ACN–water) were determined from conductivity measurements at t = 25.0 °C (CTAB in water) and t = 20.0 °C (CTAB in binary mixture ACN–water). Those values were calculated from experimental data by various procedures (conventional, the first and second derivative as well as integration), with a view to determine whether the value of the *CMC* change depending on the applied method or not, as well as finding out the optimal method for determining the *CMC* in the particular case. Thus, if there is an appropriate curvature and the break point is clear, any method is suitable for determination of the *CMC* (case of CTAB in water). The *CMC*s obtained by those methods were in a good agreement with each other. This means that the use of conventional method (Williams) is appropriate, and gives reliability to the *CMC* for CTAB in water. However, in the case of CTAB in the mixture ACN–water, the specific conductivity–concentration plot does not show a sharp transition from the premicellar and postmicellar region, but it rather exhibits a curvature. Therefore, for the precise determination of the *CMC*, the method of integration was considered, whereby calculated values of the *CMC* depend critically on the initial value of Δc (*i.e.*, the width of transition) in the process of fitting the experimental data.

Acknowledgements

The present investigations were partially supported by The Ministry of Education, Science and Technological Development of the Republic of Serbia, under projects 172015 and 172052.

REFERENCES

[1] M.J. Rosen, Surfactants and interfacial phenomena, 3rd ed., John Wiley & Sons, New York, 2004.

[2] N. Pejić, M. Aleksić, Odabrana poglavlja koloidne hemije, Farmaceutski fakultet, Beograd, 2013.

[3] J.P. Marcolongo, M. Mirenda, Thermodynamics of sodium dodecyl sulfate (SDS) micellization: an undergraduate laboratory experiment, J. Chem. Educ. **88** (2011) 629–633.

[4] J. Aguiar, A. Molína-Bolìvar, J.M. Peula-Garcìa, C. Carnero Ruiz, Thermodynamics and micellar properties of tetradecyltrimethylammonim bromide in formamide––water mixtures, J. Coll. Interf. Sci. **255** (2002) 382–390.

[5] J.N. Philips, The energetics of micelle formation, Trans. Faraday Soc. **51** (1955) 561–569.

[6] D. Atwood, A.T. Florence, Surfactants Systems: Their Chemistry, Pharmacy and Biology, Chapman and Hall, New York, 1983.

[7] T. Tadros, Applied surfactants, principles and applications, Wiley-VCH, Weinheim, 2005.

[8] A.B. Mandal, V. Ramesh, S.C. Dhar, Physico-chemical studies of micelle formation on sepia cartilage collagen solutions in acetate buffer and its interaction with ionic and nonionic micelles, Eur. J. Biochem. **169** (1987) 617–628.

[9] L.L. Schramm, E.N. Stasiuk, D.G. Marangoni, Surfactants and their applications, Annu. Rep. Prog. Chem., C: Phys. Chem. **99** (2003) 3–48.

[10] P.K. Sansanwal, Effect of co-solutes on the physico-chemical properties of surfactant solutions, J. Sci. Ind. Res. **65** (2006) 57–64.

[11] K. Manna, A.K. Panda, Physicochemical Studies on the Interfacial and Micellization Behavior of CTAB in Aqueous Polyethylene Glycol Media, J. Surfact. Deterg. **14** (2011) 563–576.

[12] M.R. Milović, J.D. Đuriš, D.D. Vasiljević, Z.R. Đurić, S.R. Ibrić, Potencijalna primena surfaktantnih sistema u formulaciji farmaceutskih oblika sa teško rastvorljivim lekovitim supstancama, Hem. Ind. **66** (2012) 667–676.

[13] W. Al-Soufi, L. Piñeiro, M. Novo, A Model for Monomer and Micellar Concentrations in Surfactant Solutions, Application to Conductivity, NMR, Diffusion and Surface Tension data., J. Colloid Interface Sci. **370** (2012) 102–110.

[14] A. Patist, in: K. Holmberg (Ed.), Handbook of applied surface and colloid chemistry, John Wiley & Sons, New York, 2001, p. 239.

[15] K. Nesměrák, I. Němcová, Determination of critical micelle concentration by electrochemical means, Anal. Lett. **39** (2006) 1023–1040.

[16] R. Williams, J.N. Phillips, K.J. Mysels, The critical micelle concentration of sodium laurylsulphate at 25 °C, Trans. Faraday Soc. **51** (1955) 728–737.

[17] M. Pérez-Rodríguez, G. Prieto, C. Rega, L.M. Varela, F. Sarmiento, V. Mosquera, A comparative study of the determination of the critical micelle concentration by conductivity and dielectric constant measurements, Langmuir **14** (1998) 4422–4426.

[18] H.N. Singh, S.M. Saleem, R.P. Singh, K.S. Birdi, Micelle formation of ionic surfactants in polar nonaqueous solvents, J. Phys. Chem. **84** (17) (1980) 2191–2194.

[19] H. Akbaş, Ç. Kartal, Conductometric studies of hexadecyltrimethylammonium bromide in aqueous solutions of ethanol and ethylene glycol, Coll. J. **68**(2) (2006) 125–130.

[20] A. Rodriguez, M. del Mar Graciani, M. Muñoz, L. Moyá, Water-ethylene glycol alkyltrimethylammonium bromide micellar solutions as reaction media: study of spontaneous hydrolysis of phenyl chloroformate, Langmuir **19** (2003) 7206–7213.

[21] A. Kroflič, B. Šarac, M. Bešter-Rogač, What Affects the Degree of Micelle Ionization: Conductivity Study of Alkyltrimethylammonium Chlorides, Acta Chim. Slov. **59** (2012) 564–570.

[22] Kabir-Ud-Din, P.A. Koya, Effect of acetonitrile on the micellization and thermodynamic parameters of tetradecyltrimethylammonium bromide: conductometric and fluorimetric studies, J. Mol. Liq. **158** (2011) 111–116.

[23] P. Carpena, J. Aguiar, P. Bernaola-Galván, C. Carnero Ruiz, Problems associated with the treatment of conductivity-concentration data in surfactant solutions: simulations and experiments, Langmuir **18**16) (2002) 6054–6058.

[24] I. Garcia-Mateos, M.M. Velázquez, L.J. Rodríguez, Critical micelle concentration determination in binary mixtures of ionic surfactants by deconvolution of conductivity/concentration curves, Langmuir **6** (1990) 1078–1083.

[25] J.L. López Fontán, J. Costa, J.M. Ruso, G. Prieto, F. Sarmiento, A nonparametric approach to calculate critical micelle concentrations: the local polynomial regression method, Eur. Phys. J. E **13** (2004) 133–140.

[26] A. Janošević Ležaić, N. Paunović, N. Pejić, Thermodynamics of micellization of hexadecyltrimethylammonium bromide in propylene glycol–water mixture: a conductivity study, Facta Univer.: Ser. Phys., Chem. Technol. **12** (2014) 17–26.

[27] H.C. Evans, Alkyl sulphates. Part I. Critical micelle concentrations of the sodium salts, J. Chem. Soc. **78** (1956) 579–586.

[28] P. Lianos, J. Lang, Static and dynamic properties of sodium *p*-(1-propylnonyl)benzenesulfonate micelles, J. Colloid Interface Sci. **96** (1983) 222–228.

[29] R. Zana, H. Lévi, Mixed micellization of cetyltrimethylammonium bromide and an anionic dimeric (gemini) surfactant in aqueous solution, Langmuir **13** (1997) 402–408.

[30] M. Del Mar Graciani, A. Rodríguez, M. Muñoz, M.L. Moyá, Water-ethylene glycol alkyltrimethylammonium bromide micellar solutions as reaction media: study of the reaction methyl 4-nitrobenzenesulfonate + Br^-, Langmuir **19** (2003) 8685-8691.

[31] J. Aguiar, P. Carpena, J.A. Molina-Bolívar, C.K. Ruitz, On the determination of the critical micellar concentration by the pyrene 1:3 ratio method, J. Colloid Interface Sci. **258** (2003) 116–122.

[32] N. Jiang, P. Li, Y. Wang, J. Wang, H. Yan, R.K. Thomas, Aggregation behavior of hexadecyltrimethylammonium surfactants with various counterions in aqueous solution, J. Colloid Interface Sci. **286** (2005) 755–760.

[33] W. Li, Y.-C. Han, J.-L. Zhang, B.-G. Wang, Effect of ethanol on the aggregation properties of cetyltrimethylammonium bromide surfactant, Coll. J. **67** (2005) 186–191.

[34] L. Moyá, A. Rodríguez, M. Del Mar Graciani, G. Fernández, Role of the solvophobic effect on micellization, J. Colloid Interface Sci. **316** (2007) 787–795.

[35] P.K. Misra, B.K. Mishra, G.B. Behera, Micellization of ionic surfactants in tetrahydrofuran-water and acetonitrile-water mixed solvent systems, Colloids Surfaces **57** (1991) 1–10.

[36] F. Jalali, A. Gerandaneh, Micellization of cetyltrimethylammonium bromide (CTAB) in mixed solvents and in the presence of potassium bromide, J. Disper. Sci. Technol. **32** (2011) 659–666.

IZVOD

ODREĐIVANJE KRITIČNE MICELARNE KONCENTRACIJE CETILTRIMETILAMONIJUM BROMIDA: RAZLIČITE PROCEDURE ANALIZE EKSPERIMENTALNIH PODATAKA

Jelena M. Goronja [1], Aleksandra M. Janošević Ležaić [2], Biljana M. Dimitrijević[2], Dragomir R. Stanisavljev[3], Anđelija M. Malenović[2], Nataša D. Pejić[2]

[1]*Farmaceutski fakultet, Univerzitet u Beogradu, Katedra za analitiku lekova, Vojvode Stepe 450, 11000 Beograd, Srbija*
[2]*Farmaceutski fakultet, Univerzitet u Beogradu, Katedra za fizičku hemiju i instrumentalne metode, Vojvode Stepe 450, 11000 Beograd, Srbija*
[3]*Fakultet za fizičku hemiju, Univerzitet u Beogradu, Studentski trg 12-16, 11001, Beograd, Srbija*

(Naučni rad)

Korišćene su različite matematičke procedure za analizu eksperimentalnih podataka s ciljem određivanja kritične micelarne koncentracije (*CMC*) katjonskog surfaktanta, heksadeciltrimetilamonijum-bromida (cetiltrimetilamonijum-bromida, CTAB) u vodi, kao i binarnoj smeši vode i korastvarača (acetonitril, ACN). Provodljivost ovih micelarnih sistema merena je na t = 25.0 °C (CTAB u vodi) i t = 20.0 °C (CTAB u smeši ACN–voda). Na osnovu podataka specifična provodljivost (κ)–koncentracija surfaktanta (c), vrednosti *CMC* su određene primenom: klasične metode, metoda diferenciranja (prvog i drugog izvoda) i metodom integracije (metode A, B, C i D, redom). U slučaju vodenog rastvora CTAB, prelaz između predmicelarnog i postmicelarnog dela krive $\kappa = f(c)$ je oštar, tako da se *CMC* određuje kao tačka preseka dve linije koje odgovaraju ovim, dobro definisanim delovima krive (metod A). Pored toga, vrednost *CMC* ovog micelarnog sistema određena je metodama B, C i D, pri čemu između dobijenih vrednosti *CMC* ne postoje statistički značajne razlike. Međutim, u odnosu na čistu vodu, dodatak ACN rezultuje u manjoj promeni specifične provodljivosti s koncentracijom CTAB u uskoj oblasti koncentracija između dva linearna dela krive κ/c, što može dovesti do nepreciznog određivanja *CMC*. Zbog toga je, za precizno određivanje *CMC* u ovom micelarnom sistemu, predložen metod integraljenja (metod D).

Ključne reči: Cetiltrimetilamonijum-bromid • Smeša acetonitril–voda • Konduktometrija • Kritična micelarna koncentracija